Trinity College Dublin
Coláiste na Tríonóide, Baile Átha Cliath
The University of Dublin

School of Biochemistry and Immunology

PLGA particle size as a critical modulator of immune tolerance via αvβ3 mechano-sensor engagement

Presented by Roisin Lynch

Supervisor- Professor Ed Lavelle

❊

2025

A PhD thesis submitted to Trinity College Dublin for the degree of Doctor of Philosophy

I have read and understood the College / University statement on plagiarism.

I declare that the attached dissertation is my own, original work undertaken in partial fulfilment of my degree. I have made no use of sources, materials or assistance other than those which have been openly and fully acknowledged in the text. If any part of another person's work has been quoted, this either appears in inverted commas or (if beyond a few lines) is indented. Any direct quotation or source of ideas has been identified in the text by author, date and page number(s) immediately after such an item, and full details are provided in a reference list at the end of the text.

I understand that any breach of the fair practice regulations may result in a fail of this dissertation and that it could also involve other repercussions. I understand also that too great a reliance on the work of others may lead to a low mark.

Abstract

The increasing prevalence of inflammatory and autoimmune conditions underscores the critical need for novel therapeutic strategies that modulate inflammation without impairing the capacity to mediate protective immunity against infection and cancer. In recent years, there has been growing interest in the use of biodegradable particles to modulate immune responses for therapeutic purposes, spanning from vaccine adjuvants to drug delivery vehicles. Notably, size was found to be a crucial physicochemical property that regulates the capacity of particulates to modulate the activation of innate immune cells. This study investigated the capacity of poly(lactic-co-glycolic acid) (PLGA) particles to induce anti-inflammatory immune responses and explored the mechanisms by which innate immune cells can respond to PLGA particles differentially based on size. This work identified that particles in the 0.5–2 μm size range can reprogram innate immune cells toward immunosuppressive phenotypes. Specifically, PLGA particles within this narrow size range were found to induce the secretion of transforming growth factor β (TGFβ), IL-1 receptor antagonist (IL-1Ra), and IL-10 from key antigen-presenting cells (APCs). Incubation of dendritic cells (DCs) with these particles resulted in an enhanced capacity to prime and expand $CD4^+$ regulatory T-cell (T-reg) in an *in-vitro* co-culture model and vaccination with antigen and particles induced enhanced antigen-specific T-reg numbers. Investigations into the mechanism by which APCs respond to particles based on size revealed significant changes in cell morphology and membrane fluidity, particularly in response to 0.5–2 μm PLGA particles. Furthermore, surface expression of the mechanosensory integrin αvβ3 was markedly upregulated by particles within this size range. A critical role for αvβ3 was identified in regulating the transduction of mechanical stimuli from the cell membrane into biochemical signalling, resulting in the observed anti-inflammatory responses. Importantly, αvβ3 was essential for the ability of DCs to activate antigen-specific T-regs by mediating the mechanical activation of latent TGFβ, providing crucial pro-tolerance signals during antigen presentation. These findings demonstrate the potential of biodegradable 0.5-2 μm PLGA particles as adjuvants for ‘inverse vaccines’ to promote immunological tolerance in a manner independent of biologic agents or potent immunosuppressants. Furthermore, these findings exhibit the importance of

mechanical cues in driving immune responses and how these can be harnessed to improve existing particle-based immune-therapies.

Publications

Lebre M. F, Boland B. J , Gouveia P, Gorman L. A , Lundahl L.E M, Lynch I. R, O'Brien J. F, Coleman J, Lavelle C E. **Pristine graphene induces innate immune training.** *Nanoscale* 12, 11192–11200 (2020).

Lynch I. R & Lavelle.C E. **Immuno-modulatory biomaterials as anti-inflammatory therapeutics**. *Biochemical Pharmacology* vol. 197 (2022).

Lundahl L.E. M, Mitermite M, Ryan D. G, Case S, Williams C. N. Lynch I. R, Lagan E, Lebre M. F, Gorman L. A, Stojkovic B, Bracken P. A, Frezza C, Sheedy J. F, Scanlan M. E, Gordon V. S, Lavelle C E. **Macrophage innate training induced by IL-4 and IL-13 activation enhances OXPHOS driven anti-mycobacterial responses**. *Elife* **11**, e74690 (2022).

Huete-Carrasco, J, Lynch I. R., Ward, W. R. & Lavelle C. E. **Rational design of polymer-based particulate vaccine adjuvants.** *Eur. J. Immunol* 54, 2350512 (2024).

Lynch I. R, Huete-Carassco J, McCluskey S, Gorman L. A, Nolan D, McManus G, Lavelle C, E. **Microparticles promote antigen-specific T-reg expansion through mechano-sensitive integrin αvβ3** (Manuscript under final preparations for submission)

Acknowledgements

First and foremost, I would like to thank my supervisor Prof Ed Lavelle, for the opportunity to work in such an incredible lab. Thank you for your unwavering support, understanding and incredible guidance. Throughout this PhD, my confidence as a scientist and passion for research has grown thanks to you.

I would also like to thank the SFI Centre for Advanced Materials and Bioengineering Research (AMBER) for the awarding me with the funding to complete this project. I am also incredibly grateful for the opportunity to carry out my PhD in the TBSI, and for all the people who manage the core facilities, especially Dr Barry Moran in the Flow Cytometry facility and Dr Gavin McManus in confocal, who are always willing to brain storm a problem with me.

Looking back on the past nine years at Trinity fills me with immense gratitude for the incredible friendships I've formed along the way. I want to express my heartfelt thanks to all the past lab members who welcomed me so warmly when I first began. Aoife, Jo, and Shauna, thank you for your guidance and unwavering patience, for teaching me everything you know, and for brainstorming with me when experiments didn't go as planned. But also, thank you so much for all the fun we had, and for all the lunches which turned into expresso martinis! Alex, thank you for always been such a calming presence and always showing up. Natalia, thank you for every piece of advice and for being a true inspiration—I've learned so much from you. And of course, Ross. I feel so fortunate to have spent my first four years in the lab with such a great friend by my side. Thank you for always being there to talk things through and for all the charcuterie, toast, and tea breaks we shared. Finally, a special shoutout to all my wonderful friends. Caoimhe, I appreciate you so much and thank you for always fighting my corner.

To the current lab members, thank you for putting up with me through the last two years in the lab. Thank you for always making me laugh Jeremy, and for the keeping me entertained with your sassy emails Dorian. The lab would not run half as smoothly without you Lorena, thank you for everything you do. Faye, you are an incredible woman, so kind and thoughtful. Thank you for all the treats you have brought in and for introducing us to Uyghur food! Nicole, it's been an absolute pleasure having you in the lab the last year and Gráinne keep being your crazy self! I've really enjoyed having yous in the lab! And to our newest addition to the lab, it's been a pleasure meeting you Liam and I have no doubt you'll do great

things. Nic, thank you so much for always being there for me and Mr Gaucho. Kate you are my angel and my saving grace. Our co-dependence has become a serious problem, but I would not have it any other way. Jorge, estoy tan agradecida de haberte tenido como amigo durante el doctorado. Siempre estuviste dispuesto a ayudar, y siempre sentí que podía confiar en ti. Muchas gracias por todo tu apoyo.

Of course, half the battle is fought at home, and I could not have asked for a more supportive family. Annette, Jean, Charlie, Gran and John, thank you for being there for us , no matter the time of day. Anna and Philip you are both my inspiration. Thank you for always giving me a reason to smile and for holding me up, even on the hard days. I appreciate you both beyond words. Lee, not only did you get me through college but you got me through this PhD. You have always been there by my side and I could not have asked for a more supportive and caring partner. Your ambition and passion in your own work helps keep my spark burning even when the tough days threaten to blow it out. And of course I owe a huge thank you to Mr Gauch, who without words has been always been there to comfort or provide laughs.

Mum and Dad, I owe everything I am to you. It is impossible to sum up into words how appreciative I am for everything you have ever done for me and for giving me every opportunity to pursue my passion. Thank you for giving me your determination, and even when your physical presence is no longer with us, your strength permeates in everything we do.

Abbreviations:

Abbreviation	
2-DG	2-Deoxy-D-Glucose
4E-BP1	Eukaryotic initiation factor 4E binding protein 1
ACL	Ammonium Chloride
AIM-2	absent in melanoma 2
AMH	Anti-Mullerian hormone
AMPK	AMP-activated protein kinase
AOI	Acute onset ischemia
APC	Antigen presenting cell
APS	Ammonium Persulfate
ATP	Adenosine tri-phosphate
B-regs	Regulatory B-cells
Baft3	Basic Leucine Zipper ATF-Like Transcription Factor 3
BCG	Bacillus Calmette–Guérin
BLG	Deaminated gliadin peptide and β-lactoglobulin
BMDM	Bone marrow derived macrophages
BMDWB	Bone marrow derived white blood cells
BMP	Bone morphogenetic protein
Brg1	Brahma-related gene 1
BSA	Bovine Serum Albumin
BTK	Bruton's tyrosine kinase
BVEGF	Vascular endothelial growth factors
c-type lectin domains	CTLD's
CAMP	Cyclic adenosine monophosphate
CAPS	Cryopyrin-Associated Periodic Syndrome
CD	Cluster of differentiation
cDC	Conventional DCs
CFSE	Carboxyfluorescein Diacetate Succinimidyl Ester
cGAS	Cyclic GMP-AMP synthase
cit-FLG	Citrullinated-filaggrin
CLO	Central lymphoid organs
cMOP	committed monocyte progenitor
CMP	Common myeloid progenitor
CNS	Central nervous system
CNS2	Conserved non-coding DNA sequence 2
cT-reg	Central T-reg
CTLA4	Cytotoxic T lymphocyte-associated antigen 4
CVD	Cardiovascular diseases
DAI	DNA-dependent activator of IFN-regulatory

DAMP	damage associated molecular markers
DC	Dendritic cell
DEPTOR	DEP domain–containing mTOR-interacting protein
DMEM	Dulbecco's Modified Eagle Medium
DNA	Deoxynucleic acid
dNTP	Deoxynucleotide triphosphate
DRE	Distal regulatory elements
EAE	Experimental auto-immune encephalomyelitis
ECAR	Extracellular acidification rate
EDTA	Ethylenediaminetetraacetic acid
eIF4e	Eukaryotic initiation factor 4E
ELISA	Enzyme linked immuno-sorbent assay
EMT	Epithelial to mesenchymal transition
eT-reg	Effector T-reg
Fab	Fragment antigen binding
$FADH_2$	Flavin adenine dinucleotide
FAS	Fatty acid synthesis
FBGC	Foreign body giant cells
FBS	Foetal calf serum
FDA	Food and Drug Authority
FGF	Fibroblast growth factor
FLNa-Ig21	Immunoglobin repeat 21 of filamin A
Flt3L	Fms-like tyrosine kinase 3 ligand
FMO	Fluorescent Minus One
FOA	Fatty acid oxidation
FoxP3	Forkhead box P3
FRAP	Fluorescent Recovery After Photobleaching
GARP	Glycoprotein A repetitions predominant
GCPRs	G-coupled receptor proteins
GDF	Growth and differentiation factors
GITR	Glucocorticoid-induced tumour necrosis factor receptor
GM-CSF	Granulocyte macrophage colony-stimulating factor
GMP	granulocyte-macrophage progenitor
GS	Gly/Ser-rich region
GSK3	Glycogen synthase kinase 3
HGF	Hepatocyte growth factor
HIF-1α	Hypoxia-inducible factor 1-alpha
HKG	House keeping genes
HRP	Horseradish peroxidase
HSC	Hematopoietic stem cells
HSP	Heat shock proteins
i.m	Intramuscular

i.v	Intravenous
i.p	Intraperitoneal
IAC	Integrin activation complexes
IBD	Inflammatory bowel disease
ICOS	Inducible costimulator
IFI16	Interferon-gamma inducible protein 16
IFN_{γ}	Interferon Gamma
Ig	Immunoglobulin
IGF	Insulin growth factors
IL	Interleukin
IL-1Ra	IL-1 receptor antagonist
ILC	Innate lymphoid cells
IPLs	Immune gene-priming lncRNA's
IRF	Interferon regulatory factor
iRNA	Inhibiting RNAs
ITE	Aryl hydrocarbon receptor ligand
ITL	Inhibitory Ig-like transcripts
JMJD3	Jumonji domain-containing protein-3
Klf4	Krüppel-like factor (
L-Glut	L-Glutamine
LAG-3	Lymphocyte activation gene 3
LAL	Limulus Lysate
LAP	Latency associated protein
LDL	Low density lipoprotein
LDP2	Laboratory of genetics and physiology 2
LFA-1	lymphocyte associated antigen 1
LN	Lymph node
lncRNA	Long non-coding RNAs
LPS	Lipopolysaccharide
Lti	Lymphoid tissue inducer
M-CSF	Macrophage-colony stimulating factor
MAL	MyD88-adaptor like
MAPK	Mitogen activated protein kinase
MCP1	Monocyte chemoattractant protein-1
MCSF	Macrophage colony stimulating factor
MDA4	Melanoma differentiation associated protein 5
MDP	Common macrophage and DC progenitor
MFI	Mean fluorescence intensity
MHC	Major histocompatibility complex
mLST8	Mammalian lethal with Sec13 protein 8
MOG	Myelin oligodendrocyte glycoprotein
MPP	Myelin proteolipid protein (PLP)

MRSA	Methicillin-resistant *S. aureus*
MS	Multiple Sclerosis
mT-regs	Memory T-regs
Mtb	M*ycobacterium tuberculosis*
mTor	Major target of rapamycin
Myc	Myelocytomatosis oncogene
nAb	Neutralising antibody
NADH	Nicotinamide adenine dinucleotide
NADPH	Nicotinamide adenine dinucleotide phosphate
NFAT	Nuclear factor of activated T cells
NFκB	Nuclear factor kappa-light-chain-enhancer of activated B cells
NK	Natural Killer cell
NLR	Nod Like receptor
NLRA	Acidic-transactivating domain NLRs
NLRB	BIR-containing NLRs
NLRC	CARD-containing NLR's
NLRP	PYRIN-containing NLRs
nm	Nanometer
NO	Nitrous oxide
Nrf2	Nuclear factor-erythroid factor 2
OCR	Oxygen consumption rate
OD	Optical density
ODN	Oligodeoxynucleotides
OPD	o-phenylenediamine dihydrochloride
OVA	Ovalbumin
OxPhos	Oxidative phosphorylation
P/S	Penicillin and Streptomycin
PAMP	Pathogen associated molecular pattern
PBS	Phosphate buffered saline
PC	Phosphatidylcholine
pDC	Plasmacytoid DCs
PDGF	Platelet derived growth factor
PDK1	3-phosphoinositide-dependent kinase
PE	Phosphatidylethanolamine
PGC-1β	PPARγ- coactivator-1beta
PI	Propidium Iodide
PI3K	Phosphoinositide 3-kinases
PIKK	Phosphoinositide 3-kinase related kinases
PLD2	Phospholipase D2
PLGA	poly(lactic-co-glycolic acid)
PLO	Peripheral lymphoid organs

PMA	Phorbol-12-myristate-13-acetate
PPARγ	Peroxisome proliferator-activated receptor-γ
PRAS40	Proline-rich Akt substrate 40 kDa
PRR	Pathogen recognition receptor
PS	Phosphatidylserine
pT-reg	Peripheral T-regs
PUFA	Polyunsaturated fatty acids
RA	Rheumatoid Arthritis
RAG	Recombinase activating gene
RAP2	Ras-related GTPases
RAPTOR	Regulatory-associated protein of mTOR
RAS	Receptor-linked tyrosine kinase
Rheb	Ras homolog enriched in brain
RICTOR	RAPTOR-independent companion of TOR
RIG	Retinoic acid-inducible gene
RLR	RIG like receptors
RNA	Ribonucleic acid
RNS	Reactive nitrogen species
ROI	Region of interest
RORγt	RAR-related orphan receptor-γ
ROS	Reactive oxygen species
RPMI	Roswell Park Memorial Institute 1640
RT	Room temperature
s.c	Subcutaneous
S6K1	p70 ribosomal S6 kinase 1
sAG	S-antigen protein
SARM	Sterile α- and armadillo-motif- containing protein
SDS	Sodium dodecyl sulfate
SHARPIN	Shank-associated RH domain-interacting protein
SIRPα	Signal regulatory protein α
SLE	Systemic lupus erythematosus
SM	Sphingomyelin
SREBP1	Sterol regulatory element binding protein 1
sRNA	Silencing RNAs
STAT	Signal transducer and activator of transcription
STING	Stimulator of IFN genes
SWI/SNF	Switch/sucrose non-fermentable
Syk	Spleen tyrosine kinase
T-cov	Conventional T-cell
T-eff	Effector T-cell
T-mem	Memory T-cell
T-reg	Regulatory T-cell

Tr1	Type 1 Regulatory T-cell
Tr2	Type 2 Regulatory T-cell
T1D	Type-1 Diabetes
T2D	Type 2 Diabetes
tAPCs	Thymic antigen-presenting cell
TAZ	Transcriptional coactivator with PDZ-binding motif.
TBS	Tris-buffered saline
TCA	Tricarboxylic acid
TCR	T-cell receptor
TGFBR	TGFβ receptor
TGFRB	TGFβ receptor dimer
TGFβ	Transforming growth factor β
TIR	Toll/Interleukin 1 receptor
TLR	Toll like receptor
TMB	5,5′-Tetramethylbenzidine
TNFα	Tumour necrosis factor α
TRAM	TRIF related adaptor molecule
TRIFF	TIR-domain containing adaptor inducing IFN-β
TRPV	Transient receptor potential vanilloid
TSC	Tuberous sclerosis complex
TSDR	Treg-specific de-methylated region
TSP1	Thrombospondin1
tT-reg	Thymus derived T-reg
VIP	Vasoactive intestinal peptide
Vit A	Vitamin A
VitD3	Vitamin D3
YAP	Yes-associated protein-1
Zeb2	Zinc-finger E-box binding homeobox 2
µm	Micrometre

List of Figures

Chapter 1- Introduction:

Chapter 2- Materials and methods

Chapter 3- Results Part I

Chapter 4- Results Part II

Figure 4.10.1 Proposed mechanism of 2 μm PLGA particle induced T-reg expansion

Chapter 5- Discussion

Figure 5.1.A Hypothesised schematic representation of potential mechanism of action for the enhancement of TGFβ expression and signalling from BMDCs by 2 μm PLGA particles.
Figure 5.1 B. Hypothesised schematic representation of potential mechanism of action linking mechanical stress imposed by 0.5-2 μm PLGA particles on cell membrane and mTOR activation.

List of Tables

Chapter 1- Introduction

Chapter 2- Materials and Methods

Table 2.2.9 B. rt qPCR program for Comparative △CT carried out on Applied Biosystems 7500 Fast system.

Table 2.2.12 A Cell density of BMDMs and THP-1 macrophages for seahorse analysis

TABLE OF CONTENT

Chapter Ⅰ; Introduction

1.1 Innate immune system

Innate immune system is the fundamental branch of the immune system, with almost all organisms and plants possessing a non-specific surveillance mechanism to detect self from non-self [1]. Despite its primitive origin, the innate immune system is highly complex, encompassing a network of cells and molecules which are not only important in early immune responses but in the development of adaptive responses and innate immune memory [2]. Innate immune cells are the first responders to a site of infection or damage. They promote inflammation in order to initiate the clearance of pathogens or debris and recruit additional innate immune cells to the area. Innate immunity is directed by myeloid cells including; monocytes, neutrophils, macrophages, dendritic cells (DCs), basophils and eosinophils. Innate lymphoid cell's such as natural killer cells (NKs), lymphoid tissue inducer cells (LTis), and 3 helper-like innate lymphoid cell subsets, group 1,2 and 3 (ILC1/2/3), are also considered part of the innate immune branch but have greater similarities to adaptive lymphocytes.

When a barrier such as the skin or mucosa is breached, following an injury or during infection, a series of "alarms" are activated which initiate action from the innate immune system. Tissue damage incurs the release of damage associated molecular patterns (DAMPs) such as IL-33 and IL-1α from lysed cells and cytoplasmic calcium, reactive oxygen species (ROSs) and polyunsaturated fatty acids (PUFAs) from cells under stress [3],[4],[5]. This is accompanied by platelet aggregation and the release of histamine which creates a chemotactic gradient, recruiting early immune responders and dilating blood vessels to allow cell extravasation [6]. Neutrophils are the first cells to arrive. Pathogen and damage recognition receptors (discussed in depth in section 1.3.1), detect DAMPs and pathogen associated molecular patterns (PAMPs) which initiate downstream signalling pathways resulting in the release of inflammatory cytokines and chemoattractants [7,8]. Monocytes arrive shortly after in response to the release of monocyte chemoattractant protein-1 (MCP-1) , extracellular matrix proteins, interferon-γ (IFN_γ) and transforming growth factor beta (TGFβ). Whilst monocytes themselves phagocytose debris, they differentiate to DCs and macrophages which are longer-lived and better adapted to phagocytosis and antigen presentation [9].

Macrophages carry out a large proportion of pathogen containment through phagocytosis, release of bactericidal ROS and degradative enzymes which break down debris. They also secrete cytokines including IL-6, tumour necrosis factor α (TNFα), and IL-1β which augment the inflammatory environment required to continue recruiting innate immune cells [10]. DCs create a link between the innate and adaptive immune branch, playing a crucial role in sampling antigens and migrating to secondary lymphoid organs, where they can activate T-cells [11]. In the following sections, the role of macrophage and DC will be discussed in more depth.

1.1.1 Macrophages

Macrophages are a highly heterogenous population of cells which are indispensable for maintaining tissue homeostasis in health and disease [12]. Whilst they are most often recognised for their role in anti-microbial defence through phagocytosis of debris and pathogens, they are also critical for tissue regeneration and clearance of dead cells during cell-turnover. The generation of macrophages is established early in development but they are also regenerated continuously from myeloid progenitors in the bone marrow.

Resident macrophages are first generated in the embryonic yolk sac, where they are seeded at various tissues sites early in development. The generation of tissue-specific macrophages is then carried out by haematopoiesis within foetal liver later in development [13]. These macrophages are highly specialised to meet the functional requirements of specific tissues types, for example microglia in the central nervous system (CNS), alveolar macrophages in the lung and Kupffer cells in the liver. Depending on the homeostatic cues within a given tissue, tissue-resident macrophages are capable of self-renewal. However the contribution of tissue resident and monocyte derived macrophages amongst the various tissue types differs. For instance microglia, epidermal and alveolar macrophages have high rates of self-renewal and are not reliant on the generation of monocyte derived macrophages [14,12].

Monocytes stem from bone marrow hematopoietic stem cells (HSCs) which undergo a series of differentiation steps resulting in the generation of semi-committed progenitors which can give rise to macrophages and DCs [15,16] . Monocytes circulate through the blood, within the bone marrow and secondary

lymphoid organs such as the spleen until they are recruited to a site of infection or damage. However, they have a relatively short life-span of about 24-48 hours if they do not receive sufficient differentiation signals to survive. Differentiation is mediated by macrophage colony stimulating factor (M-CSF) or granulocyte macrophage colony-stimulating factor (GM-CSF) under inflammatory settings [13]. Macrophages are highly heterogenous and can take on a multitude of activation states depending on the environment. The original classification of macrophages describes two polar phenotypes; the classically activated M1 macrophages, or the alternatively activated M2 macrophage. Whilst this over-simplified depiction of macrophage polarisation is commonly used, it is important to note that macrophage phenotypes are far more diverse, with M2 macrophages split into a M2 a,b,c and d phenotype and with activated macrophages being able to adopt properties of more than one phenotype [17,9,13]. The abundance of macrophage phenotypes is, therefore, better represented as a colour wheel, rather than a linear spectrum (Figure 1.1.2A) [18].

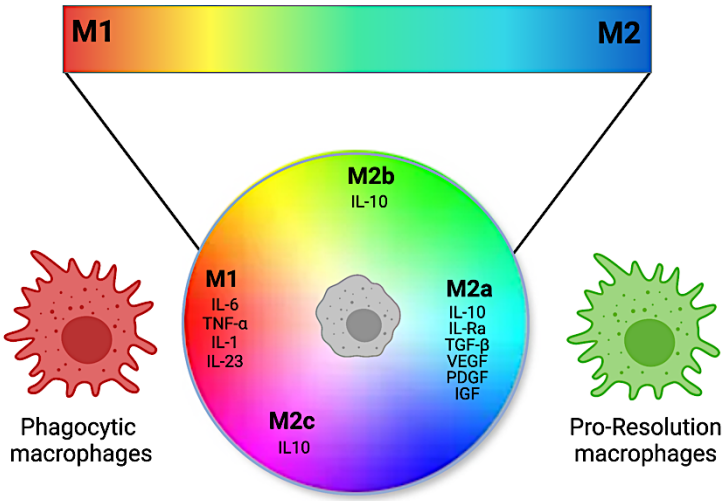

Figure 1.1.2 A Diversity of macrophage phenotypes. Macrophage activation states are commonly described as either a pro-inflammatory classically activated M1 or anti-inflammatory, alternatively activated M2 macrophages. This theory describes a linear spectrum of activation with two polar opposites. The reality of macrophage activation is more complex, with macrophages taking on less defined phenotypes depending on the environment. In an attempt to define the diversity, M1, M2a, M2b and M2c macrophages have been described, with some taking on more phagocytic capacity and others having a pro-resolution phenotype. The analogy of a colour wheel depicts the range of macrophage phenotypes more accurately than a linear spectrum.

M1-like macrophages are activated upon encountering PAMPs and DAMPs as well as pro-inflammatory cytokines, particularly TNFα and IFNγ. They are highly phagocytic and promote an inflammatory environment by secreting pro-inflammatory mediators such as IL-1, IL-6, TNFα and IL-23 as well as growth factors; Fibroblast growth factor (FGF) and platelet derived growth factor (PDGF), which recruit further monocytes, neutrophils, macrophages as well as mast cells and fibroblasts [9]. They are also adept at pathogen killing by producing bactericidal ROS and reactive nitrogen species (RNS) and break down debris and damaged tissue through the production of degradative enzymes [19]. They are, therefore, an indispensable population to combat infection, primarily bacterial and fungal, but can also help mitigate spreading of viral infections.

M2-like macrophages, are instead, anti-inflammatory and pro-regenerative. They are activated by the cytokines IL-13, IL-4 and IL-10 and in response produce immunosuppressive IL-10, IL-1 receptor antagonist (IL-1Ra) as well as growth factors; TGFβ, vascular endothelial growth factors (VEGF), PDGF and insulin growth factors (IGF) [19]. These responses are crucial for supressing excessive inflammation, which can cause further tissue damage, and for initiating tissue repair and regeneration mechanisms [20].

1.1.2 Dendritic cells

Ralph Steinman and Zanvil Cohn first described Dendritic cells (DCs) in 1973, when a unique cell population which differed from macrophages was discovered within the population of cell from a mouse spleen. Steinman described this population as extensively branched, mitochondria-rich and motile. Most importantly, they later identified this cell population to be highly adept at activating naïve T-cells [11]. These findings resulted in a surge of interest to characterise DCs and understand the mechanisms behind their capacity to activate the adaptive immune branch.

Exploration into the phenotypic characteristics of DCs, revealed that DCs are in fact a highly heterogenous population. To date, the DCs have been categorised as either being monocyte-derived or derived from the common dendritic progenitor (CDP). Within the CDP derived population, a subset of distinct cells were

characterised as plasmacytoid, Langerhans cells or conventional DCs (cDCs) [21],[22]. Plasmacytoid cells are a unique subset of DCs, which have a rounded morphology resembling plasma cells and provide anti-viral protection through high production of IFN α/β. cDCs, however, are recognised as the major antigen-presenting population, which are localised as at lymph nodes as LN-resident cDCs, or as migratory cDCs. [23,24]. . Migratory cDC patrol the periphery for pathogens or foreign entities, whilst LN-resident cDCs encounter antigens within the lymphatic system or receive antigens from APCs which have migrated to the lymph nodes [25],[26]. Finally, the specialised subset of DCs which reside in the epidermis and some mucosal tissues have been further characterised as Langerhans cells.

DCs express a number of pathogen recognition receptors (PRRs) including TLRs, C-type lectins, nod-like receptors (NLR) and rig-like receptors (RLR) which specifically recognise foreign antigens, promoting pathogen internalisation, antigen processing and maturation. DC maturation occurs as a result of a series of signalling events downstream of PRR which result in changes in the transcriptional expression of co-stimulatory cell surface markers and cytokines (Table 1.3.1A). Activation of PAMPs or DAMPs as well as the inflammatory environment in which the DC encounters the antigen defines their maturation state. These maturation markers are vital in providing the appropriate signals to activate specialised T-cell subsets [27], [28]. DCs also process and present a fraction of the antigen on specialised major histocompatibility complex (MHC) proteins. The MHC class commitment is dependent on the source and intracellular processing mechanism of the antigen.

Based on their propensity to activate $CD4^+$ or $CD8^+$ T-cells, cDCs are additionally classified as either cDC1 or cDC2 [25]. cDC1s tend to capture endogenous or viral antigens and process these antigens for presentation via MHC class I. As such, cDC1s are primarily involved in cross-presentation with $CD8^+$ T-cells, making them paramount in anti-viral and anti-cancer immunity [29]. cDC2s on the other hand, often internalise exogenous antigens which are processed and presented on MHC class II complexes[30]. cDC2s, are therefore, mainly involved in activating $CD4^+$ T-cells and the subsequent generation of humoral immunity [30]. An overview of our current understanding of these subsets are summarised in Table 1.1.3A.

cDC subset	Defining transcription factors	Defining surface marker expression	cDC cytokine secretion	cDC Function
cDC1	Basic Leucine Zipper ATF-Like Transcription Factor 3 (Baft3), interferon regulatory factor 8 (IRF8) and Id2 [25,24, 31].	CD8α (in mice and CD141 in humans), Chemokine XC receptor 1 (XCR1), CD103, DEC205, toll like receptor 3 (TLR3) [24,25].	IFNα and β, IL-12, IL-6 and TNFα [25,]	Primarily present endogenous or viral antigens to activate $CD8^+$ T-cells which provide protection against viruses and cancer.
cDC2	IRF4, IRF2, Ikaros, Krüppel-like factor (Klf4) and Zinc finger E-box-binding homeobox 2 (Zeb2) [31,30].	CD11b, Signal regulatory protein α (SIRPα) DC immunoreceptor 2 (DCIR2) [25, 31.]	Produce cytokines which promote T-helper 2 responses and B-cell activation such as IL-12, IL-6,TNFα, IL-4 and IL1β, TGFβ [30].	Primarily activate $CD4^+$ T-cells which provide protection against fungal and bacterial pathogens [30,27].

Table 1.1.3 A. Overview of functionally specialised cDC subsets and their defining characteristics.

The maintenance of immunological tolerance to self and innocuous antigens is modulated by cDCs which retain an immature or semi-mature activation state in response to antigen sampling under homeostatic or immunosuppressive environments. Immature or semi-mature DCs, are referred to as tolerogenic DC (tolDCs) and are defined by low expression of co-stimulatory CD80/86 and CD40. Furthermore, tolDCs express co-inhibitory molecules B and T lymphocyte associated/attenuator (BTLA), T-cell immunoglobulin mucin-3 (TIM-3), and produce of immunosuppressive IL-10 and TGFβ [32]. Together, the weak co-stimulatory environment and co-inhibitory molecules provide T-cells with signals which promote apoptosis, anergy or differentiation towards a regulatory T-cell (T-reg) phenotype which will be discussed in detail in section 1.2.2.

1.1.3 Innate immune memory

Immunological memory in vertebrates was once considered to be a trait exclusive to the adaptive immune system. However, evidence demonstrates that invertebrates and plants, which only possess an innate immune system, are able to respond to reinfection with a degree of "memory" [33,34]. Seminal work published by Netea *et al*, demonstrated that the innate immune system, is capable of mounting an augmented response following a secondary challenge, even after

returning to a resting state [35,36]. This was demonstrated in mice which are incapable of producing mature B and T-cells, such as the congenitally athymic CD-1 mice and $Rag^{-/-}$ mice. Despite lacking protection from the adaptive immune branch, these mice displayed enhanced protection from lethal candidiasis when pre-infected with a non-lethal dose of *C. albicans* 7 days earlier. This protection was provided by an increase in monocyte-derived pro-inflammatory cytokines, which was not mounted by the monocytes of "naïve" mice [37,38]. In another study, the adoptive transfer of macrophages from mice exposed to live *Staphylococcus aureus,* into naïve mice, conferred protection against methicillin-resistant *S. aureus* (MRSA) challenge compared to naïve mice which did not receive primed macrophages [39]. This paradigm has been termed innate memory, or innate training and has been demonstrated in monocytes, macrophages and NK cells.

The ability of certain stimuli to re-programme innate immune cells to establish a form of memory is dependent on epigenetic modifications which facilitate the access of transcriptional machinery to inflammatory genes. In addition, the metabolism of trained innate immune cells is altered to meet the increased requirements for ATP and the building blocks to increase the production cytokines and inflammatory mediators during re-activation.

Early work postulated that the timescale for innate immune memory would persist only as long as the trained cells survived. However, studies have demonstrated that innate immune training can imprint on bone marrow hematopoietic stem and progenitor cells conferring protection for weeks or even months. For instance, a cohort study published in 2015 revealed that vaccination of newborns with Bacille Calmette–Guérin (BCG) was capable of conferring non-specific protection for years compared to non-vaccinated infants [40]. Long-term protection is hypothesised to be mediated by epigenetic [41] and metabolic [42] modifications in hematopoietic stem and progenitor cells in the bone marrow [43]. Furthermore, innate training with β-glucan and BCG was shown to enhance myelopoiesis and expansion of hematopoietic stem and progenitor cells in mice [42,41,43].

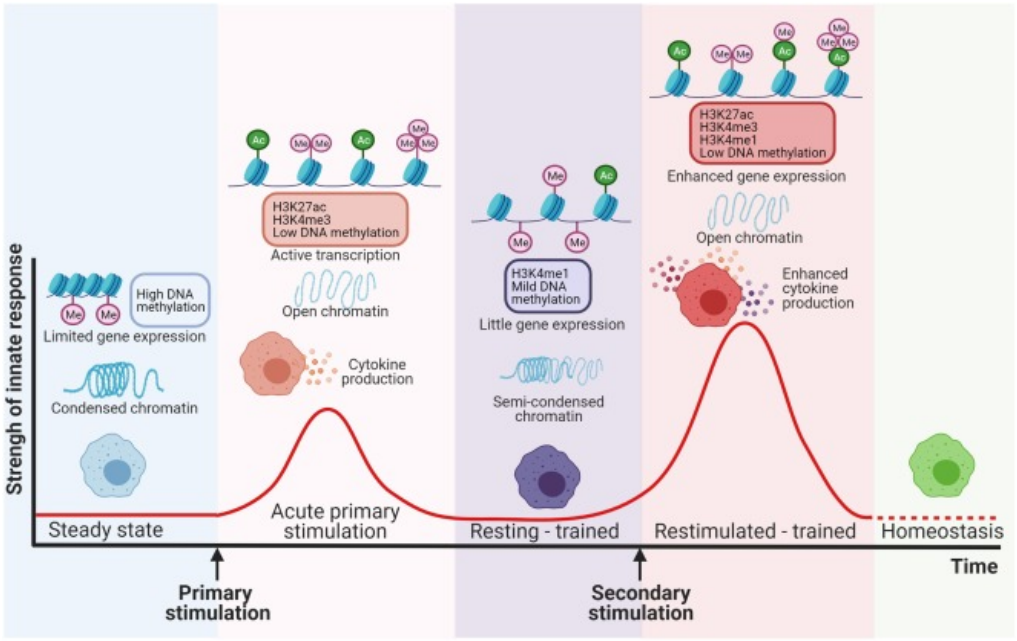

Figure 1.1.4 A. Schematic of innate immune training. The paradigm of innate immune training was coined by Netea *et al* and describes the ability of innate immune cells such as macrophages and monocytes to retain memory to a primary insult. Epigenetic alterations such as the trimethylation of H3K4 and acetylation of H3K27 occur during an acute primary stimulation and are retained even after the cell returns to a resting state. These alterations mark certain loci as "open" providing access for DNA transcription of genes. Upon a secondary stimulus, trained cells are capable of mounting a comparable or greater response, due to the enhanced accessibility to functional genes. Figure taken from Muñoz-Wolf, N. & Lavelle, E. C. Promotion of trained innate immunity by nanoparticles. *Semin. Immunol.* **56**, (2021).

Epigenetic regulation of innate immune memory

The molecular basis of innate immune memory is established by epigenetic modifications of chromatin and non-coding RNAs, which upon a secondary insult, facilitate rapid gene expression [44]. Epigenetic modifications of genes permits cells to differ phenotypically despite having the same genotype [45]. DNA is assembled into chromatin, a highly organised structure composed of DNA wrapped around histones. Each histone octamer is composed of four core proteins; H2A, H2B, H3 and H4, with 147 DNA base pairs wrapping around each histone. The compactness of chromatin determines the accessibility of the transcription machinery necessary for gene expression. The term euchromatin is given to transcriptionally active chromatin and inactive chromatin is termed, heterochromatin [46]. Post-translation modifications of histones such as methylation,

acetylation, phosphorylation and ubiquitylation as well as DNA methylation, control the remodelling of chromatin structures to alter the transcriptional state of given genes [47,48]. This is due to the interference created by these functional groups on the electrostatic tension between histones and the DNA [44]. Nucleosome and chromatin remodelling enzymes are responsible for carrying out histone and DNA modifications and usually modify loci near promoter regions or distal regulatory elements (DREs) of a particular gene [49].

During homeostasis, inflammatory genes are commonly maintained within heterochromatin. However, in response to inflammatory signalling, transcription factors such as nuclear factor kappa-light-chain-enhancer of activated B cells (NFκB), AP-1, IRFs and signal transducers and activators of transcription (STAT) family members, recruitment chromatin and nucleosome remodelling enzymes which modify chromatin to increase the access of RNA polymerase II to promoter sequences of inflammatory genes [44]. The methylation and tri-methylation of the fourth lysine on histone H3 (H3K4me) and acetylation of the 27^{th} lysine on H3 (H3K27) are common modifications found in trained innate immune cells [50].

Metabolic regulation of innate immune memory

The metabolic rewiring of innate immune cells has also been identified as a hallmark required of innate training [51]. For a detailed discussion of immunometabolism in innate immune cells, refer to section 1.5. Shifts in the cells metabolism are required to support heightened cellular responses upon re-stimulation, but also to facilitate epigenetic modifications. For instance, many co-factors and substrates required for the regulation of chromatin modifying enzymes including; NAD^+, ATP, acetyl-CoA and S-Adenosylmethionine (SAM) are generated via metabolic pathways [52,53].

The importance of metabolic rewiring for innate training was demonstrated in studies looking at the metabolic shift in macrophages and monocytes trained with BCG. Acute exposure to BCG re-directed the cells metabolism to favour glycolysis, which was dependent upon signalling via Hypoxia-inducible factor 1-alpha (HIF-1α) and major target of rapamycin (mTOR). This metabolic shift was accompanied by epigenetic modifications; He3K4Me3 and He3K27ac1. However, these epigenetic changes were not observed when glycolysis was inhibited or in HIF-1α deficient monocytes [54].

The cholesterol synthesis pathway has also implicated as a necessary metabolic program for innate training of monocytes by BCG as well as oxidised low-density lipoprotein (oxLDL). The metabolic intermediate of the cholesterol synthesis pathway, mevalonate, was shown to signal via IGF-1 receptor, resulting in downstream mTOR activation and histone modifications linked with innate training [55].

Various tricarboxylic acid (TCA) cycle intermediates such as; α-ketoglutarate and itaconate are crucial for the establishment of tolerant macrophage re-programming [56,57,58]. For instance, α- Ketoglutarate was found promote the function of the histone demethylase enzyme; Jumonji domain-containing protein-3 (JMJD3) which removes methyl groups on He3K27me3, a common silencing modification at pro-inflammatory gene loci [56,57]. Itaconate-synthesis has been shown to be essential in the induction of LPS tolerance of myeloid cells through the nuclear factor-erythroid factor 2 (Nrf2) pathway [59].

Innate immune training by particles

There is a growing body of evidence indicating that the exposure to environmental particulate matter such as air borne pollutants or biomaterials can also train innate immune cells to have heightened responses when they encounter pathogens or an unrelated stimulus [44,60]. Given the rise in air borne pollutants and the increase in the ingestion of microplastics over the last century, it is likely that the re-programming of innate immune cells is contributory to the rise in the incidence of asthma, allergies and chronic inflammation [61]. Furthermore, it highlights the repercussions of the long term effect of biomaterials and their breakdown products [50]. For example graphene based biomaterials have been proposed as an ideal material for orthopaedic implants, due to their excellent mechanical properties. Work carried out in the Lavelle lab by Dr Filipa Lebre, demonstrated that whilst pristine graphene (pGR) did not induce inflammatory cytokines from BMDMs after 24 hours, there was a significant increase in the production TNF-α and IL-6 from pGr-trained BMDMs after being restimulated with several TLR agonists a week later [62].

Alum, a widely used vaccine adjuvant, was also investigated in the lab by Dr Aoife Gorman, for its ability to train innate immune cells. Interestingly, exposure of

BMDMs and human monocytes to alum resulted in heightened secretion of the anti-inflammatory cytokines, IL-10 and IL-1Ra, upon re-stimulation with TLR agonists [63]. This has implications in terms of vaccine effectiveness and may contribute to the inability of alum-containing vaccines to mount robust Th1 responses.

This work exemplifies the need to routinely investigate how immune cells could be trained by biomaterials and micro/nano particles as well as their potential break down products. This can reduce the risk of aberrant responses and can additionally help re-purpose materials which can promote desirable innate memory for novel applications.

1.2 Adaptive immune system

Unlike the innate immune system, which can mount potent and non-specific responses, adaptive immune cells can mount targeted antigen specific responses against a broad range of pathogens, including viral infections and malignancies. In addition, the adaptative immune branch provides long term, specific immunity to a challenge, by generating a pool of memory cells which can be deployed upon re-infection in order to provide fast and efficient pathogen clearance [1].

The adaptive immune system is made up of T and B lymphocytes. Early lymphocyte development occurs in central lymphoid organs (CLO) either within the bone marrow which generate B-cells, of in the thymus, which produces T-cells. T and B-cells can then proceed to migrate to peripheral lymphoid organs (PLO) such as the lymph nodes and spleen. B-cells continue to be generated in the bone marrow through the lifetime of the host, whilst thymic regeneration of T-cells slows down. During the early development of lymphocytes in the CLO, T and B-cells acquire antigen specificity on T-Cell receptors (TCR) and immunoglobulins. The process by which specific TCRs are generated and positively selected will be discussed in section 1.2.1.

T-cells

T-cells have been classified as either conventional α/β T-cells, or non-conventional γ/δ T-cells. Conventional T-cells develop in the thymus, and undergo a series of maturation steps resulting in the expression of either CD4 or CD8. These naïve $CD4^+$ or $CD8^+$ T-cells migrate from the thymus to the reside in secondary lymphoid organs but can also migrate within the lymphatic tissue to the periphery [1,64].

T-cells remain naïve until they encounter an APC presenting an antigen, which complements their own TCR. Through engagement of MHC-TCR, as well as binding of co-stimulatory molecule, the T-cell receives the signals to give rise to specialised T-cell subsets . In addition, the cytokines produced by DC are critical to determine lineage commitment. The cytokines required to give rise to different T-cell subsets is are summarised in Figure 1.2A. T-cells can also receive negative survival signals from APCs, commonly presenting self-antigens or innocuous antigens. These negative signals or lack of co-stimulation results in T-cell deletion, anergy or alternatively the generation of regulatory T-cells (T-regs) which will be discussed in detail in section 1.2.2.

During a period of infection and inflammation, T-eff cells undergo clonal expansion and migrate to the required tissue site, supplying a specialised army of lymphocytes which can specifically target a threat [65,66]. When the tissue has been cleared of the threat, there is a period of lymphocyte “contraction” where T-eff either undergo apoptosis or generate a pool of memory T-cells (T-mem) [67]. T-mem maintain long term immunity, allowing a rapid and targeted response upon re-infection[1].

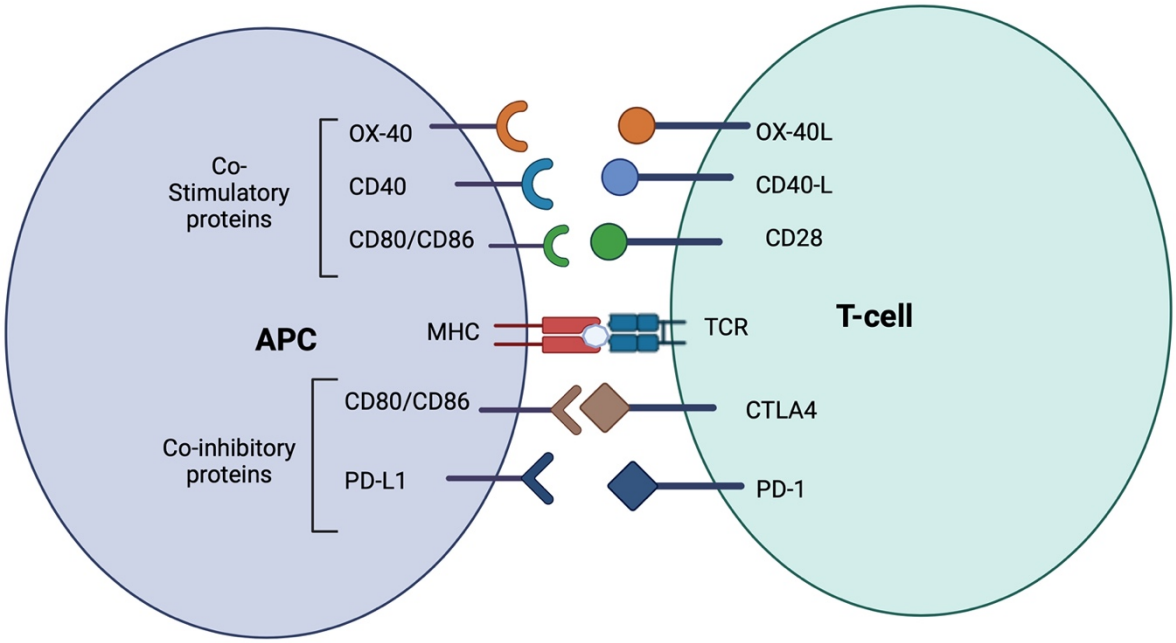

Figure 1.2A Co-stimulatory and co-inhibitory molecules presented by APCs to T-cells during antigen presentation. Co-stimulatory molecules OX-40, CD40 and CD80/CD86 (also known as B7) promote T-cell activation whilst co-inhibitory molecules; PD-1 and CD80/DC86 when binding CTLA-4 results in T-cell anergy or death.

T-cell subset	Required co-stimulatory cytokines	Transcription factors	Signature cytokines produced by T-cell	Function	References
Th1/Tc1	**IL-12,** IL-2*	T-**bet** Eomes * STAT4*	I**FNγ**	Provides protection against intracellular bacteria and viruses as well as cancer.	67, 68, 69
Th2/Tc2	**IL-4** and IL-2	**GATA-3** STAT6*	IL10 **IL-4, IL-5 and IL-13**	Provides protection against extracellular bacteria and parasites. Also involved in the development of allergies.	68, 69
Th17/Tc17	**IL-6, TGFβ, IL-21,** IL-23	**RORγT** **STAT3**	**IL-17A**	Provides mucosal defence and protection against extracellular bacteria. Also involved in pathogenesis of auto-immunity.	68, 69,
TfH	TGFβ, IL-23, IL-21, IL-12	**BCL-6** TCF-1* E1a* Runx3*	**IL-4, IL-21** IFNγ*	Help B-cell maturation and the development of humoral immunity.	68, 69, 70
T-reg	IL-10 and **TGFβ**	**FoxP3**	**IL-10, TGFβ**	Provides peripheral tolerance to self-antigens.	68, 71

Table 1.2A Overview of the co-stimulatory cytokines which promote the differentiation of CD4 and CD8 T-cell subsets and the functional characteristics of each subtype. CD4 T-cells are abbreviated as T-helper (Th) cells, and CD8 T-cells are abbreviated as T-Cytotoxic (Tc). The cytokines which are released by DCs during antigen presentation, provide signals which promote the transcriptional regulation of factors required to establish T-cell subsets. Each subset can carry out protection against diverse pathogens, which is supported by the cytokines they produce. For reference; Bold is used for factors relevant to both CD4/CD8 cells and those which only apply to CD8 T-cells only are indicated by asterisk (*).

B-cells

To further support the function of T-cells, activated B-cells pump out antigen specific immunoglobulin (Ig) proteins known as antibodies. Antigen-specific antibodies play a critical role in neutralising specific pathogens or toxins through opsonisation, facilitating enhanced phagocytosis, preventing their pathogenic function and activating the complement system which can directly lyse bacteria.

IgM and IgD are low affinity antibodies, whilst IgG, IgA and IgE are have greater affinity and produced by B-cells activated in germinal centres [1,72]. In most cases, B-cells are activated with the help from TfH cells with a complementary antigen, however, in rare cases they can also be activated by antigens themselves, which usually results in lower affinity antibody production [1,64]. The generation of humoral responses is also critical in providing long-term protection from re-infection. When an infection has been resolved, a subset of surviving B-cells differentiate to become long lived memory B-cells, which divide slowly in germinal centres, or plasma cells which secrete long-lasting and high affinity antibodies. However, B-cells have been demonstrated to play additional roles other than providing humoral responses. For example, B-cells can differentiate to take on a regulatory B-cell (B-reg) immunosuppressive phenotype through secretion of IL-10, IL-35 and TGFβ [73,74].

1.2.1 Antigen specificity, clonal deletion, central tolerance

In the early development of T and B-cells, lymphocytes acquire unique TCRs which are tested prior to maturation in order to select TCRs which are likely to complement foreign antigens and remove those with high affinity for self-antigens. Somatic gene recombination of the TCR gene during early development of conventional $CD4^-/CD8^-$ cells in the thymus generates the immense repertoire of possible TCR specificities. TCRs consist of α and beta chains, each being made up of a variable (V) and constant (C) region interspaced by joining regions (J). The β chain also contains a diversity region (D). Since the C region is unchanged, gene recombination of V(D)J region occurs yielding an abundance of possible gene combinations which are then translated to provide the cell with a unique TCR[1,75]. Upon the generation of a TCR, cells become double positive for CD4 and CD8.

Clonal selection discriminates between useful and potentially harmful TCR (figure 1.2.1). T-cells are exposed to self-ligands on MHC complexes of thymic antigen-presenting cell (tAPCs) or medullary thymic epithelial cells (mTECs). Cells which have a moderate affinity to a ligand are positively selected, whilst cells with a strong affinity are negatively selected and either undergo apoptosis (clonal deletion) or the develop into thymic T-regs (tT-regs) progenitors [76,77]. Negative selection of TCRs which strongly complement a self-antigen is the basis for central tolerance

and preventing auto-immunity, however, as we will come to discuss in section 1.2.2 and 1.4.3, this system is not foolproof [78]. TCRs which have no binding affinity, are unable to survive unless they undergo another cycle of gene rearrangement to produce a TCR which has some affinity to a ligand [75,79]. In the final stages of T-cell maturation, the CD4 or CD8 lineage is established producing single positive CD4 or CD8 cells which either reside in the thymus or populate peripheral organs until they are activated by APCs [75].

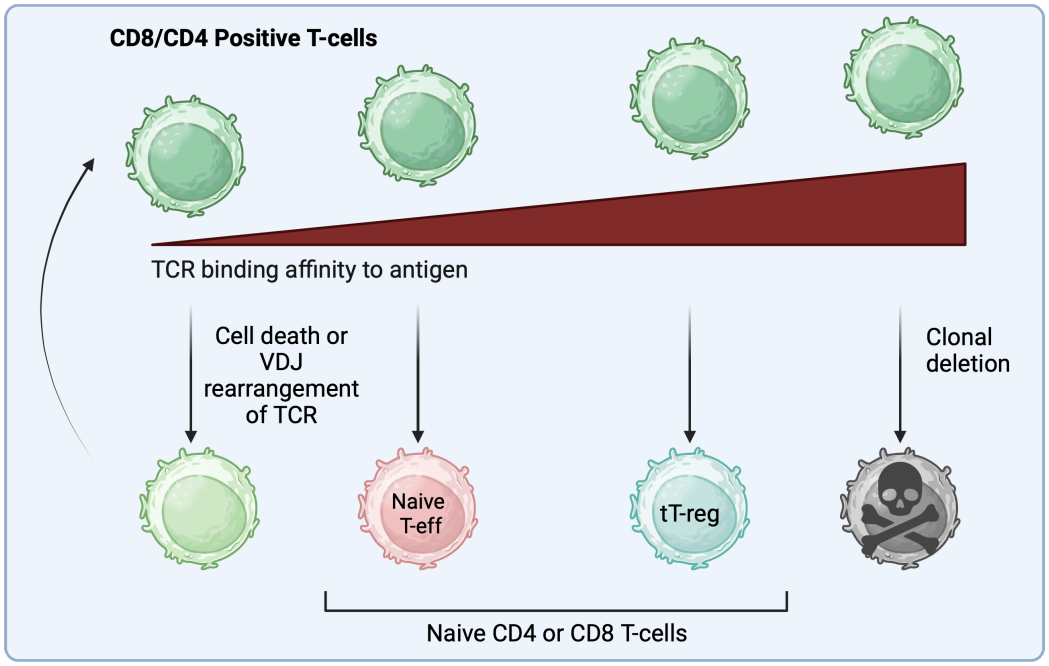

Figure 1.2.1A Fate of thymic CD4$^-$/CD8$^-$ T-cells during clonal selection is dependent on the affinity of the TCR with antigens presented by tAPCs or mTECs.

1.2.2 Regulatory T-cells and peripheral tolerance

Whilst the adaptive immune system is indispensable in providing protection from pathogens, cell damage and cancer the erroneous activation of auto-reactive T and B-cells can result in auto-immune pathology. Despite the establishment of central tolerance to remove T-cells with a TCR complementary to a self-antigen, errors during negative selection can occur. What's more, antigens can be wrongfully recognised as foreign for instance; antigens which are released during tissue or cartilage damage [80], antigens which have undergone post-translational modifications [81,82] food antigens or molecular mimetic antigens expressed by pathogens [83]. The peripheral dissemination of antigens which are restricted to

immune privileged organs such as the central nervous system (CNS), have also been shown to be a common target in auto-immunity [84]. Peripheral tolerance, therefore, provides additional lines of protection to mitigate the activation and function of auto-reactive T-cells.

In order for auto-reactive T-cells to become activated, a mature DC must present a self-antigen, together with sufficient co-stimulatory signals. However, the probability of DC maturation in response to self or innocuous antigens is low in the absence of PRR activation or inflammatory signalling. The lack of co-stimulatory molecules such as CD80/86 and T-cell polarising cytokines instead results in T-cell anergy, characterised by hypo-responsiveness and failure to respond to subsequent antigen-presentation even when the appropriate co-stimulatory signalling are presented. T-cells can also undergo deletion, whereby the cell with a TCR complementary to a self-antigen undergoes apoptotic cell death. This is mediated by the interaction between the Fas ligand with the Fas receptor (CD95) on T-cells [75, 85].

The generation of immunosuppressive T-regs provides protection from activated auto-reactive T-cells and is one of the most significant mechanisms providing self-tolerance. The dysfunction or deletion of T-regs results in spontaneous development in auto-immune diseases, which is exemplified in the T-reg deficient scurfy-mouse [86,87]. T-regs can either develop in the thymus early in life, or become activated in the periphery by DCs which provide co-inhibitory or tolerogenic signals during T-cell priming [1].

tT-regs are critical for the maintenance of tolerance, upregulating T-reg defining markers such as CD25, Forkhead box P3 (FoxP3), glucocorticoid-induced tumour necrosis factor receptor (GITR), OX40 and tumour necrosis factor receptor 2 (TNFR2) in response strong TCR binding to a self-antigen during clonal selection [76,77]. These T-reg progenitors reside in the thymus and only undergo maturation in response to IL-2 signalling, promoting the migration of mature tT-regs to the periphery [88]. The generation of peripheral T-regs (pTregs), from naïve CD4/CD8 T-cells in the periphery or secondary lymphoid organs arises from weak co-stimulatory signals provided by antigen-presenting DCs. These DCs have a tolerogenic phenotype characterised by low expression of MHC, CD80 and CD86 and the production of immunosuppressive IL-10 and TGFβ, which promotes the upregulation of T-reg defining markers such as FoxP3 and CD25. [1,75,85].

In addition to the differences in ontogeny between tT-regs and pT-regs, numerous T-reg subtypes have been identified, which further expands the diversity of T-regs. One of the main markers used to identify T-regs is the transcription FoxP3, a master regulatory of T-reg lineage identity [89,90] . However, there is still debate on the absolute necessity of FoxP3 for T-reg lineage commitment due to the identification of a subset of FoxP3$^-$ T-cells capable of supressing T-eff cells [91]. A significant portion of the research carried out on FoxP3 and T-reg generation has been carried out on lymphocytes from patients suffering from the auto-immune condition; immune dysregulation polyendocrinopathy enteropathy X-linked (IPEX) syndrome which is caused by missense or loss of function mutations on the FoxP3 gene. Severity of auto-immunity varies across IPEX patients, even amongst patients with the same FoxP3 mutation, indicating a multi-factorial regulation in the generation of immunosuppressive cell types. Single cell analysis of FoxP3 deficiency in humans and mice demonstrated that T-regs which lack FoxP3 can still retain the capacity to upregulate genes which are commonly regulated by FoxP3, and involved in providing immunosuppression such as *Il2ra*, *Tnfrsf4*, *Tnfrsf9*, *Tnfrsf18*, *Capg*, *Ikzf2* and *Ctla4* [92]. This endows FoxP3$^-$ T-regs with its immunosuppressive capacity, in spite of a partial or no FoxP3 transcription factor. Indeed, subsets of FoxP3$^-$ T-regs which demonstrate upregulation in alternative immunosuppressive responses have been described, including the functional Type 1 T-reg (Tr1) subset which produces high levels of IL-10 and TGFβ [93, 94] and tumour-infiltrating LAP$^+$/LAG-3$^+$/CD25$^+$ T-regs [95]. It has, therefore, been proposed that the only real marker of true T-reg phenotype is the capacity to supress T-eff responses rather than FoxP3 expression. That being said, various other markers have also been identified to help categorise T-reg subsets and have provide a deeper understanding of T-reg stability and function.

T-regs were first described in 1998 [96] based on the observation that CD25^{hi} T-cells were able to suppress T-eff responses. However, it is it is now understood that CD25 is the cognate receptor for IL-2 and is expressed on a variety of activated cells making it an unreliable T-reg specific marker. In fact, T-regs which do not express CD25 have been identified, specifically in the gut, lung and liver, [97,98] . It has also been demonstrated that T-regs can release surface bound CD25 as an immunosuppressive mechanism to quench IL-2 in highly inflammatory settings and then regain CD25 expression when homeostasis is restored [99,100].

Recently, expression of the transcription factor Helios was identified to be co-expressed in a subset of T-regs, particularly in those generated in the thymus. T-regs positive for Helios and FoxP3 were found to have considerably greater immunosuppressive capacity against T-eff cells and produced lower amounts of IL-2 [101]. In addition, Helios was found to enhance the stability of FoxP3 expression, preventing T-reg transition to T-eff phenotypes under highly inflammatory settings [102, 103, 104]. The stabilisation of FoxP3 by Helios co-expression is proposed to be as a result of a fully demethylated Treg-specific de-methylated region (TSDRs) which acts as a epigenetic stability marker for FoxP3 expression. In comparison, in Helios$^-$ FoxP3$^+$ cells, the TSDR is only 50% demethylated [105].

In addition, the glycoprotein A repetitions predominant (GARP) protein was found to be amplified on activated T-regs. GARP is transmembrane protein anchor which binds latent TGFβ to the surface of T-regs, exposing latent TGFβ for activation [106,107,108]. T-regs expressing GARP were found to supress T-eff cells more potently, secrete less IL-2 and promote higher levels of TGFβ and IL-10 [109,110,111]. Other surface bound receptors which have been demonstrated to be heightened on T-regs include cytotoxic T lymphocyte-associated antigen 4 (CTLA-4), inducible co-stimulator (ICOS), GITR and lymphocyte activation gene 3 (LAG-3).

A number of T-regs sub-types have been proposed, based on their ontogeny, relative expression of cell surface markers and transcription factors such as Helios and FoxP3. Table 1.2.2.A summarises the heterogeneity of the T-reg populations which have been identified in-vivo and their immunosuppressive significance in disease and homeostasis. In addition to these, T-regs which are generated *in-vitro* are referred to as inducible T-regs (iT-regs) and differ from those derived *in-vivo*. iTregs have been generated with diverse phenotypes depending on the culture conditions and signals received during differentiation [112].

T-reg subset	Function	Markers	Physiological location	Signals required to drive differentiation
Thymus Derived (tT-reg) Also referred to as natural T-regs (nT-regs)	Play an important role in preventing auto-immunity, particularly to self-antigens [76].	Increased expression of TNF receptor superfamily members such as GITR, OX40 and TNFR2, , CD25 and FOXP3. They can be distinguished from pT-regs based on the expression of neuropilin-1 and Helios [90], [105].	tT-reg progenitors are generated in the thymus but upon maturation can migrate to the periphery [77], [76].	tT-reg progenitors develop in the thymus during clonal selection in response to high affinity TCR binding to self-antigens presented by tAPCs or mTECs. Highly sensitive to IL-2 which is required for maturation and migration to the periphery [77], [76].
Central T-regs (cTregs) Also referred to as mature resting tT-regs	Mature tT-regs which reside in secondary lymphoid tissues. Precursors to eT-regs[113], [76].	Express high levels of lymphoid homing markers; S1PR1, CD62L, CCR7 as well as CD44, FoxP3, CD25, IL-7Rα [114].	Secondary lymphoid tissue.	tT-regs mature in response to IL-2 and migrate to the periphery[113].
Effector T-regs (eTreg) also reffered to as activated tT-regs or effector memory tT-regs.	Involved in maintenance of self-tolerance, immune homeostasis and tissue repair/ regeneration[115].	Can be $CD62L^{Lo}$,$CCR7^{Lo}$, $CD44^{Lo}$ or $CD62L^{Lo}$,$CCR7^{Lo}$, $CD44^{Hi}$. High expression ICOS and CTLA4 as well as chemokine receptors. Increased levels of transcription factors; IRF4, BATF and JunB. Secretion of IL-10 and TGFβ[116],[115], [117] .	Mainly Non-Lymphoid tissues, but have also found in secondary lymphoid tissues[115].	Antigen stimulation of cT-regs in the periphery[115],[117].
Peripheral T-regs (pT-reg)	Respond to both self and non-self-antigens, such as, environmental and food antigens. They also provide foetal tolerance.	Expression of FOXP3.	Peripheral organs and particularly abundant in mucosal tissue.	pT-regs develop from naïve conventional CD4+ T-cells (T-conv) receiving weak co-stimulatory signals and the IL-10, TGFβ or retinoic acid.
Type 1 T-regs (Tr1)	Restrain the effector function auto auto-reactive T-eff cells[118].	Express low CD25 and high LAG3 and CD49b but no FOXP3. Produce high levels of IL-10 and IFN_{γ}[118].	Lymphoid and non-lymphoid tissue [118].	Activated in the periphery by immature DCs which provide high levels of IL-10 [119].
Type 2 T-regs (Tr2)	Tolerance within tumour micro-environment (TME) [95], suppression of allergic inflammation and secrete IL-8, IL-9, IL-10, IFN_{γ}, TGFβ [120].	Express low CD25, CTLA4, GITR and high LAP, CD69 and CD49b but no FOXP3. Produce high levels of TGFβ [95].	TME, lung and blood [95],[120],[121].	In-vitro generation of Tr2s requires IL-8 [120] and in-vivo generation requires IL-10 and TGFβ [121].
Memory T-regs (mTregs)	Act as a reservoir of antigen specific T-regs which can expand upon re-encounter of the antigen to maintain tolerance. Crucial in anti-microbial defence and foetal tolerance[122],[123], [71].	Express high CD25, CD27, CD44, FOXP3, CTLA4 and CD127, but low expression of L-selectin [122].	Secondary lymphoid tissue and periphery[122],[123].	Memory T-regs evade apoptosis during the contraction phase and survive despite the absence of an antigen [122],[123].
CD8+ T-regs	Have a suppressive effect on CD4+ and CD8+ effector functions and proliferation in highly inflammatory environments. They also play a detrimental immune-suppressive role in cancer and viral infections[124], [69].	High expression of CD25, FoxP3, CD122, CD103, CD39 and CD73,CD152, CTLA-4, LAG3 and FasL. Low expression of CD28, CD127 and CD24RC. Secrete IFN_{γ}, IL-10 and TGFβ [124], [69], [125].	Peripheral sites during inflammation[124],[125].	Require IL-4 and IL-10 to modulate STAT-4 and STAT-6 signalling. Irrespective of TCR engagement. Elevated levels of corticosteroids have also been shown to drive CD8+ T-reg differentiation[125].

Table 1.2.2.A, Summary of T-reg sub-types.

Immunosuppressive mechanisms of T-regs

T-regs possess an arsenal of mechanisms to modulate tolerance and immune suppression through both cell-cell interactions and the production of secreted

factors Firstly, T-regs secrete high levels of the immunosuppressive cytokines, TGF-β, IL-10, and IL-35 which prevents the expansion of T-eff cells, promotes further T-reg expansion and supresses the production of pro-inflammatory mediators by innate immune cells. TGFβ was found to be of particular importance to the immunosuppressive capacity of T-regs. Mice with mutations in TGFβ developed chronic autoimmunity and had decreased levels of T-regs at 4-5 weeks [126]. Additionally, the biallelic deletion of the *tgfb1* gene promoted spontaneous autoimmunity and mice presented symptoms similar to scurfy mice which lack FoxP3$^+$ T-regs [127]. IL-10 is particularly important in regulating inflammation to environmental antigens in the intestine, colon and other mucosal tissues. Mice lacking IL-10 are considerably more susceptible to enterocolitis, inflammatory bowel disease (IBD) and reactivity to antigens within the respiratory tract [128].

T-eff responses are also disrupted by the capacity of T-regs to interfere with crucial metabolic mechanisms. For one, T-regs thwart T-eff survival and proliferation by sequestering IL-2; a critical cytokine required for T-eff maintenance. T-regs can also promote an increase in the levels of cyclic adenosine monophosphate (cAMP) to ATP, which has an immunosuppressive effect of T-eff function [129]. T-regs can enhance the surface expression of CD39 and CD73, which act as nucleosidases and convert ATP to adenosine. Subsequently, T-eff cells express adenosine A2A receptor on their surface, which results in the conversion of adenosine to cAMP [130, 131, 132].

T-regs also have the capacity to directly cause cytolysis of T-eff cells, activated auto-reactive B-cells and NK cells though the granzyme/perforin pathway and CD18 adhesion to target cells[133]. Perforin is released, creating pores in the cell membrane which permits the passage of granzymes. In the case of tT-regs they produce Granzyme A which promotes cell death independently of caspases, whilst pT-regs produce Granzyme B, which promotes caspase dependent cell death [133, 132].

Finally, T-regs can inhibit T-eff activation and expansion by interfering with antigen presentation and providing negative signals to minimise the potential for activation. They can sequester DCs by tightly binding to MHC complexes presenting self-antigens through the lymphocyte associated antigen 1 (LFA-1). This reduces the probability of antigen presentation by depleting autoreactive DCs[134]. T-regs also have high expression of CTLA-4 on their surface which binds to CD80 and CD86

on naïve T-cells with high affinity. In fact, CTLA-4 binds with higher affinity than CD28, outcompeting activation by APCs [135], [136].

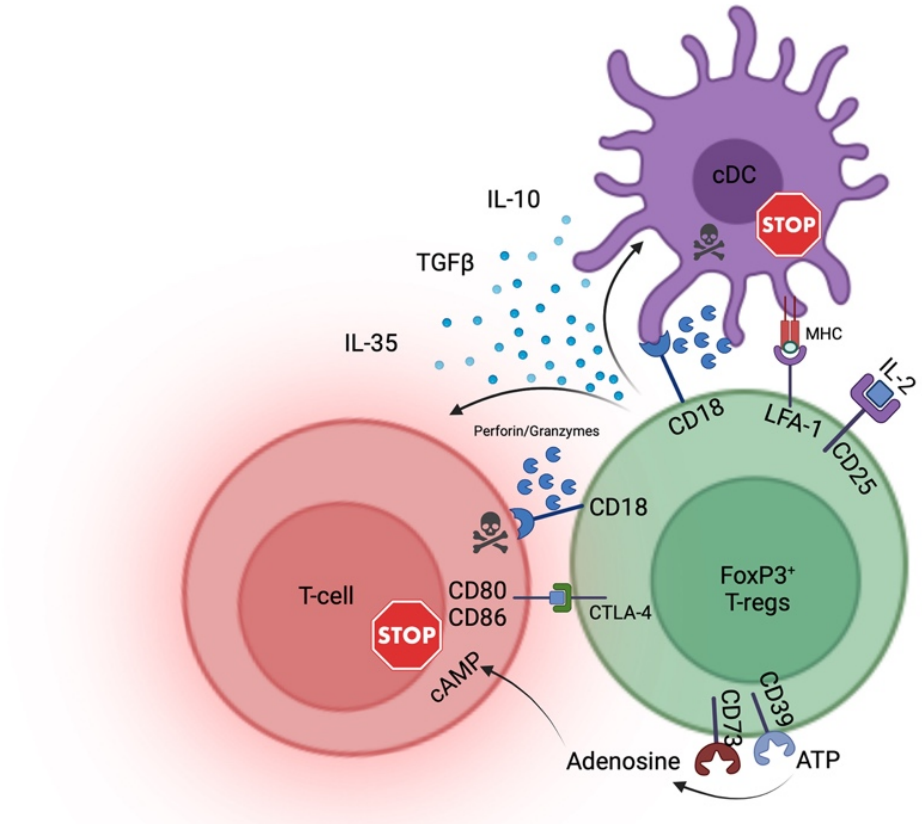

Figure 1.2.2 A. Schematic representation of the immunosuppressive mechanisms of T-regs. T-regs can supress the inflammatory activity of neighbouring T-cells as well as APCs through a variety of mechanisms including; secretion of immunosuppressive cytokines, interference with T-cell activation and metabolism, and direct cytolysis.

1.3 Immune sensing

1.3.1 Pathogen and damage sensing

Pathogen recognition receptors (PRRs) evolved as primordial means of recognising molecular patterns which are classified as non-self or released in response to cell death or damage. The capacity of recognition spans common PAMPs such as; microbial surface components, intracellular pathogenic fragments and soluble factors, as well as DAMPs such as; extracellular ATP, heat shock proteins (HSPs) and DNA [137]. These PRRs are a hallmark of the innate immune system, and precede the more elaborate and specific adaptive immune system [7,138,139,137]. TLRs are the most extensively studied PRRs. Thirteen TLRs have been identified in mammalian cells, ten of which are found in human cells [137,140].

TLRs are transmembrane glycoproteins found either on the cell membrane or on endosomes. They are composed of a ligand binding portion containing leucine rich repeats (LRRs), and a cytoplasmic domain specialised for signal transduction through toll/Interleukin 1 receptor (TIR) homology domains. Common ligands recognised by TLR receptors are shown below in figure 1.3.1A . Engagement of a ligand with a TLR ultimately results in either a pro-inflammatory response, or up-regulation of interferon inducible genes. The outcome depends on the signalling pathway downstream from the TLR which is coordinated by adaptor molecules; MyD88, MyD88-adaptor like (MAL), TIR-domain containing adaptor inducing IFN-β (TRIF), TRIF related adaptor molecule (TRAM) or sterile α- and armadillo-motif-containing protein (SARM). These highly conserved adaptor molecules subsequently cause a cascade of phosphorylation, ubiquination and protein-protein interactions which activate transcription factors. Common signalling pathways include NFκB which upregulates the expression of pro-inflammatory genes including IL6, IL1 and TNFα [141], and the activation of IRF, which activates interferon inducible genes [142].

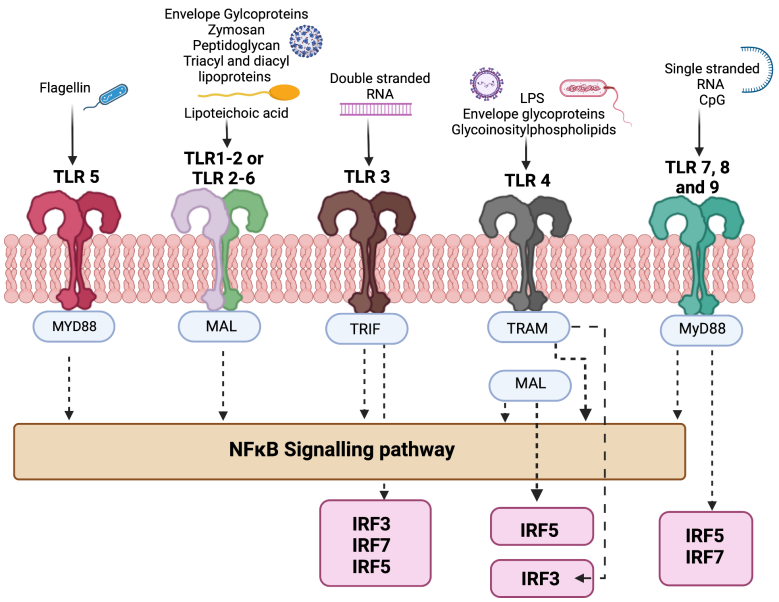

Figure 1.3.1 A. TLRs are activated by numerous ligands and signal through NFκB and IRFs. TLR 5 is activated by ligation of flagellin and signals downstream via MyD88, activating the NFκB

pathway. TLR 2 is only capable of signalling as a dimer, either with TLR 1 or TLR 6. Upon ligation of peptidoglycans, lipoproteins, and Lipoteichoic acid the NFκB pathway is activated in a MAL dependent manner. TLR3 is activated by double stranded RNA and can promote NFκB and IRF3,7 and 5 activation via TRIF. TLR4 is one of the best characterised TLRs and senses microbial patterns such as LPS, envelope glycoproteins and glycoinositylphospholipids . TLR4 can signal downstream via TRAM which activates NFκB and IRF3, or via MAL which also activates NFκB and IRF5. TLR7, 8 and 9 signalling is also dependent on MyD88 signalling and is able to activate both NFκB and IRF5 and 7, upon ligation by single stranded RNA and CpG's.

Another group of PRRs are the C-type lectins. C-type lectins can be found both as membrane bound or secreted molecules and contain c-type lectin domains (CTLDs) which bind conserved residues on carbohydrates such as; the EPN (Glu, Pro, Asn), QPN (Gln,Pro,Asp) motifs as well as mannose and galactose-like residues. These receptors require Ca^{2+} for their recognition capacity, however, a broad repertoire of Ca^{2+} independent receptors have also been identified which can recognise proteins, lipids and inorganic molecules[143,144]. The functions co-ordinated and regulated by C-type lectins are broad and diverse, serving not only as PRRs but can also respond to growth factors, antimicrobial proteins and essential components of the extracellular matrix (ECM)[144]. Furthermore, the expression of C-type lectins is not restricted to innate myeloid cells, but are also crucial for the function of adaptive immune lymphocytes. Whilst C-type lectins play a critical role in the providing protection against bacteria, fungi and even cancer, they have also been associated with the development of auto-immunity. This is exemplified in the brief summary of C-type ligand functions in various infection and disease states in Table 1.3.1 A.

	Protective responses	Pathological involvement
Bacterial and viral protection	• Critical in the response to mycobacterial infections (various CTLs inc. Mincle, MCL, DC-SIGN). • Mincle plays a critical role in the protection of *Streptococcus pneumoniae* and *Klebsiella pneumoniae* [145,146].	• CTLs such as Mannose receptor, DC-SIGN an Dectin-1 can progress disease in HIV and MtB co-infection by promoting viral transmission [147, 148]. • DC-SIGN can serve as an entry receptor for various viral pathogens including Ebola, Hepatitis C and Dengue[148].
Fungal protection	• Dectin-1 recognises glycans which decorate the fungal cell wall and activates neutrophils and $CD4^+$ T-cells[144].	• Dectin-1 can enhance inflammatory responses towards mycobiome resulting in colitis[149].
Cancer	• Dectin-2 and MCL on Kupffer cells supress liver metastasis[150]. • Dectin-1 recognises N-glycan residues on tumours initiating IRF-5 dependent responses and NK cell functions[151].	• DC-SIGN,CD39, CLEC14A and MMR support cancer interactions with endothelial cells facilitating invasion and metastasis[144]. • L-selectin facilitates lymphatic metastasis [152]. • Dectin-1 and Mincle provide macrophage-directed immunosuppression [153,154].
Auto-immunity	• The CD69 CTL receptor is involved in the development of T-regs.	• The recognition of fungal, house dust mite and pollen allergens by dectin-1 and MMR contributes to allergies. • Polymorphisms of DC-SIGN and Dectin-2 enhance susceptibility to arthritis[155] and CLEC5A and LOX1 enhance inflammation and ROS production in joints[144]. • LOX1 and MBL can be regulated by alterations in glucose metabolism in Type 1 Diabetes, which can promote diabetic complications such as fibrosis and nephropathy[156,144].

Table 1.3.1 A. Brief summary of the role of CTL receptors in regulating protective and pathogenic functions in response to bacteria, fungi, viruses and self-antigens. MCL- macrophage C-type lectin, DC-SIGN- dendritic cell-specific intercellular adhesion molecule-3-grabbing non-integrin, HIV- Human immunodeficiency virus, MtB- *Mycobacterium tuberculosis*, IRF- Interferon inducible, CLEC14A- C-type lectin domain containing 14A, MMR- monocyte mannose receptor, Lox1- lectin-like oxidized low density lipoprotein receptor 1, MBL- mannose binding lectins.

Surveillance of cytosolic PAMPs and DAMPs, such as viruses, is brought about by intracellular receptors which are not membrane-bound. Retinoic acid-inducible gene (RIG) like receptors (RLRs) are one of the main cytosolic nucleotide sensors capable of identifying viral RNA[157]. The RIG family is made up of RIG-1, melanoma differentiation associated protein 5 (MDA5) and laboratory of genetics and

physiology 2 (LGP2)[158]. Various receptors have been identified which recognise cytosolic DNA, associated with bacterial and viral infection. These include DNA-dependent activator of IFN-regulatory factors (DAIs), absent in melanoma-2 (AIM-2), interferon-gamma inducible protein 16 (IFI16) and cyclic GMP-AMP synthase (cGAS) [159] [160], however, there is a plethora of less understood DNA sensors such as DEAD-box helicase DDX41 and RNA polymerase III [140,161,162,163]. A crucial feature of cytosolic nucleotide receptors is the capacity to activate anti-viral Type I interferons critical to interfere with viral replication within cells. Another anti-viral response is the induction of cell death pathways apoptosis, necroptosis and pyroptosis by cGAS-STING activation and AIM-2, in order to mitigate viral replication within virally infected cells [159]. AIM-2 is also capable of inducing inflammasome activation required for the expression of the pro-inflammatory cytokines, IL-18 and IL1-β [164,165].

NLRs are cytosolic receptors which play a crucial role in the defence against microbes, inflammation and intracellular danger products such as uric acid, ATP, hyaluronic acid, and cholesterol crystals. Interestingly, they have also been shown to be activated in response to environmental stimuli such as asbestos, silica, aluminium and even UV radiation [166,167] . The NLR family of receptors is large and diverse, with 23 members in humans. These can be sub-divided into five further groups depending on the presence of crucial domains necessary for specific downstream signalling; (i) CARD-containing NLRs (NLRC), (ii) PYRIN-containing NLRs (NLRP), (iii) Acidic-transactivating domain NLRs (NLRA), (iv) BIR-containing NLRs (NLRB) and (vi) the most recent and elusive NLRX [157]. NLRs modulate inflammatory responses either through the inflammasome; resulting in pro-inflammatory responses, or non-inflammasome pathways; which can modulate both pro and anti-inflammatory responses (Table 1.3.2 A) [168].

Pro-Inflammatory	Anti-Inflammatory	Modulates both
NLRP1, NLRP3, NLRP6, NLRP7, NLRP12, NLRC4, NLRP10, NOD-1 and NOD-2	NLRX1, NLRC3	NLRP12

Table 1.3.2 A Modulation of pro and anti-inflammatory responses by members of the NLR receptor family [168].

1.3.2 Immune mechano-sensing

Since the concept of PAMPs and DAMPs was introduced by Charles Janeway and Polly Matzinger in the early 1990s there has been huge emphasis in the role of immune cell sensing of molecular patterns via PRRs [1,7]. This has provided a wealth of knowledge in understanding how immune cells respond to pathogens as well as in disease states such as cancer and auto-immune diseases. In the last decade, the role of mechanical sensing by immune cells to perceive their surroundings using mechano-sensitive receptors, as well as the cell membrane and cytoskeleton, has emerged. Immune cells are constantly exposed to diverse mechanical stimuli throughout the body such as shear stress, tension, compression, matrix rigidity and hydrostatic pressure, either in the resident tissues or in response to migration through blood or lymphatic vessels [169]. Immune cells also employ mechano-sensing to acquire additional information concerning physico-chemical properties of a potential target; such as size, shape and stiffness. They can also, themselves, exert forces back out onto surfaces which can function as a feedback mechanism, or onto other cells altering the nature of an interaction [170,171,172,173]. This can amplify the ability of immune cells to recognise and differentiate between a huge variety of antigens [174, 173]. An excellent example of this is the alterations in cellular stiffness during DC-T-cell interaction which significantly affect the sensitivity to and discrimination of antigens [174]. Blumenthal *et al* demonstrated that DCs undergo cortex stiffening during antigen uptake and maturation, which is dependent on the stiffness of the substrate. Subsequently, the stiffer the DC, the lower the antigen load required to activate more robust $CD4^+$ T-cell responses [175].

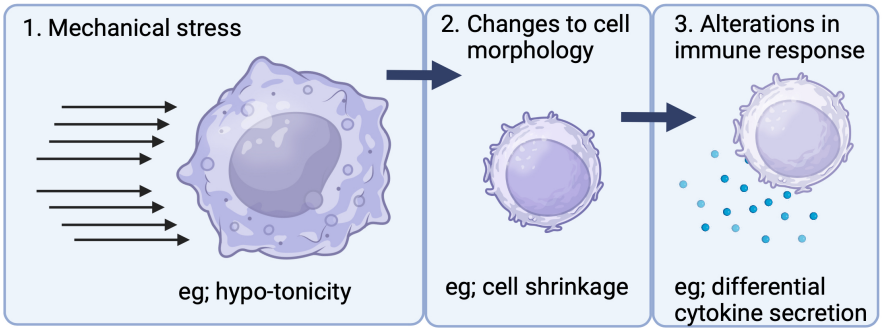

Figure 1.3.2A Simplified example of the downstream effects of mechano-transduction.
(1) Mechanical stresses activate mechano-sensors which provide the cell with information in order to (2) adapt morphologically. (3) These biochemical signals also alter the activation state of immune cells, impacting upon their phenotypic function.

The ability of immune cells to respond to mechanical cues can also contribute to disease states. For instance, changes in tissue substrate during tumour formation have been shown to promote anti-inflammatory and pro-tolerance responses, supporting immune evasion [176,177]. In the development of diseases such as atherosclerosis and liver disease, the substrate stiffness of fibrotic tissue has also been shown to promote disadvantageous immune responses such as increase TGFβ signalling, regulated in part by mechano-transduction [170]. Whilst it is clear than cells integrate numerous complex signals from their environment, studying mechano-transactions could help elucidate how immune cells become differentially activated in different environments or by seemingly inert components.

1.3.3 Mechano-receptors and sensors.

A number of mechano-sensors have been identified to play a role in the function of innate and adaptive immune cells. These include membrane bound calcium channels such as Piezo1 and transient receptor potential vanilloid 4 (TRPV4), adhesion molecules such as integrins and cadherins, as well as the membrane and cytoskeleton itself. Some of the biochemical signalling pathways downstream of these receptors include MAPKs, Yes-associated protein-1 (YAP)/transcriptional coactivator with PDZ-binding motif (TAZ) , EDN1, NFκB, and HIF-1α pathways (Figure 1.3.3 A).

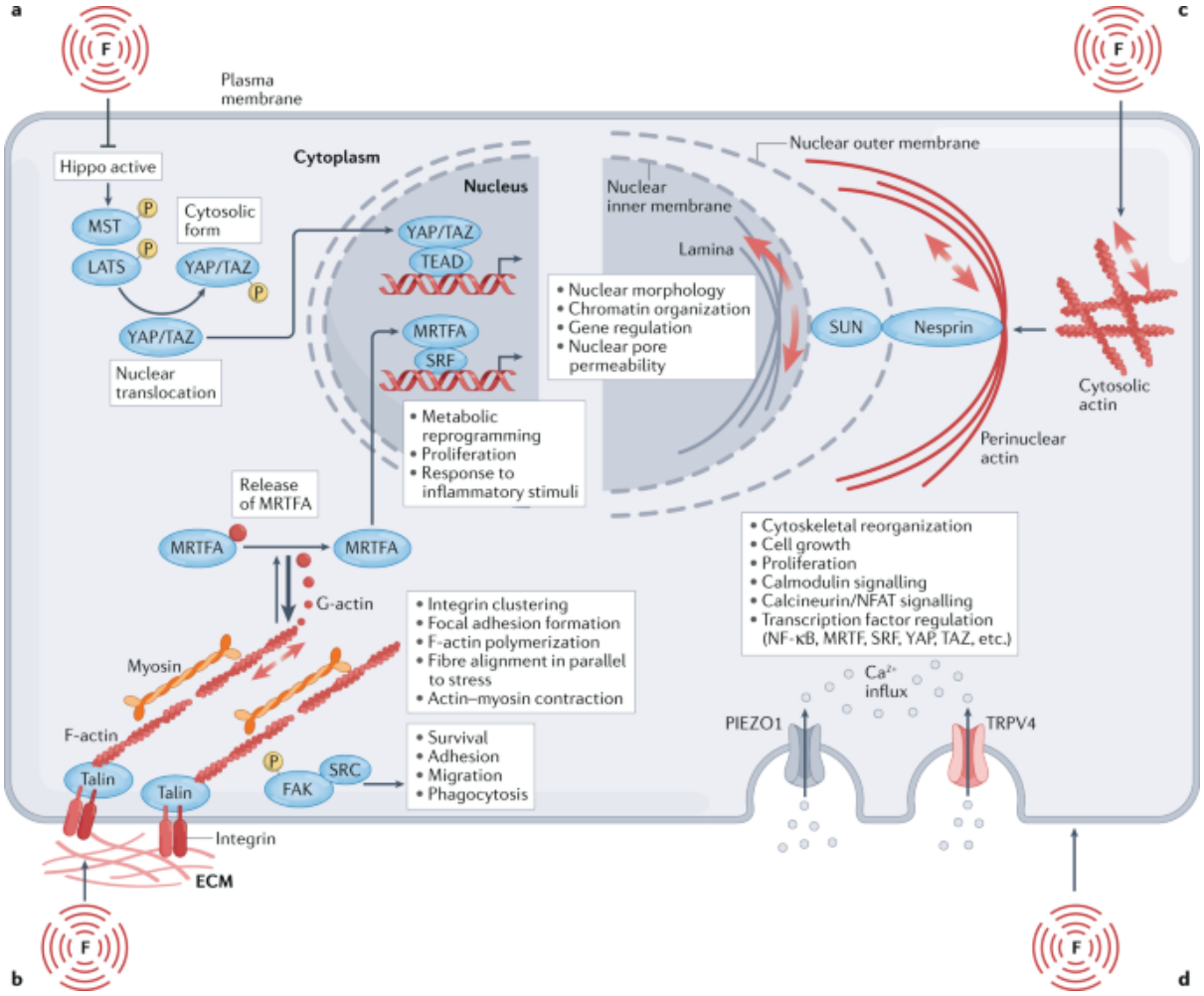

Figure 1.3.3 A. Schematic overview of the various mechanosensors involved in immune regulation and examples of known downstream signalling events. Force exerted on (a) the plasma membrane, (b) integrins, (c) the cytoskeleton or (d) calcium channels Piezo1 and TRPV4 are translated to biochemical signalling events which regulate cell behaviours such as cell growth, proliferation, cytoskeleton re-organization, metabolic reprogramming and pro or anti-inflammatory responses. Figure taken from; Du, H. *et al.* Tuning immunity through tissue mechanotransduction. *Nat. Rev. Immunol.* **23**, (2022).

Immune sensing by the cell membrane and cytoskeleton

As the interface between the cell and the its environment, the cell membrane is a crucial mechano-sensor. In eukaryotic cells, the cell membrane is composed of a fluid phospholipid bilayer composed of four principle phospholipids; phosphatidylcholine (PC), phosphatidylserine (PS), sphingomyelin (SM) and phosphatidylethanolamine (PE). It is studded with proteins which facilitate molecular transport in and out of the cell, as well as signal transduction. In addition, sterols and lipids function to regulate the fluidity and permeability of the membrane.

Cells require a degree of plasticity in terms of their topography, shape and size in order to carry out biological functions such as cell migration, extravasation and tissue remodelling[178]. In performing these functions, they experience a plethora of mechanical stresses such as tensile, compressive and shear stress [179]. In order for the cell to adapt, signalling pathways are triggered in order to restore homeostasis. A good example of this is the response to hypo-osmotic swelling. For instance, in neutrophils, hypo-osmotic tensile stress was shown to release phospholipase D2 (PLD2) from membrane invaginations which resulted in mTORC2 activation. mTORC2 regulates a plethora of immune cell functions such as a metabolism and cell survival. It was also found that mTORC2 activation was critical for actin rearrangement which allowed the cell to alter its morphology to accommodate the cell swelling without incurring cell damage [180].

Lipid rafts are also being suggested to play a critical role in regulating responses to mechanical stimuli experienced by the plasma membrane. Lipid rafts are membrane regions characterised by an compartment enriched in sterols, sphingolipids and proteins such as G-coupled receptor proteins (GCRP), integrins and signalling molecules. They can either be found as planar rafts or as invaginated caveolae which form by polymerization of caveolin proteins 1,2 and 3 [181]. These invaginations are critical to permit the plasma membrane to swell and shrink. Growing evidence suggests that mechanical stress can regulate the formation or deformation of lipid rafts, altering various downstream signalling events[182]. For instance, the disruption of lipid rafts can result in the release of embedded signalling molecules such as caveolins and PDL2, which can activate downstream signalling pathways [180,183,184,185]. Additionally, the spatio-temporal re-organization of various signalling receptors such as pathogen recognition receptors and G-coupled proteins within lipid rafts has also been demonstrated to create signalling “hot-spots” which can amplify downstream signalling [186,187,181].

The highly dynamic cytoskeleton and nucleo-skeleton is also critical in sensing and responding to mechanical stimuli. The rearrangement of the cytoskeleton and adhesion complexes in response to mechanical stress, can promote downstream signalling events which alter immune responses. The rearrangement of the cytoskeleton provides the cell with the flexibility and plasticity it requires to perform crucial functions including extravasation, adhesion, migration and phagocytosis [188,189,190]. Much of our knowledge on the mechano-sensory role of the cytoskeleton

was generated from macrophages due to their highly adhesive nature, allowing researchers to investigate the effect of substrate properties on their activation. Macrophage adherence to substrates results in cytoskeletal rearrangements which activates signalling molecules such as Rho-family small GTPase, protein kinases and nuclear proteins [191]. For instance, a study by Meli *et al* found that macrophages cultured on stiff substrates had increased activation of the nuclear factor YAP which gives rise to enhanced inflammatory responses [192]. Indeed, forcing actin rearrangement through spatial confinement is, remarkably, sufficient to influence macrophage polarisation. Macrophage morphology changes with respect to phenotype, with M1 macrophages commonly taking on a more rounded shape whilst M2-like macrophages spread out to take on an elongated morphology [193]. When cultured on micropatterned surfaces with 2 μm wide ridges, BMDMs underwent actin rearrangement and became significantly more elongated within the adherent ridges. In addition to this morphological change, BMDMs exhibited M2 characteristics such as elevated expression of Arginase-1 and secretion of IL-§4. This was not observed in BMDMs cultured on un-patterned surfaces and those with wider ridges. When actin rearrangement was inhibited using blebbistatin, cytochalasin D or Y27632, BMDMs still took on elongated morphologies, however the previously observed enhancement in M2 markers was abrogated [194].

Membrane bound receptors

Immune cells utilise ion channels as a means of translating mechano-sensory signals to biochemical signals in response to environmental changes. Two of the main mechano-sensory ion channels identified to play a role in modulating immune responses are Piezo-1 and TRPV-4. Both ion channels promote Ca^{2+} influx in response to mechanical stimuli such as lipid bilayer stretch and pressure [195].

TRPV4

The TRPV4 calcium channel be activated in response temperature changes [196] as well as mechano-messengers; arachidonic acid and epoxyeicosatrienoic acids [188]. These mechano-messengers can be released in response to strain experienced by the cell membrane, integrins and focal adhesions [197,198]. Alternatively the mechanically gated ion channel can be forced open during deformation of the plasma membrane [199,200]. TRPV4 activation opens the Ca^{2+} channel allowing influx

into cell, initiating Ca^{2+} dependent signalling such the MAPK/p38 and YAP/TAZ pathways [201, 202]. TRPV4 has been implicated as a modulator of both pro and anti-inflammatory responses, most notably in alveolar macrophages which are exposed to constant mechanical stimuli. Mechanical stress induced by lung ventilation was demonstrated to increase lung injury by enhancing ROS production and pro-inflammatory responses in a TRPV4 dependent manner [203]. On the other hand, in a model of bacterial, *Pseudomonas aeruginosa* infection in mice, TRPV4 protected the lung from injury by enhancing phagocytosis and reducing pro-inflammatory cytokine secretion [204].

Piezo1

Peizo1 was discovered in 2010 and has since been implicated in a number of physiological functions such as pain transduction, vascular development and regulation of blood pressure. It has also been found to modulate responses from macrophages, dendritic cells and T-cell in response to mechanical cues [205]. The structure of Piezo1 resembles that of a three bladed propeller. In response to external forces the structure undergoes conformational changes, providing an opening within the central channel, facilitating Ca^{2+} influx [206]. In macrophages, Piezo1 has been implicated in pro-inflammatory responses, perpetuating the inflammation in atherosclerotic and fibrotic lesions as well as pulmonary injury [207,208,209]. Piezo1 also plays a role in regulating the phagocytic capacity of macrophages, with Ca^{2+} influx promoting cytoskeletal remodelling, efferocytosis of apoptotic bodies and acidification of the phagosome [207,210].

With regards to DCs and subsequent T-cell differentiation, Piezo1 has been shown to direct Th1 responses whilst restricting T-reg expansion. This was established by several authors, demonstrating that Piezo1 deletion in both DCs and T-cells resulted in an increase in the number of T-regs which reduced the severity of experimental auto-immune encephalomyelitis (EAE) in mice [211]. This was modulated in part by an increase in the capacity of piezo1 KO DCs and T-cells to upregulate TGFβ which significantly reduced $CD4^+$ T-helper functions and diminished the numbers of activated cytotoxic $CD8^+$ T-cells [211,212,213].

1.3.4 Integrins

Integrins are membrane spanning proteins which have been extensively researched for their role in modulating immune cell adhesion to other cells and to the underlying ECM, as well as migration and phagocytosis. However, as a connection between the extracellular environment and the cell cytoskeleton, they are also important in intracellular signalling in order to provide the cell with information about its surroundings [214].

Integrin structure and activation

Integrins are composed of two glycoprotein structures, an alpha (α) and a beta (β) protein, which dimerise to yield 24 dimer combinations. Each combination has specific affinity for either leukocyte surface molecules, collagen, laminin or RGD receptors, as depicted in Figure 1.3.4 [215]

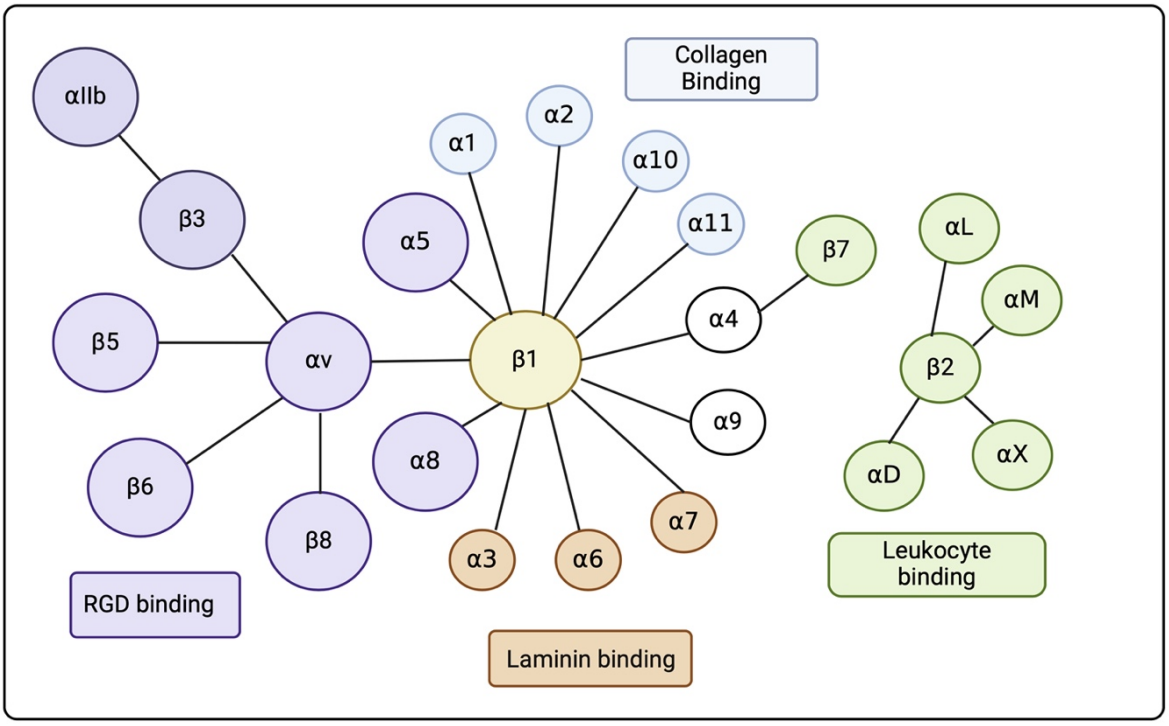

Figure 1.3.4 A. Known integrin combinations. Integrins are made up of an α and β dimer and depending on the combination have affinity to adhere to RGD motifs, laminins, collagens or leukocytes [215].

Integrins span the plasma membrane with a large globular N-terminal extracellular portion containing a ligand binding domain and a C-terminal “stalk-like” intracellular

domain. In the inactive state, the extracellular domains of both integrin dimers are maintained in the “low affinity state” whereby the globular head structures are in close proximity and in the bend conformation, shielding the ligand binding domain. The intracellular portion of both dimers clasp together (Figure 1.3.4 B) . This bent, low affinity state is maintained by various inhibitory proteins such as shank-associated RH domain-interacting protein (SHARPIN) and Immunoglobin repeat 21 of filamin A (FLNa-Ig21). Upon activation, the globular heads straighten, causing the intracellular domains of the dimers to separate and take on the “high affinity state” [216]. In order for the binding domain on the head structure to be exposed, the integrin must reach its fully extended form (Figure 1.3.4 B) [217].

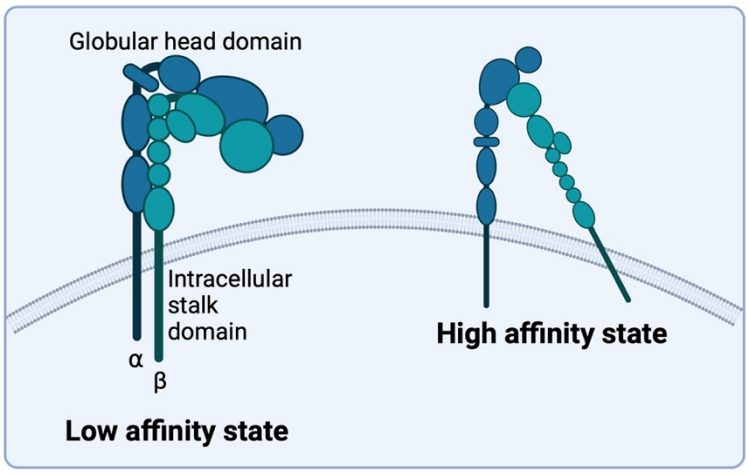

Figure 1.3.4 B Structure of low and high affinity integrins. Inactive integrins are found in the low affinity state where by the globular head is bent in a V shape and kept close the plasma membrane. The intracellular stalk domains are clasped together. Upon activation, integrins extent out and the intracellular stalk domains separate out [216].

Integrins can be activated bi-directionally from the outside-in or inside-out. [218]. Inside-out signalling is primarily regulated by the proteins talin 1 and 2 (referred herein as talin), which selectively binds the intracellular β portion of the integrin [219]. Talin is made of the FERM head domain which binds integrins (Talin H), a rod domain which binds actin (Talin R) and a compact N-terminus. The engagement of talin H with the intracellular stalk of the integrin β-dimer causes a mechanical rift between the α and β portion, forcing them apart, and promoting the integrin to take on the “high affinity state”. The activation of talin is strictly controlled, and can only bind integrins when the cell membrane becomes enriched with ;

phosphotidylinositol 4,5-bisphosphate (PIP2) [220]. The conformation at which inactive talin is maintained gives the structure a net negative charge which is normally repelled from the membrane. When the membrane is enriched with PIP_2, the cell membrane becomes significantly more negative, creating electrostatic pull of the shielded positive motif found on Talin. This causes a conformational change to the structure of talin, exposing the positive region, and allows talin to approach integrins at the cell membrane interface. The mechanism by which PIP2 can activate talin has been termed the "push-pull" [220,221] and is represented schematically in Figure 1.3.4A.

In the active form, the talin H domain can bind mechanoreceptive vinculin, paxillin, actin and KANK and the rod domain can bind phosphoinositides, rap1 GTPases and F-actin. Whilst talin is sufficient to activate integrins, an additional protein; kindlin can also cooperatively bind the intracellular domain of the β-dimer which serves as an additional adaptor protein for other signalling proteins. Through the formation of adaptor protein complexes on talin, talin binding proteins and kindlin, the activation of an integrin can potentiate signalling via cognate pathways such as spleen tyrosine kinase (Syk), Bruton's tyrosine kinase (BTK), YAP/TAZ and phosphoinositide 3-kinases (PI3K).

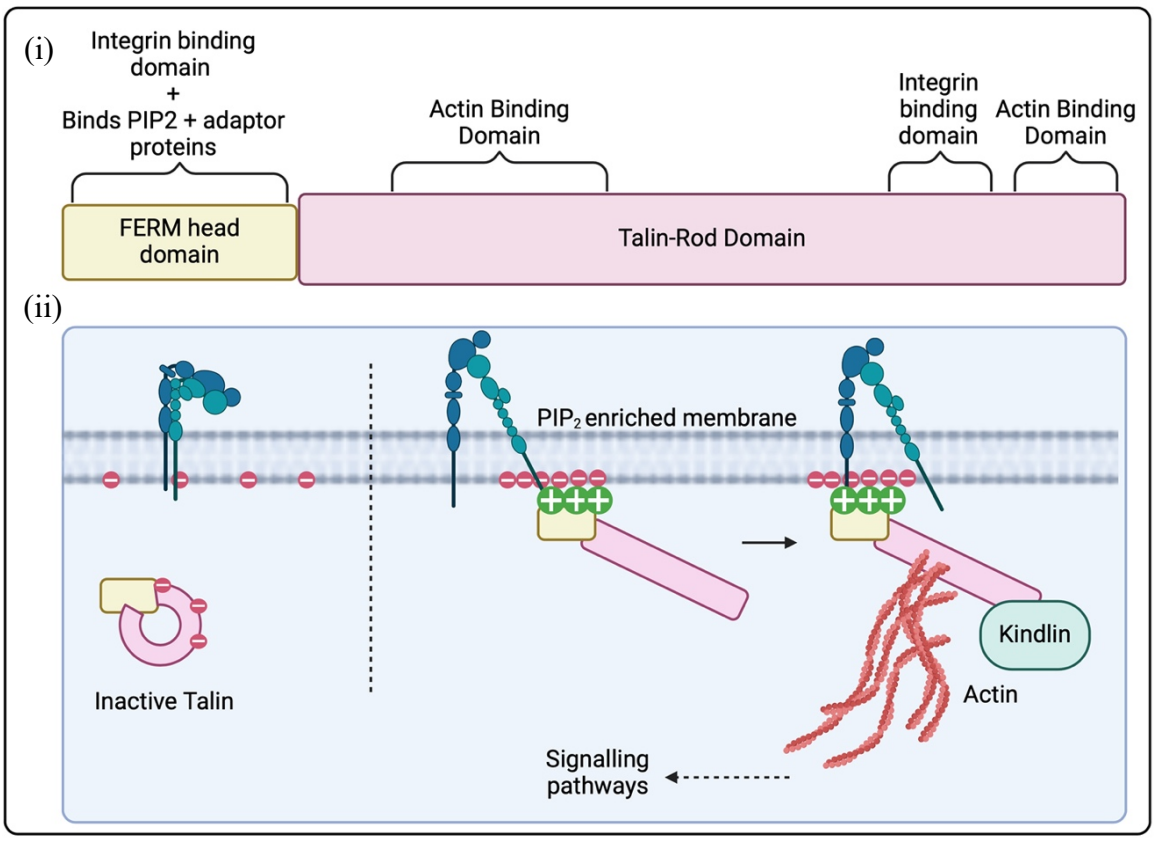

Figure 1.3.4 C. Activation of talin and inside-out activation of integrins. (i) A simplified schematic of the talin structure and the binding regions [220]. (ii) the PIP_2 dependent inside-out activation of integrins. In brief, PIP_2 enriched membranes enhance the negative charge at the plasma membrane which electrostatically forces a conformational change in the structure of talin, exposing positive motifs on the FERM-head domain. Talin can then be sequestered to the membrane to interact with talin, forcing the integrin stalks apart and mechanically activating the integrin [220,221].

Outside-in activation occurs when integrins bind the molecular patterns found on collagens, leukocytes or RGD motifs such as vitronectin, fibronectin and growth factor receptors [222,223]. Activation of integrins only occurs when there is strong affinity between ligand and integrin, permitting the assembly of integrin activation complexes (IAC) on the intracellular domain. IACs can be composed of up to 150 structural and adaptor proteins, scaffolding molecules, protein kinases, phosphatases and GTPases which incite downstream signalling events regulating the cells phenotype but also cytoskeletal dynamics to adapt cell shape, migration and growth [224]. Talin has been found to be indispensable to the formation of IACs [225]. Furthermore, the formation of integrin clusters help stabilise IACs, creating

"multi-protein hubs" at adhesion sites which significantly amplify signalling events [226]. However, there is ongoing debate on the mechanism by which integrins form clusters and the feasibility of studying these structures [227].

Mechano-transduction by integrins

Integrins play a crucial role in mechano-transduction of mechanical stress imposed on the cell membrane and cytoskeleton and can also be utilised to acquire information about their environment by exerting force on a substrate and experiencing force in return [228] . These push-pull interactions experienced at the actin-integrin intersection can modulate the formation of IAC's, and downstream signalling events. In particular the Fak/Src and YAP/TAZ signalling pathways have been identified to play crucial role in immune cell functional regulation. Integrins are also involved in a widespread cross-talk with other mechano-sensory proteins, in particular stretch activated channels such as Piezo1 and TRPV4 [229].

A good example of the functional regulation of immune cells by mechanical sensing is the conformational change of integrin αL also known as LFA-1, on dendritic cells in response to substrates with high rigidity. The conformational change to the cytoskeleton exerts force on the LFA-1 integrin, activating it, and enhancing its affinity for the intracellular adhesion molecule 1 (ICAM1) expressed on epithelia and other immune cells. This high affinity interaction enhances DC maturation, induces pro-inflammatory responses and activation of lymphocytes [230].

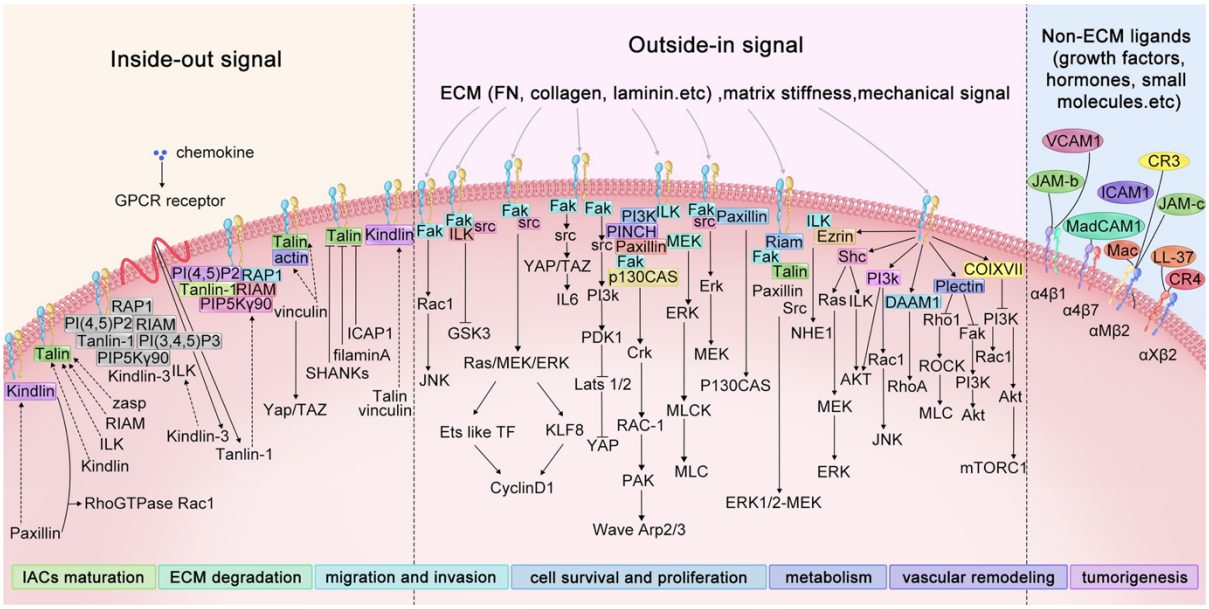

Figure 1.3.4 D. Schematic overview of signalling cascades downstream of integrins activated inside-out and outside-in. Schematic taken from; Pang, X. *et al.* Targeting integrin pathways: mechanisms and advances in therapy. *Nature Signal Transduct. Target. Ther. 2022 81* **8**, 1–42 (2023).

Regulation of TGFβ by integrins

The extensive synergy between TGFβ signalling and integrins makes them important regulators of immune responses, as well as in the development of diseases such as fibrosis and cancer [222,231, 232]. TGFβ is secreted as a latent complex, composed of the latency associated protein (LAP) which shields the TGFβ receptor binding domain. The αv containing integrins, αvβ3, αvβ5, αvβ6 and αvβ8 have an affinity to RGD-motifs, a motif which is found on the LAP protein. Tethering of integrins to the RGD motif on LAP causes a conformational change to the structure of LAP allowing TGFβ to be released. The "pull" exerted on LAP is facilitated by the integrin-cytoskeleton bond formation and actin contraction (Figure 1.3.4E) [233, 234, 235, 236, 237]. αvβ8 differs in its activation mechanism, and instead of using actin-derived contractile forces to remove LAP, it binds to LAP causing a conformational change to its structure, exposing the TGFβ binding motif [238]. The exact mechanism by which αvβ1 activates TGFβ has not been fully established, however, evidence proposes that the contractile forces might be required, with possible involvement of co-localised protease enzymes such as MMPs [239,240]. The integrins αvβ6 and αvβ8 are primarily responsible for the activation of TGFβ, with the deletion of either leading to the onset of inflammatory conditions [241]. However, this does not diminish the contributions of αvβ3 and αvβ5, which also play significant roles in TGFβ activation.

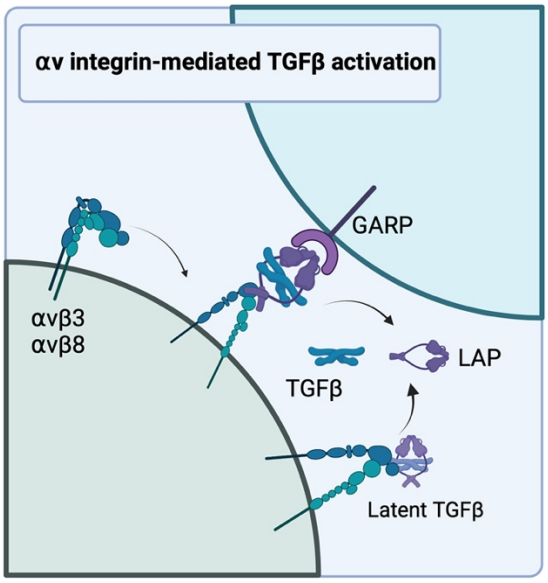

Figure 1.3.4 E. Schematic of the activation of TGFβ by αv containing integrins. Activated integrins containing the αv dimer bind the RGD domain on LAP and release TGFβ from the active TGFβ.

Interestingly, the activation of TGFβ and subsequent signalling downstream of the TGFβ receptor, enhances the gene expression of various integrins including αvβ3, αvβ5 and αvβ6 [232, 231]. This encourages a positive feedback loop to amplify TGFβ signalling axis. Indeed, the generation of TGFβ is essential for homeostasis, immune tolerance and to dampen chronic inflammation. However, this positive feedback loop can become maladapted and contribute to the pathogenesis in cancer and fibrosis. The role of TGFβ-integrin cross-talk in disease is summarised in Table 1.3.4 A. The overexpression of integrins αvβ6, and αvβ8 in particular promotes cancer growth, metastasis and angiogenesis, as well as the development of fibrosis in the skin and lung [232,242]. However, αv containing integrins also play a crucial role in promoting homeostasis through the generation of T-reg populations as well as Th17 cells to combat bacterial and parasitic infections [243].

Integrin	Immune regulation	Pathologies
αvβ3	• Low expression is critical for the polarisation of Th2 cells which bring about anti-helminth immunity [244]. • Promotes T-reg responses required for inflammatory resolution [245].	• Contributes to fibroblast differentiation in scleroderma[246] • Can facilitate cancer cell invasion in stiff tumours [247].
αvβ5	• Participates in wound healing[248].	• Contributes to fibroblast differentiation in scleroderma [249]
αvβ6	• Regulates pulmonary inflammation [250]	• Promote pulmonary, dermal and liver fibrosis [250], [251], [249]. • Exacerbates several squamous cell carcinomas [232]. • Can promote HER2 positive breast cancer metastasis [252].
αvβ8	• Modulates the differentiation of Th17 cells in the gut which regulate parasite expulsion [253]. • Essential for the suppression of T-cell mediated inflammation [254]. • Promotes epithelial homeostasis[255]. • Enhances M2-macrophage immunosuppression [256].	• Modulate Th17 expansion in models of EAE. • Promote T-regs which impair anti-tumour immune responses[257]. • Promotes Th17 cell differentiation involved in asthma[258].

Table 1.3.4 A. Immune regulation and pathologies associated with TGFβ-integrin crosstalk. The cross-talk between integrins and TGFβ provides tolerogenic immune responses which are integral for tissue homeostasis but over-expression in cancer and fibrosis can contribute to pathology.

1.4 Signalling pathways

1.4.1 TGFβ signalling

TGFβ signalling regulates the expression of 100s of genes and is crucial during development, inflammatory resolution, wound healing and establishment of

homeostasis. TGFβ signals via various TGFβ receptors (TGFR), which are made up of dimer combinations of type I (TGFRB1) and type II receptors (TGFBR2). The mammalian cell expresses seven TGFBR1, and five TGFBR2 receptors, providing a variety of pairwise combinations. When TGFβ binds the TGFBR2 dimer, a composite ligand receptor protein surface forms. The cytoplasmic tail of its adjoining TGFBR1 has a Gly/Ser-rich (GS) region upstream of a Ser/Thr kinase region, which becomes phosphorylated by TGFBR2 [259] and serves as a binding domain for Smad proteins [260]. TGFβ signalling can either proceed via the Smad dependent or independent pathway (Figure 1.4.1 A). In the Smad dependent pathway, also known as the canonical pathway, receptor regulated Smads; Smad 2 and 3 anchor to TGFBR1 within proximity to the Ser/Thr kinase region. This proximity allows Smad 2/3 to become phosphorylated by the Ser/Thr kinase, and translocate to the nucleus as a dimer, or as a trimer with Smad4, however, this trimerization is not crucial for nuclear translocation [259]. In the nucleus, the Smad complexes bind to genomic loci, and are further phosphorylated by RNA polymerase II and kinases; cyclin-dependent kinase 8 and 9 forming a protein complex which can at as a transcription factor. Signalling is then terminated by degradation or dephosphorylation of the nuclear Smad complex. The Smad signalling pathway is also regulated in the cytosol by Smad 6 and 7 which function to antagonise Smad2/3 and are usually expressed following excessive TGFβ or BMP signalling and IFN_{γ} [261,262]. TGFβ can also signal via non-canonical pathways such as MAPK pathways, JNK/p38 pathway, as well as Rho-like GTPase and PI3K/Akt pathways. However, rather than being a separate signalling pathway, there is significant cross-talk amongst different pathways and Smad proteins [263].

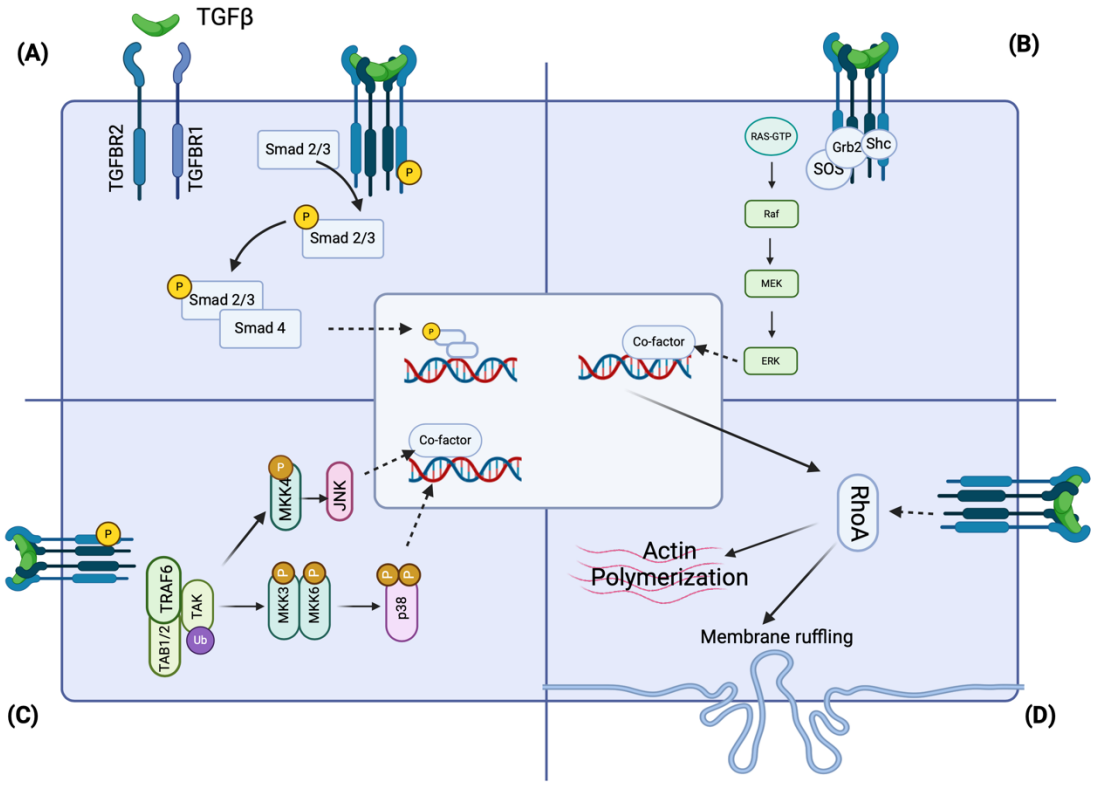

Figure 1.4.1 A. TGFβ signalling pathways. TGFβ binding to the TGFβ receptor activates downstream signalling pathways which results in the activation of transcription factors and alterations to cell functions. (A) The canonical TGFβ pathway promotes the phosphorylation of Smad2/3 transcription factors. Other non-canonical pathways include (B) the Ras/Raf/MEK/ERK and (C) p38/JNK pathways which result in the activation of co-factors which promote gene expression. (D) TGFβ receptor can also activate RhoA which can alter membrane and cytoskeletal remodelling.

1.4.2 mTOR

As a major regulator of immune signalling, the evolutionarily conserved kinase; mTOR, has been studied extensively for the role it plays in dictating immune responses [264]. The extensive phenotypic alterations which occur during immune activation and polarisation of innate immune cells such as changes in cell metabolism, morphology, cytokine secretion, migration and proliferation have been linked to mTOR regulation [265,266]. Unsurprisingly, mTOR is found downstream to many extracellular signals including engagement of TLRs [267] , growth factor receptors [268], mechanical stimuli [269,270], and intracellular signals such as nutrient availability and stress-related factors [271 272,273,265, 264].

mTORC1 and mTORC2, are serine/threonine protein kinases which belong to the family of phosphoinositide 3-kinase related kinases (PIKK). The two proteins are often referred to as just mTOR, however, it is important to note that mTORC1 and 2 can modulate different responses and become activated by separate signalling events. In its activated state, mTORC1 is composed of regulatory-associated protein of mTOR (RAPTOR) and mammalian lethal with Sec13 protein 8 (mLST8), which create further protein-protein interactions via the WD-40 domain. The activity of mTORC1 is repressed by the binding of proline-rich Akt substrate 40 kDa (PRAS40) and DEP domain–containing mTOR-interacting protein (DEPTOR). Activated mTORC2 is composed of mLST8, RAPTOR-independent companion of TOR (RICTOR), protein observed with RICTOR (PROTOR) and mSIN1. Similarly it is repressed by DEPTOR. [264,274]

The signalling network upstream of mTOR is complex, and has widespread involvement in diverse responses (Figure 1.4.2 A). It is, therefore, likely numerous additional signalling pathways converge with mTOR signalling. The ability to block mTORC1 with rapamycin has allowed a greater understanding of mTORC1 signalling [275], whilst an inhibitor to selectively inhibit only mTORC2 has not be discovered, nor can it be knocked-down without lethality [274].

mTORC1 activation is activated by Ras homolog enriched in brain GTP (RhebGTP), which is negatively regulated by tuberous sclerosis complex 1and 2 (TSC1/2). In its unphosphorylated form, TSC1/2 converts RhebGTP to RhebGDP. TSC1/2 is activated when there the cell experiences low levels of ATP, hypoxia or in response to signalling via Wnt/Glycogen synthase kinase 3 (GSK3) and 5' AMP-activated protein kinase (AMPK) pathways. On the other hand, signalling via the PI3K, Ras/Raf/MEK/ERK and MAPKs [276,271] activates mTOR by phosphorylating TSC1/2 and inhibiting dephosphorylation of RhebGTP [277]

Activated mTOR phosphorylates effectors such as eukaryotic initiation factor 4E (eIF4E)-binding protein 1 (4E-BP1) and the p70 ribosomal S6 kinase 1 (S6K1) which enhance protein synthesis [278], and positively regulates sterol regulatory element binding protein 1 (SREBP1) and peroxisome proliferator-activated receptor-γ (PPARγ) required for enhanced lipid synthesis and oxidative phosphorylation [279,280].

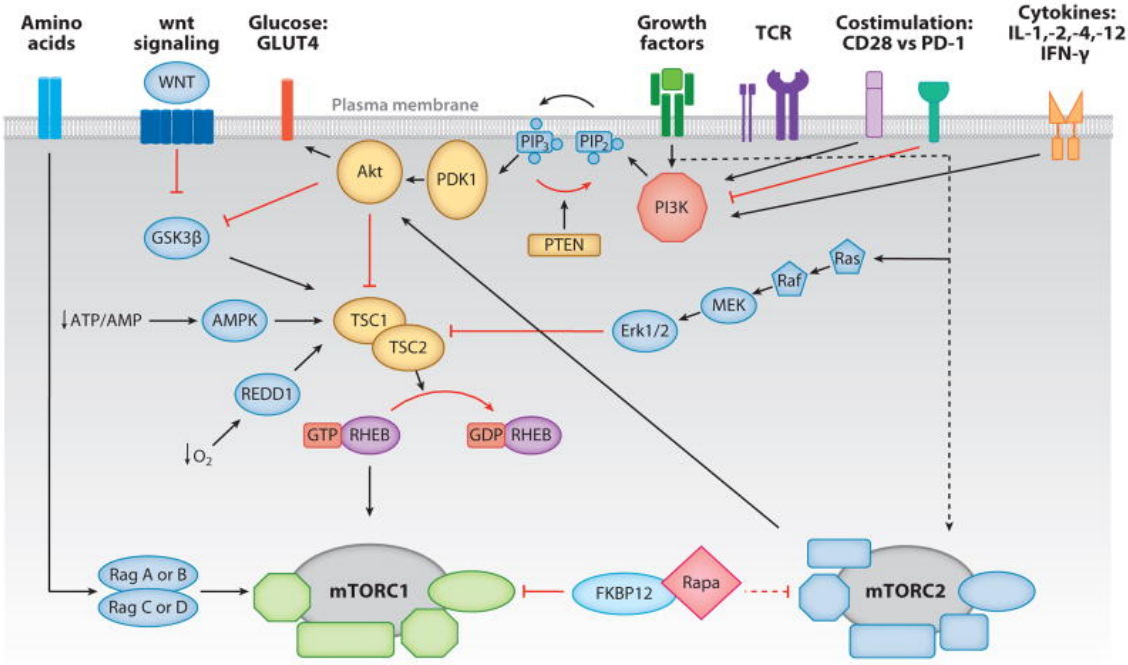

Figure 1.4.2 A. Signalling pathways which regulate mTORC1 and mTORC2. Various signalling pathways activate mTORC1/2 in response to receptor activation by growth factors or cytokines, and nutrient availability. In T-cells, mTORC1/2 can be activated by TCR and co-stimulation ligation. The main negative regulator of mTORC1 is the TSC complex which maintain RHEB in the GDP form. However, signalling via Ras/Raf/MEK/ERK or PI3K/Akt inhibit the TSC complex, allowing RHEB GTP to activate mTORC1. Activation of AMPK in response to low ATP/AMP ratios, REDD1 in response to low O_2 concentrations and WNT signalling maintain TSC activated. Figure taken from Weichhart, T., Hengstschläger, M. & Linke, M. Regulation of innate immune cell function by mTOR. *Nature Reviews Immunology* vol. 15 599–614 (2015).

Signalling via mTOR complexes is fundamental to regulating functions of both innate and adaptive immune cells including differentiation, activation, metabolism, effector functions, survival and proliferation [281,282,283, 276]. It has, therefore, been explored extensively as a potential target for directing immune responses to treat disease. For instance, rapamycin has been investigated for enhancing tolDC populations to promote T-reg expansion, but also to enhance anti-viral responses in the elderly [284,285 286].

Dendritic cell responses are strongly regulated by mTOR signalling. Early in development, mTOR is activated in response to GM-CSF and also Flt3L in the generation of $CD103^+$ cDC1 cells [283]. Importantly, in activated cells, mTOR sustains long-term glycolysis and regulates the mitochondrial production of nitric oxide (NO). Due to mTOR acting as a nutrient and energy sensing pathway it is

understandably a major regulator of metabolism. However, with that being said, inhibition of mTOR with rapamycin promotes cell survival, as it re-directs and preserves metabolic function for normal cellular functions [287]. In terms of the role of modulating either pro- or anti-inflammatory responses, the literature provides contradictory results, which are likely as a result of spatiotemporal differences in the activation of mTOR at different stages of maturation and the metabolic environment. TLR activation has been demonstrated to activate mTOR, which facilitates pro-inflammatory NO production, TNFα and Type 1 IFNs. However, during antigen-presentation in lymph nodes, mTOR activation restricted the production of IL-12, expression of CD86 and CCR7 and enhances IL-10 production [288,289,290].

mTOR is also a critical regulator of T-cell activation, for instance TSC1/2 stringently control the activation of mTOR in naïve T-cells to maintain senescence [291, 292]. mTOR is activated almost immediately after TCR stimulation and engagement of co-stimulatory molecules OX-40 and CD28. mTOR activation is maintained during antigen presentation and is augmented by the amount of antigen being presented [293,294]. It has, therefore, been proposed that mTOR plays a critical role in successfully promoting T-eff cell activation such as $CD8^+$ T-cells and Th1/Th2/Th17 cells [295]. Furthermore, mTOR has also been implicated in regulating the metabolism of T-eff cells. mTOR signalling via PI3K/AKT as well as cross talk through myelocytomatosis oncogene (Myc), enhances glycolysis which is critical to sustain $CD4^+$ T-eff functions. On the other hand, engagement with the co-inhibitory PD-L1 and weak mTOR activation as a result of brief MHC cross-presentation and co-stimulatory signals, promotes T-reg expansion [296]. This has been harnessed to enhance immunosuppression. For instance rapamycin is currently in use to prevent rejection during kidney transplantation and is being explored as a to treatment for SLE [297].

In terms of regulation of macrophage polarisation, mTORC1 promotes anti-inflammatory responses and M2 polarisation. mTORC1 activation via the PI3K/Akt pathway, was found to be essential for metabolic rewiring of macrophages towards an M2-metabolic profile [279,280] and for the secretion of anti-inflammatory cytokines such as IL-10 and IL-1Ra [277,63]. A role for mTORC2 signalling in macrophage polarisation was also identified, proving to be an important pathway for the skewing of macrophage metabolism towards oxidative phosphorylation and fatty acid

oxidation. In response to macrophage colony stimulating factor (M-CSF), mTORC2 was activated in parallel to the STAT6 pathway to bring about nuclear translocation of IRF-4, a transcription factor associated with promoting an M2-metabolic profile [298].

1.5 Immunometabolism

Cell metabolism is fundamental to the survival and effector function of all cells. They remain in a constant flux between catabolic and anabolic mechanisms depending on signals received from nutrient sensors, oxygen availability and functional requirements from the cell, such as proliferation. Catabolic metabolism breaks down molecules into smaller molecules in order to produce energy and intermediates required to support the tricarboxylic acid (TCA) cycle and the electron transport chain . These processes include glycolysis, fatty acid oxidation and breakdown of proteins. Anabolic metabolism is required for the synthesis of lipids and proteins which are essential to support proliferation and various cellular functions such as cytokine production. An overview of the six main metabolic pathways are summarised in figure 1. 5 A.

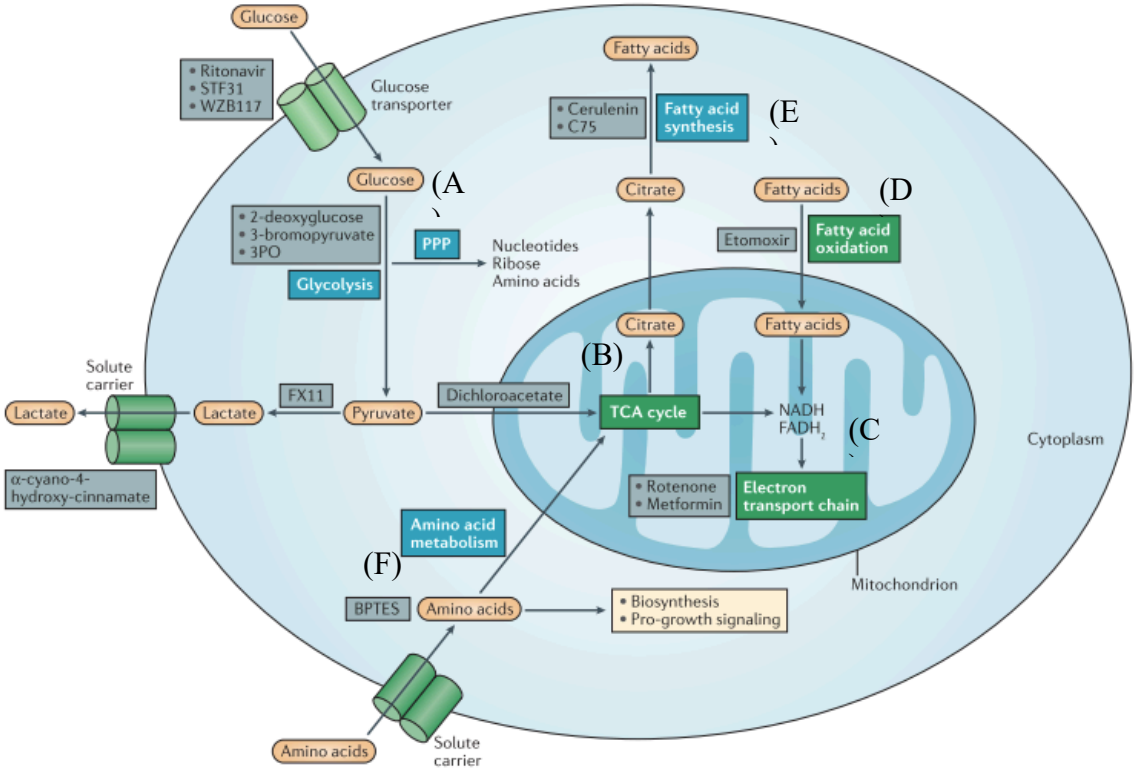

Figure 1.5 A. Overview of cell metabolism. Cells rely on six major metabolic pathways. (A) Glycolysis breaks down glucose to produce pyruvate which is either used in TCA cycle, or converted to lactate. Intermediates of glycolysis are also used for the pentose phosphate pathway (PPP). (B) The TCA cycle generates NADH and $FADH_2$ which is provides electrons to the ETC. (C) The ETC is the cell's main producer of ATP. (D) Fatty acid oxidation can also be used to produce NADH and $FADH_2$. The two main anabolic pathways are (E) fatty acid synthesis and (F) amino acid synthesis which are required for building blocks for new cells, or production of signalling proteins such as cytokines. The metabolic pathways in green boxes are dependent on oxygen whilst the boxes in blue cananaerobically. The boxes in grey denote known inhibitors to block metabolic pathways. Figure taken from O'Neill, L. A. J., Kishton, R. J. & Rathmell, J. A guide to immunometabolism for immunologists. *Nature Reviews Immunology* vol. 16 553–565 (2016).

Over the last two decades, there has been a surge of interest in immune cell metabolism and this has revealed how intricately linked immune cell metabolism is to their effector functions. It has also revealed the role immunometabolism plays in the development of diseases such as auto-immune conditions, and vice versa, how disease can alter immunometabolism [299].

The development of the extracellular flux analyser (Agilent Technologies™) has provided a highly sensitive method to measure the rate of oxidative phosphorylation and glycolysis. The rate of oxidative phosphorylation can be measured by changes in the oxygen consumption rate (OCR) which is measured

as pmol of oxygen per minute (pmolO_2/min). The rate of glycolysis relies on the minute changes to the acidification of the cell media as a result of the production of glycolytic by-product; lactate. The extracellular acidification rate (ECAR) is measured by the change in mpH/ min [300, 301]. It is, therefore, possible to measure the metabolic outputs of immune cells both at rest, and in response to inhibitors against various important metabolic functions. This can help understand the reliance of immune cells on certain metabolic pathways in health and disease. In fact it has allowed advancements in understanding immunometabolism [302,303]. Commonly used inhibitors to study how cells utilise glycolysis and OxPhos are summarised in Figure 1.5 B.

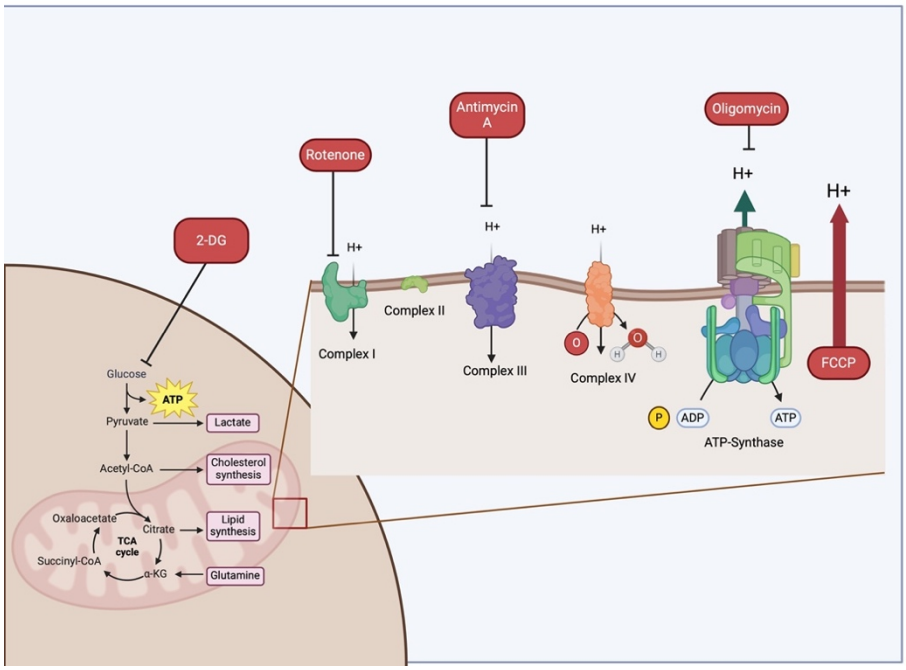

Figure 1.5 B. Schematic presenting inhibitors of glycolysis and OxPhos and targets. Oligomycin is an inhibitor of the last step of OxPhos. Blocking ATP-synthase can be used to assess the effect of both blocking mitochondrial respiration and the effect of increased stress on the cell's glycolytic capacity. FCCP can be used to uncouple the electron transport chain from Ox-Phos. This can be used to demonstrate the maximal respiration of a cell. Blocking Complex I and III using Rotenone and Antimycin-A inhibits mitochondrial respiration, and can be used to asses non-mitochondrial metabolism. Finally the 2-Deoxyglucose competes with D-glucose, and inhibits glycolysis which can be used to starve the cell of ATP.

1.5.1 Innate immune cell metabolism

Macrophages

The changes to immune cell metabolism to support immune function are exemplified well by the distinct metabolism of inflammatory and anti-inflammatory macrophages. Macrophages with an M1 phenotype, have been observed to switch their metabolic profile to favour glycolysis. In a similar way to the anaerobic glycolysis of hypoxic tumour cells, described by Otto Warburg [304], M1 macrophages utilise glycolysis as a fast source of ATP production [305] which permits macrophages to rapidly respond to infection. The TCA cycle is disrupted at two stages, releasing citrate and succinate. Citrate is required for fatty acid synthesis, nitric oxide and itaconate production whilst succinate promotes HIF-1α accumulation necessary for IL-1β expression [306]. The pentose phosphate pathway (PPP) is also utilised for the generation of metabolic intermediates [307] and nucleotide production. Furthermore, it generates nicotinamide adenine dinucleotide phosphate (NADPH) which is necessary to produce ROS and amino acids for production of cytokines [299],[308].

Anti-inflammatory M2 macrophages instead rely on the TCA cycle and then ETC. The sustained and efficient production of ATP through aerobic respiration preserves M2 macrophage viability and an intact TCA cycle provides metabolic intermediates required for biosynthesis [299]. Additionally, whilst M2 macrophages maintain the use of glycolysis to fuel the TCA cycle [298], fatty acid oxidation has been identified to be central to anti-inflammatory macrophage phenotype. Polarisation of macrophages with IL-4 was shown to activate STAT6 and PPARγ-coactivator-1beta (PGC-1β), necessary for the maturation of M2 macrophages and transition to a M2 metabolic profile.

Dendritic cells

DC activation requires a significant increase in metabolic activity to support cytokine secretion as well as processes required to degrade antigens for presentation. The stimulation of PRRs results in signalling via PI3K/Akt, resulting in an almost instant switch to glycolysis. Enhanced glycolysis is essential, with 2-DG completely blocking the generation of activated DCs [309]. Interestingly, the immunosuppressive cytokine IL-10 inhibits DC activation through antagonism of

this metabolic switch [310]. Despite this early spike in glycolysis, DCs continue to funnel pyruvate through the TCA cycle and OxPhos, in order to produce citrate. Citrate is required to fuel fatty acid synthesis which provides the building blocks to enlarge the ER and Golgi apparatus, facilitating increased protein production [311].

Tolerogenic vs immunogenic dendritic cells phenotypes depend more heavily on catabolic vs anabolic metabolism respectively [312]. PI3K/Akt signalling promotes mTOR activation shifting the metabolism towards a more "Warburg" phenotype which supports various inflammatory responses, for instance the secretion of pro-inflammatory cytokines. The increased reliance on glycolysis also allows cells to survive despite the inhibition of OxPhos by NO, which is produced in high amounts by surrounding macrophages during inflammation[313].

The antagonism of mTOR re-directs the metabolic output towards catabolic pathways to enhance the generation of ATP. Signalling via AMPK has been demonstrated to negatively regulate TLR-dependent activation and responses such as the expression of IL-17 functioning as a pathway for promoting tolerance [314]. As such, rapamycin has been investigated for its capacity to enhance the differentiation of tolDC and subsequently T-reg generation [315]. Another catabolic mechanism which has been found to modulate tolerogenic DCs , is fatty acid oxidation (FAO) which is upregulated by signalling via the Wnt/β-catenin pathway [309].

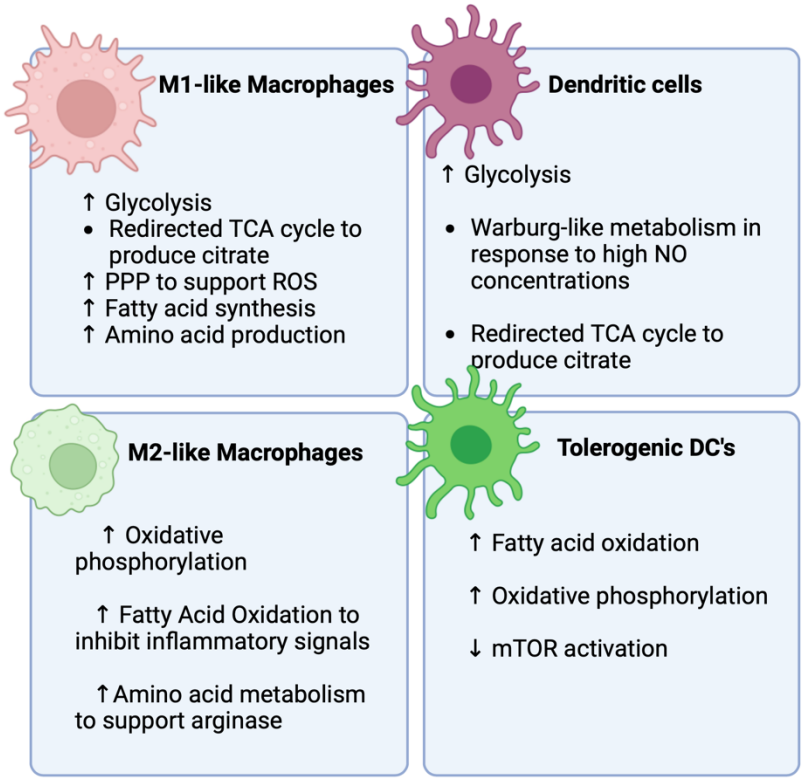

Figure 1.5.1 A. Schematic summary of the immunometabolism of differentially activated innate immune cells.

1.5.2 Adaptive immune cell metabolism

T-cells

The metabolic requirements of T-cells vary drastically depending on their activation state whether they are naïve or activated towards T-effs, T-regs or differentiated to memory cells. Prior to activation, naïve T-cells remain quiescent, producing only the basal levels of ATP, from glycolysis and OxPhos, to sustain functions for survival. During activation, T-cells have a heightened requirement for glucose which is especially paramount in the generation of Th1/Th2/TH17 cells as well as $CD8^+$ cells [299, 316]. Whilst glycolysis was not shown to be required for survival or even proliferation, it was fundamental to regulate gene expression and production of IFN_γ [317]. Despite the enhanced reliance on glycolysis for the generation of ATP, OxPhos is maintained at basal levels, particularly for production of reactive oxygen species and IL-2 production which are dependent on ECT [318]. Proliferative T-eff cells are highly metabolically active and, therefore, revert to OxPhos not only for increased ATP demand but also to synthesise the building blocks to generate

daughter cells. This requires a spike in fatty acid synthesis (FAS) and protein synthesis [319, 320]. The TCA cycle is upregulated and to fuel the cycle, glutamine is converted to alpha-ketoglutarate. The requirement for glutamine increases drastically resulting in an increase in glutamine transporters as well as glutaminolysis [321].

The metabolism which regulates T-reg activation differs, with the spike in glycolysis being less evident and an increase in the oxidation of lipids such as palmitate. This metabolism is regulated by activation of AMPK signalling pathway, which antagonises mTOR signalling [322]. OxPhos not only supports the cells energy demands but ECT complexes have been found to be essential for the regulation of genes such as PD-1, TIGIT and FoxP3 [323, 324].

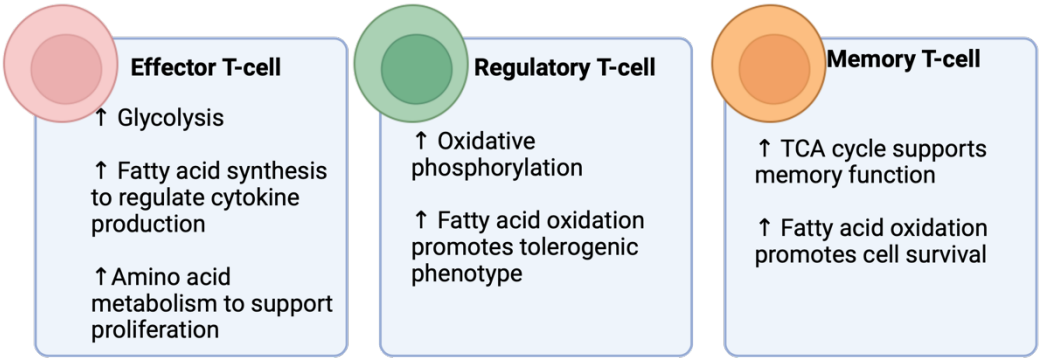

Figure 1.5.2 A. Schematic summary of the immunometabolism of effector, regulatory and memory T-cells.

1.6 Inflammation and resolution

Inflammation is often referred to as a double edged sword, being both indispensable to confer protection to the host against infection and damaged cells, but also being one of the principle drivers of chronic diseases. Risks to the host such as damage, infection or toxicity are recognised rapidly by early responding cells of the innate immune system. There is increased chemotaxis of immune cells to the site of danger, increased release of pro-inflammatory mediators, degradative enzymes, ROS and eventually activation of the highly specialised and targeted adaptive immune cells.

Once infection has been contained or the damage has been cleared, it is critical to dampen the highly inflammatory environment to prevent further tissue damage which can be caused by inflammatory mediators.

Immune resolution is an active co-ordinated task, which in healthy individuals, begins soon after the onset of inflammation [325, 326]. To begin curbing inflammation, pro-resolving mediators are produced which trigger fundamental steps towards resolution such as immune cell apoptosis and the regulation of chemokines and cytokines (Figure 1.6 A). These mediators include lipid-derived mediators such as resolvins, protectins, lipoxins and maresins, as well as protein-derived mediators such as annexin A1 and adrenocorticotropic hormones [327]. A large proportion of activated myeloid cells and lymphocytes either undergo apoptosis and are efferocytosed by macrophages, or migrate out of the tissue [328]. In addition the recruitment of immune cells wanes as the chemotactic gradient diminishes. This is particularly crucial to reduce the number of migrating neutrophils, as they carry out noxious inflammatory functions, which cause tissue damage and perpetuate inflammation [329]. Chemokines are either proteolytically cleaved by MMPs or sequestered by decoys, interceptors, scavengers, or chemokine-binding proteins [330,331]. Macrophages are prompted to switch to an anti-inflammatory state which results in the secretion of highly immunosuppressive cytokines; IL-10, TGFβ and IL-1Ra. This production of anti-inflammatory cytokines has a positive feedback effect, promoting the polarisation of further anti-inflammatory macrophages [10]. If tissue damage occurs, resolution of the inflammatory phase allows for regenerative mechanisms to take place. This involves the regeneration of damaged extracellular matrix (ECM) to support cells and re-vascularization [332,333,334,335]. In this anti-inflammatory state, macrophages secrete growth factors such as TGF-β and VEGF which results in increased infiltration of fibroblasts to the site of the wound as well as differentiation of fibroblasts to myofibroblasts, both essential for ECM fabrication [336, 337].

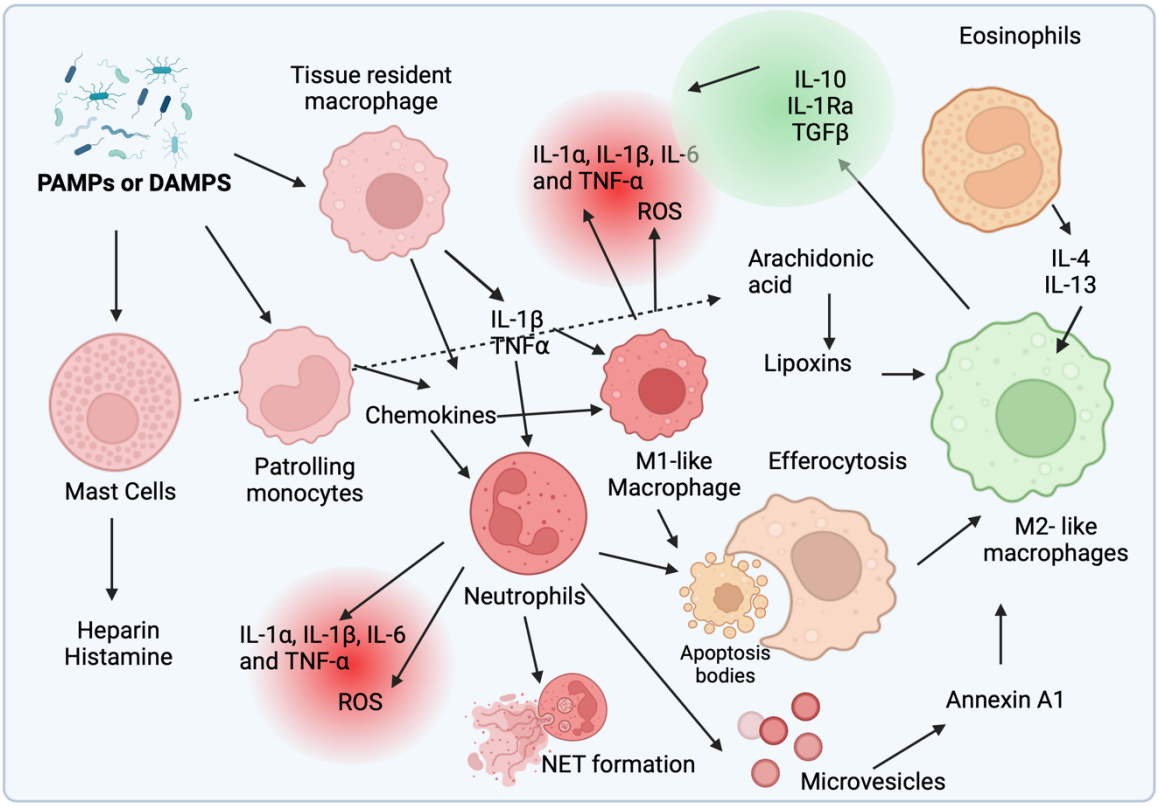

Figure 1.6 A. Schematic of the key players in inflammation and resolution. Tissue resident macrophages, patrolling monocytes and mast cells respond to PAMPs and DAMPs, which trigger downstream intracellular signalling pathways such as NFκB and interferon signalling. In response they secrete chemokines which recruit monocytes, circulating macrophages and neutrophils. The recruitment and extravasation of immune cells is facilitated by histamine which dilates blood vessels. The early production of pro-inflammatory cytokines such as IL-1β and TNFα activate macrophages and neutrophils to take on an inflammatory phenotype characterised by increased pro-inflammatory cytokine secretion and ROS, as well as formation of NET's from neutrophils. These responses perpetuate the inflammatory environment. Resolution is usually initiated early on after the inflammation is initiated to mitigate the positive feedback loop of inflammation. As immune cells in the environment undergo apoptosis, macrophages begin to efferocytose, promoting an immunosuppressive phenotype. The production of pro-resolution molecules such as Lipoxins and Annexin A1, as well as IL-4/13 from eosinophils, helps to further modulate M2-like anti-inflammatory macrophages. The production of anti-inflammatory cytokines IL-10, IL-1Ra and TGFβ dampens inflammatory cell functions and mediators.

1.6.1 Chronic inflammatory diseases and the role of macrophages

Dysregulation of any of the pro-resolving steps involved in the highly concerted resolution phase can lead a positive feedback loop in pro-inflammatory responses, creating a state of uncontrolled inflammation. In extreme cases, uncontrolled

inflammation can cause cytokine storm, which underlies life-threatening conditions such as acute respiratory distress syndrome (ARDS) and sepsis [338, 339]. However, chronic inflammation is usually low grade unresolving inflammation, which is not acutely life-threatening but can worsen over time as a result of the extensive tissue damage. This type of chronic inflammation underlies various pathologies including cardiovascular diseases (CVD), atherosclerosis, Type 2 Diabetes (T2D), chronic non-healing wounds and cancer, which put together, make up 50% of all deaths worldwide [340,341]. Worryingly the prevalence of chronic inflammation is only rising, due to an ageing population, increased rates of obesity, exposure to pollutants and inflammatory diets [340]. Two major immune cell culprits which promote chronic inflammation are neutrophils and macrophages, as a result of their integral role in recognising a diversity of PAMPs and DAMPs, initiating inflammation as well as immune resolution. As such, the levels of activated macrophages and neutrophils, as well as the levels of inflammatory mediators produced by these cells are commonly used to predict and diagnose disease [342, 343].

As discussed in section 1.1.2, macrophages can take on a plethora of activation phenotypes depending on their environment. A disadvantage of this plasticity in the dysregulated activation of the wrong macrophage phenotype at the wrong time. However, it also provides an advantage for therapeutic approaches to target macrophages to direct the polarisation of appropriate phenotypes. At homeostasis the ratio between macrophages which have an inflammatory and anti-inflammatory phenotype is relatively equal, but this increases in response to inflammatory stimuli[344]. Macrophages respond to a plethora of PAMPs and DAMPs as well as inflammatory cytokines. In response, to pro-inflammatory cytokines, activated macrophages relay this positive feedback loop, enhancing the secretion of IFN_{γ}, IL-6, IL-1 and TNFα, and IL-12 [344]. In addition, activated macrophages are a source of chemokines such as cysteine X cysteine ligand 1 and 2 (CXCL1/2), C-C motif chemokine ligand 2 (CCL2) and IL-1α and can also produce GM-CSF, G-CSF and TNF-α which extends their own lifetime, but also that of neighbouring cells and neutrophils [345,346]. The consistent pattern of macrophage recruitment and activation towards an inflammatory phenotype can result in a non-resolving cycle of chronic inflammation which can be perpetuated by chronic low-grade infection and damaged tissues which release DAMPs. The generation of DAMP's can also be

aggravated by superoxide species and degradative enzymes; MMPs and proteases, which can perpetuate further tissue damage [343,347]. The pathology of diseases such as; as colitis, arthritis and T2D is commonly as a result of this chronic tissue damage caused by inflammation.

1.6.2 Auto-immunity

Auto-immunity arises as a result of aberrant activation of T and B cells specific to an antigen which is expressed on the host's own tissues. Auto-reactive Th1, Th17 and $CD8^+$ cytotoxic cells cause significant tissue damage by exerting the functions usually aimed at containing and killing a foreign entity. Additionally, the secretion of auto-antibodies by B-cells amplifies the targeting of tissue components by both adaptive and innate immune cells [348, 349]. This tissue damage underpins the pathology of auto-immune diseases, which compromises the tissues functionality and can result in complete loss of function of tissues and entire organs. Auto-immune diseases can affect all tissue types even immune-privileged tissues such as the CNS. The underlying cause of auto-immunity to a self-antigen is complex and differs between each condition, normally progressing gradually [349]. However, they can arise as a result of a genetic pre-disposition and environmental stimuli, such as infection, tissue damage, pollutants, diet and the dysbiosis of the gut microbiota [349, 350, 351].

The generation of auto-reactive T-cells requires two steps; i) the presentation of a self-antigen by an APC which can provide adequate co-stimulatory molecules, and ii) the activation of T-cells by engagement of an auto-antigen presenting APC (Figure 1.6.2) [1]. Exposure to underlying inflammatory stimuli, for instance during infection, tissue damage or chronic inflammation can result in the DC maturation, resulting in the successful activation of T-eff cells against an antigen which does not pose a risk to the host. [1]. Alternatively, DCs might erroneously recognise self-antigens as foreign, for instance when antigens have been modified and can activate PRRs or antigens which are found in the wrong anatomical location; ie intracellular components or antigens which belong in immune privileged tissues. Furthermore, pathogens can produce self-antigen mimetic proteins which are able to activate DCs [1, 352, 348, 83].

TCRs which have a high affinity to a self-antigen are usually removed during clonal selection, however the system is not foolproof. Auto-reactive T-eff cells can persist and expand, especially in cases where peripheral tolerance mechanisms are dysfunctional. For instance, T-regs have been shown to have reduced stability and suppressive activity in diseases such as rheumatoid arthritis (RA), Type 1 Diabetes (T1D) and multiple sclerosis (MS) [353, 354,355,356]. In addition, even despite the generation of T-regs to counteract the function of T-eff cells, auto-reactive T-eff cells can become resistant or less sensitive to T-reg immunosuppression [357].

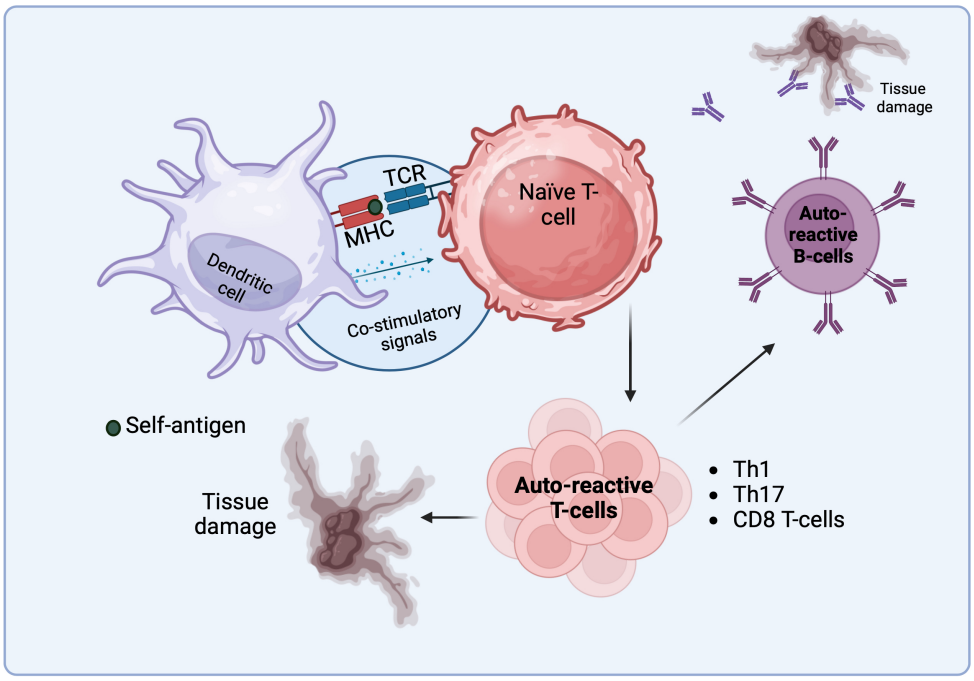

Figure 1.6.2 A. Activation of auto-reactive T and B-cells. The activation of auto-reactive T-cell subsets requires an APC presenting a self-antigen which can provide adequate co-stimulatory signals to activate a naïve T-cell which has a complementary TCR. Auto-reactive T and B-cells promote tissue damage which underlies the pathology of autoimmune diseases.

The development of auto-immune conditions is usually multi-factorial and a single cause, is usually impossible to isolate. It is likely that over time numerous events occur, whereby the normal function of central and peripheral tolerance are compromised, increasing the likelihood of the generation and expansion of auto-reactive T and B-cells. If the immune system is unable to restore homeostasis, either due to chronic inflammation, genetic mutations in key tolerogenic mechanisms, or dysregulated immune signalling, a positive feedback loop can emerge, with more tissue damage accelerating the expansion of auto-reactive cells [348].

1.6.3 Anti-inflammatory cytokines

Anti-inflammatory and pro-resolution cytokines play a crucial role in interfering with pro-inflammatory cytokines and inflammatory cell types. This is usually associated with cytokines such as IL-4, IL-13, IL-10, IL-1Ra and growth factors such as TGFβ. The classification of pro vs anti-inflammatory cytokines, however, is not black and white and a number of pro-inflammatory cytokines can also aid in inflammatory resolution. Similarly, a number of anti-inflammatory cytokines can promote inflammatory cell activation. Two of the cytokines which were explored in this work for their anti-inflammatory capacity are IL-1Ra and TGFβ and will be discussed below in more detail.

IL-1Ra

Dysregulated signalling by the pro-inflammatory members of the IL-1 cytokine family; IL-1α, IL-1β, IL-18, IL-33 and IL-36α, β and γ, has been implicated in driving pathological inflammation in a variety of disease. Their activity is highly upregulated in the majority of chronic inflammatory conditions and auto-immune diseases such as systemic sclerosis and RA [358, 359, 360, 361]. In fact, the dysregulation of IL-1 signalling is one of the main driving forces in systemic fever and cytokine-storm syndrome, life-threatening conditions which can cause systemic and severe tissue damage [362,338]. As a result, IL-1 signalling is tightly controlled. For instance, IL-1β requires two signals, usually modulated by TLR ligation, and a stimulus which activates the inflammasome. IL-1β is expressed as a the inactive precursor, which is proteolytically cleaved by caspase 1 in order to be become activated and secreted from the cell [363]. Once in circulation, the production of IL-1 cytokines is usually accompanied by a significant spike in the production of the antagonistic IL-1Ra, which competitively binds to IL-1 receptor I (IL-1R1), to negatively regulate the effect of IL-1. In fact, IL-1Ra can be secreted at 100-fold greater concentrations than IL-1β [358, 363, 364]. However, despite these controls, dysregulated IL1-driven inflammation can occur as a result of an imbalance in the ratio of IL-1/IL-1Ra. This can be caused by certain polymorphisms of IL-1 or IL-1Rn, genetic mutations of IL-1Ra or regulators of the inflammasome [365,366,367].

IL-1Ra exists as two isoforms, the secreted IL-1Ra form which is produced by activated macrophages and dendritic cells and the intracellular form (icIL-1Ra)

which lacks a signal peptide and is normally found in the cytosol of keratinocytes, only being released during cell death to regulate IL-1α [368]. From here on in, the secreted form will be referred to as IL-1Ra.

There are 10 identified IL-1 receptors with IL-1R1 being the main receptor which is bound by IL-1α and β. In order to exert downstream signalling, IL-1R1 must dimerise with IL-1R3. However, binding of IL-1Ra to IL-1R1 induces a conformational change in the receptor which prevents this IL-1R1-IL1R3 dimerization and downstream signalling [360]. The importance of the IL-1Ra regulation on IL-1α and β signalling can be exemplified by mouse models lacking IL-1Ra, which develop a plethora of auto-immune conditions and developmental issues [369,359,370,371].

The antagonistic capacity of IL-1Ra has, therefore, been extensively investigated as a method to restrict aberrant IL-1 signalling in disease states. The drug, Anakinra was developed as a recombinant version of IL-1Ra. It has been approved as a therapeutic approach to manage dysregulated IL-1-mediated inflammation in RA, Cryopyrin-associated periodic syndromes, familial Mediterranean fever, and Still's disease [372]. However, systemic blockade of IL-1 signalling (e.g. with IL-1Ra/Anakinra) puts the host at risk of opportunistic infections and can affect distal tissues. To improve tissue targeting, particle encapsulation of IL-1Ra has been explored, as well as methods of promoting the expression of IL-1Ra from immune cells [373,374].

TGFβ

Almost all cells in the mammalian body are receptive to the pleiotropic cytokine; TGFβ [262]. It takes part in the development, maintenance and homeostasis of various tissues, notably; the skin, connective tissue, cardiovascular tissues and bone. Its multi-faceted nature also means that if the signalling axis is dysfunctional it can be the driving force of diseases such as fibrosis and cancer [375, 232]. On the other hand, the diminished activity disrupts immune homeostasis, particularly in the regulation of adaptive immunity, and mice lacking TGFβ succumb to significant and spontaneous auto-immune disease [126]. The TGFβ family encompasses TGFβ1, 2 and 3 (referred to herein as TGFβ unless otherwise stated) bone morphogenetic protein (BMP), growth and differentiation factors (GDFs),

activins, Anti-Mullerian hormone (AMH) and three antagonists; Inhibin, Lefty 1 and Lefty 2 [262].

In order for the TGFβ to become bioavailable as a ligand for one of its receptors, LAP needs to be removed from the latent TGFβ-complex. Two major mechanisms have been identified to modulate the activation of TGFβ, via thrombospondin1 (TSP1) or integrins which contain the αv dimer. The adhesive glycoprotein TSP1 activated TGFβ via an exposed peptide sequence; KRFK, which has complimentary binding to the LSKL motif on LAP. Binding facilitates the mechanical dissociation of LAP from active TGFβ. However, the activation of TGFβ by integrins is far more significant. This is covered in detail in section 1.3.4.

Dysregulation of the TGF-axis has been associated with various inflammatory conditions, allergies and auto-immunity [127]. TGFβ deficit results in dysregulated T-reg generation which compromises tolerance towards innocuous antigens [127]. This is particularly notable in mucosal tissues due to the high prevalence of innocuous "foreign antigens" expressed by microbiota and food antigens. What's more, dysfunctional TGFβ signalling has been associated with increased infiltration of inflammatory cells, even in pathogen free conditions [376]. Wound closure is also delayed or can even become chronic due to persistence of inflammatory immune cells and delayed onset of cutaneous regeneration [262]. On other hand, TGFβ can also be detrimental due to its involvement in modulating cell proliferation fibroblast regulation, tissue remodelling and angiogenesis [262, 375, 377, 378]. The effect of TGFβ signalling is context dependent. For instance, whilst it is crucial for promoting the regenerative phase of wound healing, if TGFβ signalling persists it can promote over-proliferation of keratinocytes which lead to the development of hypertrophic scars [379]. In some cancers, TGFβ can act as a tumour suppressor in early stages by inhibiting cell proliferation and apoptosis of differentiating cells, however, in the later stages of tumour development it can progress tumour invasion and metastasis [380].

1.7 Polymeric particles for immunotherapy

Nano and micro-particles are used for various clinical applications, most notably for drug delivery due to the ease of tuning properties to enhance tissue targeting, controlled drug release and crossing biological barriers such as the blood-brain

barrier [381,382]. Drug encapsulation improves the safety of administering certain cytotoxic drugs, decreases the risk of side effects and improve the stability of bioactive components [383,384,385]. The use of synthetic biodegradable polymers has been favoured over non-degradable metal, silica and carbon based structures, due to their superior safety profile and clearance from the body over time [386]. The rate of biodegradation can also be adjusted, to design particles with specific drug release kinetics. Over the last two decades nano and micro-particles have been investigated for various immunotherapeutic applications from treating auto-immune diseases to enhancing the efficacy of vaccines [387,388]. The capacity to customise shape and size of particles as well as decorate their surface with chemical moieties, proteins and carbohydrates has allowed researchers to design pathogen-mimetic particles and artificial APC to activate and educate the immune system. For instance, artificial antigen presenting particles, decorated with co-stimulatory molecules on their surface have been designed to direct the *in-vivo* activation of T-regs [389,390,391], and T-eff cells [392, 393]. Immunomodulatory drugs, such as polarising cytokines can also be encapsulated within particles, to enhance desired outcomes [382,391, 394,395,384].

In this section, the influence of particle features on immune cell responses and how this can be harnessed to design the next-generation of particle based therapies for chronic inflammation and auto-immunity will be discussed.

1.7.1 Particle phagocytosis

The physico-chemical properties of particles can affect the mechanism of uptake, the time taken to engulf a target and even the activation of immune signalling pathways. Research into how phagocytes internalise particles, has demonstrated that size, charge and shape are major determinants in directing immune cell responses and the early interactions between particle and cells are likely fundamental in activating mechano-sensors and initiating downstream signalling resulting in immune polarisation.

Size plays a significant role in the mode of uptake [396]. Particles diameter below 100nm are usually taken up in a non-selective manner through pinocytosis, which has been termed “cell drinking”. Nanoparticles in the range of 100 nm up to 500 nm, which are suspended in fluid are non-selectively captured in small endosomes, created by invagination of the plasma membrane [397]. These are

formed by the assembly of coat proteins such as clathrin and caveolin into pits within the plasma membrane which bud off into the cell cytosol. The endocytic lattice formation is only capable of surrounding particles up to 500 nm, thus larger particles rely on uptake mediated by actin rearrangement [398,396]. Particles between 0.5 and 10 μm in size are internalised by phagocytosis, with particles of 2-3 μm being internalised most efficiently [399]. Phagocytosis requires substantial actin rearrangement as well as remodelling of lipids in the plasma membrane. This allows the membrane to protrude out and encapsulate the particles which are then transported into the cell in specialised vesicles called the phagosome. Upon entering the cell, the phagosome undergoes fusion with endosomes and lysosomes which mediate the degradation and recycling of the ingested material [400]. Indigestible foreign bodies which are too big to be phagocytosed, can elicit frustrated phagocytosis which drives chronic inflammatory responses such as the secretion of ROS, degradative enzymes and IL-1β production. [401]. Additionally, a foreign body response may occur as a means to isolate the material. This is characterised by macrophage fusion to create foreign body giant cells (FBGCs) which continue to release inflammatory and degradative mediators [402].

The uptake rate of particles by phagocytes is largely related to geometry and can vary from cell type to cell type. Aspect ratio and orientation of a particle are the biggest influencers in the rate of phagocytic uptake. Aspect ratio is the ratio between the width and height of a particle, giving a quantitative value to the elongation of a particle. Particles with an aspect ratio of 1 (spherical), are more readily phagocytosed [399] . The orientation of initial contact between the phagocyte membrane and particles with an aspect ratio greater or smaller than 1 (for example rod shaped, and epsilonic particles) also determines the ease at which it can be phagocytosed. As the surface area which the phagocyte must envelope increases, the rate of phagocytosis decreases [403]. The ability of a particle to trigger inflammasome activation has also been linked to high aspect ratio and needle shape, crystalline or irregular spiky particles are more likely to destabilise or rupture the membrane of lysosomes and phagosomes [404,405,406,407,403]. Similarly, rough surface topography, hydrophobic and anionic particles have been observed to be more proficient in causing membrane disruption required for inflammasome activation [408,409, 410]. As such, these particles offer potential as conventional vaccine adjuvants.

1.7.2 Influence of particle physico-chemical properties on immune responses

An interesting theory which has been proposed to explain the differential immune response to particles which lack PRR ligands is that evolutionarily, immune cells have adapted to recognise pathogens based on physical attributes such as size, shape and charge in order to better respond to new threats [411,412]. Whilst it is not fully understood how immune cells sense size and shape, it is plausible that mechano-sensors are activated and the cytoskeleton is rearranged during the early particle-cell interactions. The method of ingestion and time it takes for a phagocyte to take up a target can also determine the type of antigen presentation and subsequently the type of adaptive responses that are induced [413].

For instance, small nanoparticles, which are taken up by endocytosis, have been demonstrated to activate the NLRP3 inflammasome and Gasdermin-D mediated pyroptosis. These mechanisms promote cellular immunity required to protect the host from nano-sizes viruses [412,414, 411,415]. On the other hand, bacteria, parasites and fungi tend to be in the micron range and necessitate strong innate immune responses, humoral immunity and Th1/Th2/Th17 responses. To reflect this, particles in this size range of 200 nm – 1 μm tend to favour Th2 T-cell activation, enhance IL-4 cytokine secretion and are easily phagocytosed by macrophages [412,415,416]. Indeed, the alum adjuvant formulation; alhydrogel forms aggregates which have a mean size range of 1-3 μm , and whilst it is capable of promoting robust humoral immunity, it has a more limited capacity to promote antigen-specific cellular immunity [417].[418].

However, this theory is challenged by conflicting reports of the effects of particle size on immune responses [412]. This variability across literature could arise from the failure to maintain reproducible controls or differences in specific properties of the particles and vaccine schedules such as; particle shape, particle stiffness, charge, route of administration and antigen load, as well as in some cases endotoxin contamination [419],[420], [421,422,399,423,405,424,425]. In order to obtain a clearer understanding of how the immune system, primarily APCs, respond to particle size, studies need to be carried out where size is the only variable.

1.7.3 Particle-based drug delivery vehicles or immunomodulators

Approaches to improve treatment for chronic inflammation

Anti-inflammatory drugs and steroids are the mainstay treatment for chronic inflammation. Biological therapies such as neutralising antibodies; infliximab, tocilizumab, adalimumab and anakinra are also used in more severe inflammatory conditions, however, they are expensive and can supress the immune responses required for pathogen defence [426]. To overcome this, particle encapsulation has been explored which can provide safer, more targeted and more effective immunosuppression at a site of chronic inflammation. For instance there is interest in identifying novel methods to specifically target macrophages, due to their role in driving chronic inflammation [17,427,428,423]. This was demonstrated in the design of microparticles decorated with the fragment antigen binding (fab) portion of the F4/80 antibody and encapsulated TNF-α siRNA. The microparticle cargo was preferentially delivered to macrophages and enhanced the efficacy of the siRNA in promoting immunosuppression [429]. The ability to engineer particles with specific properties to direct biodistribution, release kinetics and cell targeting offers an exciting new approach to improving existing anti-inflammatory drugs. Additionally, the inherent immunomodulatory properties of some particles can be harnessed to design “smart-biomaterials” which augment anti-inflammatory responses through their interactions with immune cells.

Approaches to enhance peripheral tolerance using particles

The lack of specificity in targeting auto-reactive cells is also a significant issue with the current approaches taken to treat auto-immune diseases. Instead, global immunosuppressants, anti-inflammatory drugs and steroids are commonly used to dampen the overall inflammation perpetuated by the immune system, to mitigate tissue damage and offer symptom management. Not only can this put the individual at risk of infection but the long-term use of steroids and immunosuppressants are commonly associated with a high burden of side effects, making them an unfavourable option for symptom management [430]. The ideal approach to mitigating the effect of auto-reactive T-cells is thought the promotion of the body’s own peripheral tolerance. The expansion of antigen-specific T-regs can disrupt

auto-immunity and restore homeostasis, however, there is currently no approved, or effective approached to expanding antigen specific T-regs *in-vivo*.

Due to their role in directing T-cell activation, DCs are the primary target for directing T-reg expansion. In particular, TolDCs can direct the activation of T-regs or can induce anergy of auto-reactive T-cells. Additionally, they can contribute to tolerance by secreting anti-inflammatory cytokines; IL-10 and TGFβ, and metabolic modulators which dampen the immunogenicity of adjacent DCs such as heme-oxygenase-1 (HO-1) [431]. In general tolDCs have been characterised as "semi-mature" expressing low levels of co-stimulatory cell surface receptors, enhanced expression of inhibitory receptors; PDL-1 and inhibitory Ig-like transcripts (ITLs) and secretion of anti-inflammatory IL-10, TGFβ and IL-35 [106, 432, 433, 434].

Two strategies which have been explored to enhance tolDC, to mitigate auto-immunity, are; *ex-vivo* generation of antigen-specific tolDCs, or in-vivo DC targeting [435]. Over the last decade, the autologous transfusion of ex-vivo generated antigen specific tolDCs has been actively pursued as a therapeutic approach to treating auto-immunity. However, there is growing interest in using nanoparticles to promote antigen specific tolDC induction in-vivo, which can overcome some of the limitations of cell-based therapy, such as; safety concerns, cost, feasibility of isolating autologous DCs and efficacy of cell transfusion [436, 437]. Nano and microparticles with a diameter below 20 μm can easily be taken up by phagocytic cells and have, therefore, been investigated as delivery vehicles which improve the safety and targeted delivery of antigen and tolerising agents [437]. Table 1.7.3 A summarises some of the nano and micro-formulations which have been investigated to treat auto-immune diseases.

Material	Size (nm)	Therapeutic cargo	Disease target	Outcomes	Ref
Phosphatidylserine + Liposome	1000	Insulin A and B peptides	T1D	Enhanced tolDCs and impaired auto-reactive T-cell proliferation in mouse models and reduced insulitis.	[438]
PLGA and polylactide	500	OVA +PLP	MS	High molecular weight PLGA ameliorated EAE symptoms in mice and increased the accumulation of immune cells to the spleen rather than CNS.	[439]
PLGA and polylactide	500	OVA + PLP	MS	Induced long term T-cell tolerance from EAE in mice. MARCO-expressing macrophages and T-regs were found to be crucial for inducing tolerance.	[389]
PLGA	Not stated	PLP + Rapamycin	MS	Enhanced tolDCs, B-cell tolerance and T-regs in mice providing protection against EAE.	[440]
Gold	60	MOG + ITE	MS	Enhanced T-regs in mice and supressed the development of EAE.	[441]
Gold	60	Pro-insulin peptide + ITE	T1D	Enhanced tolDCs and Tregs by inhibiting NFκB. Supressed auto-immune T1D in mice.	[442]
PLGA	1000-30,000	VitaminD3, insulin B-peptide, GM-CSF, TGFβ1	T1D	Prevented T1D onset in non-obese diabetic mice (NOD) when administered s.c at 8 weeks. An enhancement in antigen specific $CD4^+$ and $CD8^+$ T-regs was shown.	[443]
PLGA	200	MOG + IL-10	MS	Prevented and reversed EAE in mice.	[444]
PLGA	1000-1800	CD40,CD80,CD86 oligonucleotides Note; no antigen used	T1D	Reversed hyperglycaemia in newly-onset diabetic mice. Enhanced antigen-specific T-regs in the lymph nodes.	[445]

Table 1.7.3 A. Particle-based therapies investigated to promote TolDCs in animal models of auto-immune disease. Myelin proteolipid protein (PLP) , Myelin oligodendrocyte glycoprotein (MOG), 2-(1*H*-Indol-3-ylcarbonyl)-4-thiazolecarboxylic acid methyl ester or Aryl hydrocarbon receptor ligand (ITE).

To re-iterate, identifying the ideal physico-chemical properties of particles to obtain desirable responses is a crucial aspect to their design. Properties such as size,

shape, charge and surface modification can improve the targeting of particles to DCs, either in the periphery or lymphoid organs. For instance, the mechanism of particle uptake differs depending on size, and this can have an effect on whether it is transported into the cell via endosomes or directly to the cytosol [397, 396]. Furthermore, size is crucial for trafficking to the lymph nodes and it has been established that nanoparticles must be <200 nm in size to freely drain to these sites. Larger particles enter the lymph nodes, but only within migratory DCs which have engulfed the particle in the periphery [446]. This has an impact on the targeting of specific DC subtypes and their proximity to naïve T-cells [447].

There has been growing evidence to demonstrate that DCs can sense particle size, as well as shape, and infer information from these attributes. For instance DCs produce more pro-inflammatory cytokine and greater antibody titres when incubated with rod-shaped gold particles, over spherical particles [407]. Nanoparticles with sharp or spiky surfaces have also been shown to be more inflammatory, due to increased lysosomal damage when internalised [405, 399]. These examples only cover of few of the ways that physico-chemical properties of particles can be tuned to target specific tissues, cell types and intracellular compartments [437]. Understanding how these physico-chemical properties direct immune responses will therefore be highly beneficial to the growing field of DC-targeted nano-particle therapies.

1.7.4 Therapeutic vaccines for auto-immune diseases

The concept of vaccines is most commonly associated with conferring immunity to a certain pathogen-derived antigen, through education and induction of immune memory, in order to mount specific and robust immune responses when the immune system re-encounters that specific antigen. Building on this paradigm, vaccines could also be designed to educate the immune system to provide tolerance towards specific self-antigens. Tolerance promoting vaccines have been termed “inverse vaccines” and could present an attractive approach to treating and preventing the generation of auto-immune diseases in an antigen specific manner [436, 448]. Various approaches have been investigated including DNA/RNA vaccines, antigen alone or modified antigen vaccines and particle-based vaccines. Most of

these approaches have been explored in animal models with a few reaching clinical testing [449, 450].

The main component for inverse vaccines is a specific antigen, which in the disease setting is known to activate autoreactive T-eff cells. Some antigens have been identified in MS, T1D and RA, however, there is still a significant lack of known antigens for a variety of diseases, and those antigen which are known, can still vary between individuals [451,348, 452]. The challenges in identifying appropriate antigens is one of the rate-limiting step in developing a "one fits-all" inverse vaccine against specific auto-immune diseases.

Early studies looking at developing inverse vaccines, explored the efficacy of administering disease-specific antigens alone in a bid to promote tolerance. Research in the 1990s demonstrated that the administration of myelin peptides under homeostatic conditions could induce antigen-specific tolerance and supress EAE in mouse models. However, when the same peptides were administered in an inflammatory setting, mice demonstrated significantly worsened EAE symptoms [453, 454]. Various clinical trials using myelin specific protein vaccines, have been conducted with some being demonstrated to be safe yet with low efficacy (NCT00468611), and other promoting significant disease progression (NCT00001781).The risk of activating auto-reactive T-eff cells with the administered antigen raises significant safety concerns, and contributes to the challenges for designing inverse vaccines.

In order to overcome the risk of promoting further auto-immunity towards an antigen, inverse vaccines also need to promote and maintain a tolerogenic environment. The main APC target for inverse vaccines are DCs due to their integral role in activating naïve T-cells. The goal of inverse vaccines would, therefore, be to prime tolDCs to either promote antigen-specific T-cell anergy or T-reg expansion. In the same way adjuvants are used to enhance and direct immune response in conventional vaccines, "inverse" adjuvants could also be used to promote tolerogenic responses. To achieve this, the addition of pro-tolerogenic and anti-inflammatory agents to vaccine formulations has been investigated [455]. The table below (Table 1.7.4 A) summarises a few potential adjuvants which have been explored to improve tolDC polarisation and T-reg promotion.

Proposed adjuvant	Response	Reference
DEC-205 antibodies	DEC205 conjugated to antigens enhanced the targeting to DCs and promoted tolerance through auto-reactive T-cell anergy and apoptosis.	[456], [457]
IFNβ + Alum	IFNβ linked to antigen and alum supressed T-eff cell proliferation and indued T-reg expansion. This was found to inhibit the progression of EAE in mice and rats.	[458]
GMCSF	GM-CSF fused to antigen mediated enhanced T-regs and tolerance even in inflammatory settings. This provided prophylactic and therapeutic protection in EAE models.	[459]
TGFβ + Rapamycin encapsulated within PLGA particles	Enhanced tolDCs, B-cell tolerance and T-regs in mice providing protection against EAE.	[440]
S-antigen protein (SAg) of *Plasmodium falciparum*	Fusion of sAg and myelin protein provided protection from EAE through increased T-regs in an IL-10 and TGFβ dependent manner.	[460]
ITE	Encapsulation of immunosuppressive AHR ligand; ITE, in conjunction with MOG or pro-insulin peptide in gold nanoparticles promoted tolDC induction and increased anti-inflammatory cytokines. Prevented the induction of EAE.	[441], [442]
Mannosylated 60-80 nm liposomes	Mannosylated liposomes loaded with myelin basic proteins prevented EAE development in mice. It was found to be safe in human phase I clinical trials (NCT02283853), but increased active CNS lesion in relapsing remitting MS patients after 7 weeks.	[461]
Glycosylation of antigens	Glycosylation of various antigens including; deaminated gliadin peptide and β-lactoglobulin (BLG) promoted robust T and B cell tolerance and expansion of T-regs. A clinical trial (NCT04248855) found the KAN-101 glycosylated antigen to be safe and tolerable and is still ongoing to assess efficacy.	[462], [463], [464]
NFκB inhibitors; Curcumin, Bay11-7082 or quercetin	Supressed T-eff cells and induced antigen specific T-regs in arthritis mouse model.	[465]
Cholera Toxin B (CTB)	Orally administered CTB- insulin conjugates have been shown to protect NOD mice from development of diabetes by enhancing antigen specific T-regs.	[466]
Heat shock protein 60 (Hsp60), Diapep277	Enhanced antigen-specific T-regs in NOD mice and protected against T1D. Clinical trials have demonstrated its safety, and enhanced protection of β-cells, affording new-onset T1D patients with less insulin to control blood glucose.	[467]

Table 1.7.4 A. Inexhaustive summary of adjuvants which have been investigated as potential adjuvants which promote antigen specific tolerance.

Despite numerous anti-inflammatory and pro-tolerance adjuvants having been identified, very few have reached clinical trials. There is still a need to refine vaccine formulations which are safe, promote stable long-term tolerance and are efficacious in either preventing or treating existing disease.

The application of inverse vaccines has been proposed for both prophylactic and therapeutic settings. Although most auto-immune diseases are only diagnosed once symptoms arise, researchers are exploring the paradigm of pre-clinical autoimmunity, where auto-reactive antibodies or T/B-cells are present, despite no obvious symptoms [348]. This could provide a window of opportunity for early preventative vaccination regimes which could mitigate the slippery slope of auto-immune disease, or at least, mitigate tissue damage [468]. However, this would require robust methods of diagnosing pre-clinical auto-immunity. The ideal vaccination regime also need to explored in more depth. As made apparent by early experiments of vaccination with antigens alone, the delivery of antigens during a window of time where there is exacerbated inflammation can jeopardise the functionality of tolerance-promoting therapies [453,454]. Taking relapsing remitting MS as an example, it would likely be more efficacious to immunise during the remitting phase of the disease. As such, an additional challenge to devising efficacious inverse vaccines would require research into the ideal spatio-temporal vaccine regime to increase the likelihood of inducing robust tolerance [469].

The route of administration also needs to considered. Numerous routes of vaccination have been explored and can be dependent on the location of the disease. For instance intra-articular vaccination would allow tissue specific delivery of therapeutic cargo to treat RA, whilst a more systemic delivery options such as intravenous (i.v), subcutaneous (s.c) or intramuscular (i.m) routes might be required for diseases such as T1D, MS or systemic lupus erythematosus (SLE).

Mucosal vaccines have been proposed as an attractive approach which can enhance the efficacy of inverse vaccines by harnessing the inherent tolerogenic nature of mucosal tissues [470]. This is exemplified well in the tolerization of food antigens such as peanut allergies via the oral delivery of food-specific antigens [471]. Indeed, oral administration of PLGA-encapsulated type II collagen antigens, in mouse models of arthritis supressed the development of symptoms [472,473, 474]. The prospect of a vaccine to treat certain auto-immune disease could be a huge move in the right direction to offering patients specific, targeted, and potentially long term reprieve from the effect of auto-reactive adaptive immune cells [469].

1.7.5 Poly- lactic (co-glycolic acid) particles

Poly Lactic-co-glycolic acid, is a commonly used synthetic polymer for medical purposes. It is one of the few polymers to be FDA approved for medical use, due to its excellent bio-compatibility, non-toxic nature, biodegradability and tuneable properties [385]. Various commercially available medical products already contain PLGA including; meshes, hydrogels, sutures, sponges, orthopaedic fillings and microparticles [475] and very few side effects have been reported in response to the polymer [476]. PLGA is a co-polymer of poly-lactic and poly-glycolic acid, which can vary in its composition of lactic to glycolic acid monomers (Figure 1.7.5 A). Lactic acid and glycolic acid both exist as L and D stereoisomers, due to the asymmetric α carbon. The composition of a PLGA polymer can therefore vary in terms of the L and D enantiomers [477]. This affects the molecular weight of a given polymer and its crystalline or amorphous nature. PLGA polymers with 30-70% glycolic acid or high content of D-lactic acid are amorphous due to a more disordered polymer chain, whereas PLA alone is crystalline particularly in the presence of L-lactic acid [477] [422]. However, most commonly, PLGA is composed of a 50:50 ratio of each co-polymer.

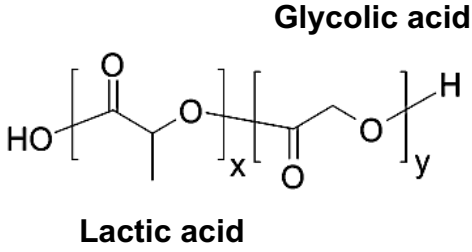

Figure 1.7.5 A. Molecular structure of PLGA. PLGA is composed of Poly Lactic and Poly Glycolic acid. X and Y is representative of the number of each co-polymer.

The clearance of implanted biomaterials has become a crucial aspect in biomaterial design to minimise adverse effects of prolonged exposure, particularly with regards to toxic breakdown products and the long term effect on immune cell activation. PLGA with a 50:50 ratio of each co-polymer has the fastest rate of degradation, however, this can be manipulated by increasing the crystallinity by adding hydrophobic lactic acid. PLGA degrades via enzymatic hydrolysis of the ester linkage formed between the polymers [478,479,385]. The breakdown products; lactic acid and glycolic acid, are endogenous metabolites which can be absorbed

by the body and broken down to release water and carbon dioxide via the Krebs cycle [480]. PLGA particles are the most commonly used for drug encapsulation [481] and can be made with varying diameter, porosity, composition and degradative kinetics, allowing targeted drug release. Particles can be easily fabricated due to their relatively hydrophobic nature, into a range of sizes from around 50 nm up to 500 μm in diameter [482,477,483]. In terms of drug delivery, different particle sizes may be more suitable to accommodate different cargo and may also determine bio-distribution and rate of drug release; important parameters for successful targeted drug delivery [477]

1.8 Hypothesis and Aims

The main hypothesis of this project is that PLGA particles in the 0.5-2 μm size range promote anti-inflammatory and pro-tolerance responses which make them the ideal particle size for therapeutic approaches to treat inflammatory conditions or as adjuvants for “inverse vaccines”.
The aims of the project are to;

- Investigate the response of innate immune cells to PLGA particles of varying sizes.

- Determine if PLGA particles in the 0.5-2 μm range can induce adaptive immune responses which promote antigen-specific tolerance.

- Identify the mechanism by which immune cells can respond to PLGA particles differentially based on size.

- Explore downstream signalling induced by PLGA particles in the 0.5-2 μm range .

Chapter II; Materials and Methods

2.1 Materials

2.1.1 General cell culture reagents

Reagent	Supplier
Roswell Park Memorial Institute 1640 (RPMI) Glutamax pH 7.2	Biosera
Dulbecco's Modified Eagle Medium (DMEM)	Biosera
Penicillin and Streptomycin (P/S)	Gibco
L-Glutamine (L-Glut)	Gibco
Foetal calf serum (FBS)	Biosera
Granulocyte-macrophage colony-stimulating factor (GMCSF)	Peprotech
Phosphate buffered saline (PBS)	Gibco
Trypan Blue	Sigma
Ethylenediaminetetraacetic acid (EDTA)	Invitrogen
Bovine Serum Albumin (BSA)	Fisher Scientific
β-Mecaptoethanol	Gibco
Sodium Pyruvate	Gibco
Non-Essential Amino Acids	Gibco
MEM vitamins	Gibco
Phorbol-12-myristate-13-acetate (PMA)	Sigma

Table 2.1.1 A. General cell culture reagents

Cell culture reagent	Composition	Cell Type
Complete RPMI (cRPMI)	500 mL RPMI 1640 supplemented with 50 units/ml Penicillin, 50 µg/ml Streptomycin and 10% FCS. For THP-1 culture, cRPMI was additionally supplemented with 0.001% β-mercaptoethanol.	Culture of BMDCs and THP-1 cells.
Complete DMEM (cDMEM)	500 mL DMEM supplemented with 2 mM L-Glut, 50 units/mL Penicillin, 50 µg/ml Streptomycin and 10% FCS.	Culture of BMDMs and L929 cells.
T-cell expansion cRPMI	500 mL cRPMI supplemented with 50 units/mL Penicillin, 50 µg/ml Streptomycin, 0.001% β-mercaptoethanol, 1% Sodium Pyruvate, 1% non-essential Amino Acids and 0.004% MEM vitamins.	Expansion of Splenocyte-derived T-cells.
Macrophage-colony stimulating factor (GMCSF)	Derived from the culture of L929 fibroblasts.	Differentiation of bone marrow derived hematopoietic stem cells to macrophages.
ACL (NH_4Cl) red blood lysis buffer	0.88g NH_4Cl was dissolved in 100ml of endotoxin-free water (H_2O) (Baxter) and filter sterilised with a 0.22 µm syringe- driven filter (Millipore).	Lysis of blood cells in bone marrow for the isolation of leukocytes.

Table 2.1.1 B Cell culture reagents prepared in house

2.1.2 Magnetic cell enrichment

Naïve CD4$^+$ T-cells

White blood cells were isolated from the spleen of OTII C57BL6 mouse strain. Naive T-cells were selectively isolated from the white blood cell suspension using the **MagniSort™ Mouse CD4$^+$ Naïve T cell Enrichment Kit** from Invitrogen.

2.1.3 Cell culture treatments

Cell treatment	Supplier	Final concentrations
Degradex™ PLGA particles (With an average diameter of; 0.2, 0.5, 1, 2, 10 or 20 µm)	Phosphorex	18.75- 300 µg/ml
Endo Grade Ovalbumin (OVA)	Hyglos	25 µg/ml
Human TGF-beta 1 (HEK293 derived)	Peprotech	25 ng/ml
Whole β-Glucan particles	Kerry Group	100 µg/ml
Recombinant murine Interleukin-13 (IL-13)	Peprotech	20 ng/ml
Recombinant murine Interleukin-4 (IL-4)	Peprotech	40 ng/ml
Recombinant murine IFNγ	BD Biosciences	50 ng/ml
Sucrose	Sigma	150 mM

Table 2.1.3 A Experimental cell treatments

2.1.4 Inhibitors and Antagonists

Inhibitor	Supplier	Target	Concentration tested
CD61 (Integrin beta 3) Monoclonal Antibody (2C9.G3)	ThermoFisher	β3	50 µg/ml
CD51 (Integrin alpha V) Monoclonal Antibody (RMV-7)	ThermoFisher	αv	50 µg/ml
Cilengitide	MCE	αvβ3, αvβ5, α5β1	250 µg/ml
Anti-mouse TGFβ 1,2,3 monoclonal antibody	R&D	TGFβ 1, 2 and 3	20 µg/ml
GsMTX4	Bio-Techne	Piezo1	1-10 µM
TRPV4 Antagonist I, RN-1734	Merck LifeSciences	TRPV4	10-50 µM
Rapamycin	Sigma	mTORC1	10 nM

Table 2.1.4 A Inhibitors and antagonists

2.1.5 Agonists

Agonist	Supplier	Target	Concentration tested
Yoda1	Merck Life Sciences	Piezo1	1-5 μM
α-PDD	Merck Life Sciences	TRPV4	1-10 mM
LPS from E. coli, Serotype R515 (Re) (TLRgrade™)	Enzo	TLR4	10 ng/ml
PAM3CSK44	Invivogen	TLR2/1	10 ng/ml
CpG Oligodeoxynucleotides (ODN) M362	Invivogen	TLR9	4 μg/ml

Table 2.1.5 A. Agonists used and their targets.

2.1.6 Flow cytometry antibodies

Antibody Target	Fluorochrome	Clone	Supplier	Vol/Sample (µl)
CD11b	PE	M1-70	Miltenyi	0.1
CD11b	PE-Cy7	M1-70	BD Biosciences	0.15
F4/80	PercP5.5	BM8	eBiosciences	0.4
CD11c	PE Cy7	HL3	BD Biosciences	0.1
CD11c	PE	M1-70	BD Biosciences	0.1
Ly6-G and L-6G (GR-1)	APC-Cy7	RB6-8C5	BD Biosciences	0.15
CD14	FITC	REA599	Miltenyi Biotech	1.3
β3	PE	REA761	Miltenyi Biotech	0.1
αv	FITC	REA181	Miltenyi Biotech	0.1
CD4	BV785	RM4-5	BioLegend	0.125
CD3	V500	500A2	BD Biosciences	0.2
CD25	PE	17A2	BioLegend	0.3
FoxP3	APC	FJK-16S	eBiosciences	0.2
Helios	Pacific Blue	22F6	BioLegend	0.5
Cell proliferation	Carboxyfluorescein Diacetate Succinimidyl Ester (CFSE)	N/A	Invitrogen	5 µM

Table 2.1.6 A Flow Cytometry antibodies.

Antibody Target	Fluorochrome	Supplier	Vol/Sample (µl)
Fixable Viability Stain V700	FVS700	BD Biosciences	0.5
Fixable Viability Stain 510	FVS510	BD Biosciences	0.5
Annexin V	FITC	MSC	1 µg/ml
PI-DNA intercalating agent	Propidium Iodide (PI)	ThermoScientific	1 µg/ml
Trypan blue	N/A	BD Biosciences	N/A
Crystal Violet	N/A	ThermoScientific	N/A

Table 2.1.6 B Cell viability antibodies and cell stains.

2.1.7 Enzyme linked immuno-sorbent assay (ELISA) kits and reagents

Cytokine	Species	Supplier	Capture antibody	Working Standard range pg/ml	Detection antibody
IL-10	Murine	Invitrogen	1/250 in PBS	32.25-4000	1/250 in 1% BSA
IL-10	Human	Invitrogen	1/250 Coating Buffer	4.6875-300	1/250 in ELISA Diluent
IL-1Ra	Murine	R and D systems	1/180 in PBS	156.25-10000	1/120 in 1% BSA
IL-1Ra	Human	Invitrogen	1/500 Coating Buffer A	31.25-2000	1/1136 in Coating Buffer B
IL-6	Murine	Biolegend	1/200 in sodium carbonate	7.8-500	1/200 in 1% BSA
IL-6	Human	Invitrogen	1/250 Coating Buffer	2-200	1/250 in ELISA Diluent
TNF-α	Murine	R and D systems	1/120 in PBS	31.25-2000	1/60 in 1% BSA
TNF-α	Human	Invitrogen	1/250 Coating Buffer	4-500	1/250 in ELISA diluent
TGF-β	Murine and Human	Invitrogen	1/250 Coating Buffer	15.625- 1000	1/250 in 1X ELISA Diluent

* 10 X Coating Buffer supplied by Invitrogen ELISA kits.
** 5X ELISA Diluent supplied as part of Invitrogen ELISA Kits.

Table 2.1.7 A. Sandwich ELISA antibodies

Reagent	Composition	Suppliers
Sodium Carbonate Buffer	4.2g $NaHCO_3$ and 1.78g Na_2CO_3 in 1L distilled H_2O, brought to pH 9.5.	Sigma
Coating Buffer A (Human IL-1Ra)	8.0g NaCL, 1.13 g Na_2HPO_4, 0.2 g KH_2PO_4, 0.2 KCl, in 1L brought to pH 7.4	Sigma
Coating Buffer B (Human IL-1Ra)	0.5 w/v BSA in Coating Buffer A with 0.001 Tween.	Thermo-Fisher
10X PBS Buffer	800g NaCl, 116g Na_2HPO_4, 20g KH_2PO_4 and 20g KCl in 10L distilled H_20 and brought to pH 7.2.	Sigma
PBS Wash Buffer	0.05% (v/v) Tween 20 in 1X PBS.	Sigma
Wash Buffer (Human IL-1Ra)	0.2 g KH_2PO_4, 1.9 g K_2HPO_4, 0.4g EDTA, 0.5ml Tween in 1.0L dH_2O	Sigma
Potassium Citrate Buffer	10.19g anhydrous citric acid and 14.6g Na_2HPO_4 in 1L distilled H_20 and brought to pH 5.5.	Sigma
o-phenylenediamine dihydrochloride (OPD) Substrate solution	OPD 0.4 mg/ml in Potassium citrate with 7 µl of H_2O_2 per 25 mL added as catalyst.	Sigma
Stop Solution	1M H_2SO_4	Sigma

Table 2.1.7 B. Additional ELISA reagents made in house

2.1.8 RNA isolation, cDNA synthesis and rt qPCR

RNA Isolation was performed using High Pure RNA Isolation Kit from Roche.

Reagent	Supplier	Final Concentration	Volume (µl)/Sample
Deoxynucleotide triphosphates (dNTPs)	Promega	2.5 mM/NTP	2.0
Reverse transcriptase buffer (5X)	Promega	1X	2.0
Random Primers 5'nnnnnn-3'/ Random hexamers	MWG Biotech	1µg/ml	0.5
Ribonuclease inhibitor (RNASEout)	Invitrogen	40 U/µl	0.25
M-MLV reverse transcriptase	Promega	200 U/µl	0.25

Table 2.1.8 A. Reagents for reverse transcription of RNA to cDNA.

Reagent	Supplier	Volume (µl)/Sample
Kapa SYBR®Fast qPCR	Kapa Biosystems	5
Nuclease Free dH_2O	Roche	1
Forward primer	Invitrogen	0.5
Reverse Primer	Invitrogen	0.5

Table 2.1.8 B. Reagents for rt qPCR

Gene target	RefSeq	Forward Seq 5'-3'	Reverse Seq 5'-3'
Tbp	NM_013684.3	CAGGAGCCAAGAGTGAAGAACA	AAGAACTTAGCTGGGAAGCCC
B2m	NM_009735.3	ATGGGAAGCCGAACATACTG	CAGTCTCAGTGGGGGTGAAT
Tgfb1	NM_011577.2	CATCCATGACATGAACCGGC	CTTCTCTGTGGAGCTGAAGCA
Itgav	NM_008402.4	GGTCGCCTATCTTCGGGATG	TGAACTGGTTCAGGATGGGC
Itgb3	NM_016780.2	GGCGTTGTTGTTGGAGAGTC	GCCTCACTGACTGGGAACTC

Table 2.1.8 C. rt qPCR Primers

2.1.9 Reagents for cell imaging

Application	Fluorochrome	Target	Supplier	Concentration
Fluorescent Recovery After Photobleaching (FRAP)	Atto-488 NHS Ester	Cell membrane proteins	Merck LifeSciences	4-6 mg/ml
IncuCyte live cell imaging	FITC conjugated particles	2μM PLGA particles	Phosphorex™	75-150 μg/ml

Table 2.1.9 A. Fluorescent stains for cell imaging analysis

2.1.10 Seahorse Reagents

	Supplier	Concentration (mM)
Complete XF DMEM medium (pH 7.4 with 5 mM HEPES an no phenol red)	Agilent	N/A
Complete XF RPMI medium (pH 7.4 with 5 mM HEPES an no phenol red)	Agilent	N/A
Glucose Solution	Agilent	10
Pyruvate	Agilent	1
L-Glutamine	Agilent	2

Table 2.1.10 A. Seahorse assay cell culture media.

Inhibitor	Target	Supplier	Final concentration (µM)
Oligomycin	ATP synthase	Sigma	10
FCCP	Mitochondrial uncoupler	Sigma	10
Rotenone	Complex II	Sigma	5
Antimycin A from streptomycin sp.	Complex III	Sigma	5
2-DeoxyGlucose	Glycolysis	Sigma	250

Table 2.1.10 B. Mitochondrial inhibitors

2.1.11 Western Blot reagents

Buffer	Composition
1.5 M Tris pH 8.8	18.15 g Tris Base In 100 mL dH_2O and brought to pH 8.8
1 M TRIS pH 6.8	12.1 g Tris Base in 100 mL dH_2O and brought to pH 6.8
10 % APS	10 g ammonium persulfate in 100 mL dH_2O
10 % SDS	10 g sodium dodecyl sulphate in 100 mL dH_2O

10 X Tris Buffered Saline (TBST)	80 g NaCl, 2 g KCL, 30 g Tris base, 10 mL Tween-20 in 990 mL of dH_2O
1 X transfer buffer pH 8.3	10.5 g glycerine, 2.25 g TRIS, 1 g SDS in 1 L dH_2O and brought to pH 8.3
3% BSA in TBST (Blocking buffer)	3 g BSA in 100 mL 1X TBST

Table 2.1.11 A. Buffers used for electrophoresis and western blot.

Resolving gel	12 %	16%
Protein size range (kDa)	40-70	10 - 45
H_2O	6.6 mL	4.2 mL
Acrylamide	8 mL	10.6 mL
1.5 M Tris	5 mL	5 mL
10% Sodium dodecyl sulphate (SDS)	200 µl	200 µl
10 % Ammonium Persulfate (APS)	200 µl	100 µl
TEMED	8 µl	10 µl

Stacking gel	
H_2O	5.5 mL
Acrylamide	1.3 mL
1 M Tris	1 mL
10% SDS	80 µl
10% APS	80 µl
TEMED	8 µl

Table 2.1.11 B SDS page resolving and stacking gels for protein electrophoresis.

Antibody	Supplier and Cat No.	Dilution
Primary antibody		
SMAD2/3 Antibody (Mouse monoclonal anti-rabbit)	Cell Signalling #3102	1:100
β-actin Primary antibody: (Mouse monoclonal anti-mouse)	Cell Signalling #8H10D10	1:5000
Phospho-SMAD2 (Ser465/467)/SMAD3 (Ser423/425) (D27F4) (Rabbit monoclonal anti-rabbit)	Cell signalling; 8828S	1:100
Phospho-SMAD2/SMAD3 (Thr8) (Mouse monoclonal anti-Rabbit)	Invitrogen # PA5-36028	1:100
Secondary antibodies		
IRDye 800CW Goat anti-rabbit IgG (H+L)	Odyssey #926-32211	1:20000
IRDye 680CW Goat anti-mouse IgG (H+L)	Odyssey #926-68070	1:10000

Table 2.1.11 C. Western Blot primary and secondary Antibodies.

2.2 Methods

2.2.1 Mice

C57BL/6 mice aged 8-12 weeks were bred in the Trinity Biomedical Sciences institute (TBSI) Comparative medicines Unit or purchased from Charles River laboratories at 5 weeks of age. Animals were maintained according to the regulations of the European Union and the Health Products Regulatory Authority (HPRA). All animal studies were approved by Trinity College Dublin Animal Research Ethics Committee (Ethical approval number 091210) and were performed under the appropriate licence. Procedures were carried out under licence numbers AE191364/P079 and AE19136/P172 and approved by the TCD Animal Research Ethics Committee (Approval Number 091210).

2.2.2 Immunisation protocol

On Day 0 and 14, female C567BL/6 mice aged 6-12 weeks were injected via the intra-peritoneal route with 200 µl of either 1X PBS, IgG Isotype control (5 mg/kg), or monoclonal anti-β3 antibody (5 mg/kg). On day 1 and 15, mice were injected with 50 µl/leg of either; 1 X PBS, OVA (10 µg/mouse) and/or 2µm PLGA particles (1 mg/mouse) via the intra-muscular route. On day 21 mice were euthanised by CO_2 and spleens and blood were collected.

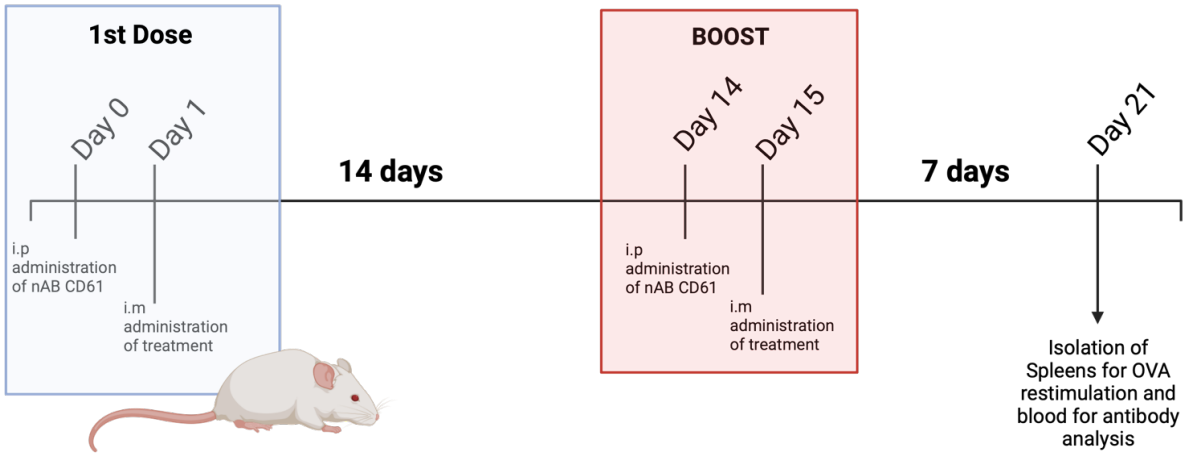

Figure 2.2.2 A. Protocol for immunisation of C57BL/6 mice with 2 µm PLGA particles and OVA, with i.p injection of β3 nAb. Mice were injected i.p with nAB against β3, IgG isotype control or PBS. The following day, mice were injected i.m with PBS, OVA and/or 2 µm PLGA particles. I.p

and i.m injections were repeated on day 14/15. Mice were sacrificed on day 21 and organs were harvested.

2.2.3 Isolation of splenic lymphocytes

To isolate white blood cells, spleens were mashed through a 40 µm filter to release cells, and a pellet was obtained via centrifugation at 400 g for 5 minutes. The pellet was re-suspended and 1 mL of 0.88% ACL was added for 2 mins to lyse red blood cells. ACL was quenched by adding 10 mL of cRPMI. Cells were centrifuged at 400 x g for 5 minutes and re-suspended in T-cell expansion media. Cell were counted as per cell counting protocol (section 2.2.5) and a $1x10^{6}$ cell/ml suspension was made up. For OVA re-stimulated group; OVA was prepared at 2X concentration of the final 25 µg/ml concentration in T-cell media. A volume of 80 µl of OVA or media was added to 96 well plates, followed by 80 µl of $1x10^{6}$ cell/ml splenocyte suspension. Cells were incubated for 72 hours before collecting cells for FACs analysis and supernatants for ELISA.

2.2.4 Whole blood and serum collection

Whole blood samples were collected in 1.5 mL and stored overnight at 4ºC to allow blood to clot . The following day blood was centrifuged at 8000 x g for 10 minutes at 4ºC. Serum was carefully pipetted, leaving the red blood cell pellet, undisturbed and stored at -20ºC for quantification of antibody titres by ELISA.

2.2.5 Cell culture

Cells were cultured at 37°C and atmospheric conditions of 5% CO_2, 95% humidity.

Cell counting

Viable cells were counted by trypan blue exclusion. Cell pellets were disrupted and re-suspended in media. An appropriate dilution of cell suspension in Trypan blue was determined and 10 µl was loaded onto a KOVA Glasstic cell counter slide with grids (Hycor Biomedical Inc.). Cells were counted under a light microscope, disregarding dead cells; visualised as dark cell structures. The final cell count in cells/mL was ascertained using the formula: Number of live cells/mL = number of live cells x 10^{4} cells/mL x dilution factor

L929 cell culture for the production of M-CSF

The murine aneuploidy fibrosarcoma cell line (L929) was transfected with a mammalian expression vector containing the cloned murine gene encoding the M-CSF. A frozen vial of L929 was rapidly thawed in a water bath at 37°C and quickly transferred to 9 mL of cDMEM at 37°C. DMSO was rinsed off by centrifuging for 5 minutes at 300 x g and the supernatant was discarded. The cell pellet was disrupted and re-suspended in 10 mL of cDMEM (w/o antibiotic). The cell suspension was then added to a T25 flask with 5 mL cDMEM which had been pre-calibrated to 37°C, 5% CO_2, and 95% humidity. Cells were incubated and checked daily.

When 90% confluence was reached, cells were split accordingly. Cells were washed with 1X PBS (Ca^{2+}/Mg^{2+} free) and incubated for 5 minutes with 2 mL Trypsin EDTA. 8 mL of cDMEM was then added and cells were detached by pipetting up and down. The cell suspension was transferred to a falcon tube and centrifuged at 400 x g for 5 minutes. The supernatant was discarded and cells were re-suspended in 25 mL of cDMEM. Cells were counted on a haemocytometer and plated at $0.5x10^6$ cell/mL in T75 of T175 flasks. Supernatant, containing L929 produced M-CSF, was harvested one week later.

Where appropriate, new stocks were stored by re-suspending $1\text{-}2x10^6$ cells in 1 mL of FBS containing 10% DMSO and frozen immediately at -80 using a “Mr Frosty” freezing container.

Testing of L929 conditioned media

L929 conditioned media was tested for its ability to promote differentiation of bone marrow derived hematopoietic stem cells to a macrophage phenotype via FACs analysis. The expression of macrophage typical surface markers; high CD11b and F4/80 and low Gr1 and Cd11c was measured.

BMDMs were differentiated as outlined below, and were supplemented with 10-30% L929 conditioned media. On day 6, cells were washed with 1X PBS and detached using 15 mL of 1 mM EDTA in PBS (not Trypsin). Plates were placed on ice for 10-20 minutes before using a pipette to rinse and dislodge cells from the bottom of the cell culture dish. Cells were pelleted by centrifugation, counted and $2x10^6$ cells/sample were added to FACs tubes (Falcon). The flow cytometry protocol is described in section 2.2.7. The gating strategy for analysis of flow cytometry data is presented below.

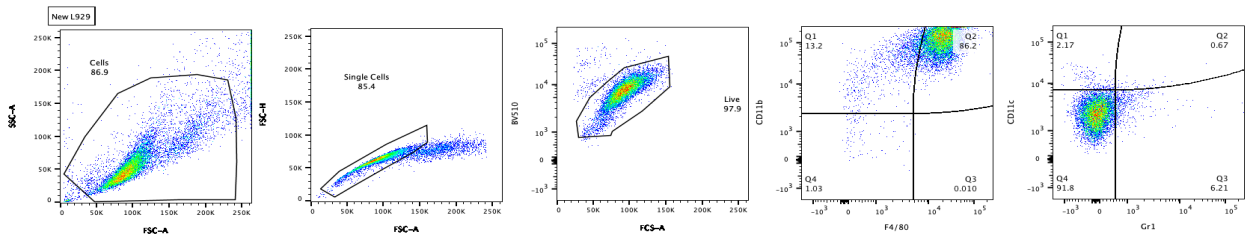

Figure 2.2.5A Gating strategy used to test differentiation of bone marrow derived stem cells to macrophages using L929 conditioned media containing M-CSF. Lymphocytes were gated by FSC-A and SSC-A measurements and doublets were excluded by the ratio of FSC-H to FSC-A. Dead cells were excluded using BV510 Viability stain. Cells were gated for their expression of macrophage markers; F4/80 and CD11b. F4/80 hi and CD11b hi cells were tested for the expression of monocyte and dendritic cell marker GR1 and Cd11c respectively. Gates were determined based on analysis of Fluorescent Minus One (FMO) controls.

THP-1 culture and differentiation

A frozen vial of THP-1 cells was rapidly thawed in a water bath at 37°C and quickly transferred to 9 mL of cRPMI at 37°C. DMSO was washed off by centrifuging the cell suspension for 5 minutes at 400 x g and discarding the supernatant. The cell pellet was re-suspended in 10 mL of cRPMI (w/o antibiotic). The cell suspension was then added to a T25 flask with 5 mL cRPMI which had been pre-calibrated at 37°C, 5% CO_2 and 95% humidity. Cells were incubated and checked daily. Flasks were split when confluence reached approximately 75%.

To count cells, the cell suspension was removed from the flask and centrifuged for 5 mins at 400 x g. The supernatant was discarded and the cell pellet was re-suspended in 5-10 mL of cRPMI. Counting was performed on a haemocytometer using trypan blue exclusion of dead cells. New flasks were set up at a cell density of $4x10^5$ cell/ml.

To differentiate THP-1 monocytes to macrophages, cells were plated into flat bottom cell culture plates at the following densities;

- 6 well; $1x10^6$ cell per well (final volume in well 2mL)
- 12 well; $0.5x10^6$ cell per well (final volume in well 1mL)
- 24 well plate; $0.25x10^6$ cell per well (final volume in well 0.5 mL)
- 96 well plate; $1.25x10^5$ cell per well (final volume in well 200 µl)

The cell suspension was made up at a 2X cell density. Before plating, cRPMI containing PMA at 2X was made up and 100 µl was added to each well. 100 µl of 2X cell suspension was then added on top. Cells were incubated with PMA for 48 hours. The plate was centrifuged at 400 x g for 5 mins, and PMA was removed and cells were washed with 1X PBS. Fresh cRPMI was added and cells were allowed to rest for 24 hours prior to experimentation. To detach differentiated THP-1 macrophages, cells were first washed with 1X PBS and then incubated with 0.05% Trypsin for 5 minutes. Cells were then gently rinsed off the bottom of the flask using a 10mL pipette. Cells were centrifuged at 400 x g for 5 minutes and supernatant was discarded.

Testing differentiation of THP-1 by PMA

THP-1 cells were differentiated as outlined in section 2.2.5, supplemented with various concentrations of PMA (10-100 µM). After 48 hours incubation with PMA and a 24 hour rest period, cells were washed with 1X PBS and detached using 0.05% Trypsin for 5 minutes. Cells were gently rinsed from the flask surface with a 10 mL pipette and pelleted by centrifugation, counted and $2x10^5$ cells/sample were added to FACs tubes (Falcon). The flow cytometry staining protocol is described in section 2.2.4 and antibodies were used against the macrophage surface markers, $CD11b^+$ and $CD14^+$. The gating strategy for analysis of Flow cytometry data is given below.

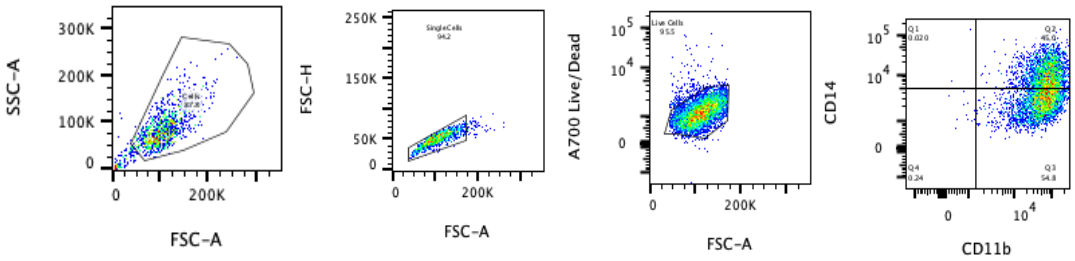

Figure 2.2.5 B. Gating strategy used to test differentiation of THP-1 monocytes to macrophages by PMA. Lymphocytes were gated by SSC-A and FSC-A measurements and doublets were excluded by the ratio of FSC-H to FSC-A. Dead cells were excluded using A700 viability stain. The expression of the THP-1 macrophage markers, CD11b and CD14 was assessed. Gates were determined based on analysis of FMO controls.

Murine Bone Marrow isolation

Murine bone marrow was isolated to obtain hematopoietic stem cells for differentiation into primary innate immune cells. The media used in the bone marrow protocol differs depending on cell type (refer to materials section for comprehensive component list).

Cell type	Media
BMDM	cDMEM
BMDC	cRPMI

Table 2.2.5 A Media used for primary immune cell culture.

Female C57BL/6 mice between the ages of 8-12 weeks were euthanised using CO_2 and death confirmed via cervical dislocation. The femurs and tibiae were isolated, removing all tissue and muscle, and then sterilised by washing briefly in 70% ethanol.

A 10 mL syringe was loaded with media and a 27G needle attached. The extreme ends of the femur and tibia were severed using sterile sharp medical scissors, avoiding the bone marrow. The 27G needle was inserted into the ends of the bone and flushed with media into a sterile petri dish, attempting to collect as much bone marrow as possible. A 10 mL syringe was attached to a 19G needle and clumps were disrupted by repeat pipetting the suspension. The suspension was then transferred to a 50 mL falcon tube, through a 40 µm cell strainer and centrifuged for 5 minutes at 400 x g. Supernatant was discarded and the cell pellet was disrupted. Red blood cells were lysed by adding 1 mL of ACL for 2 minutes. 15 mL of media was then added to stop the reaction and cells were centrifuged for 5 minutes at 300 x g to remove ACL. Supernatant was discarded and the pellet was again disrupted. Cells were suspended in 10 mL of media and counted using Trypan Blue exclusion.

BMDM differentiation

A $1x10^6$ cells/ml suspension of bone marrow derived white blood cells (BMD-WB) was made up in cDMEM with 25% L929 -M-CSF. Sterile, non-treated petri dishes were washed with 10 mL of cDMEM and cells were plated at a final volume of 10 mL. Cells were then incubated for 6 days prior to re-plating, with supplementary feeding of 10 mL cDMEM with 25% L929-M-CSF on day 3. On day 6 of cell culture, cells were confluent and fully differentiated to BMDMs.

To detach BMDMs, cDMEM was removed and cells were washed with ice cold PBS. PBS was removed and replaced with ice cold PBS containing 0.1% EDTA. Tissue culture dishes were placed on ice for 5-10 minutes until BMDMs were seen to detach under the microscope. Cells were rinsed off the surface of the dish using a 10 mL pipette. The cell suspension was then centrifuged at 400 x g for 5 mins. Cells were resuspended to a density of $1x10^6$ cells/ml in cDMEM containing half the concentration of L929 M-CSF (12.5%) and plated into 6 well plates for qPCR/ FACs analysis or flat bottom 96 well plate for ELISA.

- 6 well plate; $2x10^6$ cell/well (Final volume of 2 mL)
- For acute stimulation: 96 F well plate; 1.25 $x10^5$ cell/well (Final volume 125 µl)
- For training protocol: 96 F well plate; $2x10^5$ cell/well (Final volume 200 µl)

NOTE: Refer to confocal microscopy and seahorse analysis methods section for specific cell plating protocol for these experiments.

BMDMs were rested for minimum of 24 hours before applying experimental treatments.

BMDM training

For innate immune training analysis, BMDMs were treated with PLGA particles (150µg/ml) in the 0.2-20 µm size range for a period of 24 hours. Cells were washed with 1 X PBS and fresh cDMEM with 12.5% L929 supernatant was added. BMDMs were incubated for 6 days before being exposed to a secondary stimulus; LPS (10 ng/mL), PAM (10 ng/ml) CpG (4 µg/ml). For cytokine analysis, supernatants were collected after 24 hours.

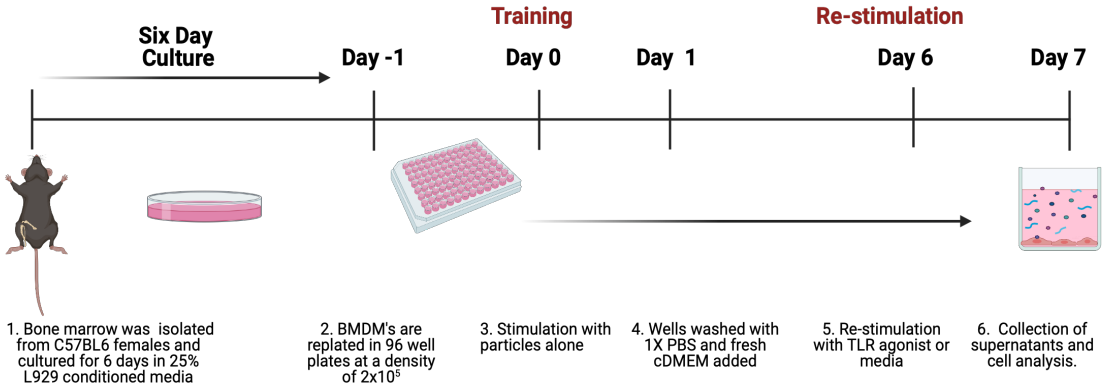

Figure 2.2.5 C. Outline of the training protocol. Training of BMDMs was performed to analyse the long term effect of PLGA particles on macrophage behaviour, at extended time points after removal of the particles. In brief, bone marrow was isolated from female C57BL/6 mice and cultured in cDMEM supplemented with 25% L929 supernatant for six days. On day -1, BMDMs were replated as described in section 2.2.2. On day 0, BMDMs were incubated with PLGA particles (37.5-150 µg/ml) alone for 24 hours. Cells were washed with PBS and fresh media was added to cells. On Day 6, BMDMs were re-stimulated with various TLR agonists for 24 hours, before collecting samples for analysis. Figure created on Biorender.com

GMCSF BMDC differentiation

A 4.25x10^5 cell/ml suspension of BMD-WB was made up in cRPMI supplemented with 20 ng/ml GM-CSF and 35 ml of cell suspension was cultured in T175 flasks. On day 2, cells were fed with an additional 30 ml cRPMI containing 20 ng/ml GM-CSF. On day 5, the complete volume of supernatant containing non-adherent cells was discarded and 30 ml of cRPMI with 20 ng/ml GMCSF was added. Finally on day 7, 30 ml of cRPMI with 20 ng/ml GM-CSF was added. On day 9 of cell culture, cells were confluent and fully differentiated to BMDCs. To detach BMDCs for the surface of the cell culture flask, the surface was carefully rinsed using a 10 mL pipette. The surface was carefully washed 3-4 times to detach as many semi-adherent cells as possible. Media was removed and spun down at 400 x g for 5 mins. Cells were resuspended to a density of 6.25x10^5 cell/ml in cRPMI containing half the concentration of GM-CSF (10 ng/ml) and plated into 12 well plates for qPCR/ FACs analysis or U bottom 9 well plates for ELISA.

- 12 well plate; 6x10^5 cell/well (Final volume 950 µl)
- 96 U well plate; 1.25x10^5 cell/well (Final volume 200 µl)

DCs were rested for a minimum of 2 hours before applying experimental treatments.

Inhibitor pre-treatment.

Inhibitor pre-treatment was performed a minimum of 1 hour prior to experimental treatment. Concentrations of inhibitors and neutralising antibodies are described in the materials section.

2.2.6 Co-Culture

BMDCs used for CD4+ T-cell co-culture were weaned off conventional FBS to minimise the exposure to TGF-β found in serum. BMDCs were gradually adapted to X-VIVO 15 Serum-free Hematopoietic Cell Media (LONZA) using the following culturing protocol. On the first feed on day 3, cells were cultured in 25% X-VIVO Media and 75% standard cRPMI. On the second feed, cells were cultured in 50:50 ratio and on the final feed the percentage of X-VIVO media was increased to 75%. All media supplementation was prepared with 20 ng/ml GMCSF. BMDCs were then re-plated into 96 well U-Bottom plates in 100% X-VIVO media with 10 ng/ml GMCSF, ready to proceed to stimulation after a 2 hour recovery period.

BMDC stimulation

BMDCs were rested for 2 hours, before pre-treatment with the anti-β3 monoclonal antibody (mAb) (50 µg/ml) for one hour. BMDCs were then treated with the following stimulations; 2 µm PLGA particles (300 µg/ml), TGF-β (10 ng/ml), or LPS (30 ng/ml). Each experimental group was also co-stimulated with or without endotoxin-free OVA (25 µg/ml). BMDCs were incubated for 24 hours before co-culture with T-cells.

Naïve $CD4^+$ T-cell isolation

Splenocytes were isolated from female C57BL/6-Tg(TcraTcrb)425Cbn (OTII mice) as described in the protocol in section 2.2.5. Cells were counted on a haemocytometer by trypan blue exclusion and re-suspended to a density of $1x10^8$ cells/mL in PBS supplemented with 2% FBS. T cells were isolated using the

MagniSort™ mouse naïve CD4+ T cell Enrichment Kit (ThermoFisher) as per manufacturers protocol. In brief; 200 µl of MagniSortTM Enrichment Antibody Cocktail was added for every 1 mL of cells and pulse vortexed before incubating for 10 minutes at RT. Cells were washed with 2% FBS-Buffer. The supernatant was discarded and cells were transferred to a 12 x 75 mm, 5 mL tube at a concentration of $1x10^8$ cell/mL (without exceeding 2 mL per tube) Cells were then incubated with the same volume of MagniSortTM Negative Selection Beads as the antibody cocktail. The suspension was thoroughly mixed and incubated for 5 mins at RT. An equal volume of 2% FBS Buffer was added to the cell-bead suspension and pipetted up and down with a P1000 pipette. The 5 mL tube was placed within the EasySep™ magnet (StemCell) and the unbound cells were decanted into a 50 mL tube. The tube was washed several times with 2% FBS-Buffer. The collection tube containing enriched naïve CD4+ T-cells was centrifuged at 400 x g for 5 minutes. The pellet was resuspended in 10 ml of T-cell expansion media, cells were counted and resuspended at a density of $1x10^6$ cell/mL and allowed to recover for 1 hour prior to co-culture.

CFSE staining

After a 1 hour rest-period. T-cells were stained with CFSE to measure cell proliferation. Sufficient cells for a CFSE negative control were left unstained. T-cells were centrifuged at 400 x g for 5 mins and the pellet was resuspended in 1 ml of PBS containing 5% (v/v) FCS. A 5 µm solution of CFSE was prepared in PBS and added to T-cells. Cells were mixed on a vortex and incubated for 20 mins in the dark at 37ºC and 5% CO_2. CFSE was quenched with T-cell media and cells were allowed to rest for 5 minutes before centrifugation at 400 x g for 5 mins. Cells were counted on a haemocytometer using trypan blue exclusion of dead cells. Cells were resuspended at a density of $2x10^6$ cells/ml.

Co-Culture of BMDCs and T-cells

To prepare the co-culture, the supernatants on the treated BMDCs were carefully removed, without disrupting the BMDC cell pellet and 100 µl of fresh T-cell media was added. In the groups receiving anti-TGFβ neutralising antibody, the 100 µl T-cell media was made up with neutralising anti-TGFβ mAb (20 µg/ml). This was

followed by addition of 125 µl of T-cell suspension at $2x10^6$ cell/ml. The co-culture was incubated for 72 hours before analysis.

2.2.7 Flow Cytometry

Extracellular staining

Cells were removed as per the specific cell type protocol described in section 2.2.5 and pelleted by centrifugation at 400 x g for 5 mins. The supernatant was discarded and the pellet was briefly vortexed to re-suspend cells. Cells were incubated in 250 µl of viability stain at 1:500 dilution in PBS for 15 minutes in the dark at RT. Cells were washed with 1 mL of 1X PBS and pelleted. Supernatants were discarded and cells were resuspended in 100 µl of FACs Buffer (2% FCS in PBS) with Fc Block at 1:20 dilution. Cells were incubated on ice for 10 minutes in the dark.

A master mix was then made up with fluorescent tagged antibodies (dilutions described in materials section) in FACs buffer. The master mix (MM), containing 10 µl of each antibody (final volume of MM added = number of antibodies x 10 µl) was added to cells and incubated for 30 minutes at room temperature in the dark. Single Stains (SS) (cells or OneComp Beads) and Fluorescent Minus One (FMOs) controls were also prepared. After a 30 minute incubation, cell samples, SS and FMOs were washed with PBS and pelleted down by centrifugation. Supernatants were discarded and cells were fixed with 100 µl of 4% paraformaldehyde (PFA). Cells were incubated for 20 minutes at room temperature in the dark. A final centrifugation step was carried out to pellet cells. Supernatants were discarded and cells were either re-suspended in FACs Buffer or stained for intracellular markers (protocol below). Cells were analysed using BD LSRFortessa Flow Cytometer or Cytex Aurora spectral Flow Cytometer

Intracellular staining

Fixation and permeabilization for intracellular staining was performed using eBiosciences™ Foxp3/Transcription factor staining kit. The manufacturers protocol was followed. In brief; 4X Fix/Perm concentrate was prepared in Fix/Perm Diluent at a ratio of 1:3 and 1 ml was added to cells after the final wash step carried out during extracellular staining. Cells were incubated at room temperature for 30 mins or 60 mins at 4ºC.

10 X Permeabilization Buffer was then prepared in dH_2O at a ratio of 1:9 and 2 mL was added at the end of 30-60 minute incubation. Cells were centrifuged at 400 x g for 5 minutes and supernatant was discarded. The pellet was disrupted by brief vertexing. Intracellular fluorescent tagged antibody was added in a volume of 10 µl at dilutions stated in materials section. Cells were incubated in the dark for 30 mins at room temperature. At the end of the 30 min incubation, 2 mL of 1X permeabilization buffer was added to each sample and cells were spun down by centrifugation at 400 x g for 5 mins. Cells were resuspended in 2mL of 1X permeabilization buffer, centrifuged and supernatants discarded. Cells were resuspended in 200 µl of FACs buffer before Flow cytometry. Cells were analysed using BD LSRFortessa Flow Cytometer or Cytex Aurora spectral Flow Cytometer

Data analysis for co-culture

When co-culture samples were run on the Cytex Aurora spectral Flow Cytometer the entire sample was analysed. It was, therefore, necessary to normalise the number of single cell events across the experimental groups. The number of live and $CD4^+CD3^+$ cells were normalised to $5x10^4$ single cell events. An example of the table used to normalise cell number is provided below;

Normalised	N1	Media	2 um	TGF	LPS	OVA	OVA 2 um	OVA LPS	OVA TGF	Events
A1	Single cells	20259	46680	14965	32633	54108	20073	68834	46245	50000
A2	Normalisation	2.4680389	1.07112254	3.3411293	1.53219134	0.92407777	2.49090819	0.72638522	1.08119797	
A3	Live cells	14977	17750	11678	26573	19092	12253	18679	17906	
A4	Normalised Live cells	36963.8185	19012.425	39017.708	40714.9205	17642.4928	30521.098	13568.1495	19359.9308	
A5	CD3/CD4	10609	13361	10146	20588	15774	11039	15837	13261	
A6	Normlaised CD3/CD4	26183.4247	14311.2682	33899.0979	31544.7553	14576.4028	27497.1355	11503.7627	14337.7662	
A7	FoxP3	301	669	95	487	524	1059	302	693	
A8	Normalised FoxP3	742.879708	716.580977	317.407284	746.177183	484.216752	2637.87177	219.368335	749.270191	
A9	Proliferating FoxP3	78	112	62	93	36	924	0	505	
A10	Normalised Proliferatin	192.507034	119.965724	207.150017	142.493795	33.2667997	2301.59916	0	546.004974	

Table 2.2.7 A. Representative table of normalisation calculations for analysis of co-culture samples. The following formulae were used. (A1) number of single cell events. (A2) $5x10^4$ divided by A1. (A3) Number of live cells (A4) Number of live cell multiplied by A2. (A5) Number of $CD3^+CD4^+$ T-cells. (A6) Number of CD3/CD4 T-cells multiplied by A2. (A7) Number of $FoxP3^+$ cells (A8) Number of $FoxP3^+$ cells multiplied by A2. (A9) Number of proliferating cells (A10) Number of proliferating cells multiplied by A2.

2.2.8 Enzyme Linked Immunosorbent Assay (ELISA)

Cytokine ELISA

Commercially available murine and human ELISA kits from R &D Systems, Biolegend and Invitrogen were used to measure cytokine secretion into the culture

supernatant. All antibody and reagent dilutions for individual ELISA kits are listed in the materials section.

All washing steps were done using PBS-Tween wash buffer and repeated three to four times unless otherwise stated by the manufacturer. During incubations, plates were placed on orbital rotators unless otherwise stated. In brief, high binding plates (Grenier Bio One) were coated with 50 µl/well of Capture antibody, accounting for sufficient wells to accommodate all samples and a standard curve. The plate was left to incubate overnight at either room temperature (RT) or 4°C, depending on manufacturers recommendation. Plates were washed and 100 µl of 1% BSA (Blocking buffer) was added to each well to block non-specific binding of antibodies. Plates were incubated for 1-2 hours depending on manufacturer's protocol, at RT.

Plates were washed, and 50 µl of supernatant was added to corresponding wells. Supernatants were stored at -20ºC and thawed prior to this step. Supernatants were diluted depending on the relative secretion of a given cytokine by the cell type. The standard curve was prepared as per manufacturers recommendations and a 7-fold serial dilution of 1:2 was performed in triplicate. A blank control was also included as a control for background signal. Plates were incubated at RT on an orbital shaker for 2 hours or overnight at 4ºC, washed, and 50 µl of detection antibody was added to each well and left to incubate for either 1 or 2 hours depending on manufacturers recommendations.

Plates were washed, and 50 µl of Horseradish peroxidase (HRP) conjugated streptavidin was added to each well and left to incubate in the dark for 20 or 30 minutes depending on the manufacturers protocol. The plates were washed a final time, taking care to wash plates extensively to remove all unbound HRP-Streptavidin. 50 µl of OPD or 5,5′-Tetramethylbenzidine (TMB) was added to each well and monitored for colour development. The enzyme reaction was stopped by addition of 25 µl of 1 M H_2SO_4 when the plate had developed to the desired intensity. The optical density (OD) values were read spectrophotometrically at 492 nm for OPD and 450 nm for TMB using the VersaMax Micro-plate reader. Cytokine concentrations in the supernatants were determined from the standard curve generated using recombinant cytokines of known concentrations. The blank was subtracted to remove background signal.

Total OVA specific-IgG ELISA

ELISA was performed using commercially available antibodies listed in section 2.1.9. All washing steps were done using PBS-Tween wash buffer and repeated three to four times. Antibody dilutions were made in blocking solution made with 1% (w/v) semi-skimmed milk in 1 X PBS. During incubations plates were placed on orbital rotators unless otherwise stated.

Medium binding ELISA plates (Grenier BioOne) were coated with 50 µl OVA solution (10 µg/ml) in sodium carbonate buffer and incubated overnight at 4ºC. Plates were washed three time and blocked with blocking solution for 2 hours at RT. Plates were washed and serum samples were added onto the plate in a serial dilutions starting at 1:1000 (12 x 1:2 dilutions). Dilutions were made in blocking solution. Serum samples were incubated for 2 hours. Plates were washed and 50 µl of HRP- conjugated anti-mouse IgG antibody was added as per dilutions stated in section 2.1.9. Plates were incubated at RT for 1 hour and washed a final time. 50 µl of OPD was added and monitored for colour development. The enzyme reaction was stopped by adding 25 µl of 1 M H_2SO_4. The optical density (OD) values were read spectrophotometrically at 492 nm using the VersaMax Micro-plate reader. The blank was subtracted to remove background signal.

2.2.9 qPCR

RNA isolation

RNA from cell cultures were isolated using High Pure RNA isolation kits (Roche) according to the manufacturers protocol. In brief, culture media were discarded and cells were washed with 1X PBS. Cells were lysed by adding an appropriate volume (300-600 µl) of cell lysis/binding buffer and promptly transferred into a high pure filter column inserted into a collection tube. Tubes were centrifuged for 15 seconds at 8000 x g and flow through was discarded. DNase mixture (1:9 DNase: Incubation buffer) was added to the top of the filter column and incubated for 15 minutes. Two washing steps were carried out with a 15 second centrifugation at 8000 x g, followed by a final 2-minute centrifugation at 13000 x g. Collection columns were inserted into clean, sterile nuclease-free micro-centrifuge tubes and Nuclease free dH_2O (50-100 µl) was added to the top of the column and centrifuged at 8000 x g for 1 minute. RNA concentration from the flow through was obtained

by nano-drop spectrophotometry read at 260 nm. Quality check of RNA was performed with the following criteria; 260/280 >2.0 for pure RNA and 260/230 >2.0 for uncontaminated RNA samples.

Reverse transcriptase; cDNA synthesis

RNA isolated from treated cells was used to synthesise cDNA. A master mix was made up with reverse transcriptase enzyme (RT), random hexamer primers, dNTPs, RNAse out and RT buffer. The ratios of each component are stated in the materials section, with the quantities scaled up to the number of samples required. A final volume of 5 µl of master mix was pipetted into the bottom of PCR tube strips using nuclease free filter pipette tips. A final volume of 5 µl of RNA sample was added to corresponding PCR tubes, adjusting the concentration of RNA samples to 200 ng using nuclease free water. Two controls were also included; a “No RT” sample as a negative control for the RT-PCR cycle, and a “No DNA” sample as a control for contamination.

The following thermo-cycler program was used for cDNA synthesis.

Temperature (ºC)	Time (s)
25	10
42	60
95	3
4	∞

Table 2.2.9 A. Thermo-cycler protocol for cDNA synthesis.

qPCR

A master mix was made up containing KAPPA SYBR®, forward and reverse primers for the desired gene, and nuclease free water. The ratios of each component are stated in the materials section, with quantities scaled up to the number of samples being screened for each gene. A final volume of 7 µl of master mix was added to the bottom of well in a 96 well PCR plate using nuclease free filter pipette tips. 3 µl of DNA sample was added to the respective wells. Plates were sealed using adhesive PCR plate seals and centrifuged briefly to ensure a homogenous mixture is brought to the bottom of the plates. Samples were run on an Applied Biosystems 7500 Fast system on the following program;

Temperature (ºC)	Time (s)	Cycles
50	120	1
95	120	1
95	3	40
60	30	40

Table 2.2.9 B. rt qPCR program for Comparative △CT carried out on Applied Biosystems 7500 Fast system.

Dissociation curve analysis was performed after a completed real-time qPCR to exclude non-specific products. Changes in gene expression given as CT values (cycle threshold values) were normalised to *β-actin* and *mTERT* expression.

2.2.10 Confocal microscopy

Cell membrane staining for FRAP

BMDMs or BMDCs were seeded into 35 mm glass bottom tissue dishes at a cell density of $2x10^6$ cell/ml and left to adhere overnight. Cells were washed with 1X PBS to remove non-adherent cells and all proteins from cell culture media. Cell membrane proteins were then labelled with ATTO 488 NHS Ester (4-6 mg/ml) in 1 X PBS for 30 minutes at 37°C.

Cells were washed once with PBS and fresh media was added. Prior to fluorescent bleaching and imaging, cells were treated with PLGA particles (150 µg/ml) for 1 hour, or hyper osmotic media (150 mM sucrose in cDMEM) or hypo osmotic media (1:5 dH_2O: Media) in the minutes prior to imaging.

FRAP Confocal microscopy

FRAP measurements were performed using the Zeiss LSM 710 confocal microscope with a 63x/1.4 oil immersion objective. Photobleaching was performed using a 80 mw 488 argon laser and 0.3% laser power during imaging 100% laser power during photobleaching on a square area of 4 x 4 µm. Cells were imaged for 5 frames pre-bleach, 1 frame during the bleach and 150 frames post-bleach. For each experimental group, a minimum of 6 cells were analysed.

Individual FRAP measurement curves were generated using the FRAP application on Leica LAS X life Sciences software. Parameters were set in place to select the

highest quality FRAP attempts for each group, minimising the interference from cell movement and fluorescence dimming. The generated rates of recovery (s) were averaged for each experimental group. Statistical significance between the conditions was assessed by two-way ANOVA with multiple comparisons on PRISM software.

2.2.11 Live imaging of cells

IncuCyte SX1® (Sartorius) cell incubator was used for live imaging of cells over a period of 48 hours after incubation with FITC-conjugated 2 µm PLGA particles (Phosphorex Degradex® PLGA) (75 µg/ml). Cells were replated into 96 well flat bottom plates as per the specific cell type protocol and allowed to rest overnight prior to incubation with PLGA particles and transfer to the IncuCyte®. HD phase imaging with green fluorescent channel was performed every 30 minutes at a magnification of 20X.

Analysis of particle localisation was performed using Fuji Image J software. Jpeg images from IncuCyte SX1® were loaded onto ImageJ software in the RGB stack format. The following functions were applied to all images.

- Cropped to 100 x 142 (+/- 1) pixels to isolate a smaller region of the image
- Noise reduction; de-speckle function.
- Enhance contrast and sharpen.

These functions were applied to improve identification of cell boundaries. Using the freehand selection tool, a region was isolated indicating the cell boundaries denoting the region of interest (ROI). The analysis tool was then used to generate a histogram of fluorescent intensity across the ROI. Mean intensity of fluorescence in the green channel within the ROI was calculated from the histograms for 6 cells per 100 x 144 region and plotted for each time point to monitor internalisation of FITC-conjugated 2 µm PP.

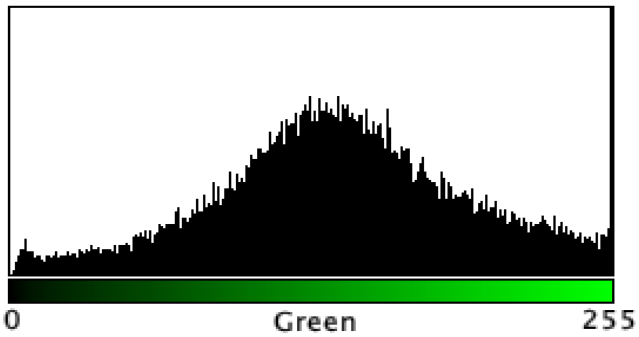

Figure 2.2.11 A. Example of histogram generated for the intensity of green fluorescence detected within a ROI. Each event indicates the intensity across the scale, per pixel.

2.2.12 Seahorse Assay

Mitochondrial and Glycolytic Stress Test

Cells were seeded into a 96 micro-well XF Seahorse cell culture plate in a volume of <100 µl to ensure cell adherence to the bottom of the micro-well. Cell density was dependent on cell type and experiment duration.

Cell type	Experiment duration	Cell/well
BMDM	24 hour	$1x10^6$
BMDM	6 days	$1.5x10^6$
THP-1	24 hour	$1.5\ x10^5$
THP-1	6 days	$1.5\ x10^5$

Table 2.2.12 A Cell density of BMDMs and THP-1 macrophages for seahorse analysis

NOTE: THP-1 monocytes were differentiated with 10 ng/ml PMA in the XF Seahorse microwell plate as per protocol in section 2.2.5.

Cells were incubated for 24 hours to allow adhesion. The following day, cells were treated with PLGA particles (300 or 150 µg/ml), β-glucan (100 µg/ml), mIL4 and mIL13 (20 and 40 ng/ml respectively) or LPS and mIFN$_\gamma$ (10 ng/ml and 25 ng/ml respectively).

The day prior to analysis, a Seahorse cartridge was hydrated by immersing the cartridge sensors in sterile water in the hydration cartridge. The cartridge was incubated for at least 12 hours at 37 °C , in an incubator at 0% CO_2. A 50 mL tube with calibration fluid was also incubated at 37°C devoid of CO_2. The day of analysis, the sterile water was discarded, and the cartridge sensors were immersed in the

pre-calibrated, calibration fluid (pH 7.4) for 90 minutes. An hour prior to analysis, the cell culture media was replaced with Seahorse XF DMEM with no phenol red and supplemented with 10 mM glucose, 1 mM pyruvate and 2 mM L-glutamine. After 90 minute calibration of the cartridge, inhibitors were added to their respective ports; oligomycin (port A, 10 µM), FCCP (port B, 10 µM), rotenone and antimycin-A (port C, 5 µM each) and 2-DeoxyGlucose (Port D, 250 mM). Note: a further 1/10 dilution will occur when inhibitors are injected into the well. Real-time measurements of oxygen consumption rate (OCR) and extracellular acidification rate (ECAR) were measured by using Seahorse system: Seahorse XFe96 Analyzer (Agilent) as per manufacturers protocol.

Calculating basal respiration, ATP production from oxidative phosphorylation and maximal respiration were calculated using the following equations;

1) Basal respiration = resting OCR - non mitochondrial respiration
2) ATP production OXPHOS = resting OCR- proton leak - non mitochondrial respiration
3) Maximal respiration = OCR after FCCP- proton leak - non mitochondrial respiration

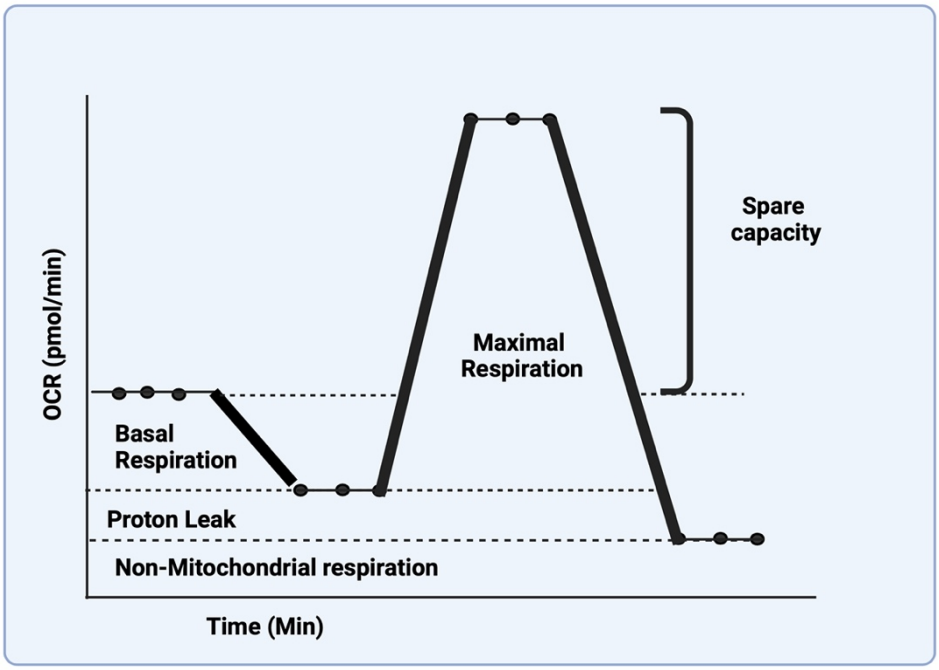

Figure 2.2.12 A. Metabolic outputs which can be calculated from OCR vs time plot. OCR measurements following injection of mitochondrial inhibitors Oligomycin, FCCP and Antimycin A + Rotenone can be used to calculate the following rates; basal respiration, proton leak, non-mitochondrial respiration, maximal respiration and spare capacity.

2.2.13 Western Blot

Cell lysate preparation

Cells were treated for specified time points before centrifuging the plate and removing supernatants. Cells were gently washed with 1 x TBST whilst kept on ice. Cells were then lysed using 50-100 µl lysis buffer. Cells were kept on ice for 5 minutes before detaching using a cell scraper and transferring cell lysate to a 1.5mL Eppendorf tube. Lysates were boiled for 10 minutes at 90ºC and stored at -20ºC until required.

SDS PAGE Gel preparation

Gels were prepared depending on the size range of the protein of interest. Table 2.16 details the composition for specific resolving gels. Each reagent was added in the order listed in the table. Gels were cast in 1.5 mm glass plates (12.5 cm x 6.5 cm), allowing for the resolving gel to set before adding the stacking gel. 16 well combs specified for 1.5mm casts were used to create protein loading wells. Gels were used straight away or stored at 4ºC for a maximum of one week.

Gel electrophoresis

Gels were assembled in an electrophoresis tank filled with 1X SDS Running Buffer. The comb was carefully removed and 10-20 µl of sample was added to the designated wells. 5 µl of protein molecular weight ladder was also added. The tank was connected to the power pack and set to 90 V for the first 30 minutes of running, and 110V for the remaining 1-2 hrs. Electrophoresis was stopped when the loading buffer line reached the end of the gel. The gel was carefully removed and prepared for transfer to a nitrocellulose membrane.

Semi-Dry Protein transfer

Filter paper and a 0.2 µm nitrocellulose membrane (BioRad) were soaked in 1X transfer buffer before assembly of a transfer sandwich. Assuming the bottom plate was the positive plate, the sandwich was prepared in the following order; filter paper, nitrocellulose membrane, gel, filter paper. During the stacking, bubbles were eliminated to prevent unsuitable transfer. The negative plate was positioned on top and a weight was placed on top of the fully assembled Fast-Blot semi-dry transfer

system (Analytikjena™) to maintain pressure. The transfer system was connected to a power pack set at 120 mA for one gel and 150 mA for two. Depending on the size of proteins being transferred the system was allowed to run for 1-2.5 hours.

Primary and Secondary antibody staining

The nitrocellulose membrane was washed using 1X TBST and incubated overnight with rotation at 4ºC in 10 ml 3% BSA (w/v) made up in 1X TBST to minimise non-specific binding. The primary antibody was prepared in 5 mL blocking solution and incubated with the nitrocellulose membrane for 12-24 hours at 4ºC with rotation. The membrane was washed three times using 1X TBST and incubated with 5 mL of secondary antibody in blocking solution. The secondary antibody was incubated at RT with rotation for 1-2 hrs. The membrane was washed 3-4 times and visualised on the LiCor OddessyFX at 700 and/or 800 nm. Analysis to quantify the florescence intensity of each band was performed on the Empiria Software and fold change of band intensity was normalised.

2.2.14 Cell viability assays

LDH assay in cell culture supernatants

CyQuant™ LDH cytotoxicity assay was carried out according to the manufacturer's instructions (ThermoFisher). Prior to commencing the assay, the 100% death control were prepared by using 10X lysis buffer for 45 minutes at 37°C, 95% humidity and 5% CO2. The reaction mixture was prepared by mixing 600 µl of assay buffer with 11.4 ml of substrate stock solution. The reaction mixture was stored in the dark. Once the 100% cell death controls were ready, 50 µl of supernatant from experimental groups, from spontaneous cell death group (cells in media with vehicle control) and the 100% cell death group were transferred to a 96 well plate in triplicate. An aliquot of 50 µl of reaction mixture was then added to each well and incubated for 30 minutes at room temperature and in the dark. Stop solution (50 µl) was added after 30 minutes and the OD was measured by a plate reading spectrophotometer at an absorbance of 492 nm. To subtract background absorbance, the plate was also read at 680 nm, and these values subtracted from the optical density values of the reading at 492 nm.

Live/Dead analysis by FACs

A control for cell death was also prepared by incubating cells in 70% EtOH or 10% DMSO for 15 minutes prior to detaching cells from cell culture plates. To measure cell viability, cells were incubated in 250 µl of viability stain in PBS, at the dilutions indicated in the materials section for 15 minutes in the dark at RT. Cells were then washed with 1 mL of 1X PBS and centrifuged at 400 x g for 5 mins. Cells were either further stained extra and intracellularly or analysed immediately using the BD LSRCanto Flow Cytometer or Cytex Aurora spectral Flow Cytometer. Dead cells were characterised as populations with high fluorescence intensity of live/dead stain and decreased FSC or increased SSC.

Annexin V Apoptosis assay

Apoptosis and cell death were assessed using Annexin V and PI staining. For Annexin V staining, all washes, incubations and measurements were performed in 1x Annexin V binding buffer (see materials section for buffer composition). PI staining was performed in PBS. Cells were stimulated for 24 hrs, then washed and incubated with 1 µg/ml Annexin V-FITC in 200 µl and incubated for 5 mins at RT in the dark. Cells were then washed and resuspended in 200 µl of 1X Annexin V buffer. Finally, PI was added directly to FACS tubes (1 µg/ml) immediately before acquiring the samples on the Cytex Aurora spectral Flow Cytometer. Live cells were characterised as double negative for Annexin V and PI, cells in early apoptosis were positive for Annexin V but negative for PI, and double positive cells are indicative of cells in late apoptosis.

Crystal violet assay

Supernatants from adherent cells was removed and cells were gently washed twice with PBS. Crystal violet staining solution (50 µl) was added to each well and incubated for 20 mins at RT. The staining solution was gently removed and cells were washed twice with PBS. The plate was then allowed to air-dry overnight. A 1:2 solution of PBS with Tween® detergent was prepared and 100 µl was added to solubilise the crystal violet. The plate was incubated on an orbital shaker for 20 minutes at RT and the OD was measured at 570 nm. The background OD (well with no cells) was subtracted from each reading.

2.2.15 Statistical analysis

All statistical analysis was carried out using GraphPad Prism software (version 10.0.3) the statistical tests used are detailed in relevant figure legends.

Chapter 3; Results part I

Anti-inflammatory macrophage responses to PLGA particles are dependent on size and modulated by αvβ3 and mTOR.

3.1 Chapter 3 Introduction

Innate immune cells, namely, macrophages, and monocytes are the first responders to a site of damage or infection [337,484]. They play an indispensable role in providing an adequate response to restore homeostasis by removing pathogens and debris, as well as modulating the recruitment of additional immune cells. Whilst inflammatory responses are critical, inflammation must be resolved to restore homeostasis and allow healing mechanisms to begin [20].

Chronic inflammation can occur when inflammation is un-regulated, resulting in aggressive feedback of pro-inflammatory responses and tissue damage [17]. This can lead to disease states such as chronic wounds [485], diabetes [486], IBD [487] and sepsis [488]. It is also a serious complication associated with organ transplants [489], implantation of medical devices and biomaterials [490,491]. Therapeutic approaches to address chronic inflammation focus on breaking the cycle of inflammation through promotion of anti-inflammatory immune cell expansion [492]. Anti-inflammatory cytokines secreted by macrophages and dendritic cell such as; IL-10, IL-1Ra and TGFβ, help mitigate the positive feedback loop of pro-inflammatory responses, and can initiate healing mechanisms which restore homeostasis. Macrophages are key drivers of non-specific inflammation, but are also, adept at controlling and modulating anti-inflammatory and healing responses. The highly plastic nature of macrophages allow them to take on a spectrum of phenotypes, from highly inflammatory to anti-inflammatory activation states [493,494]. As both the causative agent and the mitigator of inflammation, macrophages are key targets for the treatment of inflammatory diseases and in the prevention of implant rejection.

Current treatments to combat chronic inflammation rely on suppressing the immune responses by using steroids, anti-inflammatory drugs or targeted cytokine blockade such as anakinra [495]. A major drawback of these, is the risk of systemic immunosuppression as well as high risk of adverse effects, toxicity and poor tissue targeting. A method to overcome some of these limitations, is to use polymeric biodegradable particles as drug delivery vehicles [496, 497]. This approach improves tissue targeting and dosing, increases the stability of bioactive components and improves the safety profile of existing drugs [381, 498]. However, in order to take full

advantage of particle-based therapies, the immune response towards the particles themselves also needs to be understood.

A major interest within the Lavelle lab, has been in identifying how physico-chemical properties of polymeric particles, such as size, shape and charge participate in altering and enhancing immune responses [499,405 ,500,399]. These findings can help inform which particle properties are best suited for certain applications, either as drug delivery vehicles, or stand-alone therapies [422]. A physical property which was found to have a notable influence on immune response is particle size. Previous work in the lab has demonstrated that PLGA particles in the 50-100 nm size range drive potent cellular immunity through the expansion of $CD8^+$ T-cells, incurring interest in their potential as vaccine adjuvants [414]. On the other hand, unpublished work by Dr Sean McCluskey, identified that larger 0.5 μm PLGA particles drive anti-inflammatory IL-10 secretion from dendritic cells and macrophages, making them poor adjuvants but advantageous for applications aimed at regulating inflammation [501].

The research presented here seeks to expand on the anti-inflammatory properties of PLGA particles in the 0.5-2 μm range. With macrophages being critical drivers of chronic inflammation, we sought to verify the ability of particles in this size range to drive the secretion of other anti-inflammatory cytokines whilst maintaining low pro-inflammatory responses. This could present a novel means of utilising immunomodulatory particles to enhance anti-inflammatory and pro-resolution macrophage populations to combat chronic inflammation.

Another important area of focus, is looking at long term effect of particles on immune cells. Influential work by Netea and colleagues, elucidated the capacity of innate immune cells to retain memory to an encounter, amplifying responses to a secondary non-related stimulus [502]. Indeed, the breadth of pathogen-derived components, pollutants and biomaterials which are able to generate innate immune memory has expanded over the years.[503]. It is, therefore, critical to investigate how foreign particles might promote a trained phenotype in key innate immune cells such as macrophages, to prevent the risk of exacerbating chronic inflammation.

Finally, understanding the underlying mechanisms which dictate size-dependent immune responses to particles could provide better evidence-based implementation of particles for clinical applications. With size being the only independent variable and PLGA not binding to any known receptor, we propose a

role for mechanically sensitive receptors, which instead respond to alterations to the cell membrane. The ever-growing overlap between immunology and mechano-biology has revealed new-found appreciation for mechanical signals in driving immune cell responses and phenotypes, particularly in response to biomaterials [172,188,171,200,170].

Taking into account these critical aspects of particle-driven immune-modulation the overall hypothesis of this chapter is that PLGA particles in the 0.5-2 μm range drive macrophage polarisation, through cell membrane disruption and engagement of a mechano-sensitive receptor. We propose this to be the mechanism by which particles differentially respond to particles based on size, and responsible for down-stream signalling, promoting an anti-inflammatory phenotype.

To address the hypothesis for this chapter, the following experimental aims were formulated;

1) Investigate the role of PLGA particle size on macrophage inflammatory phenotype.
2) Investigate the long term impact of PLGA particles on macrophages and propensity to drive innate immune memory.
3) Identify the mechanism by which macrophages can differentially respond to particles based on size.
4) Identify downstream signalling pathways involved in modulating macrophage phenotype.

Chapter 3 - Results

3.2. BMDMs treated with PLGA particles in the 0.5- 2 μm range demonstrate anti-inflammatory cytokine secretion and M2 typical metabolism after 24 hrs.

Macrophage responses to polymer particles were investigated with the intention of identifying an immunomodulatory particle size which could drive anti-inflammatory immune responses. Dr McCluskey previously demonstrated an enhanced propensity for DCs to secrete anti-inflammatory IL-10 following treatment with LPS and PLGA particles of 0.5 μm in size. However, it was unclear if macrophages would respond in a similar manner.

To gain insight into the effect of particles alone, BMDMs were incubated with PLGA particles from 200 nm to 20 μm in diameter (150 μg/ml) for 24 hours. LPS at 10 ng/ml, was also included as a positive control for pro-inflammatory macrophage activation. None of the tested particle sizes on their own promoted increased secretion of pro-inflammatory IL-6 or IL-12p40 or anti-inflammatory IL-10 as compared to untreated cells (Figure 3.2.1 C-E). However, basal secretion of IL-12p40 was reduced from BMDMs treated with 0.5-2 μm particles, particularly those treated with 2 μm particles. Additionally, there was a significant enhancement in the secretion of IL-1Ra from BMDMs treated with PLGA particles in the 1-2 μm range (Figure 3.2.1 A) in a concentration dependent manner (Figure 3.2.1 B).

Next, BMDMs were cultured with PLGA particles and TLR4 ligand LPS to assess if any of the tested sizes could magnify or suppress endotoxin induced inflammatory responses in macrophages. After a 24 hour incubation, the secretion of pro and anti-inflammatory cytokines were compared to BMDMs treated with LPS alone. PLGA particles in the 1-2 μm range significantly amplified the secretion of IL-1Ra (Figure 3.2.2 A) and promoted a moderate increase in IL-10 (figure 3.2.2 B). None of the tested PLGA particle sizes caused any significant change in the secretion of IL-6 or IL-12p40 (Figure 3.2.2 C-E).

In order to verify that the trends in IL-10 and IL-1Ra were not attributable to increased cell proliferation or viability, the number of live cells remaining after culture with PLGA particles was determined. The percentage of live cells was quantified using BV510 fixable viability stain (FVS) which was analysed by flow

cytometry. There was no change in the percentage cell viability of BMDMs treated with PLGA particles of all sizes, as well as a variety of TLR agonists; LPS, PAMCSK4, heat killed *Mycobacterium tuberculosis* (MtB) and β-glucan (Figure 3.2.4 A). This was further corroborated by the negligible cytotoxicity of particles (Figure 3.2.4 B). Cytotoxicity was analysed using the LDH colorimetric assay, which measures the release of LDH from cells with a damaged cell membrane. The % toxicity of each treatment was calculated by comparing the absorbance values to that of 100% cell death control. Finally, the number of adherent cells remaining in culture was quantified using crystal violet stain. The number of cells is proportional to the amount of crystal violet stain. The crystals can then be solubilised and measured spectrophotometrically as a readout to compare cell density to untreated control wells. The absorbance readings increased by a fold change of approximately 0.25 in the particle treated BMDMs compared to untreated BMDMs, however, this was not found to be statistically significant (Figure 3.2.3 C).

An additional method to characterise macrophage activation state is by analysing the metabolism of the cell. It has been established that the metabolic profile of macrophages shifts depending on their activation state in order to meet the requirements of the cell. Briefly, pro-inflammatory macrophages require a fast energy output which is met by upregulating glycolysis. Anti-inflammatory macrophages instead require a more consistent anabolic metabolism, which is not susceptible to exhaustion. This is facilitated by funnelling pyruvate through the TCA cycle and increased rates of oxidative phosphorylation. To further investigate the phenotype of BMDMs treated with PLGA particles in the 1-2 μm size range, extracellular metabolic flux analysis was performed on cells and their metabolic profile was compared to M1-polarised (LPS and IFN_{γ} treated), M2- polarised (IL-4 and IL-13 treated) and untreated BMDMs. The oxygen consumption rate (OCR) of IL-4/IL-13 treated cells was enhanced compared to untreated cells, and injection of mitochondrial inhibitors, Oligomycin and Rot/AA affected oxygen uptake corroborating the dependence on mitochondrial OxPhos, typical of M2-polarised macrophages. The basal OCR of BMDMs treated with IFN_{γ} and LPS was lower than untreated BMDMs (Figure 3.2.4 A) and instead they displayed an increase in the extracellular acidification rate (ECAR). This metabolic profile is characteristic of M1 macrophages which required a heightened rate of glycolysis (Figure 3.2.4

B).

BMDMs treated with 1 μm PLGA particles demonstrated an increase in basal OCR (Figure 3.2.4 C) and the production of ATP was found to be dependent on oxygen consumption (Figure 3.2.4 D). In fact the OCR of particle-treated BMDMs was greater than that displayed by IL-4/IL-13 treated BMDMs. Finally, by plotting the OCR vs ECAR, the metabolic profile of each BMDM group can be evaluated (Figure 3.2.4 E). BMDMs treated with 1 μm PLGA particles were classified as more aerobic in nature. IL-4/IL-13 treated BMDMs were slightly less aerobic, whilst IFN_{γ}/LPS treated BMDMs were very highly glycolytic.

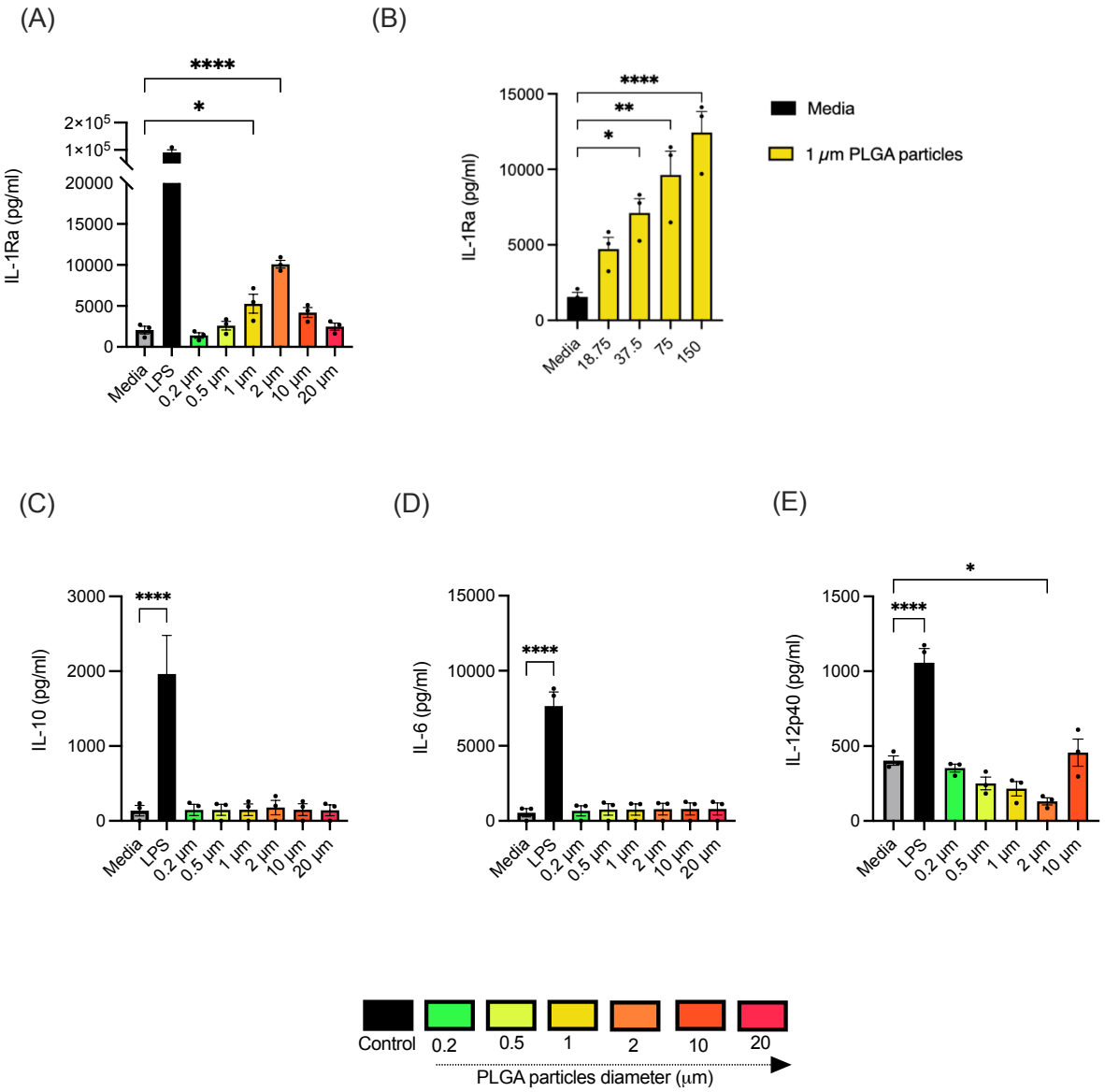

PLGA micro-particles in the 1-2μm size range enhance the secretion of anti-inflammatory IL-1Ra by macrophages in a concentration dependent manner. BMDMs cultured from bone marrow of C57BL/6 mice (6.25x10^5 cell/ml) were treated with PLGA particles in a range of sizes (150 μg/ml) or (B) 1 μm PLGA particles at a range of concentrations (18.75-150 μg/ml) for 24 hours. Secretion of (A-B) IL-1Ra, (C) IL-10 (D) IL-6,and (E) IL-12p40 in the supernatant was measured by ELISA. One way ANOVA was used to determine statistical significance as compared to control, where *p<0.05 **p<0.01 ***p<0.001 and **** p<0.0001. Error bars show mean ± SEM for three individual experiments.

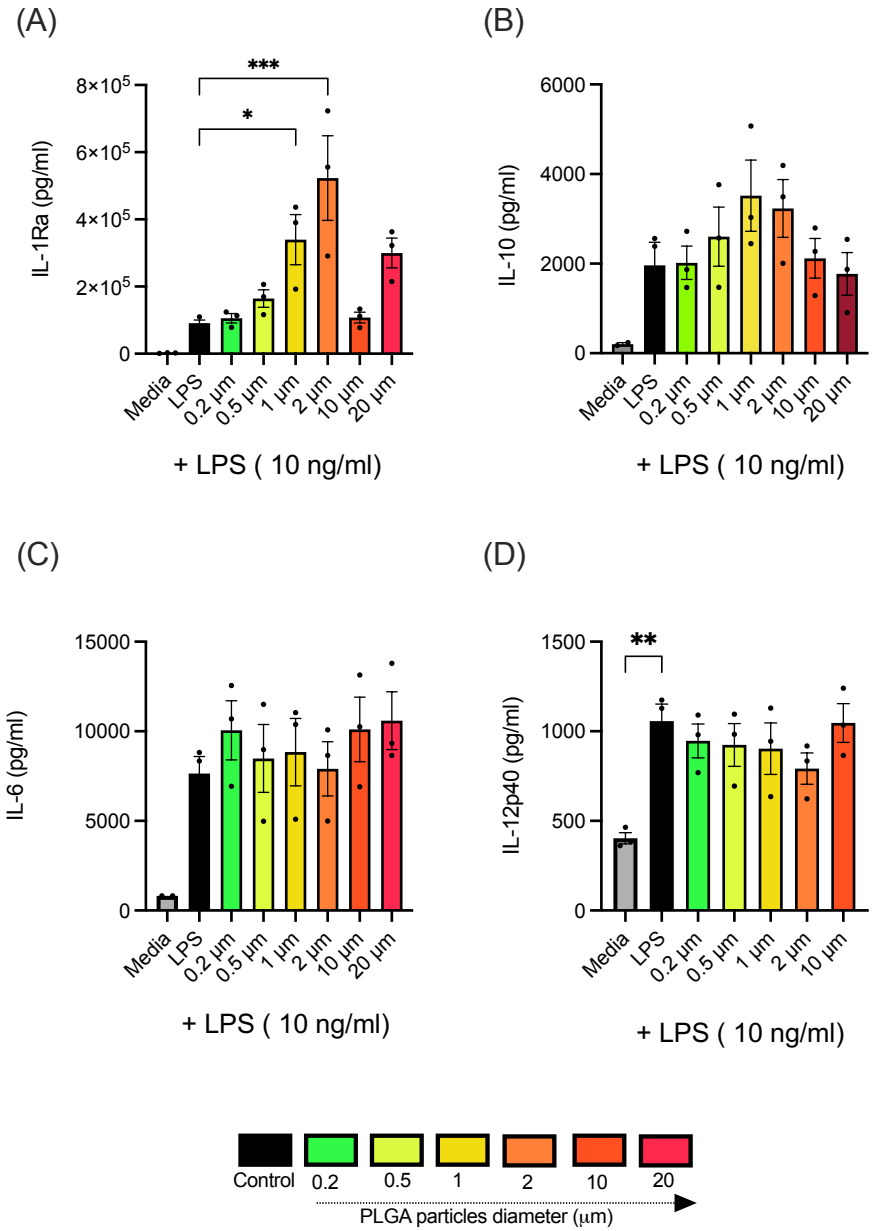

Figure 3.2.2 PLGA particles in the 1-2 µm range enhance the secretion of IL-1Ra and IL-10, but not IL-6 or IL-12p40 from BMDMs co-stimulated with LPS. BMDMs (6.25x10^5 cell/ml) were treated with PLGA particles across a range of sizes (150 µg/ml) and LPS (10 ng/ml) for 24 hours. Secretion of (A) IL-1Ra, (B) IL-10, (C) IL-6, (D) IL-12p40 into the supernatant was measured by ELISA. One way ANOVA was used to determine statistical significance as compared to control, where *p<0.05 **p<0.01 and ***p<0.001. Error bars show mean ± SEM for three individual experiments.

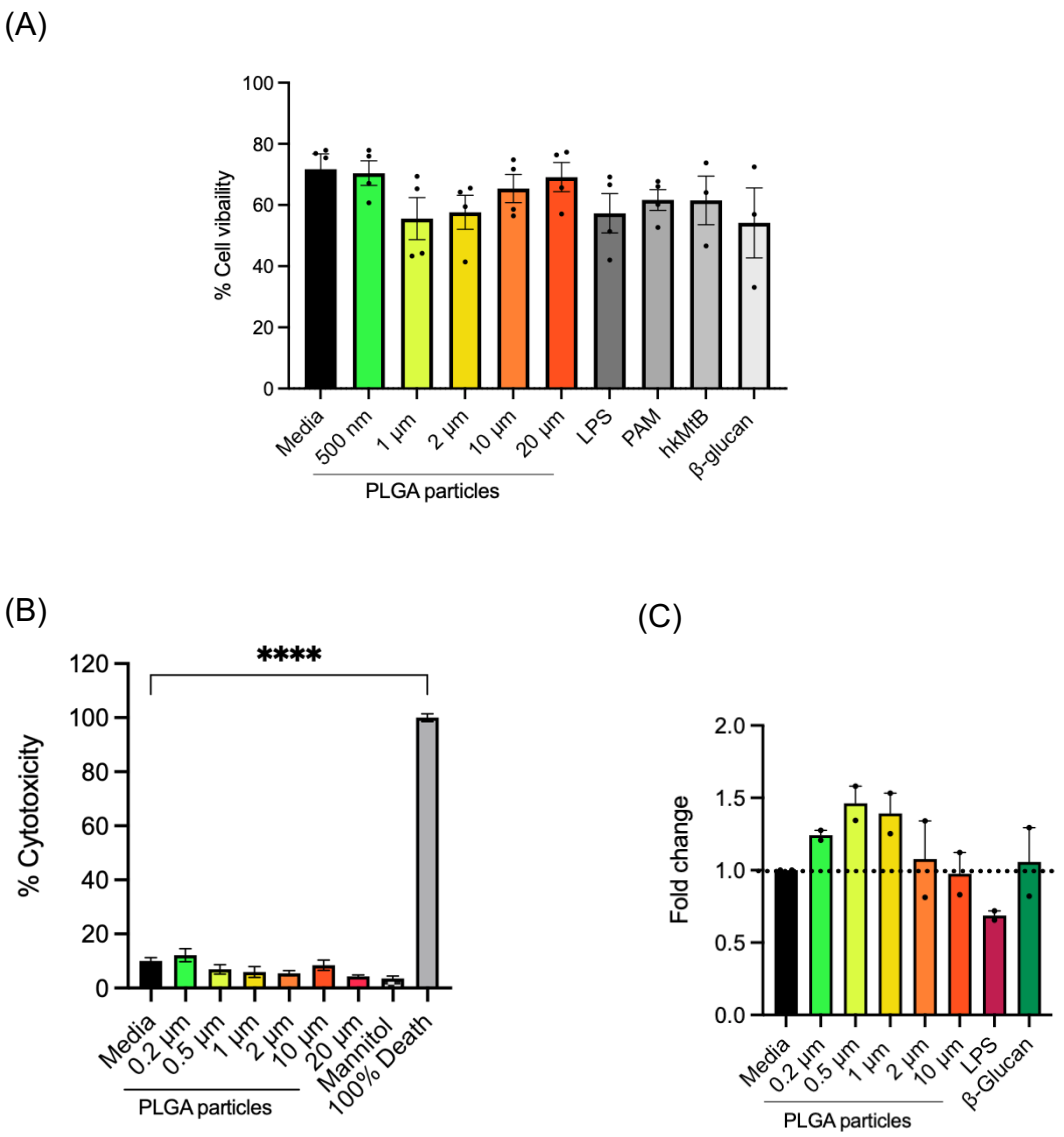

Figure 3.2.3 Incubation of BMDMs with PLGA particles of 0.2-20 µm in size did not affect cell viability or cell number. BMDMs (6.25x10^5 cell/ml) were treated with PLGA particles in a range of sizes (150 µg/ml), LPS (10 ng/ml), β-glucan (100 µg/ml) PAMCSK4 (10 ng/ml) or heat killed Mtb (hkMtB) (25µg/ml). The effect of 24 hour stimulation on cell viability and proliferation was assessed using three methods. (A) % of live cells analysed by Flow Cytometry (B) LDH assay where % cytotoxicity is given as the percentage absorbance value compared to a 100% cell death control. (C) Cell number was measured using a crystal violet assay where the fold increase in cell number was given as a fold change over untreated cells. One way ANOVA was used to determine statistical significance as compared to control, where *p<0.05 **p<0.01 ***p<0.001 and **** p<0.0001. Error bars show mean ± SEM for (C) two, (B) three or (A) four individual experiments.

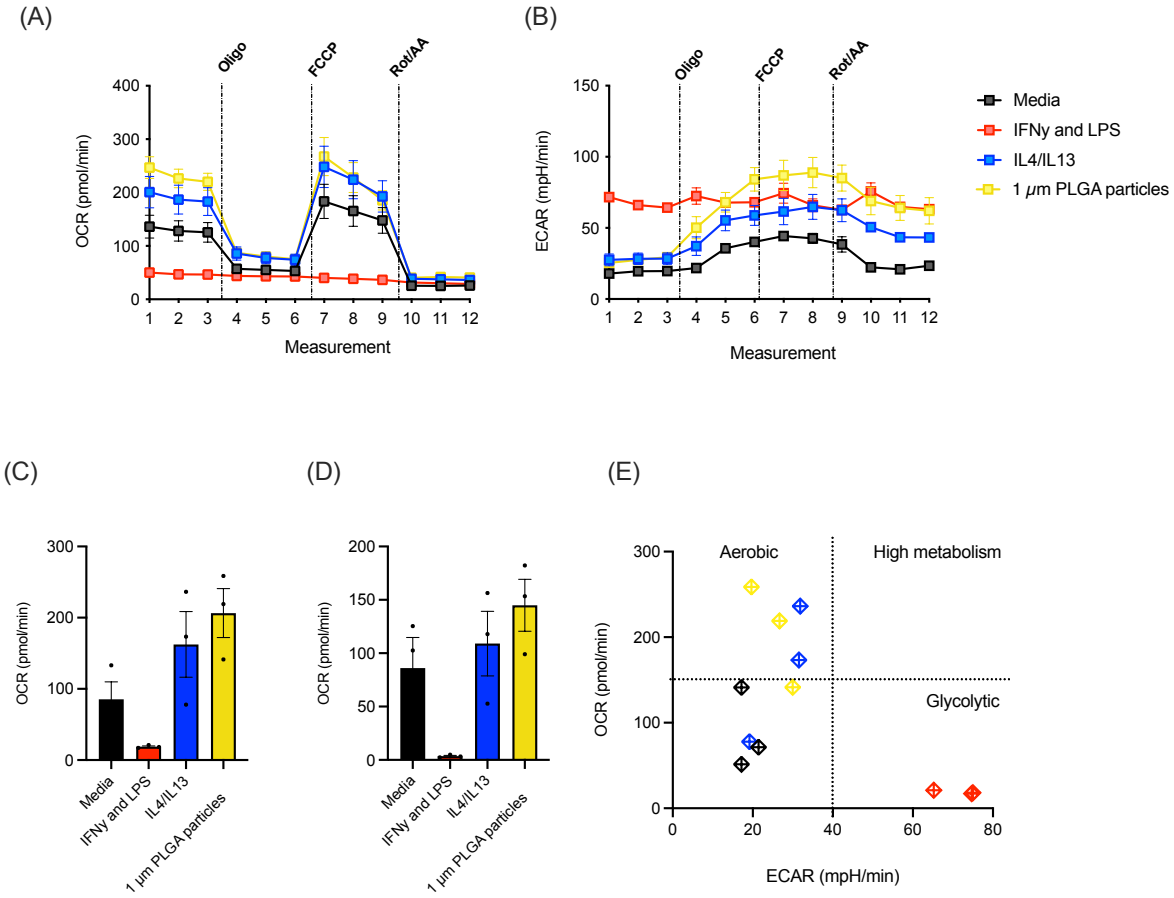

Figure 3.2.4 Acute treatment of BMDMs with 1 μm PLGA particles shifts their metabolic output towards a M2-typical metabolism. Extracellular flux analysis was carried out on BMDMs ($1.25x10^5$ cell/well) treated for 24 hrs with 1 μm PLGA particles (150 μg/ml), M2-polarising cytokines (IL-4 and IL-13, 40 and 20 ng/ml respectively) or M1- polarising cytokines (IFN_γ and LPS 50 ng/ml). A mito-stress assay was conducted on Agilent XFe96 Seahorse analyser using the following mitochondrial inhibitors; Oligomycin (Oligo), FCCP, and Rotenone (Rot) and Antimycin A (AA). Measurements of (A) Oxygen consumption rate (OCR) and (B) extracellular acidification rate (ECAR) were plotted for each group with three measurements made in 5 minute intervals after inhibitor injection. (C) Basal respiration and (D) OCR used for ATP production were plotted and are also depicted as an energy phenotype plot (E). Error bars show mean + SEM and statistical significance in (C-D) was calculated using one-way ANOVA. Error bars show mean ± SEM for three individual experiments.

3.3 BMDMS treated with 0.5- 2 μm PLGA particles exhibit sustained anti-inflammatory cytokine secretion for up to 7 days.

The innate immune memory paradigm has increased the requirement for in-depth analysis of how innate immune cells such as macrophages respond in the weeks and even months post-treatment. Studies have provided evidence to show that biomaterial particles can imprint memory on innate immune cells which can alter treatment outcomes [34,28]. Training is characterised by metabolic and epigenetic modifications which permit innate immune cells to amplify responses upon a secondary insult [35, 36,37]. In terms of measuring innate memory, cells are routinely tested for altered responsiveness after 6 days, once they have returned to a resting state.

BMDMs were treated with a range of PLGA particle sizes at a concentration of 150 μg/ml for 24 hours, and then rested for 6 days in fresh media. They were then re-stimulated with a variety of TLR agonists for a further 24 hours. The cytokine response of particle-trained BMDMs to LPS which targets TLR4, CpG oligodeoxynucleotides which target TLR9 and PAM3CSK44 which targets TLR1/2, was assessed.

Interestingly, PLGA particles were able to re-program cells to amplify anti-inflammatory cytokine secretion in a size dependent manner. However, it was noted that the trend in cytokine secretion of particle-trained BMDMs was different depending on the TLR agonist used. For instance, the secretion of IL-10 by BMDMs restimulated with LPS was enhanced following training with 2 μm PLGA particles. However, there was little size-dependent difference in IL-10 secretion when BMDMs were re-stimulated with CpG or PAM3CSK44 (Figure 3.3.1 A). With regards to a size-dependent trend in IL-1Ra, only PLGA particles in the 0.5-2 μm were able to train BMDMs to significantly upregulate IL-1Ra in response to CpG and PAM3CSK4. However, training with all PLGA particle sizes was able to significantly enhance IL-1Ra in response to LPS. That being said, BMDMs trained with 0.5-2 μm PLGA particles produced the greatest levels of IL-1Ra in the LPS-restimulated groups (Figure 3.3.1B).

Looking at the pro-inflammatory cytokine secretion of particle-trained BMDMs it is clear that no particle size amplified the propensity of cell to produce IL-6 or TNFα above basal levels. However, BMDMs trained with PLGA particles in the 0.5-2 μm

range secreted significantly less IL-6 in response to re-stimulation with PAM3CSK4 (Figure 3.3.2 A) and moderately decreased levels of TNFα when re-stimulated with CpG and PAM3CSK4 (Figure 3.3.2 B).

These trends demonstrate the importance of assessing the response to different TLR agonists to gain a broader understanding of the trained phenotype in the context of different unrelated stimuli. Overall, the results indicated that training of BMDMs with 0.5-2 μm PLGA particles enhances anti-inflammatory responses following rechallenge of the cells with TLR ligands.

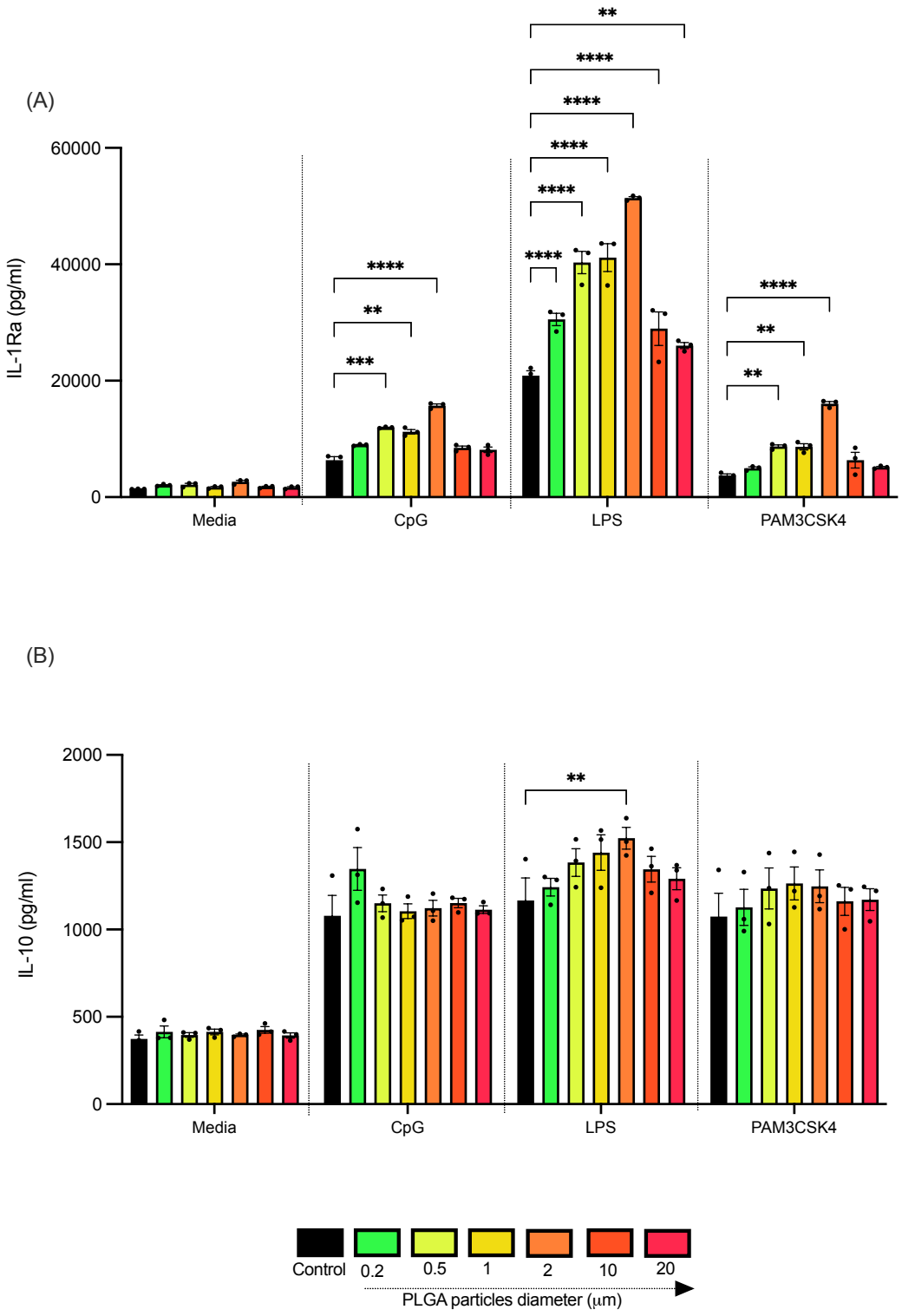

Figure 3.3.1 Training BMDMs with PLGA particles in the size range of 0.5-2 μm enhances anti-inflammatory cytokine secretion after TLR ligand re-stimulation. BMDMs ($6.25x10^5$ cell/ml) were treated with PLGA particles in the size range of 0.2-20 μm in diameter (150 μg/ml) for 24 hours. Media with particles was removed and cells were rested for 6 days, before re-stimulation with LPS (10 ng/ml) PAM3CSK44 (10 ng/ml) or CpG (4 μg/ml) for a further 24 hours. Supernatants

were collected and ELISA was performed to measure the concentration of (A) IL-10 and (B) IL-1Ra. Two way ANOVA with Dunnet's multiple comparison test was used to determine statistical significance compared to untrained controls where *p<0.05 **p<0.01 ***p<0.001 and **** p<0.0001. Error bars show mean ± SEM for three individual experiments.

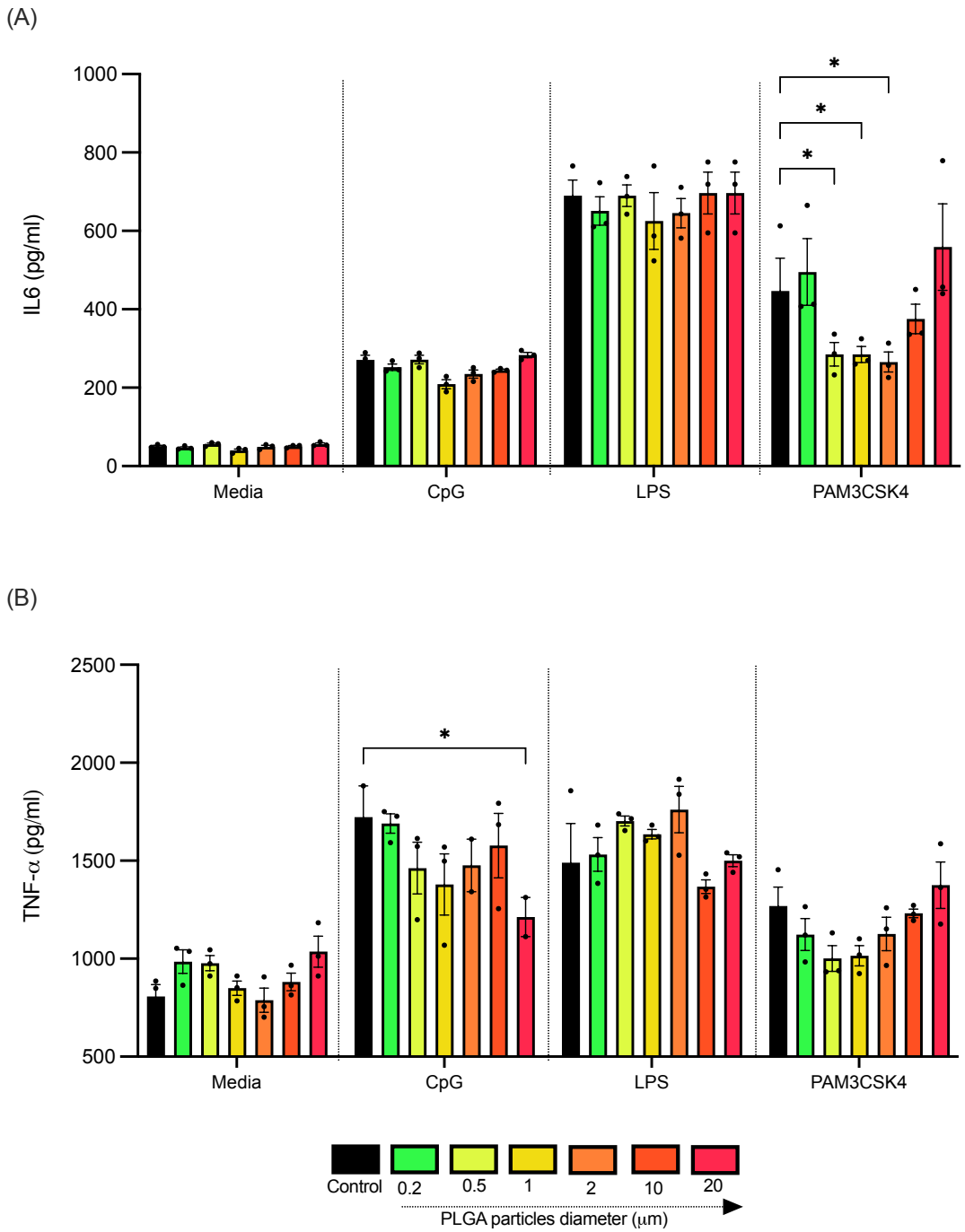

Figure 3.3.2 Training BMDMs with PLGA particles in the size range of 0.5-2 μm does not enhance the secretion of pro-inflammatory cytokines after TLR ligand re-stimulation. BMDMs ($6.25x10^5$ cell/ml) were treated with PLGA particles in the size range of 0.2-20 μm in diameter (150 μg/ml) for 24 hours. Media with particles was removed and cells were rested for 6 days, before re-stimulation with LPS (10 ng/ml) PAM3CSK44 (10 ng/ml) or CpG (4 μg/ml) for a further 24 hours. Supernatants were collected and ELISA was performed to measure the concentration of (A) IL-6 and (B) TNF-α. Two way ANOVA with Dunnet's multiple comparison test was used to determine statistical significance compared to untrained controls where *p<0.05. Error bars show mean ± SEM for three individual experiments.

3.4 BMDMS trained with 0.5-2 μm PLGA particles maintain heightened aerobic metabolism 7 days after interaction compared to untrained BMDMs.

A key feature of trained innate immune cells is the re-programming of their metabolism which supports cell longevity and rapid re-activation upon re-stimulation. The effect of 1 μm PLGA particles on the metabolism of BMDMs was, therefore, examined. Mitochondrial and glycolytic stress tests were performed to investigate the reliance of BMDMs on both glycolysis and OxPhos. As an established inducer of trained immunity, whole β-glucan particles (100 μg/ml) was used as a positive control. The rate of glycolysis was measured based on the extracellular acidification rate (ECAR) of the media, and the rate of oxidative phosphorylation was measured by the oxygen consumption rate (OCR).

Based on the ECAR plot, it is evident that β-glucan trained BMDMs had an elevated glycolytic rate which was severely dampened when the glycolytic inhibitor 2-Deoxy-D-Glucose (2DG) was injected (Figure 3.4.1 A). Whilst particle trained BMDMs had a slightly enhanced basal glycolytic rate compared to untrained BMDMs (Figure 3.4.1 C), injection of 2-DG had a minimal effect on ECAR (Figure 3.4.1 A).

The OCR of β-glucan trained BMDMs was significantly upregulated, with mitochondrial inhibitors having a negative effect on OCR. Particle trained BMDMs also demonstrated elevated OCR and basal OCR which was significantly impacted when mitochondrial inhibitors were used (Figure 3.4.1 B and D). The overall basal metabolic profile of β-glucan vs particle treated BMDMs indicates that β-glucan induces a highly metabolic phenotype, whereas training with 1μm PLGA particles induced a moderate increase aerobic metabolism (Figure 3.4.1 E)

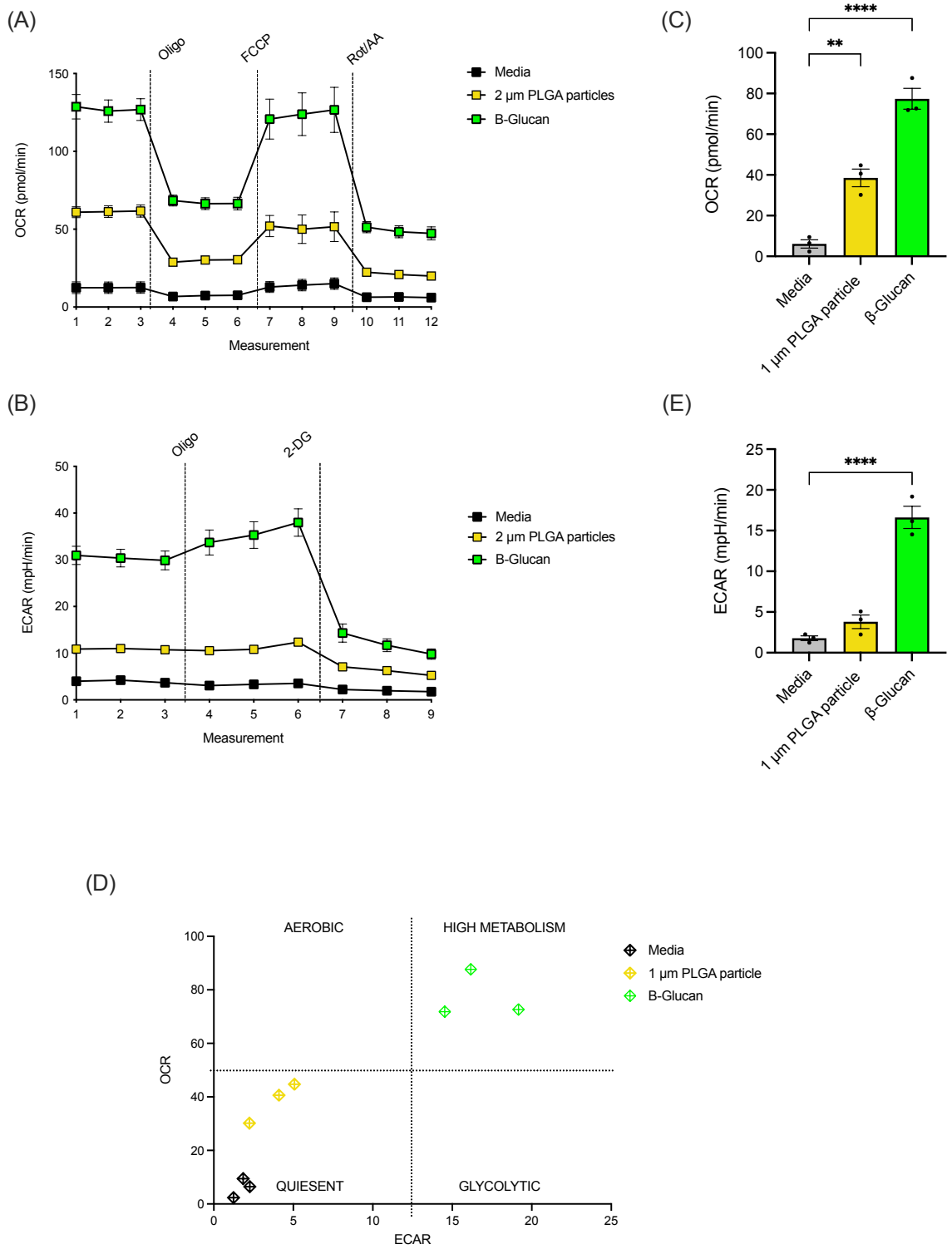

Figure 3.4.1 Training BMDMs with 1 µm PLGA particles promotes a metabolic switch, enhancing aerobic respiration. BMDMs (1x10^6 cell/ml) were treated with 1 µm PLGA particles (150 µg/ml) or β-glucan (100 µg/ml) for 24 hours. Cells were washed and fresh media was added. Cells were incubated for 6 days before carrying out mitochondrial and glycolytic stress assays on an Agilent XFe96 Seahorse analyser using the following mitochondrial inhibitors; Oligomycin

(Oligo), FCCP, and Rotenone (Rot) and Antimycin A (AA) and the glycolysis inhibitor; 2-DG. Measurements of (A) Oxygen consumption rate (OCR) and (B) extracellular acidification rate (ECAR) were plotted for each group with three measurements made in 5 minute intervals after inhibitor injection. (C) Basal respiration and (D) basal glycolysis were plotted and are also depicted as an energy phenotype plot (E). Statistical significance in C and D were calculated using one-way ANOVA compared to media control, where *p<0.05 **p<0.01 ***p<0.001 and **** p<0.0001. Error bars show mean ± SEM for three individual experiments.

3.5 Human THP-1 macrophages treated with PLGA particles in the 0.5-2 μm size range demonstrate enhanced anti-inflammatory cytokine responses after training.

Experiments were then carried out to address whether the particle induced responses seen in murine macrophages was also observed in human macrophages. An established human model is the immortalised human leukaemia monocyte cell line, THP-1, which can be differentiated to macrophages using phorbol-12-myristrrate-13-acetate (PMA) treatment for 48 hours.

The optimal PMA concentration was investigated by measuring the extent of differentiation to macrophages, cytotoxicity and impact on inflammatory cytokine secretion. A concentration range between 10 and 100 nM was assessed. Across the range of concentrations, there was minimal variation in % live cells following 48 hour PMA treatment, with 25 nM PMA yielding the greatest cell viability (Figure 3.5.1 A). To test the concentration of PMA required to promote differentiation of THP-1 monocytes to macrophages, the expression of macrophage differentiation markers; CD11b and CD14 were examined. All concentrations of PMA promoted a shift towards a double positive population, with 10 nM promoting the greatest % of double positive cells, at 51% (Figure 3.5.1 B). Another feature of PMA treatment which was assessed was its propensity for altering cytokine secretion, as it has previously been described to influence the expression of pro-inflammatory genes [504, 505]. Incubation of cells with 10-100 nM PMA had no significant effect on IL-6 secretion after 48 hour incubation (Figure 3.5.1 C). The secretion of TNFα was affected by PMA in a concentration dependent manner, with significant enhancement in response to 50 and 100 nM (Figure 3.5.1 D). In light of these results, the optimal concentration chosen for our THP-1 differentiation protocol was 10 nM.

Having established an adequate concentration of PMA which promoted macrophage differentiation but did not enhance inflammatory responses, the effect of PLGA particles on cytokine secretion was assessed. Exposure of THP-1 macrophages to PLGA particles (300 μg/ml) across a range of sizes did not influence secretion of IL-1Ra or IL-10 (Figure 3.5.2 A-B). Furthermore, when LPS at 100 ng/ml was used as a co-stimulus there was no significant particle induced enhancement of IL-10 or IL-1Ra secretion (Figure 3.5.2 C-D).

The metabolic profile of particle treated THP-1 macrophages was also tested by carrying out mitochondrial and glycolytic stress tests. β-glucan was used here as a control, as it has been described to attenuate inflammatory responses in THP-1 macrophages [506, 507]. Treatment of cells for 24 hrs with 1μm PLGA particles or β-glucan enhanced the basal OCR and ECAR of THP-1 macrophages compared to controls (Figures 3.5.3 C-D). The injection of mitochondrial inhibitors brought the OCR back to baseline, indicating a strong reliance on OxPhos. Additionally, the glycolytic inhibitor 2-DG reduced ECAR to baseline (Figures 3.5.3 A and B) indicating a high glycolytic rate. These results taken together indicate a shift towards a highly metabolic phenotype, with readouts for both glycolysis and OxPhos increasing significantly following β-glucan and PLGA particle treatment (Figure 3.5.3 E).

The size dependent trained response to PLGA particle size in THP-1 macrophages was also assessed. THP-1 macrophages were incubated with PLGA particles across a range of sizes at 300 μg/ml for 24 hours, rested for 6 days and re-stimulated with LPS (100 ng/ml). The secretion of IL-10 and IL1Ra was enhanced but only from THP-1 macrophages trained with 1 and 2 μm PLGA particles following LPS re-stimulation (Figures 3.5.4 A and B). There was also a slight increase in IL-1Ra secretion from 1-2 μm particle treated THP-1 macrophages which were not re-stimulated with TLR agonists.

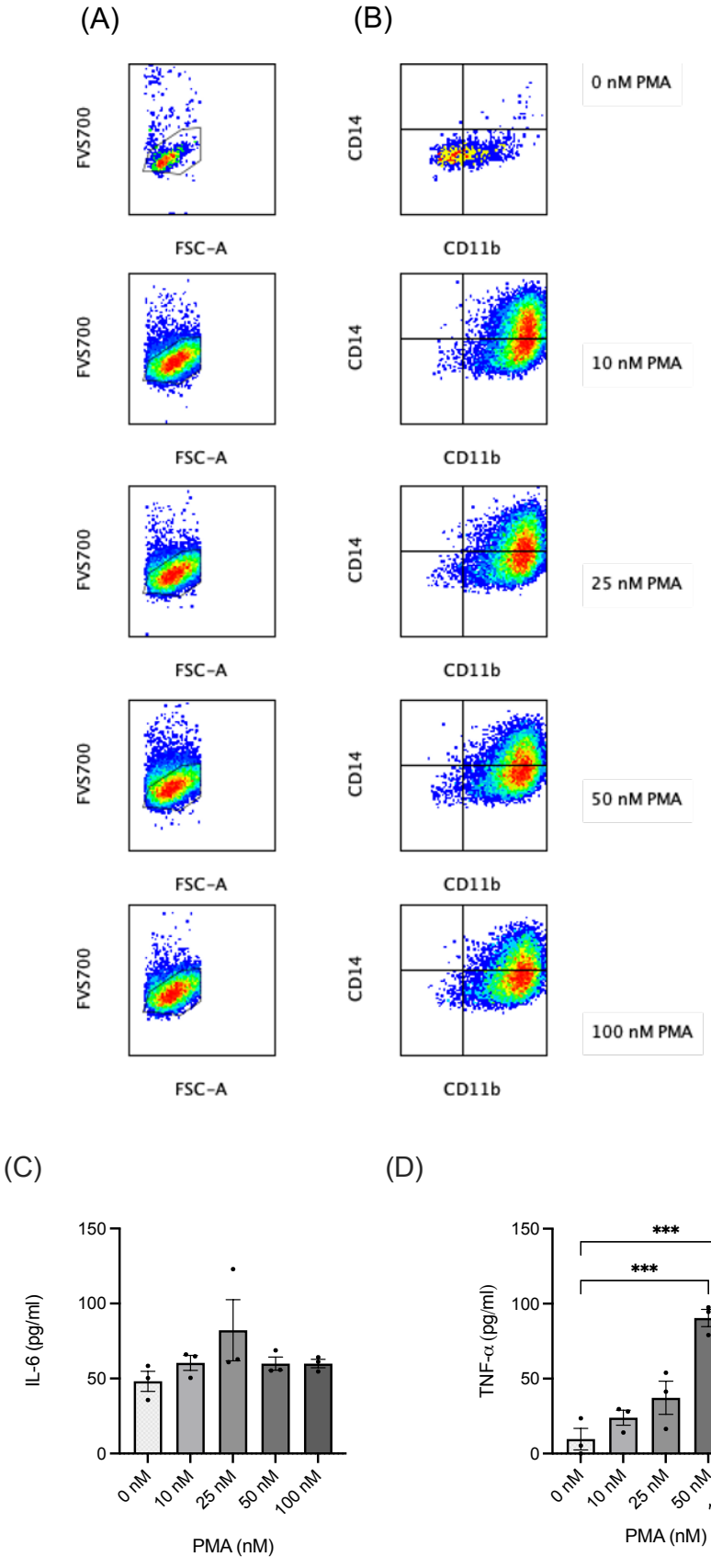

Figure 3.5.1 10 nM PMA promotes THP-1 differentiation towards a macrophage phenotype, without promoting pro-inflammatory responses. THP-1 monocytes ($0.5x10^6$ cell/ml) were left

untreated or treated with PMA at a concentration of 10-100 nM for 48 hours. Following a 24 hour rest period, THP-1's were stained with fixable viability stain FVS700 and for THP-1 derived macrophage markers; CD11b and CD14. Analysis by flow cytometry was carried out and representative dot plots for (A) cell viability and (B) the CD14/CD11b populations. Supernatants were also collected to measure pro-inflammatory (C) IL-6 and (D) TNFα secretion. Error bars show mean ± SEM and statistical significance was calculated using (C-D) one way ANOVA. Statistical significance was displayed as; *$p<0.05$ **$p<0.01$ and ***$p<0.001$. Experiment was performed (A-B) twice and (C-D) in triplicate using THP-1 cells from distinct passages.

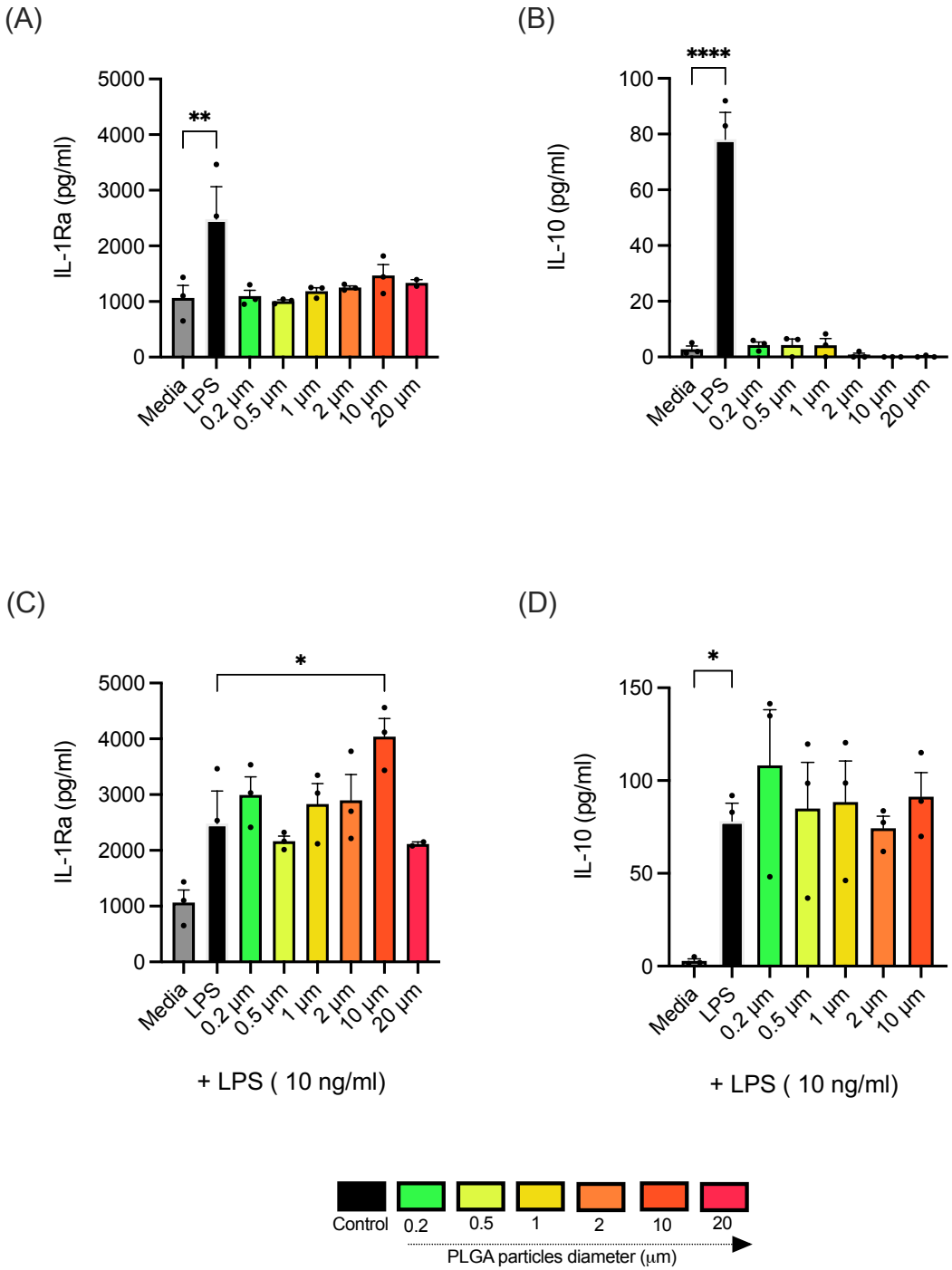

Figure 3.5.2 PLGA particles in the 0.2-20 µm range do not enhance anti-inflammatory cytokine secretion from THP-1 derived macrophages. THP-1 derived macrophages ($0.5x10^6$ cell/ml) were incubated with PLGA particles in the size range of 0.2-20 µm (300 µg/ml) alone (A-B) or with LPS (100 ng/ml) for 24 hours. Secretion of IL-1Ra (A and C) and IL-10 (B and D) in the supernatant was measured by ELISA. One way ANOVA was used to determine statistical significance compared to untreated control (A-B) or LPS control (C-D) , where *p<0.05 **p<0.01 ***p<0.001 and **** p<0.0001. Error bars show mean and ± SEM for three individual experiments.

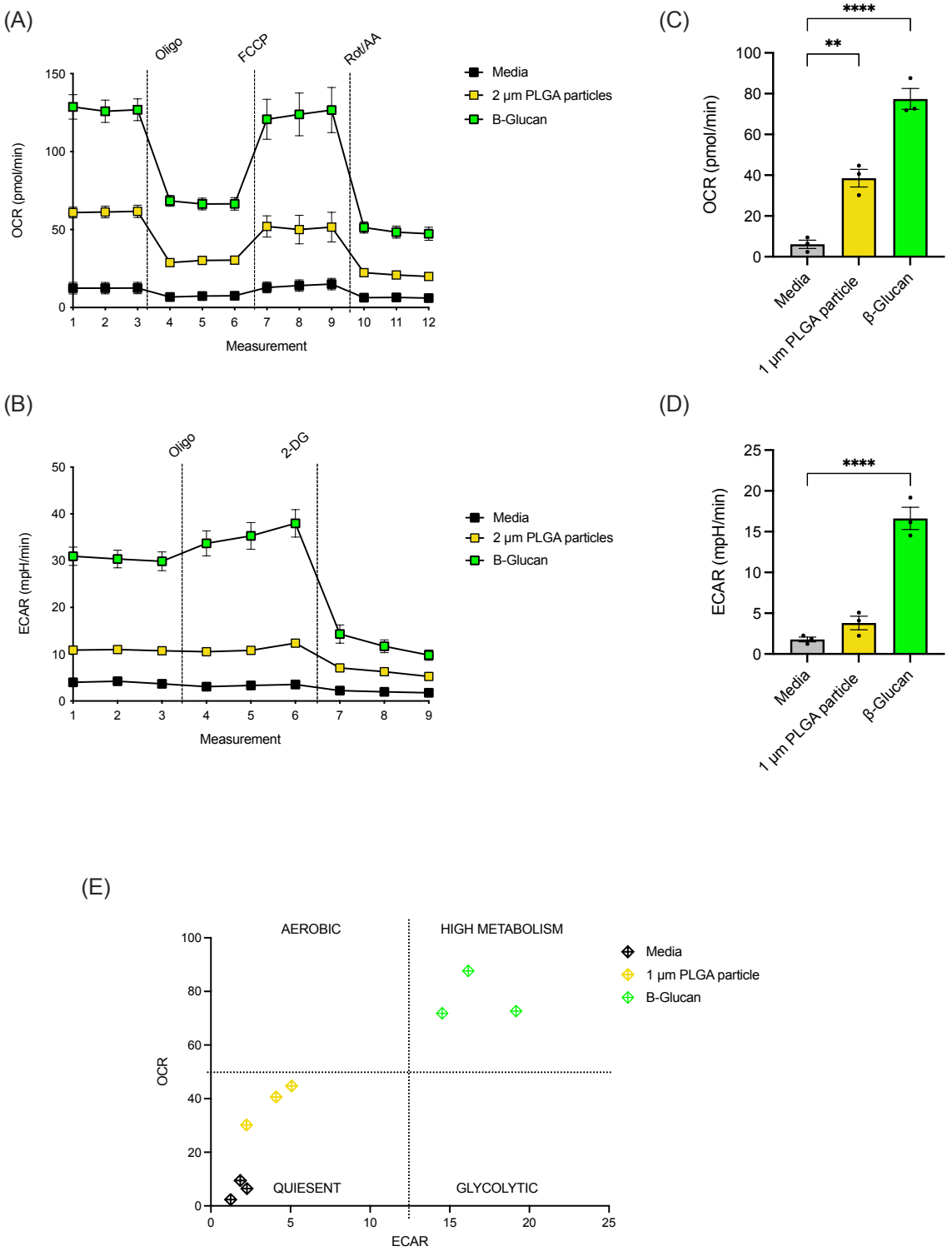

Figure 3.5.3 1 µm PLGA particles promote a shift in THP-1 derived-macrophage metabolic profile, enhancing both OxPhos and glycolysis. THP-1 derived macrophages ($1.5x10^5$ cell/well) were treated with 1 µm PLGA particles (300 µg/ml) or β-glucan (100 µg/ml) for 24 hours. A mitochondrial and glycolytic stress assay was conducted on Agilent XFe96 Seahorse analyser using the following

mitochondrial inhibitors; Oligomycin (Oligo), FCCP, and Rotenone (Rot) and Antimycin A (AA) and glycolysis inhibitor; 2-DG. Measurements of (A) Oxygen consumption rate (OCR) and (B) extracellular acidification rate (ECAR) were plotted for each group with three measurements made in 5 minute intervals after inhibitor injection. (C) Basal respiration and (D) basal glycolysis were plotted as bar charts and are also depicted as an energy phenotype plot (E). Error bars show the mean ± SEM and statistical significance in (C-D) were calculated using ordinary one-way ANOVA against media control, where *$p<0.05$ and **$p<0.01$. Experiment was performed in triplicate using cells from three distinct passages.

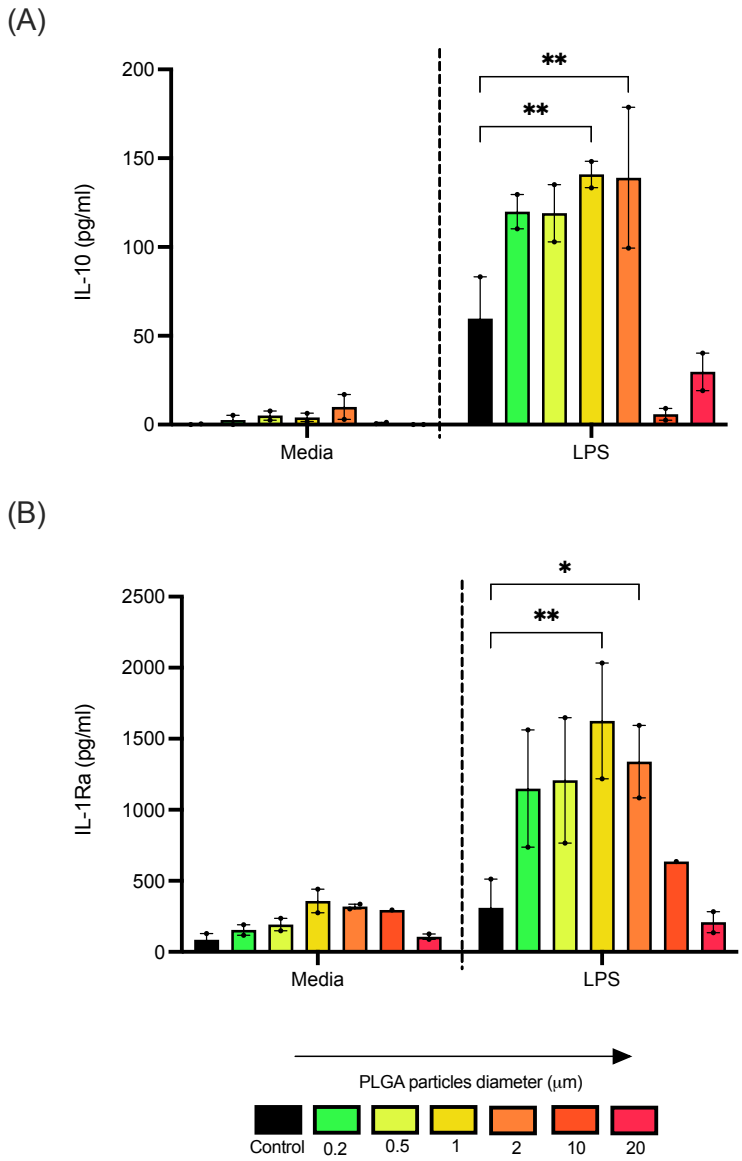

Figure 3.5.4 Training THP-1 derived macrophages with PLGA particles of 1-2 µm in size up-regulates secretion of the anti-inflammatory cytokines IL-1ra and IL-10. THP-1 derived macrophages ($1x10^6$ cell/ml) were treated with PLGA particles of 0.2 - 20 µm in diameter (300 µg/ml) for 24 hours. Media with particles was removed and cells were rested for 6 days, before being re-stimulated with LPS (10 ng/ml) for a further 24 hours. Supernatants were collected and ELISA was performed to measure the concentration of (A) IL-10 and (B) IL-1Ra. Two way ANOVA with Dunnet's multiple comparison was used to determine statistical significance compared to control where *$p<0.05$ and **$p<0.01$. Error bars show mean ± SEM for two individual experiments using THP-1 cells from distinct passages

3.6 BMDMs treated with PLGA particles in the 0.5-2 μm size range have altered morphology and reduced membrane fluidity.

Having established the capacity of PLGA particles in the 0.5-2 μm range to skew BMDMs towards an anti-inflammatory phenotype, the mechanisms underlying these responses were investigated.

In order to assess the fate of 2 μm PLGA particles when cultured with BMDMs, FITC-conjugated particles were used. The capacity of BMDMs to internalise the particles over a period of 24 hours was measured, based on the increase in the fluorescence within the cell boundary of images captured using a live cell imager (Incucyte®). The fluorescence within BMDMs increased in the first 2-6 hours, before reaching a plateau. This demonstrated the capacity of BMDMs to efficiently phagocytose 2 μm PLGA particles with cells becoming saturated by the 6 hour timepoint.

One of the key differences noted after 24 hour incubation with PLGA particles, was that BMDMs treated with 0.5-2 μm particles were notably smaller, had fewer protrusions and appeared more compact. These physical properties were quantified by flow cytometry (Figure 3.6.1 A-E), comparing the forward and side scatter (FSC and SSC respectively) of BMDMs left untreated (grey histogram) or treated with particles of various sizes (coloured histograms) (150 μg/ml). Forward scatter is indicative of cell size, with greater FSC-A intensity being proportional to larger cells. Side scatter measures the internal complexity of the cell, with more granular cells having higher SSC. There was a pronounced decrease in intensity of FSC-A in the BMDMs treated with 0.5-2 μm particles, as well as an increase in SSC-A (Figure 3.6.1 A-C). BMDMs treated with larger 10 μm particles had no significant shift in FSC-A or SSC-A when compared to untreated BMDMs (Figure 3.6.1 D). The unique morphological alterations observed in by flow cytometry were also evident in the confocal microscopy images presented in Figure 3.6.1 E and F. Untreated BMDMs (Figure 3.6.1 E) appeared spindle-like with many protrusions whilst BMDMs treated with FITC-conjugated 1 μm PLGA particles were significantly smaller, rounder (Figure 3.6.1 F).

Next, the effect of particles in this size range, on the cell membrane was investigated. The cell membrane and cytoskeleton play integral roles as sensors to alert the cell to changes in its environment, allowing the cell to adapt and survive

to changes imposed on its morphology. It was hypothesised that, a decrease in membrane fluidity would accompany the observed shrinkage of BMDMs in response to 0.5-2 μm PLGA particles. Fluorescent recovery after photobleaching (FRAP), a confocal microscopy technique, was used to measure changes in membrane fluidity. The protocol is schematically represented in Figure 3.6.2 A . Fluorescently labelled cell-membrane proteins in a small region on the cell surface were photobleached with a high intensity argon laser. This is depicted in the images taken post photo-bleaching in Figure 3.6.2B. The images are representative of the fluorescent recovery within the photobleached ROI at time 0,10 and 30 sec, of cells in hyper-osmolar media. Over time, unbleached membrane bound proteins migrate back into the photobleached region. Depending on the membrane fluidity, the rate at which these proteins move can be tracked by the half time required to recover fluorescence intensity in the ROI. The membrane fluidity of cells exposed to different osmolarities was used as controls. Cells exposed to hypo-osmolar media (1:5 $_{d}H_2O$ in media) swell, which should in theory enhance membrane fluidity. Indeed, the membrane fluidity of BMDMs in hypo-osmolar media increased, denoted by a distinct decrease in the rate of recovery half-time to about 20 seconds, from the rate of recovery of 40 seconds in untreated BMDMs. BMDMs exposed to hyper-osmolar media (150 mM sucrose) should in theory shrink, resulting in reduced membrane fluidity. This was demonstrated here as an significant increase in the rate of recovery of 94 seconds compared to untreated BMDMs. Cells exposed to 1 μm PLGA particles had a recovery rate of approximately 64 seconds, which was significantly longer than the recovery rate of untreated BMDMs, indicating a decrease in membrane fluidity (Figure 3.6.2 C).

The morphological alterations specific to BMDMs treated with 0.5-2 μm PLGA particles could be indicative of cell apoptosis [508]. To verify that PLGA particles do not induce apoptotic cell death, Annexin V was used to quantify the exposed phosphatidylserine (PS); inner membrane component only exposed in early and late apoptosis. The membrane-impermeable propidium iodide (PI) was also used to measure cell death. PI intercalates with DNA which is released during cell membrane fragmentation, a sign of programmed cell death. Increase in Annexin V staining but not PI is usually characteristic of early apoptosis, whilst increase of both indicates late apoptosis. Increased PI alone is usually indicative of cell death via an alternative pathway such as necroptosis or pyroptosis. As a positive control

for apoptosis, BMDMs were treated with hydrogen peroxide, a known inducer of apoptosis at concentrations less than 4 mM [509]. The % live cells in the 1-2 μm particle treated groups were comparable to untreated BMDMs indicating no significant cell death. Furthermore, particles did not induce early or late apoptosis after a 24 hour incubation, which was clearly induced in the positive control (Figure 3.6.3 A-B). These results indicate that the morphological alterations observed in cells incubated with the 1-2 μm PLGA particles are not demonstrative of apoptosis.

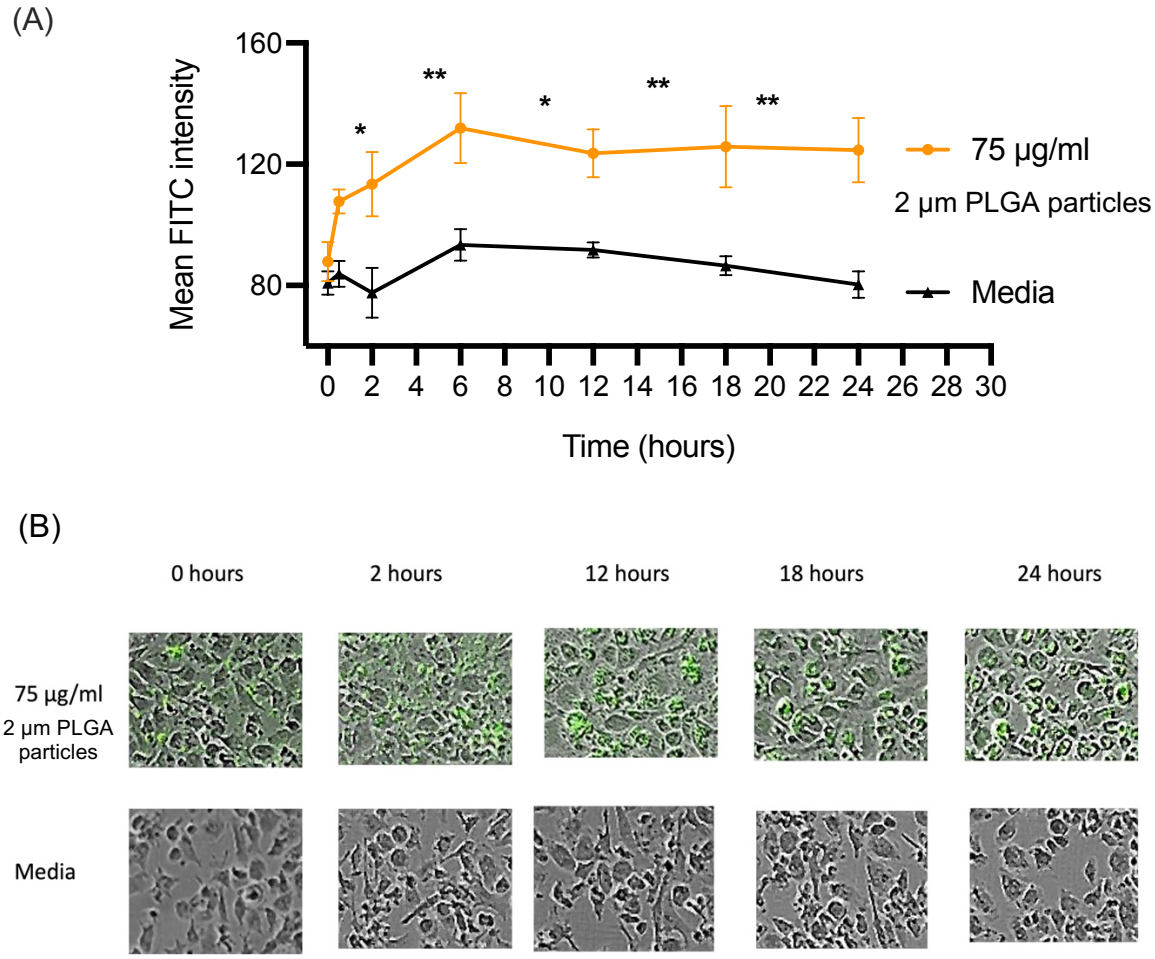

Figure 3.6.5 BMDMs begin to internalise 2 µm PLGA particles within the first hour after incubation. The internalisation of FITC-labelled 2 µm PLGA particles over time by BMDMs isolated from C57BL/6 mice was measured from images acquired on Incucyte® live-cell analyser. (A) The mean fluorescence intensity in the green-fluorescent channel was measured within the cell boundary over time. The fluorescence intensity was measured within 6 cells per image, and three images per condition and time point. Analysis was carried out using Fiji ImageJ software using the histogram analysis function. (B) Representation of corresponding images generated by the Incucyte® live-cell imager over time, which were used to measure FITC intensity within BMDMs. Presented images have undergone cropping and processed to reduce noise. Two-way ANOVA with Šídák's multiple comparisons test was used to determine statistical significance as compared to media control, where *$p<0.05$ and **$p<0.01$. Error bars show mean and ± SEM for the average of 6 cells measured per image, and analysis of three images per group per time point.

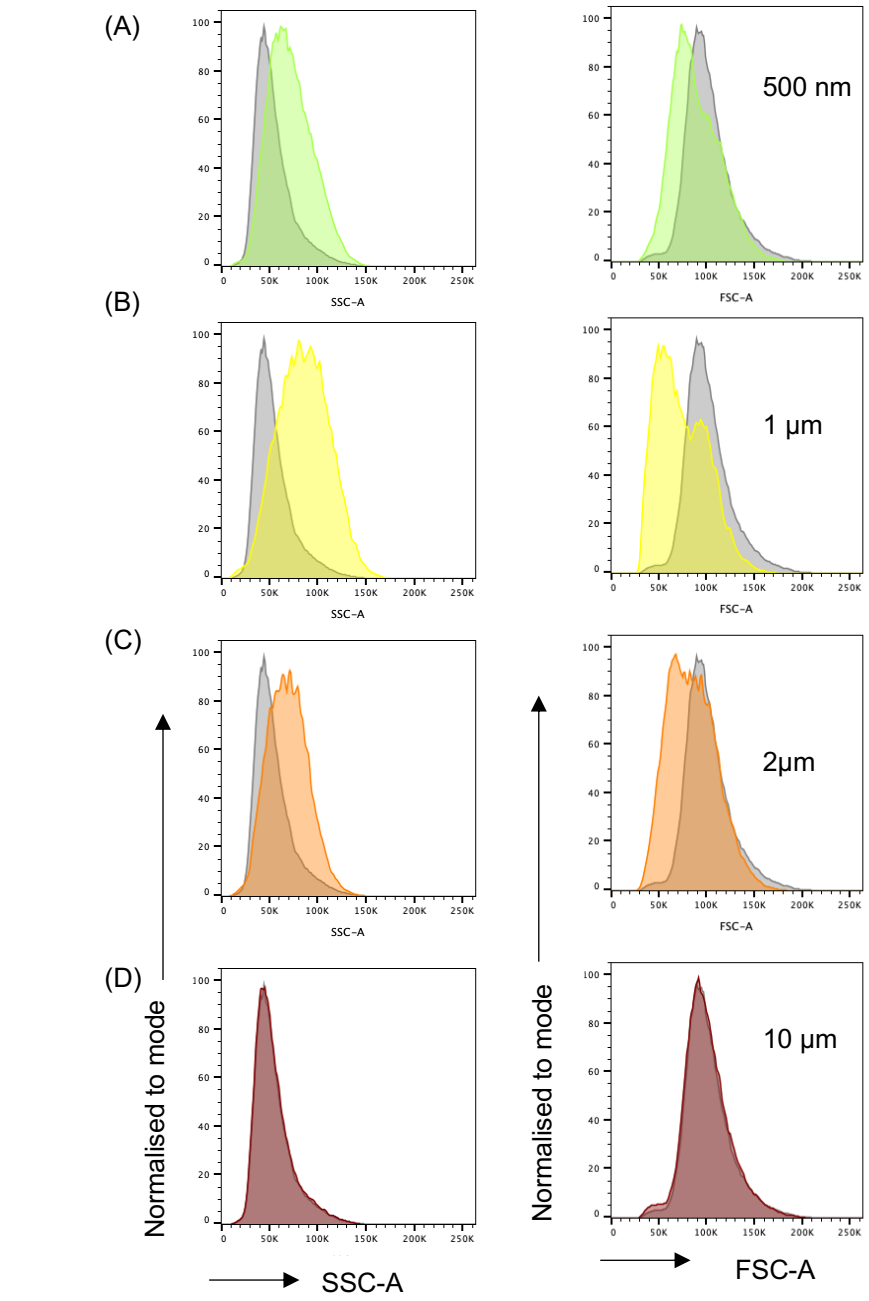

(E)

(F)

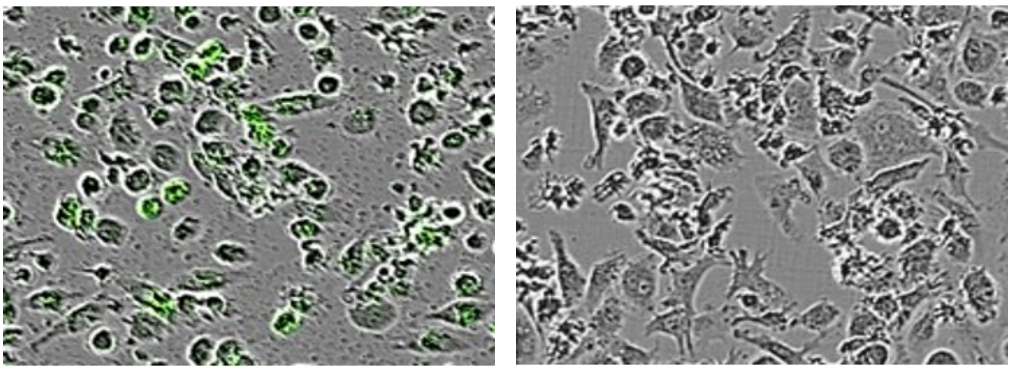

Untreated

2 µm PLGA particles- FITC

Figure 3.6.2 BMDMs incubated for 24 hours with PLGA particles of 0.5-2 μm in size exhibit decreased size and increased granularity. Changes in morphology were analysed by flow cytometry and represented as histograms for forward and side scatter (FSC and SSC respectively). Histograms for untreated BMDMs (grey histogram) were compared against BMDMs treated with (A) 0.5μm (B) 1μm (C) 2μm, (D) 10 μm (300 μg/ml) (coloured histograms). Representative phase contrast images for BMDMs left untreated (E) and treated with FITC-conjugated 1 μm PLGA particles (F) were obtained by the IncucyteSX5 live-cell analyser after 24-hour incubation. Histograms are representative of three biological replicates obtained over three distinct experiments.

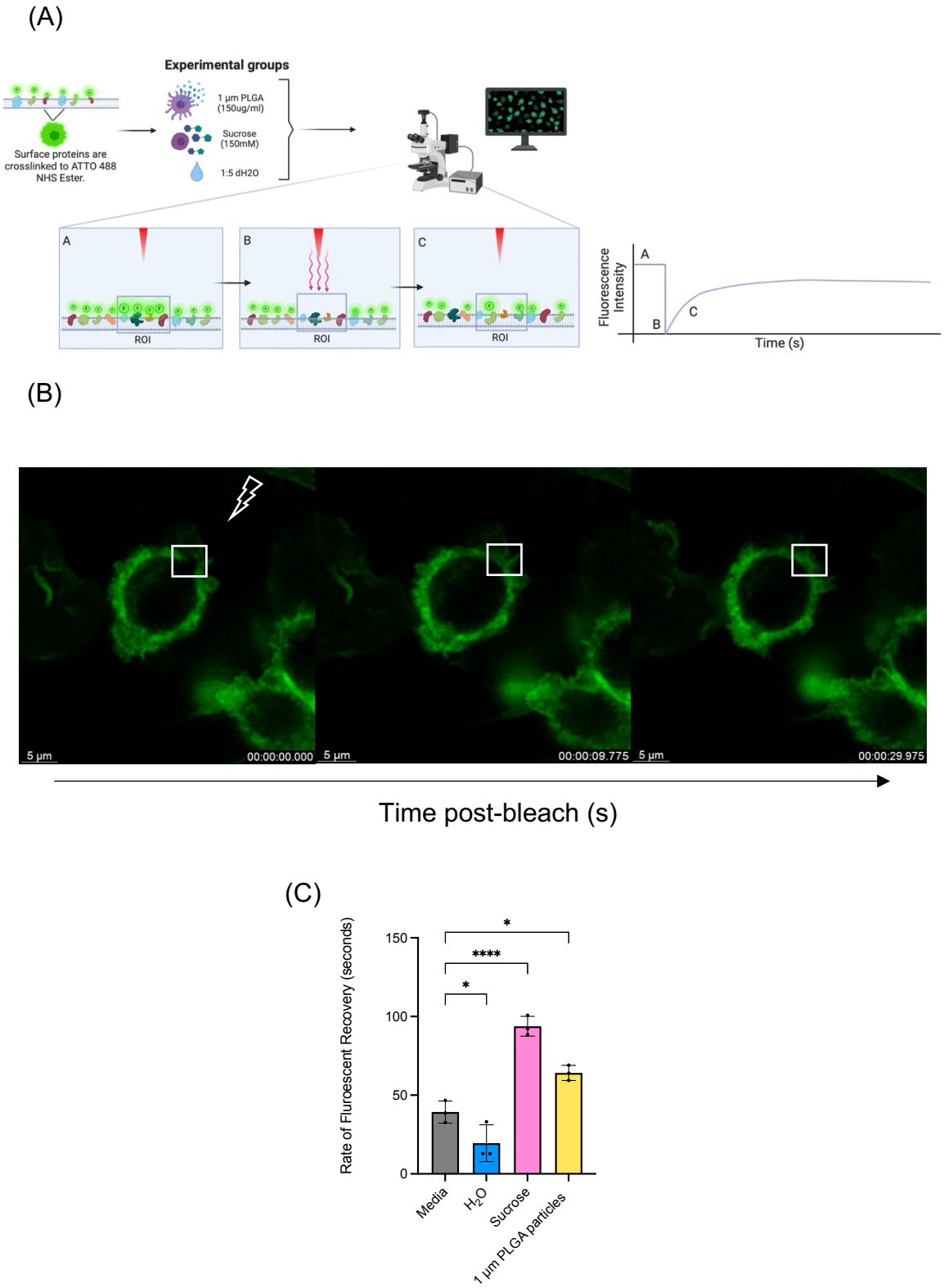

Figure 3.6.3 Incubation with 1µm PLGA particles decreases the membrane fluidity of BMDMs after 1 hour incubation. Membrane proteins on BMDMs (1x10^6 cell/ml) were tagged with Atto 488 NHS ester. BMDMs were then treated with 1 µm PLGA particles (150 µg/ml), a hypo-osmotic control

(1:5 H_2O in media) and hyper-osmotic control (150mM sucrose in media) for 1 hour before being subjected to FRAP analysis on a on Leica TCS SP8 STED confocal microscope. A high-intensity argon laser was used to photo-bleach a 4 μm² region of interest (ROI) of fluorescently labelled cell membrane. The rate of fluorescence recovery into the ROI was recorded post-bleach. (A) Images were captured instantly after photo-bleaching, at 10 sec post bleach and 30 sec post bleach. (B) Schematic describing the FRAP protocol. (B) Fluorescent recovery half-time for each experimental group was calculated using the Leica LAS x-Software FRAP analysis tools which generates rate of recovery curves providing half-time for the rate of recovery in seconds. Fluorescence recovery half-time was graphed as mean ± SEM for three individual experiments using distinct biological replicates. One-way ANOVA was used to determine statistical compared to untreated control, where *$p<0.05$ **$p<0.01$ ***$p<0.001$ and **** $p<0.0001$.

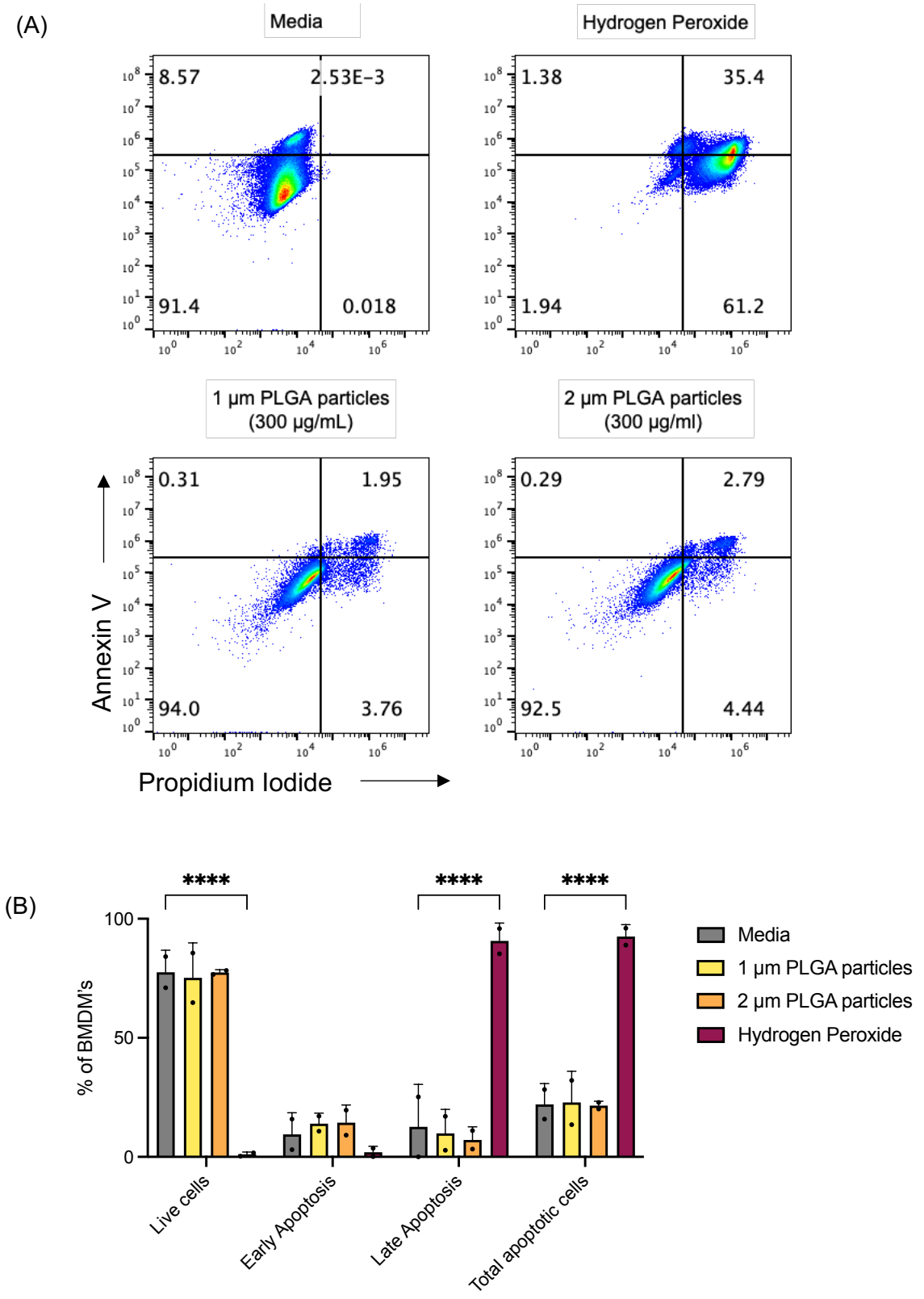

Figure 3.6.4 Treatment of macrophages with PLGA particles in the 1-2 µm range does not induce significant apoptosis after 24 hours incubation. BMDMs ($6.25x10^6$ cell/ml) were treated with 1 or 2 µm PLGA particles (300 µg/ml) or hydrogen peroxide (500 µM) for 24 hours. BMDMs were then fluorescently stained with Annexin V and propidium iodide (PI) and analysed by flow

cytometry. (A) Representative histograms of the intensity of Annexin V and PI in single cells left untreated or treated with particles or hydrogen peroxide. (B) % of live cells quantified as double negative for PI and Annexin V, % of early apoptotic cells quantified as Annexin V positive, % of late apoptotic cells quantified as double positive and % of the total apoptotic cell population. Two-way ANOVA with Dunnet's multiple comparison was used to determine statistical significance as compared to media control, where *$p<0.05$ **$p<0.01$ ***$p<0.001$ and **** $p<0.0001$. Error bars show mean and ± SEM for two individual experiments.

3.7 The mechano-sensor; αvβ3 is required for particle induced IL-1Ra secretion and is upregulated in BMDMs treated with PLGA particles of 0.5-2μm in size.

The size-dependent effect of particles on membrane dynamics, described in results section 3.6, suggests a potential role for a mechano-sensor in modulating BMDMs towards an anti-inflammatory phenotype. Mechano-sensors which have been linked to immune modulation include the ion channels; Piezo1 and TRPV4 [172], as well as integrins such as $\alpha_v\beta_3$, $\alpha_v\beta_6$, $\alpha_v\beta_8$ integrin [510]. The involvement of these mechano-sensors was investigated using specific inhibitors and agonists and measuring the changes to the secretion of IL-1Ra. The secretion of IL-1Ra was chosen due to the capacity of 0.5-2 μm PLGA particles enhance IL-1Ra alone, without the need for a secondary TLR agonist. This provides a valuable system to determine the involvement of mechano-sensors in the anti-inflammatory response without the interference of TLR signalling.

Taking advantage of RNA-sequencing data obtained by a previous lab member; Dr Aoife Gorman, changes to the gene expression pertaining to mechano-sensitive proteins or receptors was investigated to refine the investigation [45]. This data set was generated from RNA isolated from alum-treated BMDMs, which was demonstrated to also upregulate IL-1Ra signalling. It was, therefore, used as a reference rather than a direct comparison to particle treated BMDMs. The *itgb3* gene, which encodes the β_3 integrin dimer was identified as a significantly upregulated gene in response to alum. It's potential involvement in particle induced IL-1Ra was, therefore, addressed.

The surface expression of β_3 was measured in BMDMs that were treated with 0.5-2 μm PLGA particles (150 μg/ml) for 24 hours, using a fluorescently labelled antibody against β_3 to measure the mean fluorescent intensity (MFI). Histograms were generated comparing untreated and treated BMDMs (Figure 3.7.1 A-F). BMDMs treated with 0.5-2 μm PLGA particles demonstrated a significant shift in the intensity of β_3 expression (Figure 3.7.1 A-C), with an increase in MFI of approximately 10-30% as compared to the MFI of untreated BMDMs (Figure 3.7.1 G). However, BMDMs treated with the larger 10 and 20 μm particles and LPS did not demonstrate this increase β_3 expression (Figure 3.7.1 D-F). β_3 has been shown to dimerize with αv as well as $\alpha_{IIB,}$ however, owing to the role of $\alpha_v\beta_3$ in innate

immune cell regulation it was prioritised for this investigation.

Next, the role of $\alpha_v\beta_3$ in the particle-mediated secretion of IL-1Ra by BMDMs was determined by using the inhibitor, Cilengitide (75-300 μM) and neutralising antibodies (nAb) against β_3 and α_v (50 μg/ml). Blockade of αvβ3 with either the inhibitor or the nAb led to a reduction in particle-induced secretion of IL-1Ra (Figure 3.7.2 A-B). The decrease in IL-1Ra in the inhibited groups was significant, however, it was not brought down to the basal level. Cilengitide was tested at concentrations ranging from 75-300 μM, with all concentrations having equal inhibitory properties (Figure 3.7.2 A). Blockade of one or both integrin dimers was sufficient to reduce IL-1Ra secretion to the same extent, indicating a redundancy of integrin signalling when one is blocked (Figure 3.7.2 B).

The role of αvβ3 in innate immune training by 0.5-2 μm PLGA particles was also assessed, using the nAbs one hour prior to training. When αv or β3 was inhibited, 2 μm PLGA particle trained BMDMs were unable to mount the enhanced IL-1Ra secretion which was previously demonstrated after LPS restimulation. However, it must be noted that the secretion of IL-1Ra in untreated BMDMs was also decreased in response to the nAb, indicating a potential global reduction in IL-1Ra signalling rather than a particle-specific mechanism. Neutralisation of both dimers demonstrated a slightly greater inhibitory effect than one or the other alone (Figure 3.7.3 A).

The partial reduction in IL-1Ra secretion following blockade of αvβ3 (Figure 3.7.2) suggested a potential involvement of a second mechano-sensor in the mechanism of action of 0.5-2 μm particles. Inhibitors RN1374 and GsMtX4, against the ion channel mechano-sensors TRPV4 and Piezo1 respectively were, therefore, assessed for their impact on IL-1Ra signalling. BMDMs were also treated with specific mechano-sensors agonists; αPDD and Yoda1, as well as 2 μm PLGA particles. Blocking TRPV4 had no significant effect on IL-1Ra secretion, nor did the agonist; αPDD, enhance IL-1Ra secretion (Figure 3.7.4 A). Whilst the Piezo1 agonist; Yoda1 at 1 and 5 μM promoted IL-1Ra secretion in a similar manner to 2 μm particles, the inhibitor did not block these response (Figure 3.7.4 B). This could either indicate a poor inhibitory capacity of GsMtX4 at the concentrations tested or a more complex role of Piezo1 activation in IL-1Ra signalling.

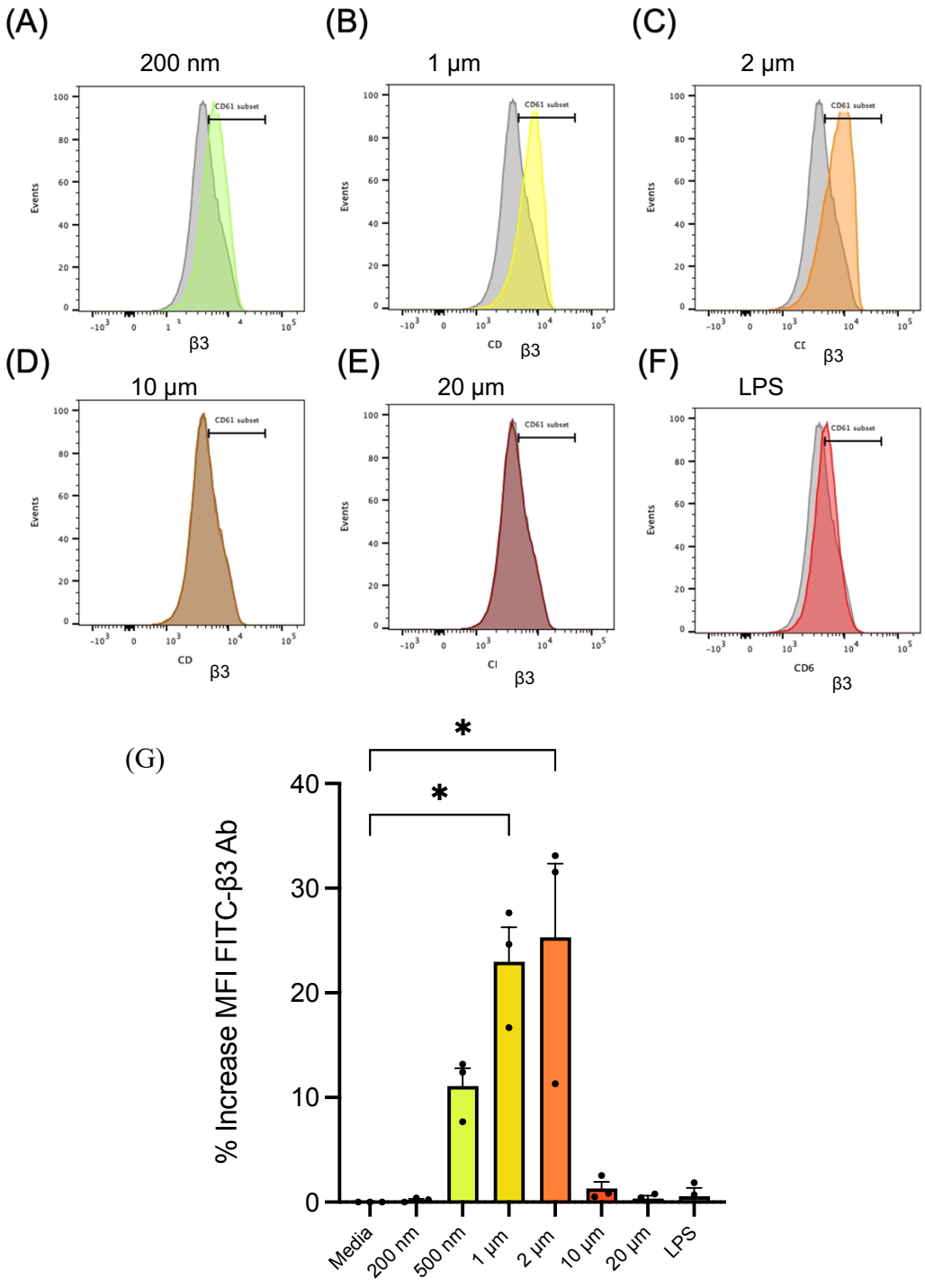

Figure 3.7.1 BMDMs treated with PLGA particles in the 0.5-2 µm size range significantly upregulate surface expression of β3. BMDMs were assessed for the surface expression of β3 by flow cytometry. BMDMs ($1x10^6$ cell/ml) were treated with PLGA particles of various sizes (150 µg/ml) and LPS (10ng/ml) for 24 hours. BMDMs were detached and stained with fixable viability stain BV510 and FITC conjugated β3 antibody. Histograms for untreated BMDMs were compared against BMDMs treated with (A) 0.5 (B) 1 (C) 2 and (D) 10 µm (E) 20 µm PLGA particles and (F) LPS. (G) MFI of FITC-β3 was calculated and the % difference in MFI of treated groups vs untreated

was plotted. Histograms are representative of three biological replicates obtained over three distinct experiments. Kruskal-Wallis test was used to determine statistical significance where *$p<0.05$.

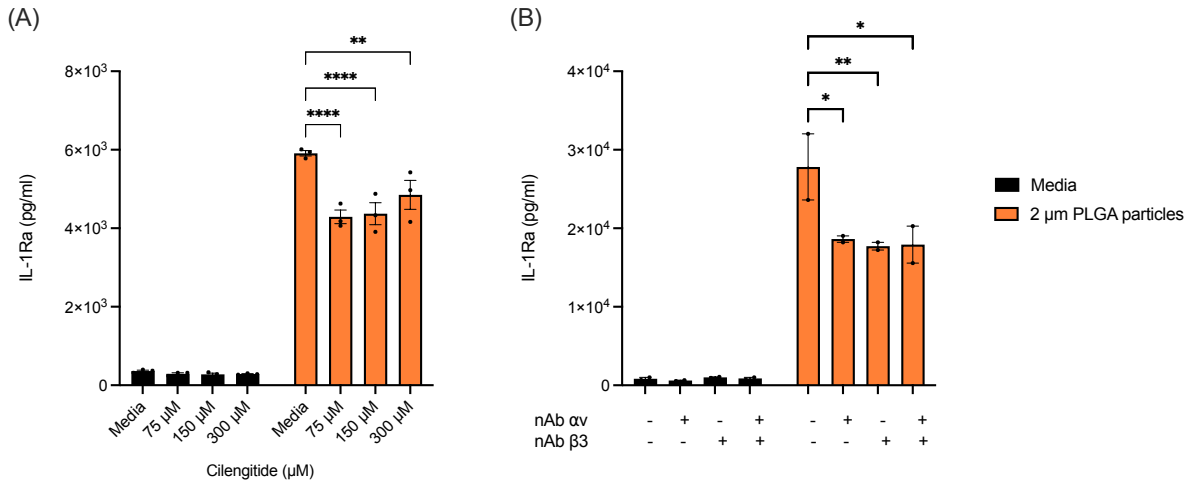

Figure 3.7.2 Blocking αvβ3 results in a partial reduction in IL-1Ra secretion from BMDMs treated with 2 µm PLGA particles. BMDMs were pre-treated with either (A) Cilengitide (75-300 µM) or (B) neutralising monoclonal antibodies against αv and β3 (50 µg/ml) for one hour and then treated with 2 µm PLGA particles (150 µg/ml) for 24 hours. Supernatants were collected to quantify the concentration of IL-1Ra by ELISA. Two way ANOVA with Dunnet's multiple comparison was used to determine statistical significance compared to uninhibited control where *p<0.05 **p<0.01 ***p<0.001 and **** p<0.0001. Error bars show mean ± SEM for (A) three or (B) two biological replicates.

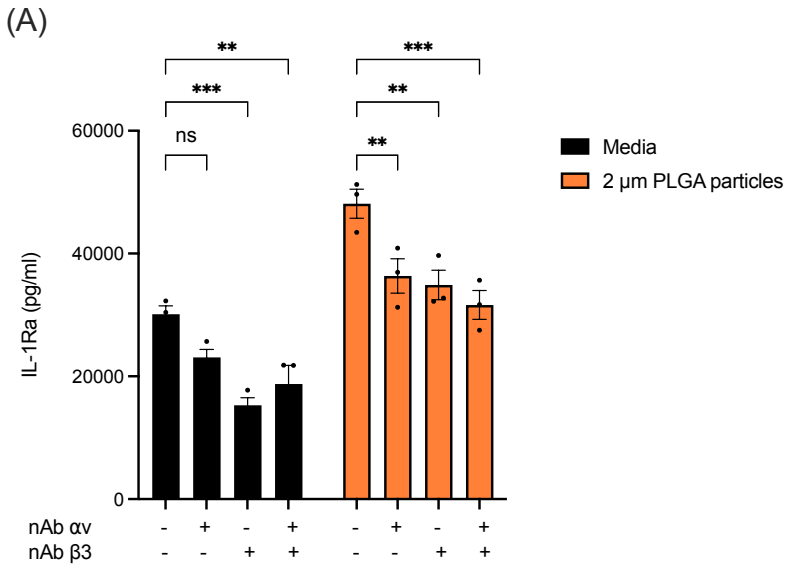

Figure 3.7.3 Blocking αvβ3 reduces IL-1Ra production from BMDMs trained with 2 µm PLGA particles. BMDMs (1x10⁶ cell/ml) were pre-treated with neutralising monoclonal antibodies against αv and β3 for one hour and then treated with 2 µm PLGA particles (300 µg/ml) for 24 hours. Supernatants were removed and replaced with fresh media, and cells were incubated for a further 6 days. On day 6, BMDMs were re-stimulated with LPS (10 ng/ml) for 24 hours. Supernatants were collected to quantify the concentration of IL-1Ra by ELISA. Two-way ANOVA with Dunnet's multiple comparison was used to determine statistical significance compared to uninhibited control where *p<0.05 **p<0.01 and ***p<0.001. Error bars show mean ± SEM for three biological replicates.

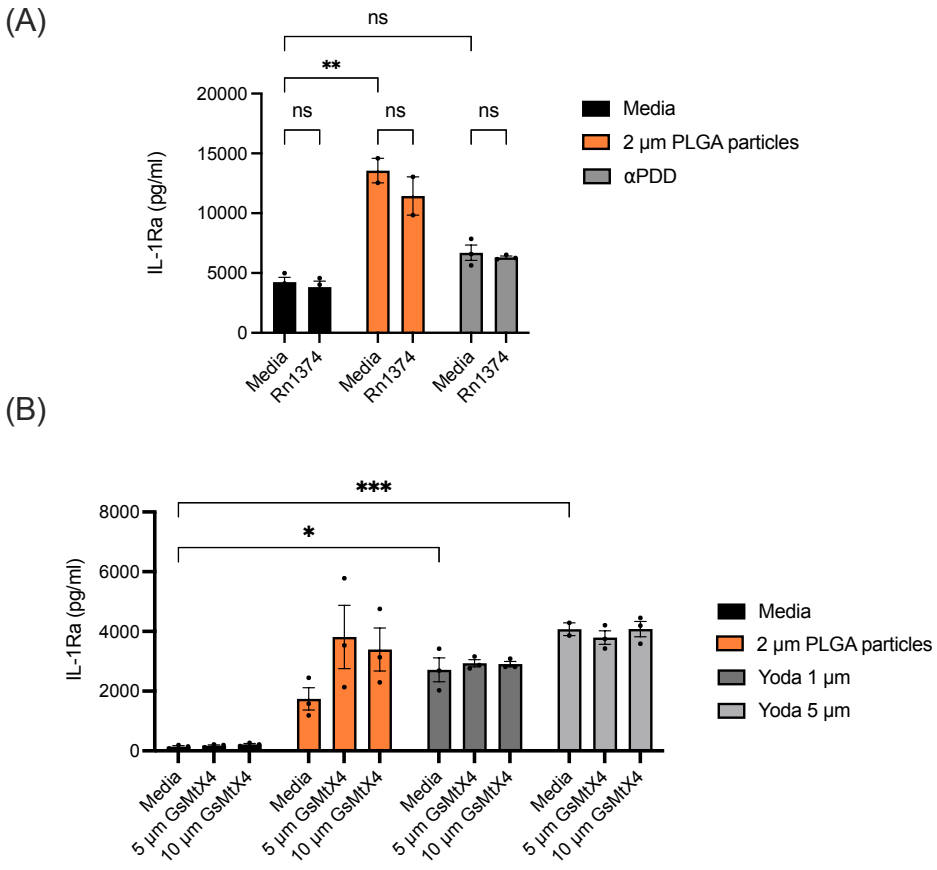

Figure 3.7.4 Blocking calcium channel mechano-sensors; Piezo1 and TRPV4 does not affect IL-1Ra secretion from BMDMs treated with 2 µm PLGA particles. BMDMs (6.25x10^{5}cell/ml) were pre-treated with either (A) TRPV4 inhibitor (RN1374) (50 µM) or (B) Piezo1 inhibitor (GsmTx4) (5-10 µm) for one hour. BMDMs were then treated with either 2 µm PLGA particles (300 µg/ml, (A) TRPV4 agonist (αPDD) (10 µM) or Piezo1 agonist (Yoda 1) (1-5 µM) for 24 hours. Supernatants were collected to quantify the concentration of IL-1Ra by ELISA. Two-way ANOVA with Dunnet's multiple comparison was used to determine statistical significance compared to uninhibited control where *p<0.05 **p<0.01 and ***p<0.001. Error bars show mean ± SEM for three individual experiments.

3.8 mTORC1 is required for IL-1Ra production by BMDMs treated with 0.5-2 μm PLGA particles.

A deeper understanding of how BMDMs respond to PLGA particles in the 0.5-2 μm size range requires assessment of downstream signalling responsible for establishing the anti-inflammatory and innate immune training responses. Referring back to the mechanism behind the enhanced IL-1Ra secretion in alum treated BMDMs, Dr Gorman found that the mTOR pathway was critical in promoting IL-1Ra secretion, but also in the metabolic alterations and capacity to establish innate immune training [63].

To assess the involvement of the mTOR signalling axis in BMDM responses to 0.5-2 μm PLGA particles, BMDMs were pretreated with the specific mTORC1 inhibitor, rapamycin (10 nM). Interestingly, the secretion of IL-1Ra was also significantly reduced when mTORC1 was inhibited in BMDMs treated with 1 or 2 μm PLGA particles at concentrations of 75 or 150 μg/ml (Figure 3.8.1 A-B).

Having established a role for mTORC1 in the acute upregulation of IL-1Ra in response to 1 and 2 μm PLGA particles, the involvement of mTORC1 in establishing training was investigated. BMDMs were pre-treated with rapamycin prior to training with 1 μm PLGA particles (150 μg/ml) and IL-1Ra in the supernatant was measured after LPS (10 ng/ml) or PAM3CSK44 (10ng/ml) re-stimulation, 6 days later. Training with 0.5-2 μm PLGA particles was previously shown to enhance the secretion of IL-1Ra from BMDMs re-stimulated with LPS and PAM3CSK44 (Figure 3.3.1A). When mTOR was inhibited, this enhancement in IL-1Ra was completely abrogated (Figure 3.8.2 A-B). However, rapamycin also inhibited increased IL-1Ra secretion from untrained BMDMs. This could indicate that mTOR plays a role in the global regulation of IL-1Ra signalling in response to TLR agonists, rather than a specific involvement in the establishment of innate immune training by PLGA microparticles.

To ensure that there was no discrepancy in the number of cells remaining after the training protocol, crystal violet analysis was performed on BMDMs on day 7 after re-stimulation. The results demonstrated no significant difference in cell number across all experimental groups (Figure 3.8. C).

Another characteristic of particle trained BMDMs is the metabolic shift towards a predominantly aerobic metabolism. Analysis of the metabolic output of BMDMs

pre-treated with rapamycin prior to training was performed to further investigate the role of mTORC1 in training. 1 μm PLGA particle-trained BMDMs pre-treated with rapamycin had a significantly lower basal OCR and a moderate decrease in ECAR on day 6 tests compared to uninhibited counterparts (Figure 3.8.3 A-D). Looking at the energy profile in Figure 3.8.2 E, the aerobic phenotype resulting from particle training, was brought down by rapamycin, with cells taking on a more quiescent phenotype, although, not as quiescent as untrained BMDMs.

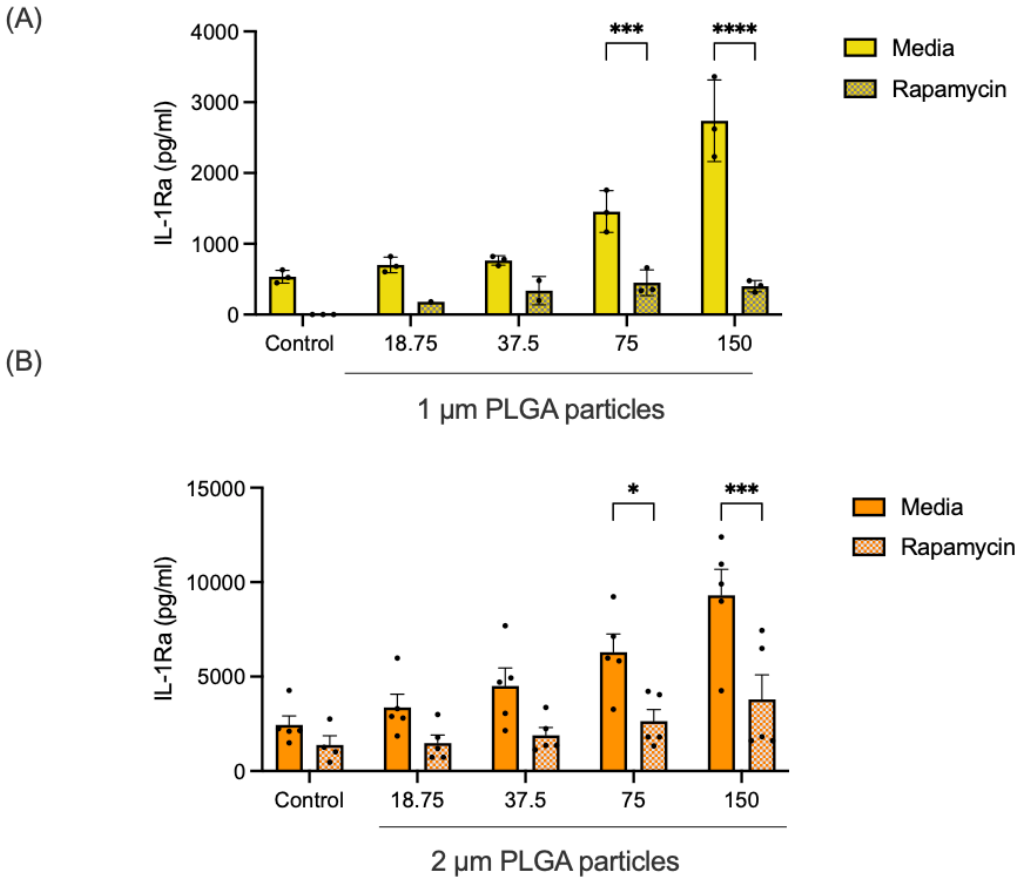

Figure 3.8.1 Rapamycin inhibits the up-regulation of IL1-Ra by 1 and 2 µm PLGA particles. BMDMs ($6.25x10^5$ cell/ml) were pre-treated with Rapamycin (10 nM) or media for 1 hour. BMDMs were then treated with (A) 1 or (B) 2 µm PLGA particles (18.75-150 µm) for 24 hours. Secretion of IL-1Ra in the supernatant was measured by ELISA. Two way ANOVA with Dunnet's multiple comparison was used to determine statistical significance where *p<0.05 **p<0.01 ***p<0.001 and **** p<0.0001. Error bars show mean and ± SEM for (A) five and (B) three individual experiments using distinct biological replicates.

(A)

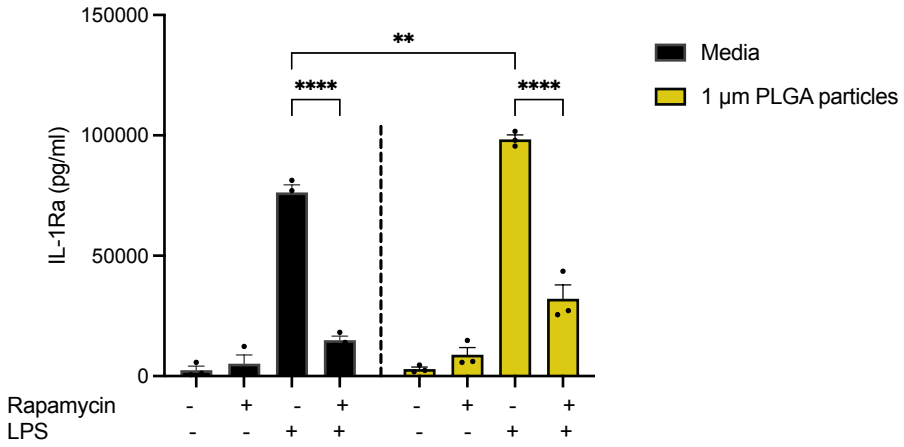
150000
100000
50000
0
IL-1Ra (pg/ml)
**
****
****
Media
1 µm PLGA particles
Rapamycin
LPS

(B)

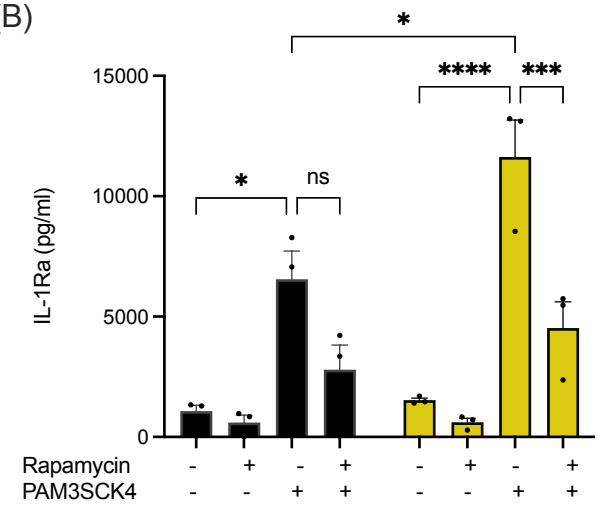
15000
10000
5000
0
IL-1Ra (pg/ml)
*
****
***
*
ns
Rapamycin
PAM3SCK4

(C)

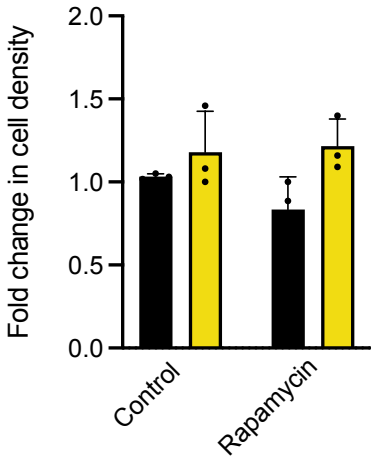
2.0
1.5
1.0
0.5
0.0
Fold change in cell density
Control
Rapamycin

Figure 3.8.2 Rapamycin inhibits the enhanced IL-1Ra response in BMDMs trained with 1 µm PLGA particles. BMDMs ($1x10^6$ cell/ml) were pre-treated with Rapamycin (10 nM) or left untreated for 1 hours. BMDMs were then treated with 1 µm PLGA (150 µg/ml) for 24 hours. Media was replaced after 24 hours and BMDMs were incubated for 6 days before re-stimulating with (A) LPS (10 ng/ml) or (B) PAM3CSK44 (10 ng/ml) . Secretion of IL-1Ra in the supernatant was measured by ELISA. (C) Crystal Violet analysis to quantify the number of adherent cells in culture on day 7 was performed and presented as fold change as compared to untreated group. Two way ANOVA with Dunnet's multiple comparison (A-B) or One way ANOVA (C) was used to determine statistical significance where *p<0.05 **p<0.01 ***p<0.001 and **** p<0.0001. Error bars show mean ± SEM for three individual biological replicates.

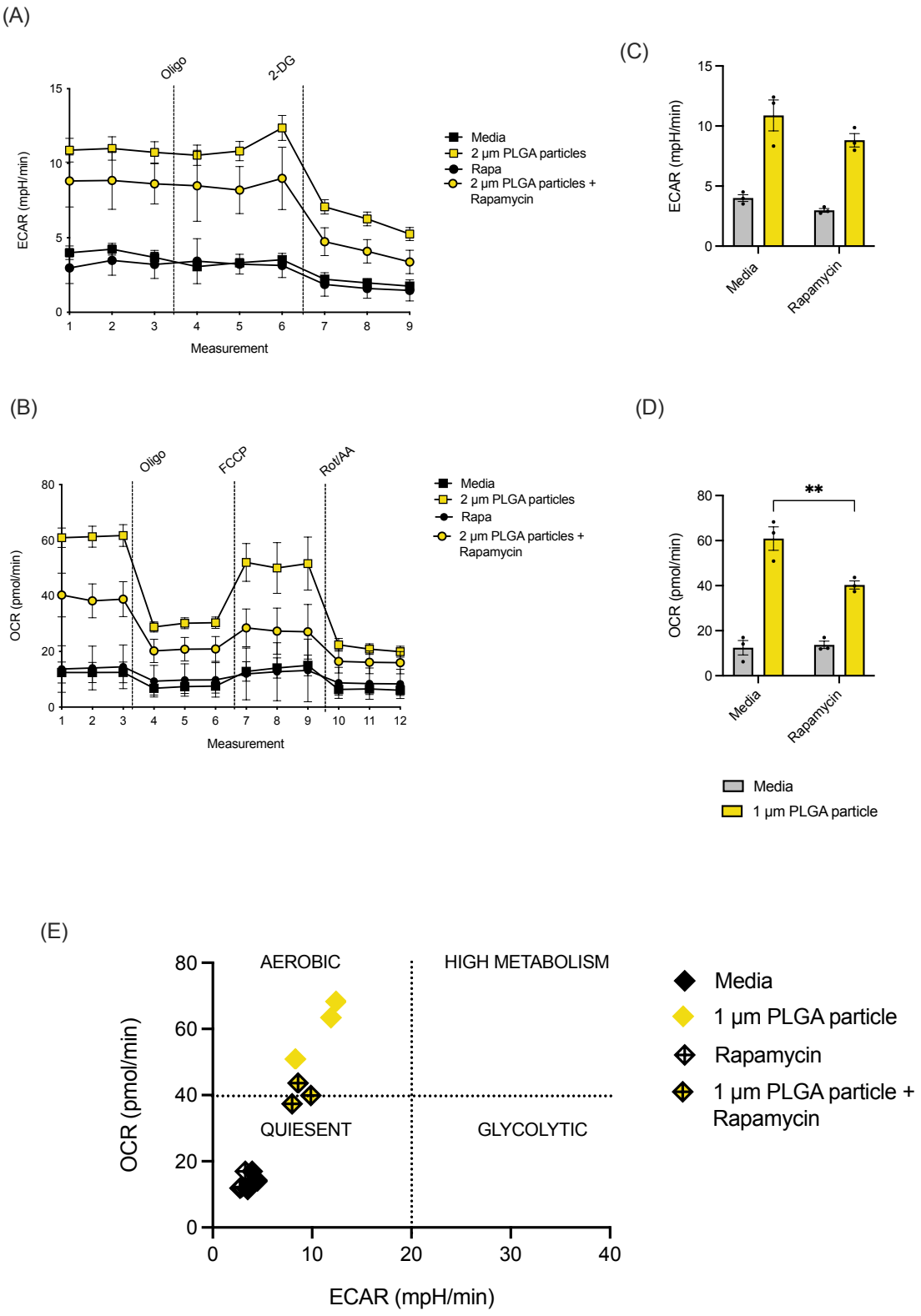

Figure 3.8.3 Rapamycin inhibits metabolic rewiring of BMDMs trained with 1 µm PLGA particles BMDMs (1x10^6 cell/ml) were pre-treated with Rapamycin (10 nm) for 1 hour and then treated with 1 µm PLGA particles (150 µg/ml) for 24 hours. Cells were washed and new media was added. Cells were incubated for 6 days before carrying out the mitochondrial and glycolytic stress assay on an Agilent XFe96 Seahorse analyser using the following mitochondrial inhibitors;

Oligomycin (Oligo), FCCP, and Rotenone (Rot) and Antimycin A (AA) and the glycolysis inhibitor; 2-DG. Measurements of (A) extracellular acidification rate (ECAR) and (B) Oxygen consumption rate (OCR) were plotted for each group with three measurements made in 5 minute intervals after inhibitor injection. (C) Basal glycolysis and (D) basal respiration were plotted as bar charts and against one another to generate an energy profile plot. Error bars show the mean ± SEM and statistical significance in (C-D) were calculated using Two way ANOVA with Dunnett's multiple comparisons compared to media control, where *$p<0.05$ and **$p<0.01$. Error bars show mean ± SEM for three individual experiments.

3.9 Chapter 3 Discussion

The clinical application of biodegradable particles has played a significant role in overcoming the limitations of existing drugs and cell therapies [498,511]. Research in the last two decades has optimised physico-chemical properties of these particles to refine tissue targeting, tune release kinetics [385,477] and protect unstable or easily degraded cargo [50]. However, the implications of these physico-chemical properties on the immune response has commonly been overlooked or poorly understood as the particles themselves were not seen as active agents but rather as delivery systems.

The research presented in this chapter seeks to obtain a better understanding of how PLGA particle size affects macrophage responses, with the objective of identifying particles which promote anti-inflammatory responses. Previous work by Dr McCluskey in the Lavelle lab established that 0.5 μm PLGA particles drive enhanced IL-10 and reduced IL-12p70 secretion from dendritic cells, suggesting that these specific particle sizes may be weak vaccine adjuvants for inducing effector T cell responses [501]. However, these findings illuminated an alternative application for particles in this size range, as modulators of anti-inflammatory responses which could prove advantageous for the treatment of chronic inflammatory diseases. This work explores the anti-inflammatory properties of PLGA particles in the 0.5-2 μm size range from BMDMs acutely after particle treatment, but were also in the generation of innate immune memory. Innate immune training has previously been studied for non-specific protection against pathogens, but the promotion of “long-term” anti-inflammatory memory has not been widely recognised. The mechanism by which macrophages respond differentially to particle size was also investigated and based on the observation of gross morphological alterations in 0.5-2 μm treated macrophages, a role for mechano-sensors was hypothesised. Through the use of a panel of inhibitors, the role of the mechano-sensor αvβ3 in driving IL-1Ra signalling was identified. Furthermore, the downstream signalling required to establish anti-inflammatory responses as well as metabolic alterations required for innate immune training was found to be dependent on the mTORC1 signalling axis.

Particles used in this research were composed of poly (D,L-lactide-co-glycolide) with an L/G ratio of 50/50 and MW of 30,000. All properties were kept constant,

other than particle diameter allowing a clearer understanding of size dependent responses without interference of charge, shape or surfactants. PLGA particles were selected due to their safety profile, biodegradability and prior Food and Drug Authority (FDA) approval for biomedical applications [480,478,512].

Macrophages have a significant influence in propagating chronic inflammation, but are also capable of regulating inflammation by fostering an anti-inflammatory phenotype through secretion of immunosuppressive cytokines [335,17]. Moreover, macrophages constitute one of the first and most abundant innate immune cell recruited to a site of damage, infection or inflammation. The response of macrophages to a foreign entity, such as a particle, is dependent on physico-chemical properties such as size, shape and charge. As the principal phagocytic cell of the innate immune system, macrophages will internalise particles, and the ease which they can do so and the effect of particles on cell integrity can determine the inflammatory reaction ensued. The effect of particle size and shape on phagocytosis has been explored extensively [397,513,398] however, its effect on macrophage inflammatory responses has not been fully resolved.

Assessment of the cytokine profile of BMDMs treated with PLGA particles across a range of sizes from 0.2–20 μm was performed to investigate their proclivity to modulate anti-inflammatory and pro-inflammatory cytokine responses from BMDMs. Prior research into the effect of PLGA particles on BMDMs and BMDCs demonstrated that PLGA particles do not induce cytokine secretion without a secondary TLR agonist. However, here it was demonstrated here that 1-2 μm PLGA particles, were in fact, able to upregulate the secretion of IL-1Ra on their own in a concentration dependent manner which was further amplified in the presence of LPS. In fact, at the highest concentration tested, BMDMs treated with 1 and 2 μm particles alone produced 4-8 fold greater amounts of IL-1Ra compared to untreated BMDMs.

IL-1Ra is a competitive antagonist to the IL-1 receptor, preventing binding of both IL-1α and IL-1β and downstream inflammatory signalling. Production of IL-1Ra from innate immune cells is one of the many homeostatic controls in place to prevent severe IL-1-mediated toxicity and has been shown to be endogenously produced to buffer IL-1 family cytokines. This, however, has been found to be species dependent with studies indicating mice generate greater IL-1Ra in response to IL1α and β than humans [514]. Aberrant IL-1 family signalling is a

common cause of a broad spectrum of inflammatory diseases including Cryopyrin-Associated Periodic Syndrome (CAPS), acute onset ischemia (AOI), diabetes and RA. As such, the blockade of IL-1 signalling has become the gold-standard therapeutic approach for many of these diseases [495]. Most notably, the IL-1Ra mimetic; anakinra, has been used for treatment of RA since 2001, followed by its use to treat CAPS in 2013 and deficiency of IL-1RA autoimmune disorders in 2020 [515]. Identification of a novel means to modulate IL-1Ra endogenously could prove advantageous to enhance IL-1Ra levels in disease states where pro-inflammatory cytokine signalling surpasses immunosuppressive functions.

IL-10 is another potent immunosuppressive cytokine which inhibits the secretion of a myriad of pro-inflammatory cytokines including IL-6, TNFα, IL-18, IL-1α and IL-1β from neighbouring macrophages, DCs and monocytes [516]. None of the tested PLGA particle sizes was capable of driving IL-10 production on their own, but there was a modest increase in response to LPS in 0.5-2 μm treated BMDMs.

The secretion of IL-6, IL-12p40 and TNFα by BMDMs was not enhanced above basal levels by particles alone or in the presence of LPS. Excessive inflammatory signalling through secretion of these cytokines commonly results in non-resolving inflammation, material rejection and tissue damage. This is brought about through heightened chemotaxis of macrophages, dendritic cells and monocytes, and enhancement of their pro-inflammatory capacity, creating an environment which can aggravate or promote chronic inflammatory disease. In addition, IL-6 can also serve as a good indication of endotoxin contamination. Endotoxin contamination originates from the gram negative bacterial cell membrane, and even at low concentrations can initiate potent inflammatory feedback through TLR4 [419,420]. Due to the serious risk of endotoxin exposure, particle-based therapies must not exceed the FDA limit of 0.5 EU/mL. The IL-6 secretion from BMDMs treated with PLGA particles of all sizes did not exceed basal levels as compared to untreated BMDMs. These results are encouraging in indicating the particles tested here are not contaminated with endotoxin [517].

Immune cells undergo profound metabolic alterations following activation in order to fulfil the energy requirements to support functional roles of specific polarisation states [299,312]. A distinct shift in the immunometabolism of macrophages has been described in pro or anti-inflammatory phenotypes, and can, therefore, be used to gain a deeper understanding of their activation state. Macrophages which are

activated with LPS and IFN_{γ} shift towards a pro-inflammatory phenotype and produce high levels of pro-inflammatory cytokines, degradative enzymes, reactive oxygen species and enhance phagocytic capacity. As such they require a fast reliable source of energy which can be met by funnelling glucose through anaerobic glycolysis. Polarising macrophages with IL-4/IL-13 promotes an anti-inflammatory phenotype. Anti-inflammatory macrophages are usually longer lived and require a steady source of energy. In response, they upregulate OxPhos which is powered by aerobic glycolysis and an intact Krebs cycle [518]. The advent of metabolic flux assays, such as Seahorse XF analysers (Agilent), has allowed quantification of the outputs of metabolic pathways through the measurement of oxygen consumption rate (OCR) by mitochondria and extracellular acidification rate (ECAR) as a result of the production of lactate during glycolysis. Inhibitors of glycolysis or mitochondrial complexes involved in OxPhos are also used to assess the effect of imposing stress on the cell metabolism.

The overall cytokine profile of BMDMs treated with particles in the 0.5-2 μm range suggests polarisation towards an anti-inflammatory phenotype so experiments were carried out to determine if this was reflected in the metabolic profile. Indeed, BMDMs treated with 1 μm PLGA particles demonstrated a significant enhancement in OCR, demonstrating an increase in OxPhos. In fact, ATP was produced almost exclusively through OxPhos when the mitochondria were intact. When mitochondrial complexes were blocked, OCR was hampered, resulting in a switch towards increased glycolysis, reflected in the increase in ECAR. Comparing the metabolic profile of 1 μm PLGA particle-treated BMDMs to IL-4/IL-13 polarised macrophages indicated that particle treated BMDMs were re-programmed towards an anti-inflammatory M2 typical metabolism. Taking the cytokine and metabolic evidence together, this suggests that PLGA particles in the 0.5-2 μm range are a suitable size range to promote anti-inflammatory macrophage responses.

For decades, immunological memory was attributed solely to lymphocytes of the adaptive immune system. Seminal work by Netea and colleagues published in 2011 proposed that innate immune cells such as monocytes and macrophages are also capable of establishing memory to certain stimuli, allowing more robust responses upon re-stimulation [502]. Unlike adaptive immune cells, innate immune memory is non-specific and responses can be elicited by unrelated stimuli. The range of agents capable of generating memory has grown over the last decade,

with various biomaterial particulates such as pristine graphene [62] and alum being added to the list [387],[60]. The repercussions of biomaterial induced trained immunity could result in adverse reactions and future complications, which need to be rigorously explored.

Training of BMDMs with particles in the 0.2-20 μm range was carried out over a 24 hour incubation period, followed by a 6 day resting period to bring cells back to a resting state. On day 7, BMDMs were re-stimulated with a variety of TLR agonists and cytokines secreted into supernatants was measured. Surprisingly, particles in the 0.5-2 μm range promoted a trained phenotype characterised by heightened anti-inflammatory cytokine responses following re-stimulation. In contrast, the secretion of pro-inflammatory IL-6 and TNFα was either unaffected or reduced by particles in the 0.5-2 μm range. However, there was variability in the trends observed based on the TLR agonist used. For example, all PLGA particle sizes enhanced IL-1Ra secretion when re-stimulated with LPS, whilst only 0.5-2 μm particles amplified IL-1Ra in response to PAM3CKS4 and CpG. It is therefore imperative to study the response to various agonists representing different infection types; i.e. viral, bacterial or fungal to assess the overall trend in responses.

Innate immunity has customarily been associated with heightened inflammatory immunity and non-specific protection against pathogens, for example in response to BCG training [43]. The innate immune training results presented in response to 0.5-2 μm particles, proposes a potential third avenue of innate immune training which is neither tolerance or induction or heightened inflammation, but instead an "anti-inflammatory" memory [519].

Previous unpublished work by Dr Gorman in our lab, demonstrated a similar trained phenotype from alum treated BMDMs, in particular with regards to their propensity to enhance IL-1Ra secretion. Interestingly, the alum adjuvant used in this work; alhydrogel, forms aggregates which are most commonly found in the 2-3 μm range [417]. The size effect of alum aggregates has previously been postulated to contribute to the inability to promote immunity to certain pathogens or cancer , and this could be in part, affected by the propensity to drive IL-1Ra [520]. These results suggest a potential role of particle size in directing trained immune phenotypes and future work looking at particles of different compositions could help elucidate if the ability to promote anti-inflammatory trained immunity could be based on particle size.

The development of memory in innate immune cells is dependent on metabolic

and epigenetic alterations which provide a means for fast and robust response to a secondary stimulus [521, 53]. The metabolic profile of 1 μm PLGA particle trained BMDMs was compared to that of whole β-glucan particles. β-glucan is one the most studied innate immune training agents, found to contribute to non-specific protection against viral, bacterial and fungal pathogens through enhanced IFNs, IL-1β and IL-6 responses. Memory to β-glucan exposure is dependent on the metabolic adaptations promoting heightened glycolysis and OxPhos. Whilst particle training did not elevate the metabolic output to the same extent as β-glucan trained BMDMs, they retained a heightened basal rate of OxPhos compared to untrained BMDMs. The metabolic state at day 7 might be sufficient to upregulate anti-inflammatory responses whilst heightened anabolic outputs, as seen in β-glucan trained BMDMs, may be required to enhance pro-inflammatory and protective immune responses.

Results thus far have provided evidence of size dependent PLGA particle-induced anti-inflammatory responses from murine BMDMs. Modelling of immune responses in mice is indispensable in biomedical research and in many regards there is overlap in human and mouse responses. Indeed, when comparing the mouse and human genome, there are only 300 genes which are not shared between the species [522]. However, that being said, there are discrepancies within critical features of the adaptive and innate immune system, for example in TLRs, ratios of leukocyte subsets and cytokine/chemokine receptors, to name a few [523,522]. Validation of immune responses in human immune cells is essential in order to translate research findings. A commonly used immortalised human monocyte cell line is the THP-1 monocytes derived from an acute monocytic leukaemia patient. Treatment with PMA over a period of 48 hours promotes monocyte-macrophage differentiation, providing an *in-vitro* human macrophage model. The capacity of PMA at various concentrations to promote human macrophage markers; CD14 and CD11b was addressed, as well as its effect on cell viability and inflammatory phenotype. Treatment with 10nM PMA was sufficient to promote significant differentiation whilst preventing cytotoxicity and enhancement in IL-6 and TNF-α.

THP-1 derived macrophages (THP1-M0) treated with PLGA particles in the 0.5-2 μm size range did not enhance either IL-10 or IL-1Ra secretion, on their own or with LPS, as previously demonstrated in BMDMs. However, THP-1s treated with

1 μm PLGA particles demonstrated an elevation in basal OCR and ECAR, indicating an increase in metabolic functions. Experiments were then conducted to assess if PLGA particles in this size range could train THP1-M0s to promote anti-inflammatory cytokine secretion. There was an increase in IL-10 and IL-1Ra secretion in response to LPS on day 7 in the BMDMs trained with 1-2 μm particles, which coincided with trends seen in BMDMs. However, these results are only preliminary, and trends in response to other agonists, as well as the trend in IL-6 and TNFα secretion would need to be carried out to establish a clearer picture.

Unfortunately, the THP1-M0 model has some drawbacks which did not make it the most suitable *in-vitro* model to study the response of human immune cells to PLGA particles. Whilst the use of THP1-M0s is convenient, the immortalised cancer cell line does not reliably replicate the behaviours and response spectrum of primary macrophages isolated from a host. For example, THP1-M0 have significantly lower expression of TLR-2 and TLR-4 as compared to human monocyte derived macrophages, meaning much greater concentrations of TLR agonists had to be used [524]. These findings indicate that further work needs to be done to investigate the translation of particle-mediated immunomodulation between the species using a more reliable model such as human PBMCs.

The ability of PLGA particles within the specific size range of 0.5-2 μm to modulate anti-inflammatory responses led to the question of how BMDMs respond differentially to particles, based solely on size. Immune responses are commonly driven by specific ligand-receptor engagement through cytokine receptors or PRRs. PLGA particles are co-polymers of lactic and glycolic acid and whilst neither is a specific ligand to a known receptor, cells are capable of lactate sensing through GCPRs and lactate transport into the cell [525,526]. However, this would not explain the size dependent responses seen across PLGA particles of different sizes. Furthermore, at the time of BMDM exposure to particles, lactic and glycolytic acid are emulsified into a co-polymer particle which prevents acidification of the microenvironment or free lactate release. The degradative rate of PLGA particles depends on MW, ratio of each copolymer and size [527]. The only parameter which was altered between tested particles was size, with smaller particles degrading fastest. However, studies accessing the degradation rate of 200 and 500 nm PLGA particles *in-vitro*, did not demonstrate significant loss of particle MW within the first 24-48 hours [528]. It was, therefore, concluded that the impact of lactic acid or media

acidification on macrophage modulation was likely insignificant during early particle-cell interactions.

It was noticed that particle size had a significant effect on BMDM morphology. BMDMs incubated with 0.5-2 μm particles were notably smaller and less granular than BMDMs incubated with 0.2, 10 and 20 μm PLGA particles or with LPS. This was quantified by flow cytometry demonstrating that the FSC of BMDMs treated with particles in this size range was significantly lower, and the SSC was increased. On initial observation, there were concerns that these morphological alterations were indications of apoptosis. It was, however, ruled out through assessment of extracellular staining by membrane impermeable Annexin V and PI. Additionally, 1-2 μm particle treated BMDMs had comparable cell viability to untreated BMDMs. Immune cells are highly dynamic and can respond to external forces imposed on the cell membrane such as stretch, sheer stress, osmolarity and morphological deformation. Cell sensing is critical to allow the cell to respond to these stresses and alter their physiology to compensate for changes to their environment or even disease.

Overlap in the fields of mechanobiology and immunology have made it evident that immune cells rely on mechano-sensation, alongside PRR's, to influence immune responses [188,529,172]. Various mechanically gated receptors have since been linked to immune cell regulation, allowing the conversion of mechanical to biochemical signals. Moreover, activation of certain receptors such as the TGFβ receptor [530], integrins [531],[532],[533],[534] and GCPRs [535] have been found to be regulated by spatial re-organization of the cell membrane, creating receptor clustering and downstream signalling independently of ligand interaction.

The effect of 0.5-2 μm particle-mediated cell shrinkage on the cell membrane was, therefore, assessed through the confocal microscopy using FRAP as a readout for membrane fluidity. Proteins in the cell membrane of BMDMs were crosslinked to a fluorophore, and a small region of interest (ROI) was photobleached. Over time unbleached proteins migrate back into the ROI and the rate of fluorescent recovery can be measured to create recovery vs time plots. Controls for high and low membrane fluidity were prepared by altering the osmolarity of media with either high sucrose content or water in media. It was hypothesised that due to the shrinkage of BMDMs following the interaction with 1-2 μm PLGA particles, membrane fluidity would decrease significantly mirroring the effect of hyper-

osmolarity on cells. As expected, treatment of cells with 1 μm particles decreased the rate of fluorescent recovery indicating a significantly more rigid membrane, as compared to untreated BMDMs. The mechanism by which particles bring about membrane modifications is yet to be understood. However, key parameters such as method of internalisation, rate of phagocytosis and the period of time the cell membrane remains in contact with a particle can all affect cell morphology and membrane dynamics [399,513,398]. Based on the observations and crude analysis of particle internalisation, PLGA particles appear to be internalised within the first 30 mins of incubation, and reach a peak at around 6 hours. Therefore, 1-2 μm PLGA particles may induce membrane stress, or membrane ruffling during the period of time that they surround the cell, prior to phagocytosis of the particle.

The membrane disruptions and morphological alterations in BMDMs incubated with PLGA particles of 0.5-2μm in size suggested involvement of a mechano-sensor. Mechano-sensors found to influence immune responses include; TRPV4, Piezo1 and various integrins [188,200,172,536,537]. Involvement of each of these mechano-sensors was investigated using specific inhibitors and agonists to measure their effect on IL-1Ra secretion. The ability of 0.5-2 μm PLGA particles to drive IL-1Ra secretion on their own, made it a convenient read-out for inhibitory studies, without having to consider the influence of a TLR agonist.

In order to refine the search for a mechano-sensor involved in driving anti-inflammatory responses, reference RNA sequencing data acquired from alum-treated BMDMs as part of Dr. Gorman's research [63] was exploited. Dr Gorman identified the capacity of alum adjuvant to drive IL-1Ra secretion from BMDMs both acutely and in training protocols, providing a commonality between the two particulates. The *itgb3* gene which encodes β3 portion of integrins such as αvβ3 and $\alpha_{iib}\beta3$, was significantly upregulated in alum-treated BMDMs. Numerous integrins have been linked to immunomodulatory roles including; αvβ3 [538], αvβ8 [539], αvβ6 [537], $\alpha M\beta_2$, therefore, the αvβ3 heterodimer was focused on. The surface expression of each dimer was assessed via flow cytometry to verify the translation of the RNA sequencing data to responses from PLGA particle treated BMDMs. Interestingly, only PLGA particles in the 0.5-2 μm upregulated the surface expression of αv and β3, with larger particles and LPS having little or no effect. Although the αvβ3 integrin has not previously been linked to regulation of IL-1Ra

secretion, it has been shown to drive both pro and anti-inflammatory responses. For instance, in a model of human blood monocytes and monocyte-derived macrophages, ligation to the αvβ3 cognate ligand vitronectin resulted in NFκB activation and expression of pro-inflammatory cytokines IL-6 and TNFα, IL-8 and IL-1β, whilst the expression of anti-inflammatory IL-10 was significantly decreased [246]. However, as will be discussed in more detail in chapter 4, αvβ3, as well as other αv containing integrins are essential for the activation of TGFβ, an important anti-inflammatory cytokine in the promotion of adaptive immune tolerance and tissue regeneration [541,542].

The role of αvβ3 in driving IL-1Ra secretion was assessed using the chemical inhibitor Cilengitide and neutralising antibodies (nAb) against αv and β3. The results indicated a partial role for αvβ3 in modulating IL-1Ra signalling acutely and in training. However, the IL-1Ra levels were still greater than media controls indicating that blocking αvβ3 is not sufficient to completely shut down IL-1Ra signalling. A secondary mechanism must also be at play in the 2 μm PLGA particle induced anti-inflammatory responses.

The role of other mechano-sensors was assessed for their contribution to IL-1Ra signalling, however, TRPV4 and Piezo1, were ruled out as regulators of IL-1Ra secretion induced by 2 μm PLGA particles. The TRPV4 antagonist RN1734 had a very limited effect on IL-1Ra secretion and activation of TRPV4 using αPDD also had no effect. The results for Piezo1 inhibition using GsMtx4 were interesting, as instead of seeing a reduction or no effect, there was an increase in the secretion of IL-1Ra. Additionally, the Piezo1 agonist, Yoda1 heightened IL-1Ra secretion, surpassing particle treated BMDMs, however, this enhancement was not affected by GsMtx4 pre-treatment. These results are contradictory, with both the agonist and antagonist increasing IL-1Ra secretion. Work by Atcha *et al* demonstrated that Piezo1 KO mice were less inflammatory and upregulated various anti-inflammatory responses [97]. Therefore, by blocking Piezo1, the anti-inflammatory outputs of BMDMs treated with 2 μm PLGA particles may be further amplified. The enhancement of IL-1Ra in response to Piezo1 agonism would be harder to explain. IL-1Ra might be upregulated in response to a Piezo1-driven increase in IL-1 cytokine secretion. However, addressing this would require further work looking at IL-1 secretion from Piezo1 activated BMDMs. Owing to increasing evidence linking

Piezo1 in regulating pro-inflammatory responses [98,99,97,100], as well as the contradictory results obtained from its inhibition, the role of Piezo1 was deemed outside of the scope of this project.

mTORC1 and 2 (collectively referred to as mTOR) play vital roles in responding to stress, energy availability and growth factors, which go on to shape innate immune function and metabolic reprogramming [101]. The role of mTOR in driving similar responses in 0.5-2 μm PLGA particle treated BMDMs was, therefore, assessed. The specific inhibitor of mTORC1, rapamycin, was used to verify the dependence of mTORC1 signalling on particle-mediated IL-1Ra production. Rapamycin pretreatment brought the secretion of IL-1Ra from BMDMs treated with 1 and 2 μm PLGA particles down to basal level, indicating that this response was mTORC1 dependent. Furthermore, various stimuli have been shown to induce innate immune training through mTOR activation including alum and β-glucan [102,103]. Indeed, pre-treatment with rapamycin prior to training, inhibited the capacity of BMDMs to enhance IL-1Ra secretion upon re-stimulation 7 days later. Rapamycin also reduced the rate of mitochondrial respiration in particle-trained BMDMs, resulting in a more quiescent metabolic output indicating a role in the metabolic reprogramming during training.

Whilst an association between the mechanical regulation of IL-1Ra and mTOR activation has not been established here, cross-talk between these pathways could be hypothesised based on previous work carried out in the lab and from published work. Dr McCluskey demonstrated that 0.5-2 μm PLGA particles were able to enhance IL-10 through activation of ERK/PI3K/p38 signalling in BMDCs [26]. The phosphorylation of ERK blocks TSC phosphatase, allowing the accumulation of Rheb-ATP which activates mTOR [104]. Dr McCluskey also proposed that signalling was brought about by the formation of lipid rafts on the membrane in response to the mechanical stress imposed by particles in this size range. What's more, it is possible that lipid raft formation is involved in modulating mechano-sensor activation in response to mechanical stimuli on the membrane [105,106]. The formation of lipid rafts not only increases membrane rigidity but can also promote co-localisation of membrane bound proteins, imposing a spatio-temporal clustering effect [86,87,88,89]. Lipid rafts have been implicated in regulating the activation of integrins within these clusters through both inside-out and outside-in activation. For example the lipid raft component; oxysterol 25-hydrocholesterol was found to

activate αvβ3 through binding to the integrin head [107]. On the other hand, formation of integrin foci within lipid rafts, has been postulated to recruit talin to the intracellular integrin tail domains, promoting inside-out activation[108]. With this in mind, αvβ3 activation, has been shown to activate various pathways including; PI3K [95], ERK, FAK, Src[109] and Rho GTPases [110]. Therefore, it can be proposed that 0.5-2 μm PLGA particles induce membrane alterations, resulting in lipid raft formation and αvβ3 clustering which through ERK/PI3K signalling pathways modulate mTOR. Activated mTOR is then capable of inducing transcription of IL-1Ra and metabolic reprogramming involved in the anti-inflammatory phenotype. However, further research linking integrins to lipid rafts and downstream ERK signalling would be required to verify this hypothesis.

The results presented here indicate an indispensable role for mTORC1 in IL-1Ra signalling and innate immune "anti-inflammatory" memory. Signalling via αvβ3, however, is only partially responsible for IL-1Ra responses. If our hypothesis linking αvβ3 and mTORC1 activation is correct, it is also plausible to theorise an alternative pathway for mTOR activation other than through αvβ3 signalling. The consequences of phagocytosis and intracellular breakdown of 1-2 μm PLGA particles has not been fully elucidated and could contribute to activation of signalling pathways either through intracellular disruption or release of degradation products. Based on live cell imaging, it is clear that BMDMs begin to ingest PLGA particles within the first 30 minutes, and by 24 hours, are saturated with particles. Macrophages are highly adept at phagocytosing particles on the micron range between 0.5- 10 μm. In fact most air and water borne bacterial pathogens are within this size range, indicating an evolutionary adaptation for pathogen containment. PLGA particle degradation within the cell occurs naturally via hydrolysis releasing lactic and glycolic acid. It has been demonstrated that ester hydrolysis within the phagosome, enhances the speed of degradation, due to low pH and hydrolytic enzymes [111]. As an endogenous metabolic product of glycolysis, lactic acid has been described as immunosuppressive and negative regulator of glycolysis in innate immune cells[79]. Lactate accumulation downregulates LPS-induced cytokine secretion [112], inflammasome activation [113] and macrophage migration[114]. These responses have been postulated to be in part modulated by mTOR. For instance, studies investigating lactate accumulation as a consequence of the Warburg effect

in cancer cells demonstrated that lactate induced mTOR activation downstream of PI3K/Akt signalling [115, 116]. Furthermore, a study by Lui *et al*, demonstrated lactate-associated mTOR activation in tumour-associated macrophages, contributing to the immunosuppressive environment within tumours [117]. It would, therefore, be reasonable to theorise that if lactic acid accumulates intracellularly from the breakdown of PLGA, it could also be involved in mTOR activation.

Future work would be required to validate the hypotheses proposed here; (i), PLGA particle size dependent αvβ3 activation is partially involved in mTOR signalling and (ii) Internalisation and degradation of PLGA particles in this size range drives lactate-associated mTOR activation. Hypothesis 1 could be explored by inhibiting αvβ3 and measuring mTOR signalling proteins such as phosphorylated SK61 and 4EBP1. Hypothesis 2 would require analysis of lactate accumulation intracellularly and the effect of this on mTOR activation. Alternatively polystyrene particles of the same diameter could be used in lieu of PLGA particles, to assess the mechanism of mTOR activation through αvβ3 in the absence PLGA degradation products.

In summary of the work carried out for this chapter, PLGA particles in the 0.5-2 μm size range were identified to induce significant anti-inflammatory cytokine secretion from BMDMs, most notably IL-1Ra. A metabolic shift towards "M2" like metabolism characterised by enhanced OxPhos was also demonstrated. The capacity of this specific particle size range to induce anti-inflammatory innate immune memory was identified, with BMDMs having an enhanced propensity to secrete IL-1Ra, and maintain heightened OxPhos. Delving into the mechanism of action, established a role for the mechanosensitive αvβ3 integrin and mTOR signalling. This work provides compelling evidence for the further investigation into the use of PLGA particles in this size range for clinical applications for inflammatory diseases, whether as a drug delivery vehicle or stand-alone therapy. It also demonstrates the immense impact a single parameter, such as particle size, can have on immune responses, and how the evolutionary adaptation of immune cells to sense size could be harnessed to improve therapeutic approaches.

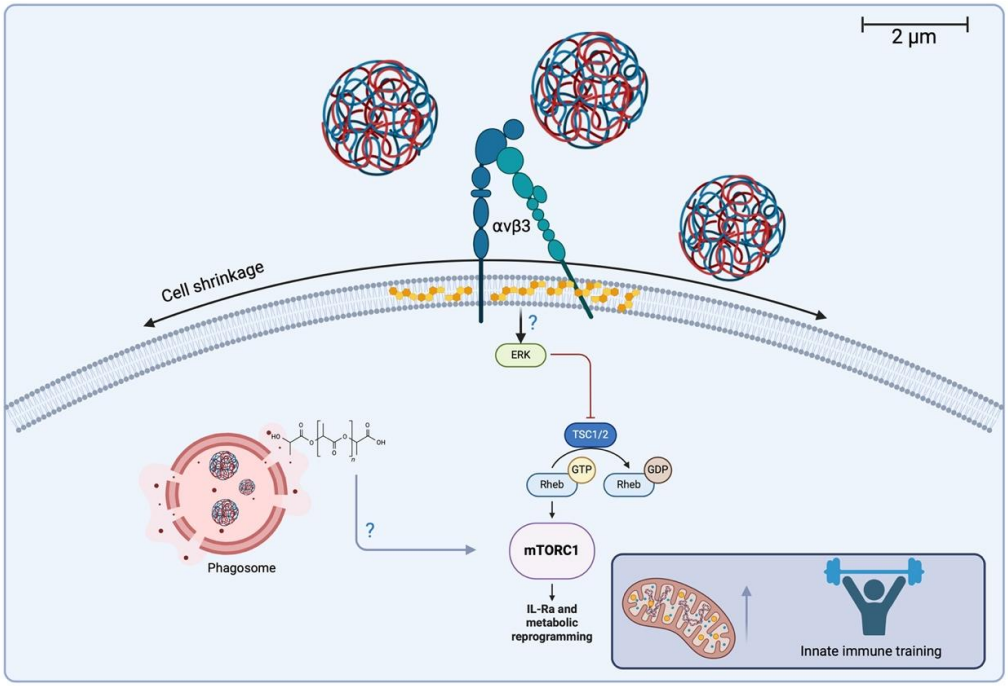

Figure 3.9.1 Proposed mechanisms of action of 0.5-2 µm PLGA particle-mediated anti-inflammatory responses and innate immune training. PLGA particles in the 0.5-2 µm range interact with the cell membrane of BMDMs inducing mechanical stress resulting in cell shrinkage and morphological alterations. This results in increased activation of αvβ3, proposed to be as a result of the formation of lipid rafts. Downstream signalling is proposed to involve ERK/mTOR pathway which promotes enhanced IL-1Ra signalling, metabolic reprogramming and anti-inflammatory innate immune training.

Chapter 4; Results part II

PLGA particles drive T-reg differentiation in a size dependent manner through the engagement of mechanosensitive αvβ3

4.1 Chapter 4 Introduction

In chapter 3, the propensity of PLGA particles in the 0.5-2 μm range to drive anti-inflammatory macrophage responses was demonstrated. It was proposed that particles in this size range could be harnessed as drug delivery vehicles, or as stand-alone therapies for chronic inflammatory diseases. In this chapter, the effect of size on PLGA particle modulation of DCs and priming of T cell responses was addressed.

DCs play a fundamental role in sampling antigens in the periphery and mounting an appropriate response. Upon uptake and processing of an antigen, a cascade of signalling events results in maturation and antigen presentation on either MHC I or MHC II receptors [543,11]. The maturation state of DCs directs T-cell priming in order to expand a T-cell population specialised to either mount effector responses, or promote tolerance [28]. TolDCs commonly develop during homeostasis or in the presence of an anti-inflammatory environment and are characterised by a semi-mature state with enhanced secretion of anti-inflammatory cytokines IL-10 and TGFβ, and an enhanced propensity to prime T-regs [544,435].T-regs act as a contingency plan to mitigate the harmful effects of autoreactive T-cells, which become erroneously activated [68]. However, despite both central and peripheral tolerance, auto-immune pathologies such as T1D, RA and MS are all too common. Whilst the mechanisms leading to auto-immunity are complex and diverse, they can broadly be characterised by a specific immune response against an innocuous self-antigen resulting in tissue damage and exacerbated inflammation, as well as inadequate development of T-regs [545,546].

The standard treatment for most auto-immune diseases focuses on symptom management using anti-inflammatory and immunosuppressive drugs, rather than on targeting the underlying cause. The risk of global immunosuppression and high burden of side effects make many of these drugs unfavourable [492,430]. An alternative approach is to boost the immune systems own tolerance, through augmented expansion of tolDCs or T-regs. Clinical trials have already been carried out, looking at the success and safety of transfusing *ex-vivo* expanded autologous DCs [435,547,548] and T-regs [549,550] with bioactive components which promote their differentiation [551,552,553]. However, a common issue encountered, is the instability of transfused cells, short lived responses and non-specific effects when utilising

bioactive compounds such as a polarising cytokines [549,554,555.] An attractive alternative would be to develop an “anti-inflammatory” vaccine, also referred to as an “inverse vaccine”, which can boost the expansion of antigen-specific T-regs. Based on the results presented in Chapter 3, demonstrating the capacity of PLGA particles in 0.5-2 μm size range to promote anti-inflammatory responses from macrophages, we proceeded to carry out further exploration to assess their capacity to function as “anti-inflammatory adjuvants” [501].

The mechanism by which innate immune cells can sense and respond differentially based on particle size is yet to be fully elucidated, however, the recognition of the role of mechano-sensors in immune cell signalling offers clues as to how immune cells respond independently of PRRs [190,556,172]. In fact, the ability of innate immune cells to sense surface properties is likely an evolutionarily conserved mechanism which enhances both phagocytic capacity and the establishment of an appropriate response to clear pathogens [399]. As a relatively underappreciated aspect in immunology, there is huge potential to be found in understanding the mechanical regulation of immune cells.

In this chapter, the “anti-inflammatory adjuvant” paradigm is explored by investigating the capacity of 0.5-2 μm PLGA particles to promote tolDC responses and antigen-specific T-regs. In chapter 3, the partial role of αvβ3 integrin in modulating IL-1Ra secretion from BMDMs was established, and here it is theorised that the integrin could also play a role in the promotion of anti-inflammatory responses by BMDCs. In order to address these hypotheses, the following aims were formulated

1. To address the role of PLGA particle size in modulation of BMDC responses.
2. To determine the capacity of 0.5-2 μm PLGA particles to promote antigen-specific T-reg expansion in co-culture.
3. To investigate the capacity of 0.5-2 μm PLGA particles to promote antigen-specific T-reg expansion *in-vivo*.
4. To elucidate the role of mechano-sensors in DC responses to PLGA particle size and explore the mechanism of action behind anti-inflammatory signalling.

Chapter 4 Results

4.2 PLGA particles in the 0.5-2 μm range promote the secretion of IL-10 and TGFβ signalling

IL-10 is a highly immunosuppressive cytokine which blocks Th1 and Th17 responses, but promotes Treg responses [516]. Incubation of DCs with PLGA particles in the 0.5-2 μm size range, at a concentration of 300 μg/ml, led to significantly enhanced IL-10 secretion when cells were co-stimulated with 5 ng/ml LPS (Figure 4.2.1 A). The secretion of pro-inflammatory cytokines was also assessed with and without LPS stimulation to assess the effects of particles over a range of sizes. PLGA particles of all sizes, were unable to mount significant IL-6 or TNFα secretion on their own, nor did they amplify the response to LPS (Figure 4.2.1 B-C) There was, however, notable variation in TNFα secretion across biological replicates, particularly with the larger particles (Figure 4.2.1 C).

In addition to IL-10, TGFβ is critical in maintaining homeostasis through modulation of immunosuppressive cell phenotypes [557,108, 106]. TGFβ is released in a latent form, composed of the bioactive TGFβ surrounded by latency associated protein (LAP) which conceals the receptor binding motif. The release of LAP from the TGFβ complex requires the denaturing or mechanical deformation of LAP [107]. Whilst it is possible to measure activated TGFβ concentrations in the supernatant by ELISA, *tgfb1* gene expression was instead assessed by rt qPCR to circumvent variability arising from activating latent TGFβ. Interestingly, BMDCs treated with 1 μm PLGA particles enhanced the expression of *tgfb1* gene, to a level superior to BMDCs treated with TGFβ (Figure 4.2.2 A-B).

Signalling via the canonical TGFβ pathway was also assessed through measurement of the phosphorylation of downstream promoter proteins; Smad2 and 3. The level of pSmad2/3 in BMDC protein lysates was quantified by western blot analysis and bands were normalised against total β-actin and total Smad. BMDCs treated with 1 μm PLGA particles (300 μg/ml) and TGFβ (25 ng/ml) demonstrated an increase in phosphorylated Smad2/3, on both the pSmad2 (Ser465/467)/pSmad3 (Ser423/425) (Figure 4.2.3 A) and pSmad2/3 (Thr8) residues (Figure 4.2.3 B). The enhancement of pSmad2/3 was evident at the 1- and 3-hour time point (Figure 4.2.3 C) but not after 30 minutes. Representative

blots depicting the β-actin and total Smad bands, used for normalisation, are presented in Figure 4.2.3 D.

The number of cells in culture after 24-hour treatment was compared to ensure that the enhancement of IL-10 was not due to an enhanced cell number. Crystal violet staining was used to compare cell density. The fold change in the absorbency readings for each treatment group was calculated compared to the untreated group. BMDCs incubated with 0.5-20 μm PLGA particles alone and with LPS demonstrated a fold increase in the absorbance reading of approximately 0.25 compared to the absorbance of untreated BMDCs and the LPS control . However, the fold increase was not found to be statistically significant, and there was no difference across the difference size groups (Figure 4.2.4 A). Furthermore, there was no difference in cell viability in BMDCs treated with 0.5-2 μm PLGA particles (Figure 4.2.4 C). The % of live cells was quantified by flow cytometry and indicated that none of the PLGA particle sizes assessed, caused significant cell death. This has also been established previously in the lab, with only PLGA particles of <100 nm promoting cell death [558,501].

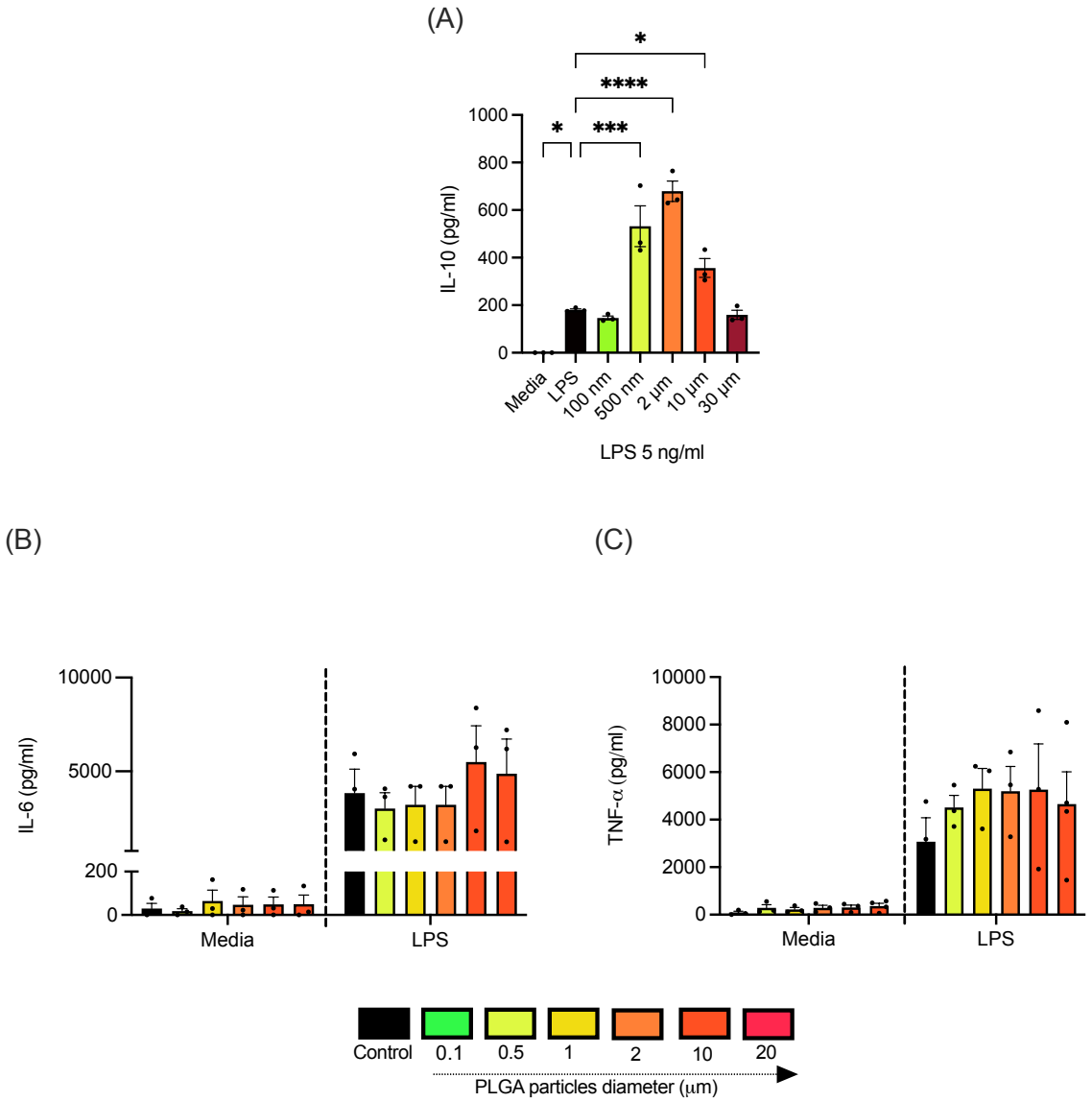

Figure 4.2.1 PLGA particles between 0.5- 2 µm in size enhance the secretion of IL-10, but not IL-6 and TNFα from BMDCs treated with LPS. BMDCs ($6.25x10^5$ cell/ml) were treated with PLGA particles in a range of sizes (300 µg/ml) and LPS (5 ng/ml) for 24 hours. Secretion of (A) IL-10 (B) TNF-α and (C) IL-6 in the supernatant was measured by ELISA. One way ANOVA (A) or two-way ANOVA (B-C) with Dunnet's multiple comparison test was used to determine statistical significance as compared to untreated, or LPS control, where *p<0.05 **p<0.01 ***p<0.001 and **** p<0.0001. Error bars show mean and ± SEM for three biological replicates.

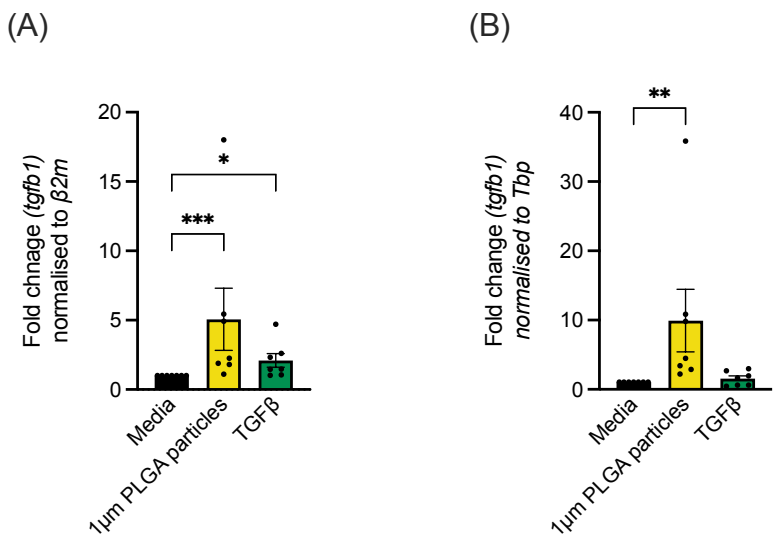

Figure 4.2.2 BMDCs treated with 1µm PLGA particles have enhanced *tgfb1* gene expression. BMDCs (6.25x10 ^{5} cell/ml) were treated with 1 µm PLGA particles (300 µg/ml) or TGFβ (25 ng/ml) for 24 hours. mRNA was isolated and cDNA was prepared for rt qPCR. Expression of *tgb1* was normalised to the expression of (A) *β2M* and (B) *Tbp*. One way ANOVA was used to determine statistical significance as compared to untreated control, where *p<0.05 **p<0.01 and ***p<0.001. Error bars show mean and ± SEM for three individual biological replicates, with rt qPCR performed two individual times, per sample.

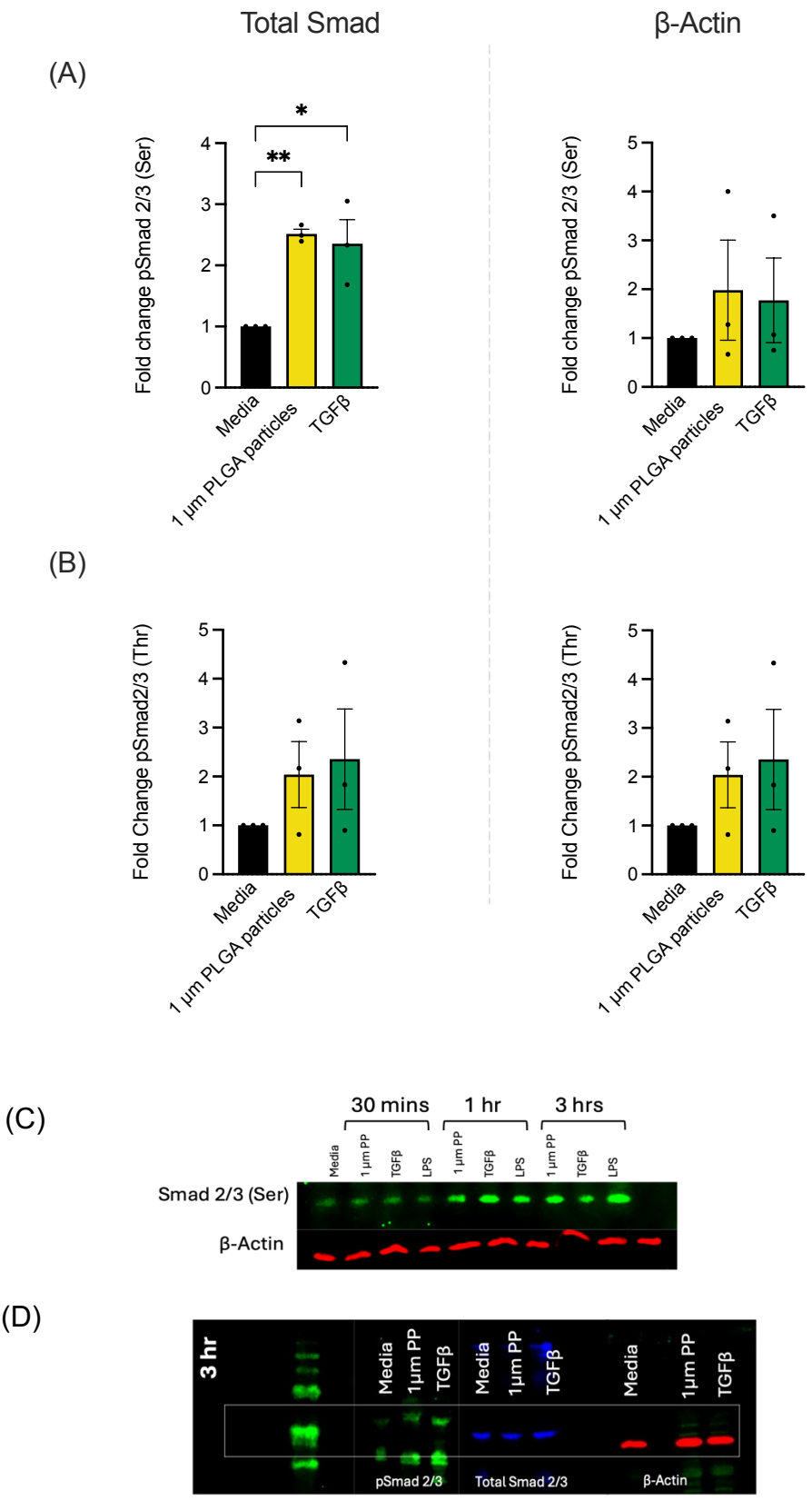

Figure 4.2.3. BMDCs treated with 1µm PLGA particles (1 µm PP) demonstrate increased phosphorylation of Smad2/3. BMDCs (6.25x10 ^{5} cell/ml) were treated with 1µm PLGA particles (300 µg/ml), TGFβ (25 ng/ml) or LPS (10 ng/ml) for 30 mins, 1 or 3- hours. Protein was isolated,

denatured and separated based on size by gel electrophoresis. Proteins were transferred to a nitrocellulose membrane and phosphorylation of Smad proteins was measured using antibodies specific to; pSmad2 (Ser465/467) pSmad 3 (Ser423/425) and pSmad2/3 (Thr8). Secondary antibodies were used with IR fluorescence to detect protein bands. Densitometry analysis of fluorescent signal for each band was performed using EmpiriaStudio software (Li-Cor) and normalised against the signal for β-actin and total Smad2/3. Fold change of normalised fluorescent signal for (A) pSmad2/3 (Ser) and (B) pSmad2/3 (Thr) were calculated against untreated control. Representative blots portray bands specific to (C) pSmad2/3 (Ser) and β-actin at each time point and (D) pSmad2/3 (Ser), total Smad and β-actin at 3 hours. One way ANOVA was used to determine statistical significance as compared to untreated control, where *$p<0.05$ and **$p<0.01$. Error bars show mean and ± SEM for three individual biological replicates.

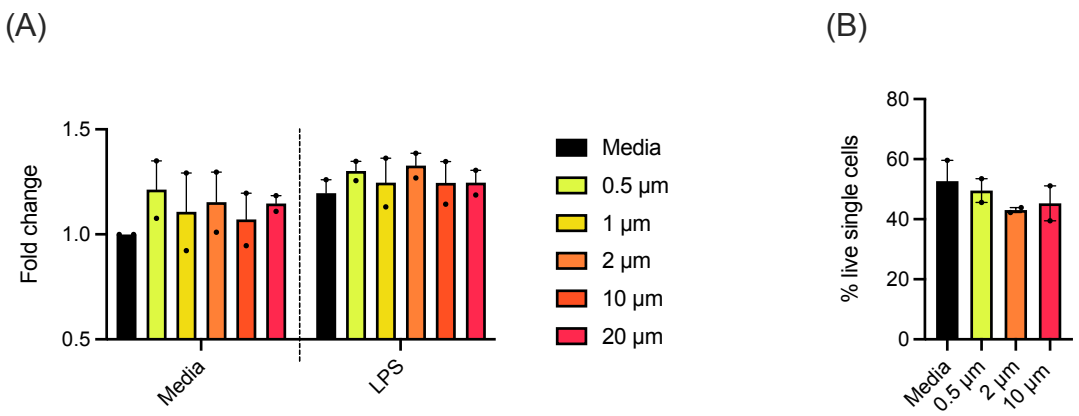

Figure 4.2.4 PLGA particles in the 0.5-20 µm size range do not induce cell death or affect cell density. BMDCs ($6.25x10^5$ cell/ml) were treated with PLGA particles in a range of sizes (300 µg/ml) and/or with LPS (10 ng/ml) for 24 hours. (A) Cell number was compared using of crystal violet staining as a spectrophotometric readout for the number of adherent cells in culture treated with particles alone or with LPS. The fold increase was given as a fold change in absorbance compared to untreated cells. (B) % of live cells was analysed by Flow Cytometry using BV510 live/dead stain . One way ANOVA was used to determine statistical significance as compared to untreated or LPS control. Error bars show mean ± SEM for two individual biological replicates.

4.3 BMDCs treated with 2 µm PLGA particles promote the expansion of OVA-specific T-regs in co-culture.

The promotion of tolerance-inducing cytokines such as IL-10 and TGFβ from BMDCs treated with 0.5-2 µm PLGA particles prompted further investigation into their propensity to direct T-cell priming. A co-culture model was designed to measure the expansion of T-regs by BMDCs *in-vitro* using the ovalbumin (OVA) antigen and OVA-reactive T-cells isolated from OTII-mice.

BMDCs were treated with or without OVA, as well as 2 µm PLGA particles, TGFβ or LPS for 24 hours. Naïve CD4 T-cells were isolated from OT-II mice and stained with CFSE in order to track proliferation. BMDCs and T-cells were co-cultured for 72 hours prior to staining for flow cytometry. A graphical description of this protocol is depicted in Figure 4.3.1A. To quantify T-reg populations, cells were gated on single, live cells expressing the T-cell makers; CD3 and CD4. The FoxP3 T-reg markers was used to quantify T-regs, and $CFSE^{+}$ T-regs were selected for proliferation modelling. The gating strategy is presented in Figure 4.3.1 B.

Firstly, the number of live cells and $CD3/CD4^{+}$ T-cells per 5 $x10^{5}$ single cell events. was compared across the groups to ensure that there was no significant T-cell death during the co-culture protocol which could subsequently affect the number of T-regs. There was no significant difference in fold change in either the number of live cells or $CD4/CD3^{+}$ cells when compared to the media only control group (Figure 4.3.1 C-D). However, when the number of T-regs were compared, there was a notably increase in the number of OVA-specific $FoxP3^{+}$ T-cells in the co-cultures with BMDCs treated with OVA + 2 µm PLGA particle. (Figure 3.4.1 E-F).

Another marker which has emerged as a potentially robust marker for T-regs is the TGFβ anchor protein; GARP. To compare the expression of GARP across the groups, the fold change in the mean fluorescent intensity (MFI) of the GARP antibody was compared to OVA alone. Interestingly, only T-cells primed by 2 µm particle + OVA treated BMDCs, demonstrated an increase the surface expression of GARP (Figure 4.3.2 A-B). A population of $GARP^{hi}$ T-cells can be clearly distinguished in the FSC-A vs GARP dot plots (Figure 4.3.2 E). There was no increase in the MFI of GARP on T-cell primed by BMDCs treated with TGFβ and OVA, despite the increase in $FoxP3^{+}$. In addition to GARP, the expression of TGFβ bound LAP was measured. TGFβ/LAP complex can be secreted bound to cell-

membrane receptor GARP, and can be indicative of inactivated TGFβ levels. There was a significant decrease in the MFI of LAP on $CD4^+$ T-cells which were co-cultured with 2 μm PLGA particles (Figure 4.3.2 C-D), and notable LAP^{lo} population in dot plots (Figure 4.3.2 F). This could be indicative of an increase in TGFβ activation.

The proliferation of T-regs is a fundamental feature required to expand antigen-specific populations which can bring about tolerance *in-vivo*. Therefore, the number of proliferating cells which stem from the initial $CD4^+$ population was tracked with CFSE staining. In brief, as cells undergo cell division, the fluorescent CFSE is split between parent and daughter cells. As such, populations with a lower CFSE intensity are generated and several peaks can be visualised depending on the number of division events. The proliferation modelling to quantify the number of proliferated cells at each generation was performed by FloJo software (BD Biosciences). The number of proliferating $FoxP3^+$ cells significantly increased in the T-cells primed by BMDCs treated with OVA + 2 μm PLGA and OVA + TGFβ (Figure 4.3.3 A and B) which contributes to the increase in the total T-reg number shown in Figure 4.3.1E.

(A)

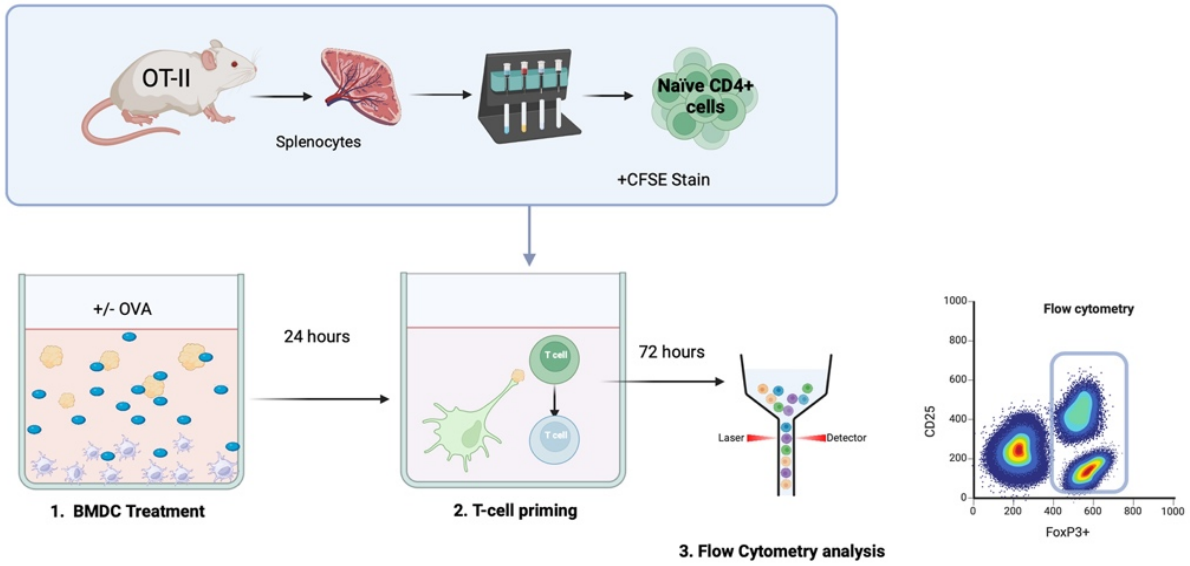
OT-II
Splenocytes
Naïve CD4+ cells
+CFSE Stain
+/- OVA
24 hours
72 hours
Laser
Detector
1. BMDC Treatment
2. T-cell priming
3. Flow Cytometry analysis
Flow cytometry
CD25
FoxP3+

(B)

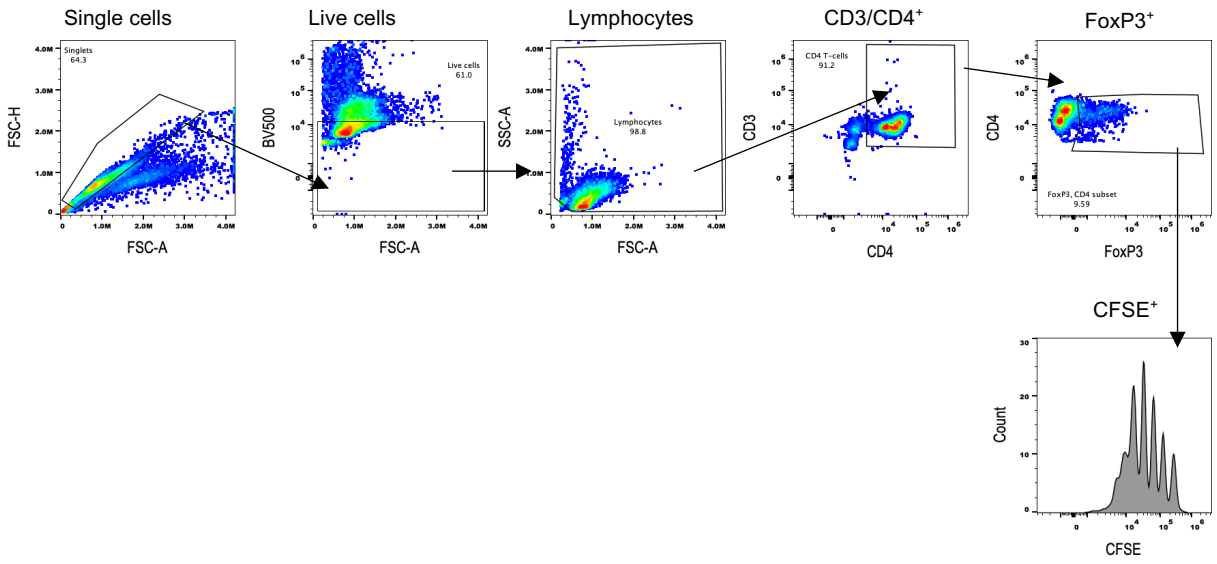
Single cells
Live cells
Lymphocytes
CD3/CD4+
FoxP3+
FSC-H
FSC-A
BV500
SSC-A
CD3
CD4
FoxP3
CFSE+
Count
CFSE

(C)

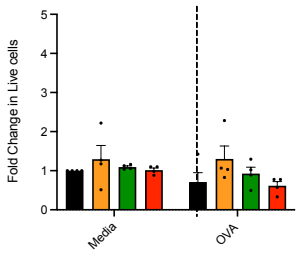
Fold Change in Live cells
Media
OVA

(D)

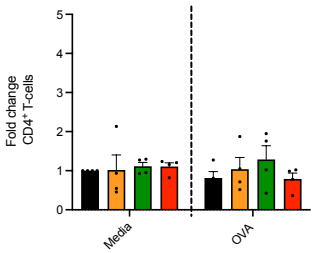
Fold change CD4+ T-cells
Media
OVA

(E)

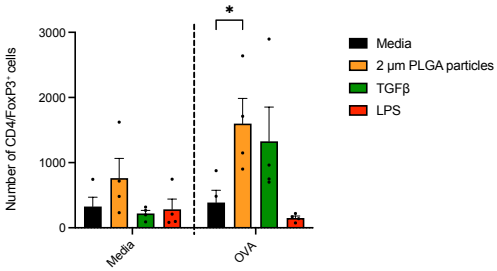
Number of CD4/FoxP3- cells
Media
OVA
Media
2 µm PLGA particles
TGFβ
LPS

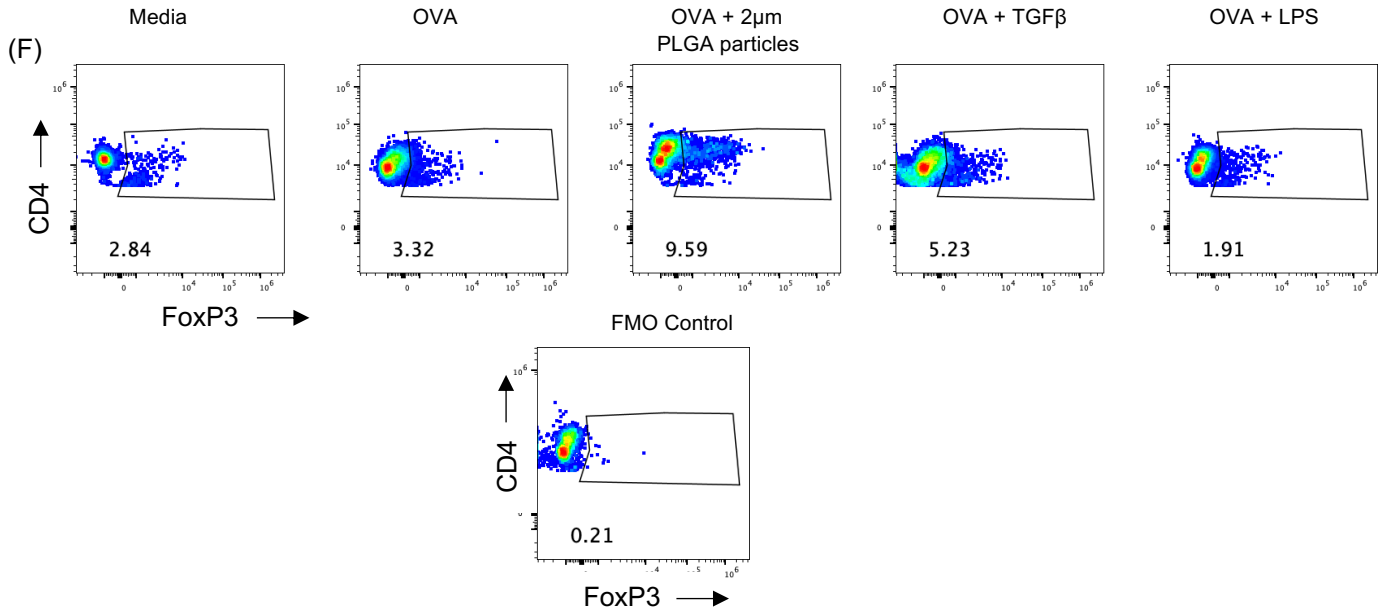

Figure 4.3.1 BMDCs treated with 2 µm PLGA particles promote FoxP3$^+$ T-cell differentiation. BMDCs cultured from bone marrow isolated from C57BL/6 mice (2x10^5 cell/ml) were treated with 2µm PLGA particles (300 µg/ml), TGFβ (25 ng/ml) or LPS (10 ng/ml) with or without OVA (25 µg/ml) for 24 hours. Enriched CD4$^+$ T-cells isolated from splenocytes from OTII mice (4x10^5) were stained with CFSE and added to the co-culture for 72 hours. Cells were stained with fixable viability stain (FVS), as well as fluorescent antibodies specific to CD3, CD4 and FoxP3. A schematic of the co-culture protocol is presented in panel (A). The gating strategy used to quantify cell populations is presented in panel (B). Flow cytometry was used to quantify (C) % live cells, (D) number of CD3/CD4$^+$ cells and (E) number of CD3/CD4/FoxP3$^+$ cells. Histograms depicting (F) FSC-A vs FoxP3 for each experimental group and the fluorescent minus one (FMO) control for FoxP3 antibody are also displayed. (C-D) Kruskal-Wallis or (E) Two-way ANOVA with Dunnet's multiple comparison test was used to determine statistical significance as compared to untreated control, where *p<0.05. Error bars show mean ± SEM for three individual co-culture experiments.

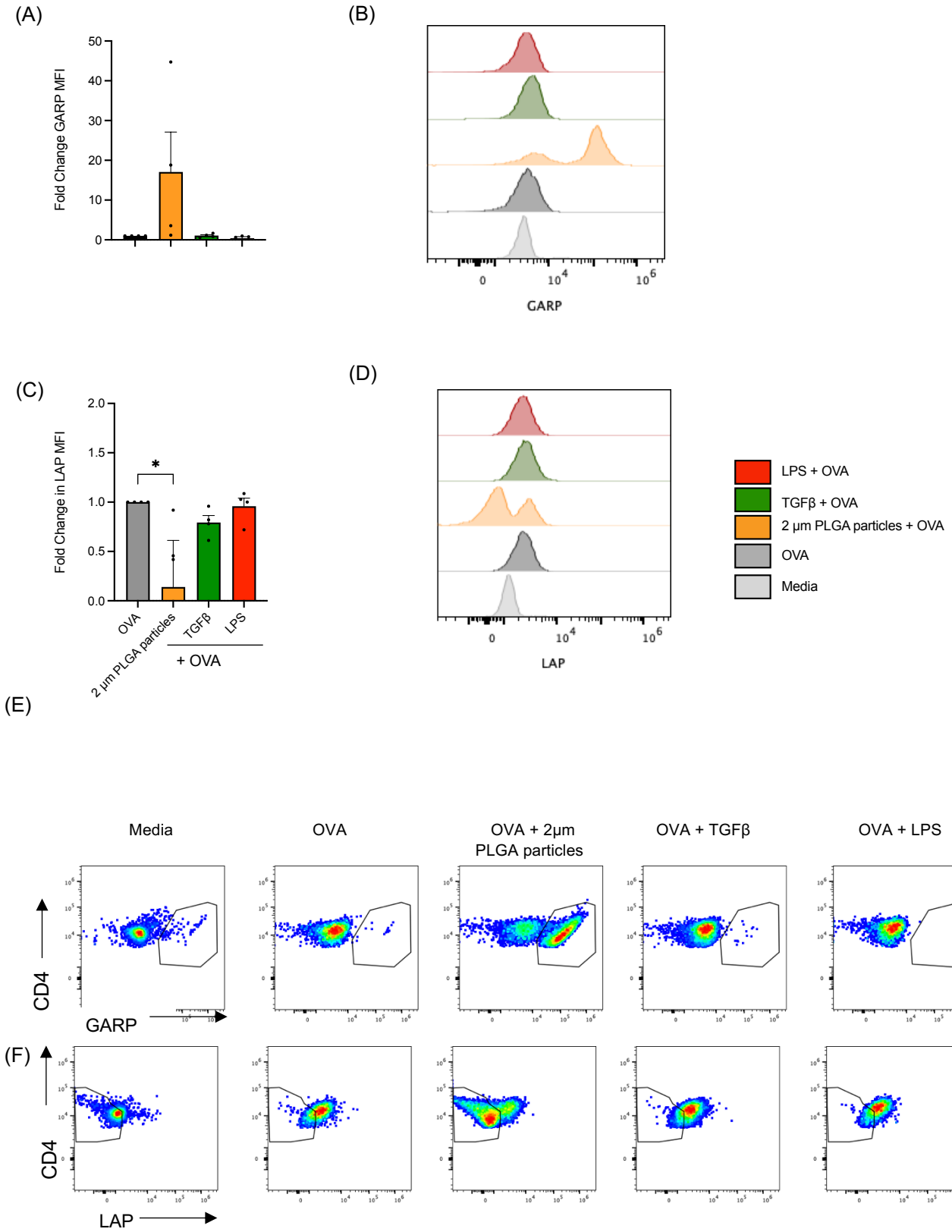

Figure 4.3.2 BMDCs treated with 2 µm PLGA particles promote increased expression of GARP and decreased LAP on CD4⁺ T-cells. Co-culture was carried out as specified in Figure 4.3.1A. using fluorescent antibodies specific for GARP and LAP. Cells were gated for live, single CD3/CD4⁺ cells. Fold change in the surface expression of (A) GARP and (C) LAP were calculated by

comparing the MFI of each treatment to the untreated control. Histograms of depicting the expression of (B) GARP and (D) LAP as well as dot plots of (E) FSC-A vs GARP and (F) FSC-A vs LAP were also included. Kruskal-Wallis test was used to determine statistical significance as compared to untreated control, where *$p<0.05$. Error bars show mean ± SEM for three individual co-culture experiments.

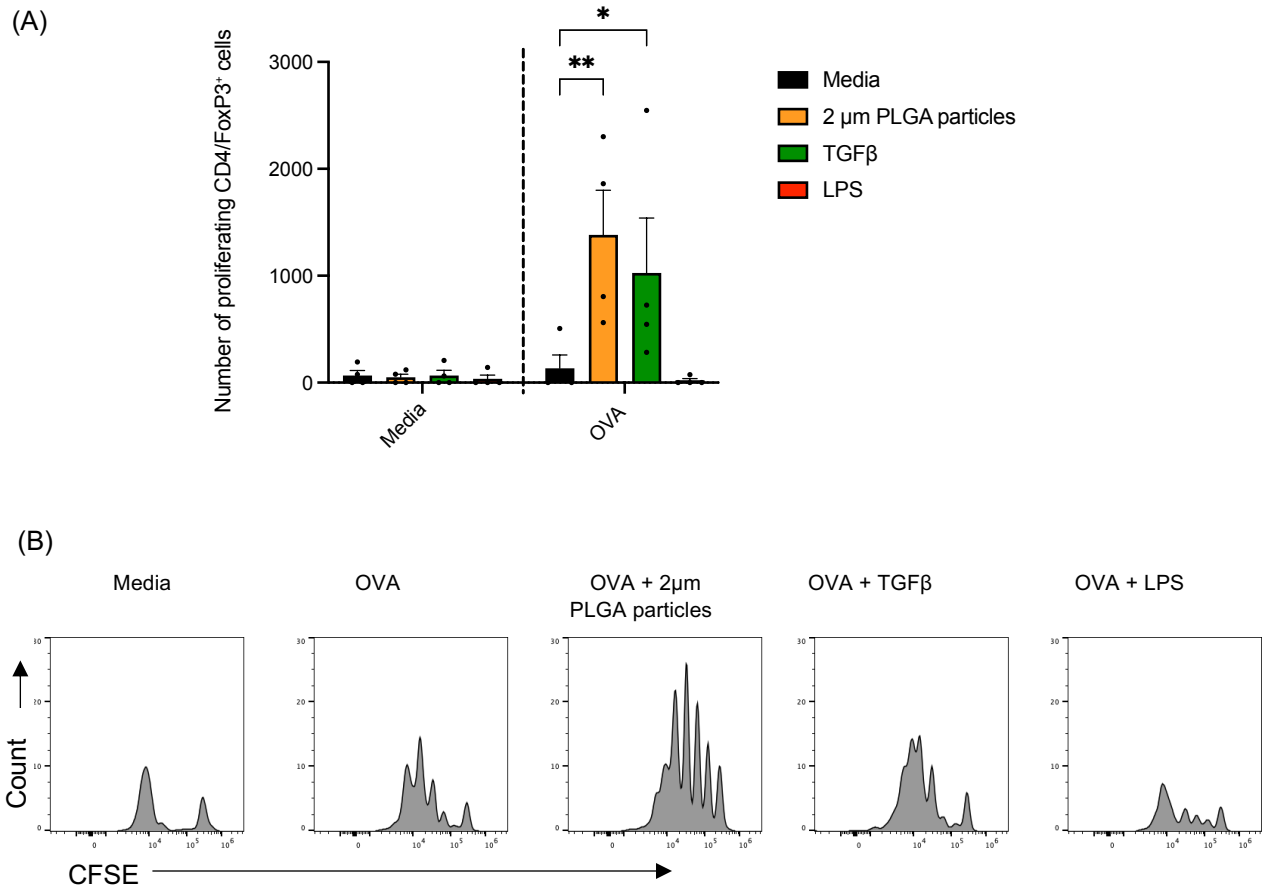

Figure 4.3.3 BMDCs treated with 2 µm PLGA particles expand FoxP3$^+$ T-cells. Co-Culture was carried out as specified in Figure 4.2.1A. Cells were gated for live, single CD3/CD4/FoxP3/CFSE$^+$ cells. Proliferation modelling was carried out using FlowJo Software (BDSciences). (A) The proliferation modelling function was used to calculate the total number of proliferating cells (B) Representative histograms of CFSE peaks (X-axis depicts the cell count and ranges from 0-120) . Two-way ANOVA with Dunnett's multiple comparison test was used to determine statistical significance as compared to untreated control, where *p<0.05 and **p<0.01. Error bars show mean ± SEM for three individual co-culture experiments.

4.4 2 μm PLGA particles promote OVA-specific CD4$^+$ T-reg expansion *in-vivo*

Following on from the promising results obtained from the *in-vitro* co-culture, the capacity of 2 μm PLGA particles to enhance antigen-specific T-regS in an *in-vivo* model was addressed. Female C57BL/6 mice were injected intramuscularly (i.m) with OVA, 2 μm PLGA particles or in combination, and boosted 14 days later. A week later, spleen-derived lymphocytes were isolated and re-stimulated *ex-vivo* with OVA for 72 hours to selectively expand OVA reactive populations. A graphical representation of the vaccination regime is depicted in Figure 4.4.1 A. T-reg defining markers; FoxP3, Helios and CD25 were used to characterise CD4$^+$ populations. The gating strategy used to quantify T-regs is depicted in Figure 4.4.1 B.

The number of live cells which were acquired after *ex-vivo* re-stimulation of splenic lymphocytes was not significantly different across the different treatment groups (Figure 4.4.1 C). There was, however, an increase in number of CD3/CD4$^+$ T-cells in the ex-vivo culture of spleens from mice vaccinated with OVA + particle combination (Figure 4.4.1D). What's more, these mice produced a significantly greater number of OVA specific T-regs which were positive for FoxP3 and CD25 (Figure 4.4.1 E and G), as well as Helios (Figure 4.4.1F and H). The groups which were vaccinated with antigen or PLGA particles alone did not demonstrate any increase in OVA-specific CD25$^+$, FoxP3$^+$ or Helios$^+$ above basal levels (PBS injected mice). Lymphocytes which were cultured *ex-vivo* without OVA, did not have elevated T-reg numbers in any of the groups (Figure 4.4.2 A-B).

FoxP3$^+$ T-regs can also arise from CD8$^+$ T-cells, providing a regulatory cytotoxic function against antigen-primed CD4$^+$ and T-follicular helper cells [559]. They have also been found to play a crucial role in supressing immune rejection following tissue transplantation [560,125,124.] The number of CD8/FoxP3$^+$ and CD8/Foxp3/Helios$^+$ were quantified following *ex-vivo* re-stimulation with OVA. The number of CD8$^+$ T-cells acquired was equal across the groups and made up about 1% of the total lymphocytes (Figure 4.4.3A). However there was no notable enhancement in FoxP3$^+$ or Helios$^+$ T-reg populations in any experimental groups. (Figure 4.4.3B).

The supernatants from the *ex-vivo* cultured lymphocytes were collected at 72 hours to assess the secretion of IL-10 from total splenic lymphocytes. Cells isolated from

mice vaccinated with 2μm PLGA particles and OVA secreted higher basal concentrations of IL-10 compared to mice treated with one or the other alone (Figure 4.4.4A). Interestingly, this response was seen equally in groups receiving OVA re-stimulation and those left without re-stimulation. Whilst the concentrations were relatively low, ranging between 50 and 100 pg/ml, the trend was significant. A greater cell density could be required to obtain higher IL-10 concentrations, considering in this protocol lymphocytes were plated at a density of $8x10^5$ cell/well, with a 72 hour culture period.

Finally, the effect of vaccination with antigen and 2 μm PLGA particles on antibody responses were assessed through measurements of serum IgG titres. It has previously been demonstrated by Dr Sharp in the Lavelle lab, that PLGA particles of a broad size range can promote humoral immunity [35]. Mice vaccinated 2 μm PLGA particles and OVA produced a significant amount of OVA-specific IgG compared to mice vaccinated with particle alone or antigen alone (Figure 4.4.5A-B).

(A)

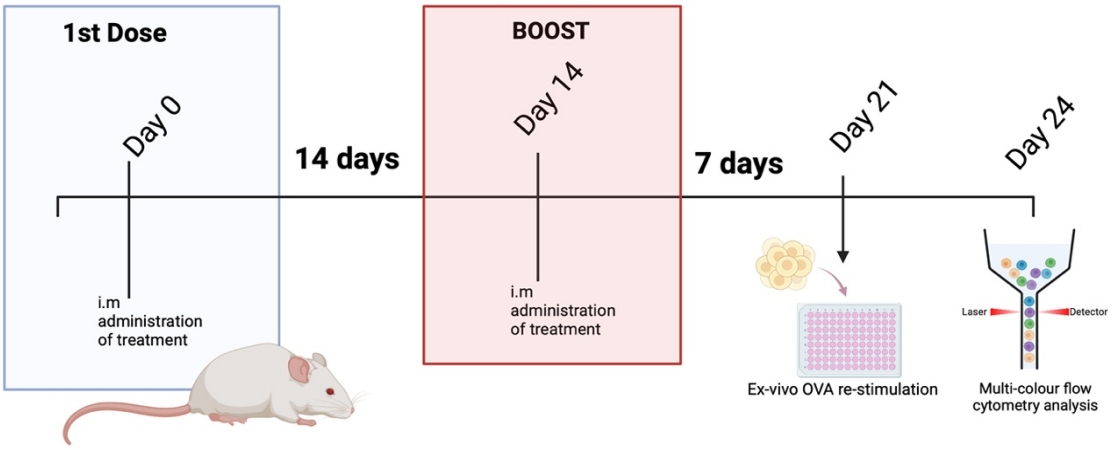
1st Dose
Day 0
14 days
BOOST
Day 14
7 days
Day 21
Day 24
i.m
administration
of treatment
i.m
administration
of treatment
Ex-vivo OVA re-stimulation
Laser
Detector
Multi-colour flow
cytometry analysis

(B)

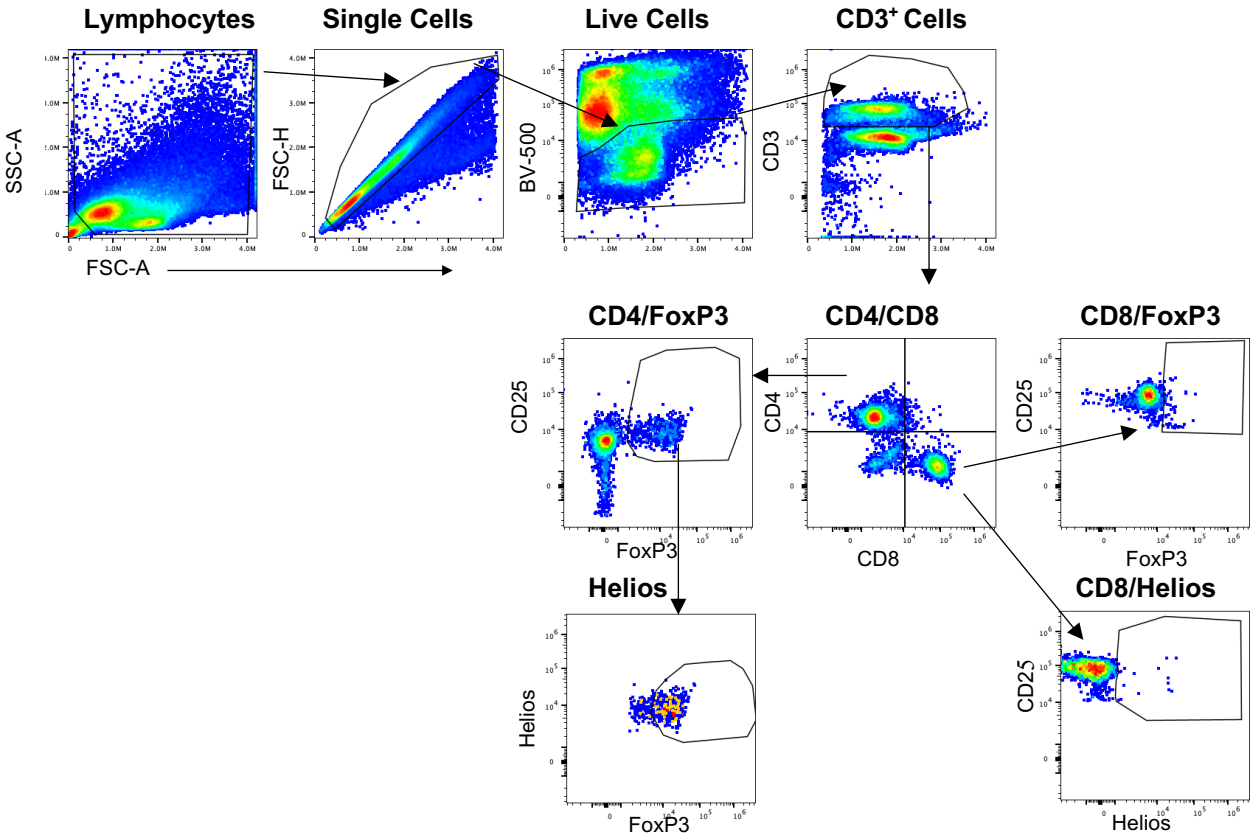
Lymphocytes
Single Cells
Live Cells
CD3⁺ Cells
SSC-A
FSC-A
FSC-H
BV-500
CD3
CD4/FoxP3
CD4/CD8
CD8/FoxP3
CD25
FoxP3
CD4
CD8
CD25
FoxP3
Helios
CD8/Helios
Helios
FoxP3
CD25
Helios

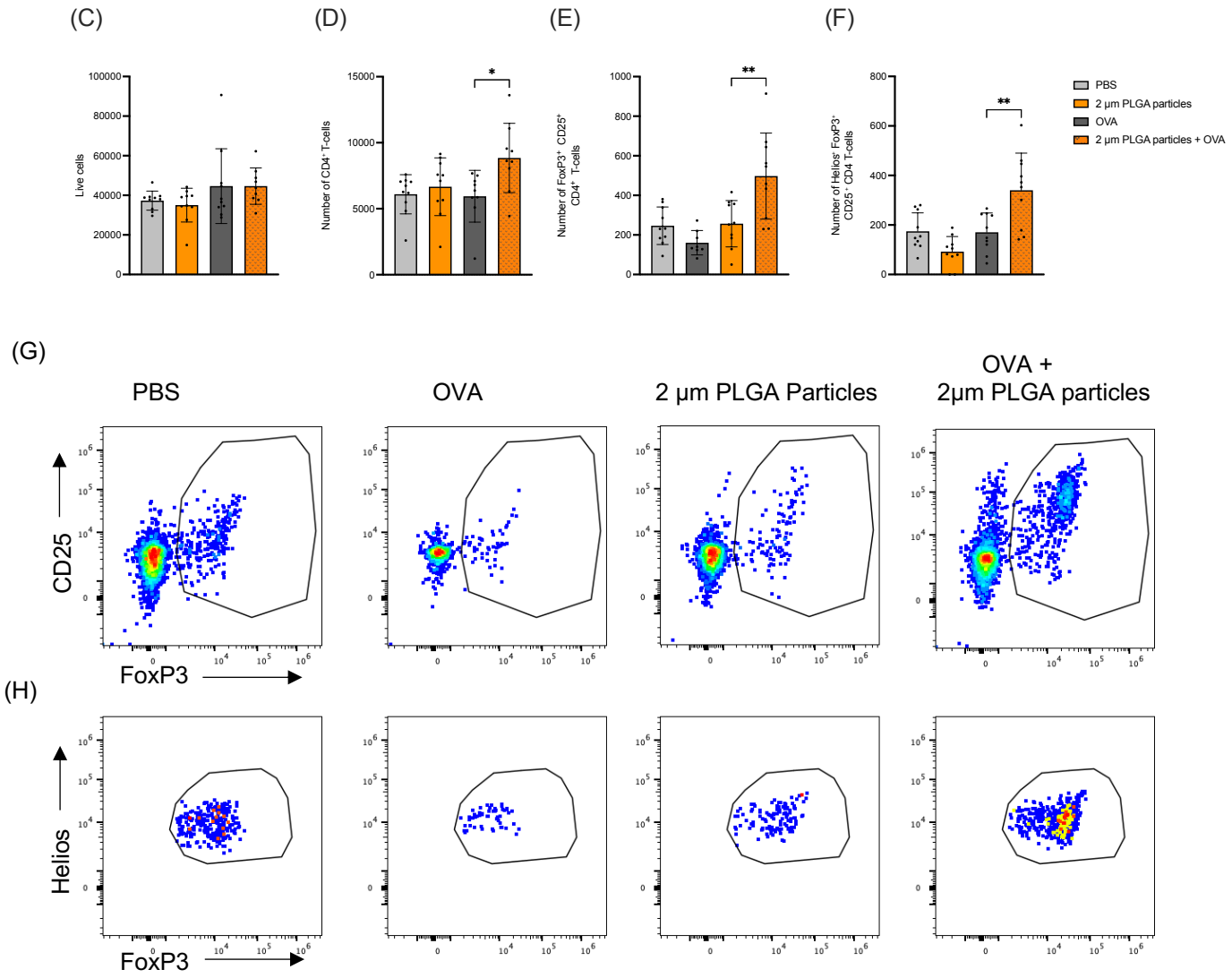

Figure 4.4.1 Intramuscular injection of 2 µm PLGA particles and OVA enhances OVA-specific T-reg subsets. C57BL/6 mice were injected i.m with PBS, OVA (10 µg/mouse), 2 µm PLGA particles (1 mg/mouse) or OVA + particle combination, on day 0 and boosted on day 14. On day 21, mice were sacrificed and spleens were collected. Lymphocytes were isolated and re-stimulated with OVA (25 µg/ml) *ex-vivo* for 72 hours. The schematic of the vaccination protocol is depicted in (A). Lymphocytes were stained with FVS and antibodies specific to CD3, CD4, CD8, CD25, FoxP3 and Helios and cell populations were quantified by flow cytometry. The gating strategy is depicted in (B). The number of (C) single live cells (D) CD3/CD4$^+$ (E) CD4/CD25/FoxP3 and (F) CD4/CD25/FoxP3/Helios were quantified for each experimental group. Representative histograms of (G) double positive (CD25/FoxP3$^+$) and (H) triple positive (CD25/FoxP3/Helios$^+$) populations are depicted. Statistical significance was determined using One-Way ANOVA compared to OVA treated group. Data are represented as mean ± SEM. Asterisks (*) represent *$p < 0.05$ and **$p < 0.01$. Mouse injection regime was performed on a total of 9 C57BL/6 female mice per group.

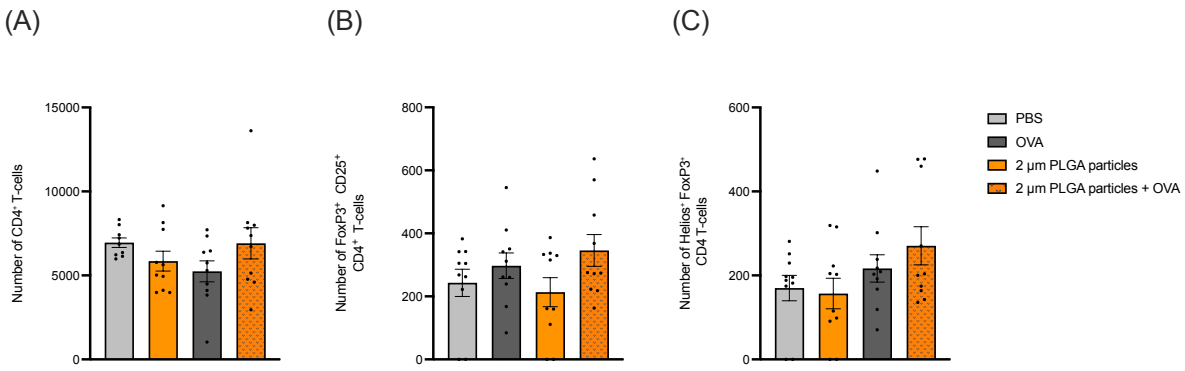

Figure 4.4.2 There was no difference in T-reg number following ex-vivo culture of spleenocytes without OVA. C57BL/6 mice were injected i.m with PBS, OVA (10 µg/mouse), 2 µm PLGA particles (1 mg/mouse) or OVA + particle combination, on day 0 and boosted on day 14. On day 21 mice were sacrificed and spleens were collected. Lymphocytes were isolated and cultured *ex-vivo* for 72 hours. Cells were stained with FVS and the following antibodies; CD3, CD4, CD8, CD25, FoxP3 and Helios. Populations were gated as per the gating protocol described in figure 4.4.1B. The number of (A) live, single, CD3/CD4 cells positive for (B) CD4/CD25/FoxP3 and (C) CD4/CD25/FoxP3/Helios were quantified. Statistical significance was determined using One-Way ANOVA compared to OVA treated group. Data are represented as mean ± SEM. Mouse injection regime was performed on a total of 9 C57BL/6 female mice per group.

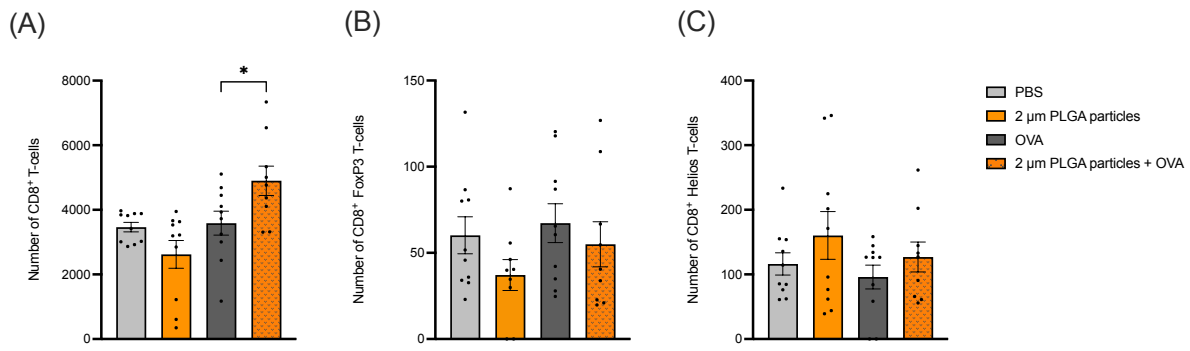

Figure 4.4.3 Intramuscular injection of 2 µm PLGA particles and OVA does not enhance CD8$^+$ T-regs subsets. C57BL/6 mice were injected i.m with PBS, OVA (10 µg/mouse), 2 µm PLGA particles (1 mg/mouse) or OVA + particle combination, on day 0 and boosted on day 14. On day 21 mice were sacrificed and spleens were collected. Lymphocytes were isolated and re-stimulated with OVA (25 µg/ml) *ex-vivo* for 72 hours. Cells were stained with FVS and the following antibodies; CD3, CD4, CD8, CD25, FoxP3 and Helios. Populations were gated as per the gating protocol described in Figure 4.3.1B. The number (A) of live single CD3/CD8 cells positive for (B) CD8/FoxP3 and (C) CD8/FoxP3/Helios were quantified. Statistical significance was calculated using One-Way compared to OVA treated group. Data are represented as mean ± SEM. Asterisks (*) represent *p < 0.05. Mouse injection regime was performed on a total of 9 C57BL/6 female mice per group.

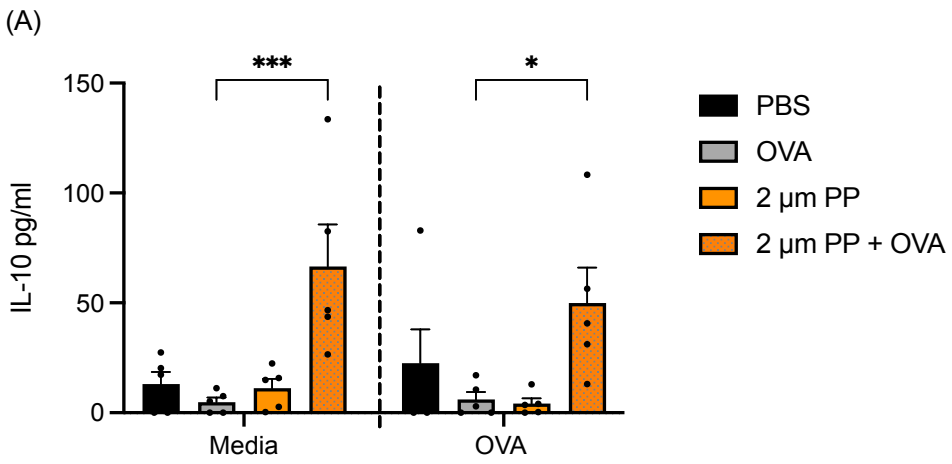

Figure 4.4.4 *Ex-vivo* cultured lymphocytes isolated from mice injected with 2 µm PLGA particles and OVA have enhanced IL-10 secretion. C57BL/6 mice were injected i.m with PBS, OVA (10 µg/mouse), 2 µm PLGA particles (1 mg/mouse) or OVA + particle combination, on day 0 and boosted on day 14. On day 21 mice were sacrificed and spleens were collected. Lymphocytes were isolated and re-stimulated *ex-vivo* for 72 hours with or without OVA (25 µg/ml). (A) Supernatants were collected and the secretion of IL-10 was quantified by ELISA. Statistical significance was determined using Two-Way ANOVA with Dunnett's multiple comparison against OVA vaccinated group. Data are represented as mean ± SEM. Asterisks (*) represent *$p < 0.05$, **$p < 0.01$ and ***$p < 0.001$. Mouse vaccination regime was performed on a total of 5 C57BL/6 female mice per group. Supernatants were only collected from the second *in-vivo* experiment which was carried out on 5 mice.

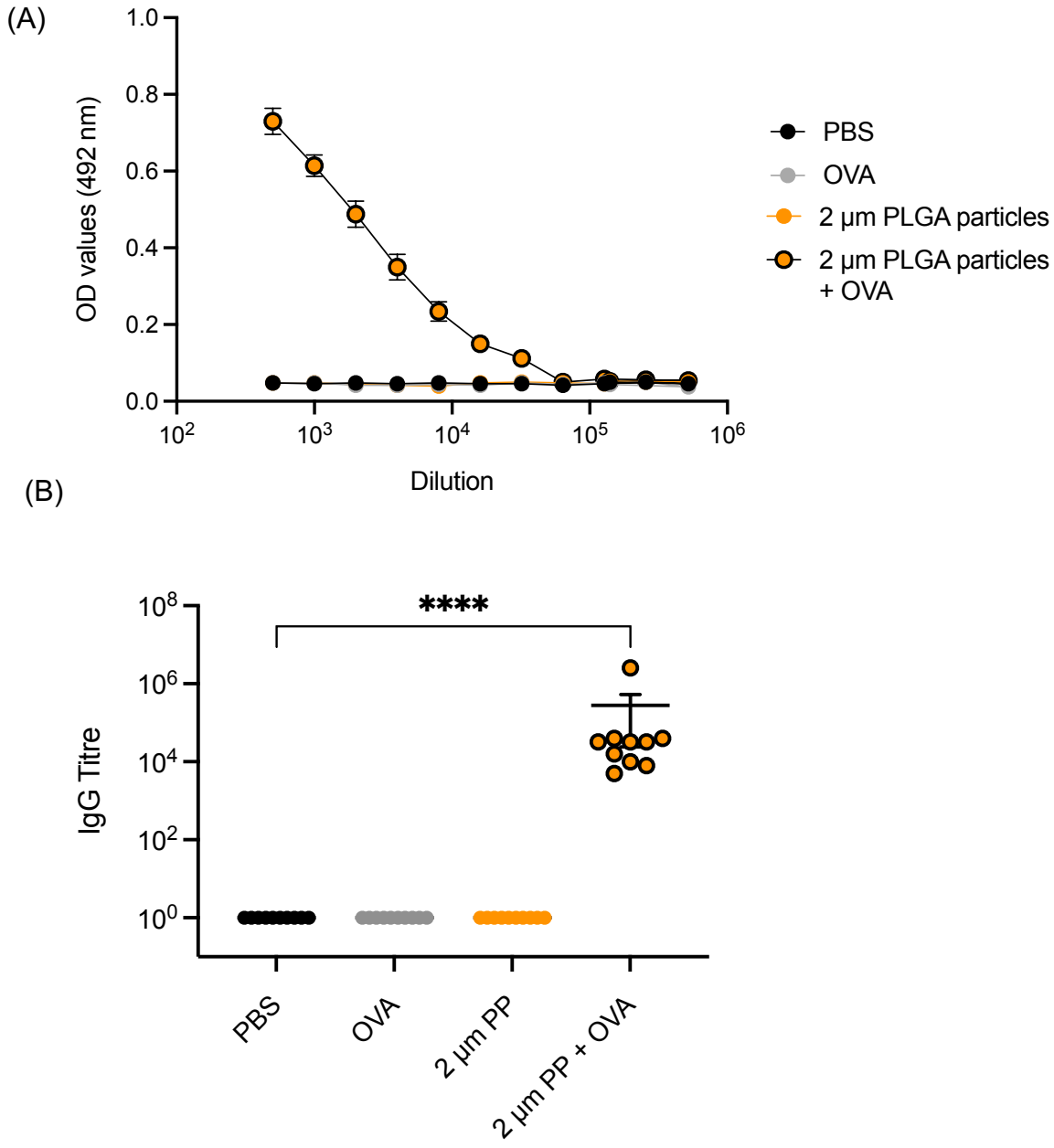

Figure 4.4.5 Intramuscular injection with 2 µm PLGA particles and OVA promotes enhanced serum OVA-specific IgG. C57BL/6 mice were injected i.m with PBS, OVA (10 µg/mouse), 2 µm PLGA particles (1 mg/mouse) or OVA + particle combination, on day 0 and boosted on day 14. On day 21 mice were sacrificed and blood was collected. Blood serum was isolated and OVA-specific IgG ELISA was performed on a serial dilution of serum, starting at 1:500 dilution. (A) The OD value of each dilution was measured and dilution curves were created and (B) IgG titres were calculated. Mouse injection regime was performed on a total of 9 C57BL/6 female mice per group. Kruskal-Wallis test was used to determine statistical significance as compared to untreated control, where *p<0.05 **p<0.01 ***p<0.001 and **** p<0.0001. Error bars show mean ± SEM for three individual co-culture experiments.

4.5 BMDCs treated with 1- 2 µm PLGA particles have altered morphology and membrane fluidity.

Observation of BMDCs treated with PLGA particles of between 0.5-2 µm in size *in-vitro* demonstrated gross morphological changes. The decrease in BMDC size following 3 hour treatment with 1 µm PLGA particles can be clearly visualised when compared to untreated BMDCs in the confocal microscopy images presented in Figure 4.5.1A. For comparison, BMDCs treated with hypo (1:5 dH_2O) and hyperosmolar (150 mM Sucrose) media were used to induce cell expansion and shrinkage respectively. To quantify these morphological changes, flow cytometry of BMDCs treated with PLGA particles (300 µg/ml) of various sizes or LPS (10 ng/ml) was carried out. BMDCs were gated for live cells using fixable viability stain (FVS), and FSC and SSC were compared across the groups. BMDCs treated with PLGA particles in the 0.5-2 µm range had a decreased FSC, and a slight increase in SSC, indicating a decrease in size and increase in internal complexity. Cells incubated with larger 10-20 µm PLGA particles and LPS had a FSC and SSC comparable to untreated BMDCs.

Despite previous work demonstrating that the particles in the 0.5-2 µm size range do not induce cytotoxic responses, an apoptosis assay was carried out to ensure that the observed cell shrinkage was not a sign of early apoptosis. BMDCs treated with 1 or 2 µm PLGA particles (300 µg/ml) were stained with PI and Annexin V. Hydrogen peroxide (500 µM) was used to induce apoptosis as a positive control, and the cells can be clearly shown as double positive for PI and Annexin V (Figure 4.5.2A). BMDCs treated with both particle sizes did not demonstrate an increase in either cell death (PI^+), early apoptosis (Annexin V^+) or late apoptosis (PI^+/Annexin V^+).

Based on the cell shrinkage observed in BMDCs treated with PLGA particles in this size range, FRAP analysis was conducted to verify if membrane fluidity was altered. A graphical representation of the protocol is shown here in Figure 4.5.3A. In brief, a small ROI of fluorescently labelled membrane was photobleached and the time required for half of the fluorescence to recover within this ROI was measured. The photobleaching in a ROI is depicted in Figure 4.5.3 B, demonstrating the fluorescent recovery over time in an untreated BMDC. As a control for rigid membranes, BMDCs were incubated in media containing 150 µM

sucrose (hyperosmolar media) which caused the cell to shrink. As a control for a highly fluid cell membrane, 1:5 ratio of water in media (hypo-osmolar media) was used, which caused the cell to swell. BMDCs were treated with 1 μm PLGA particles for 0.5, 1 and 3 hours. The half time for fluorescent recovery for particle treated BMDCs increased significantly compared to untreated BMDCs, as early as 30 mins post-incubation. This indicated a decrease in membrane fluidity comparable to BMDCs in hyperosmolar media (Figure 4.5.3 C).

(A)

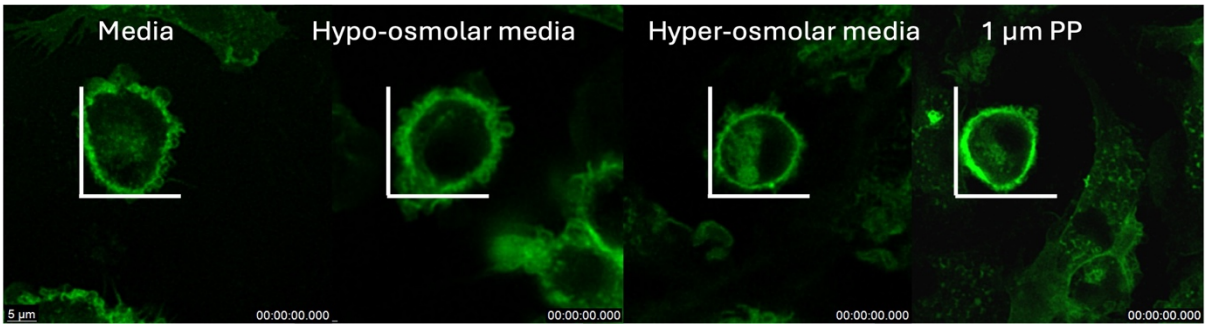

(B)

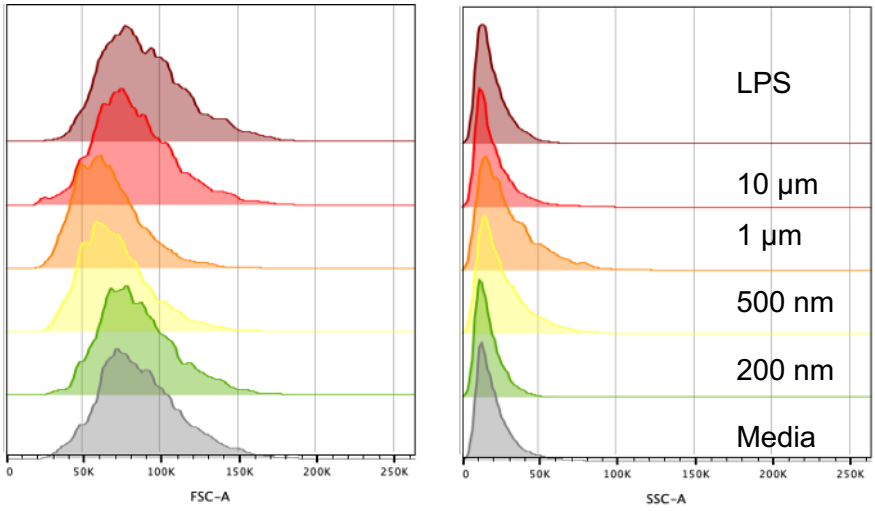

Figure 4.5.1 BMDCs incubated for 24 hours with PLGA particles (PP) in the 0.5-2 µm size range exhibit decreased size and increased granularity. (A) Confocal microscopy images of fluorescently tagged membrane proteins on BMDCs which were treated with hyper/hypo osmolar media and 1 µm PLGA particles for 1 hour. (B) Changes in morphology of BMDCs treated with 0.5-10 µm PLGA particles (300 µg/ml) or LPS (10 ng/ml) were analysed by flow cytometry and represented as histograms for forward and side scatter (FSC and SSC respectively). Histograms are representative of three biological replicates obtained over three distinct experiments.

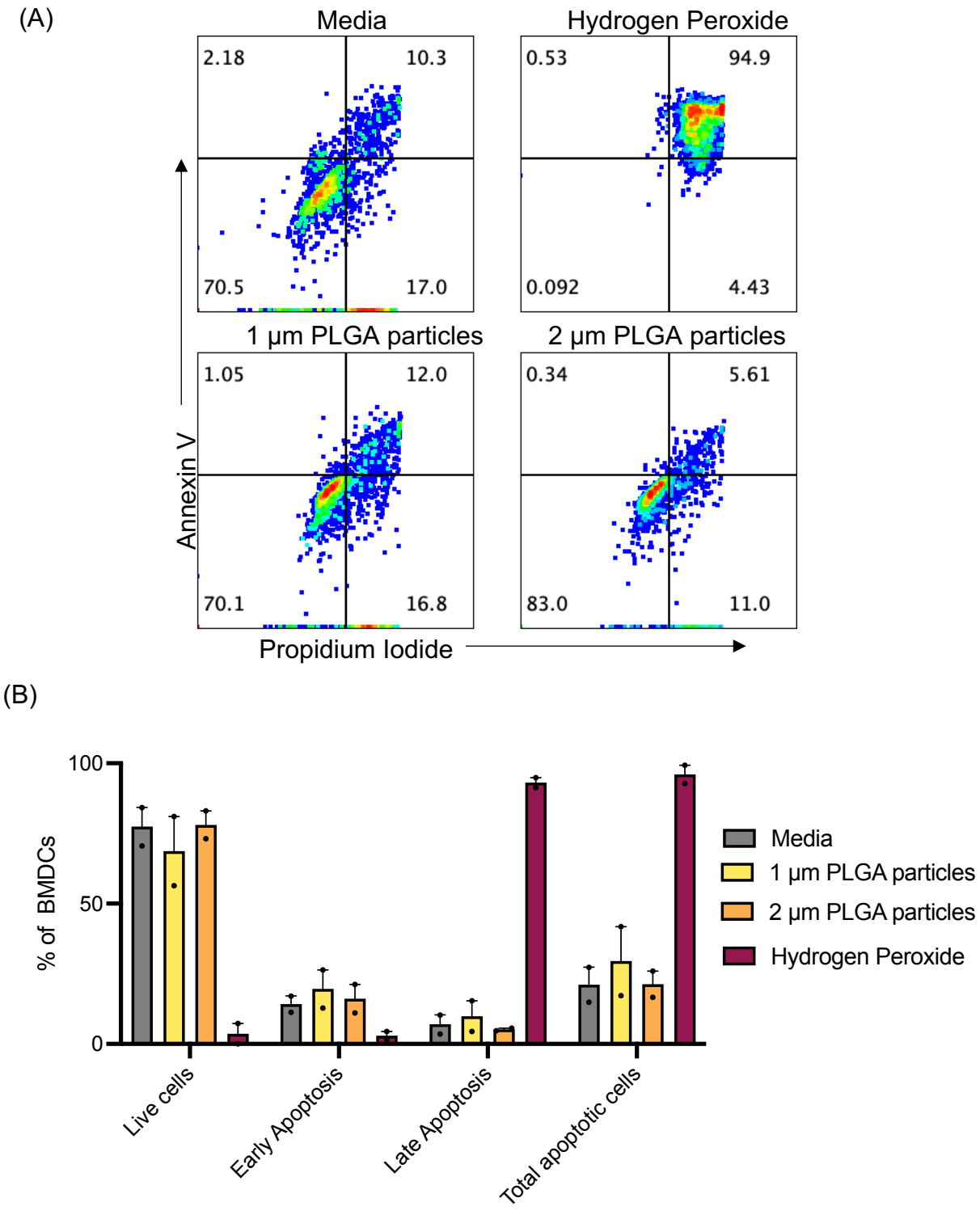

Figure 4.5.2 PLGA particles in the 1-2 µm size range do not induce significant apoptosis after 24 hours incubation. BMDCs ($6.25x10^6$ cell/ml) were treated with 1 or 2 µm PLGA particles (300 µg/ml) or hydrogen peroxide (500 µM) for 24 hours. BMDCs were then fluorescently stained for Annexin V and live/dead indicator Propidium Iodide (PI) and analysed by flow cytometry. (A) Representative histograms of the intensity of Annexin V and PI in single cells treated with particles, or hydrogen peroxide. (B) % of live cells quantified as double negative for PI and Annexin V, % of early apoptotic cells quantified as Annexin V positive and % of late apoptotic cells quantified as

double positive. % of the total apoptotic cell population includes the % of cells in early or late apoptotic cells. Error bars show mean ± SEM for two individual experiments performed on two biological replicates.

(A)

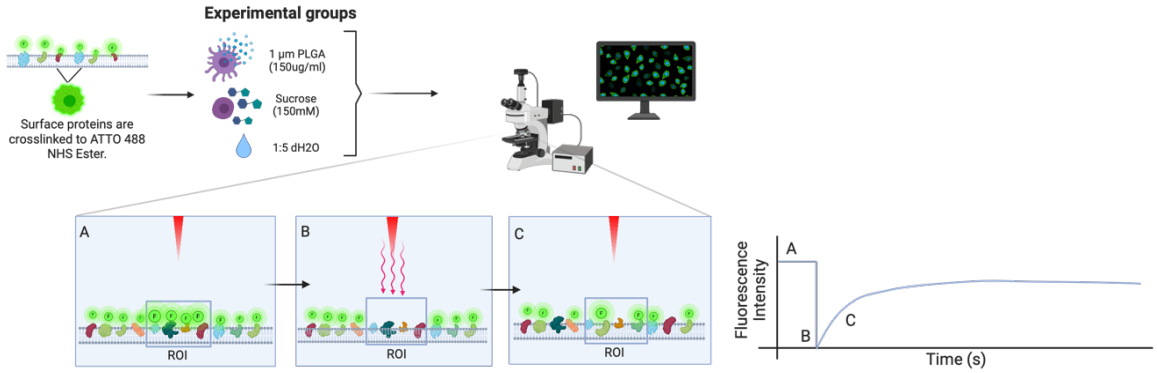

(B)

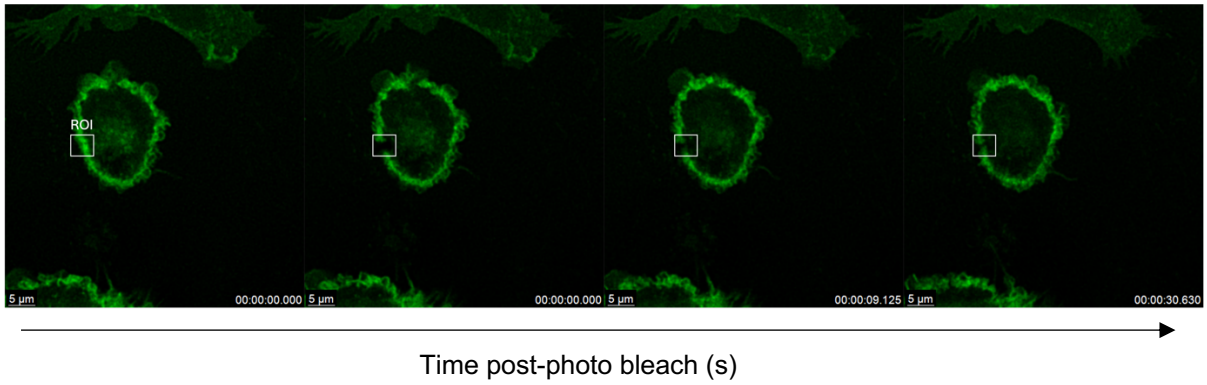

Time post-photo bleach (s)

(C)

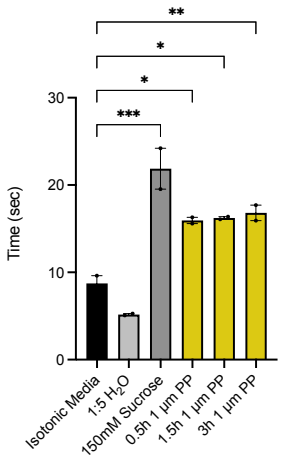

Figure 4.5.3 Exposure to 1µm PLGA particles (PP) decreased the membrane fluidity of BMDCs as early as 0.5 hours after incubation. Membrane proteins on BMDCs cultured from bone marrow isolated from C57BL/6 mice ($1x10^6$ cell/ml) were tagged with Atto 488 NHS ester. BMDCs were then treated with 1 µm PLGA particles (150 µg/ml) for indicated time points, a hypo-osmotic control (1:5 H_2O in media) and hyper-osmotic control (150mM sucrose in media) for 1 hour before being subjected to FRAP analysis on a Leica TCS SP8 STED confocal microscope. A high-intensity argon laser was used to photo-bleach a 4 µm² region of interest (ROI) of fluorescently labelled cell membrane. Rate of fluorescence recovery into the ROI was recorded post-bleach. (A)

Schematic describing the FRAP protocol and (B) representative images of photobleaching within the ROI. (C) Fluorescent recovery half-time for each experimental group was calculated using the Leica LAS x-Software FRAP analysis tools which generate rate of recovery curves providing half-life for the rate of recovery in seconds. Fluorescence recovery half-time was graphed as mean ± SEM for two individual experiments. One-way ANOVA with was used to determine statistical significance compared to untreated control where *$p<0.05$ **$p<0.01$ and ***$p<0.001$.

4.6 Treatment of BMDCs with 0.5-2 μm PLGA particles enhanced the expression of αvβ3, which is required for TGFβ signalling but not gene expression.

In chapter 3, BMDMs treated with 0.5-2 μm PLGA particles were found to upregulate the expression of αvβ3 which was also found to be involved in the upregulation of IL-1Ra. The αvβ3 integrin has mechano-sensing properties, providing both inside-out and outside-in signalling in response to various mechanical strains, for example changes to membrane tension [561]. Since BMDCs were also found to be morphologically affected by 0.5-2 μm PLGA particles, expression of each dimer of the αvβ3 complex was assessed.

The surface expression of αv and β3 was quantified by their MFI and the expression compared to untreated BMDCs. Treating BMDCs with 2 μm PLGA particles for 24 hours, enhanced the surface expression of both αv and β3 dimers, whilst treating BMDCs with LPS resulted in a decrease of approximately 8% (Figure 4.6.1 A-D). The gene expression for each dimer was also quantified and 2 μm PLGA particles enhanced the expression of *itgb3* and *itgav* when compared to untreated BMDCs.

Next, the involvement of αvβ3 in the tolerogenic phenotype exhibited by BMDCs treated with 0.5-2 μm PLGA particles was determined. In section 3.6, it was demonstrated that blockade of αvβ3 using the chemical inhibitor, Cilengitide, and neutralising antibodies partially inhibited the secretion of IL-1Ra. Therefore, the effect of Cilengitide pre-treatment on the expression of *tgfb1* in BMDCs was investigated. Blocking αvβ3 had no effect on *tgfb1* gene expression in 1 μm PLGA particle- or TGFβ- treated BMDCs when normalised to house-keeping genes (HKGs) *β2M* or *Tbp* (Figure 4.6.2 A-B). However, various integrins including αvβ3 have been shown to modulate the TGFβ axis by promoting the activation of TGFβ rather than its gene expression [562,231,537]. Therefore, experiments were carried out to determine if blocking αvβ3 would reduce the activation of TGFβ and consequently, reduce signalling downstream of the TGFβ receptor. BMDCs were pretreated with Cilengitide prior to treatment with PLGA particles or TGFβ for 1 and 3 hours and the phosphorylation of pSmad2 (Ser465/467)/pSmad 3 (Ser423/425) and pSmad2/3 (Thr8) was measured in protein lysates. There was a reduction in the intensity of the bands corresponding to phosphorylation of smad2/3 when αvβ3

was inhibited prior to BMDCs treatment with 1 μm PLGA particles or TGFβ (Figure 4.6.3 A). Densitometry analysis of the bands was performed and a fold change in normalised signal was calculated to quantify the difference in pSmad2/3 expression. BMDCs pre-treated with Cilengitide had decreased pSmad2/3 levels compared to uninhibited counterparts. This demonstrated, that by blocking αvβ3 on BMDCs, particle-induced TGFβ signalling mediated via the canonical TGFβ pathway was reduced (Figure 4.6.3 B) (Figure 4.6.3 C).

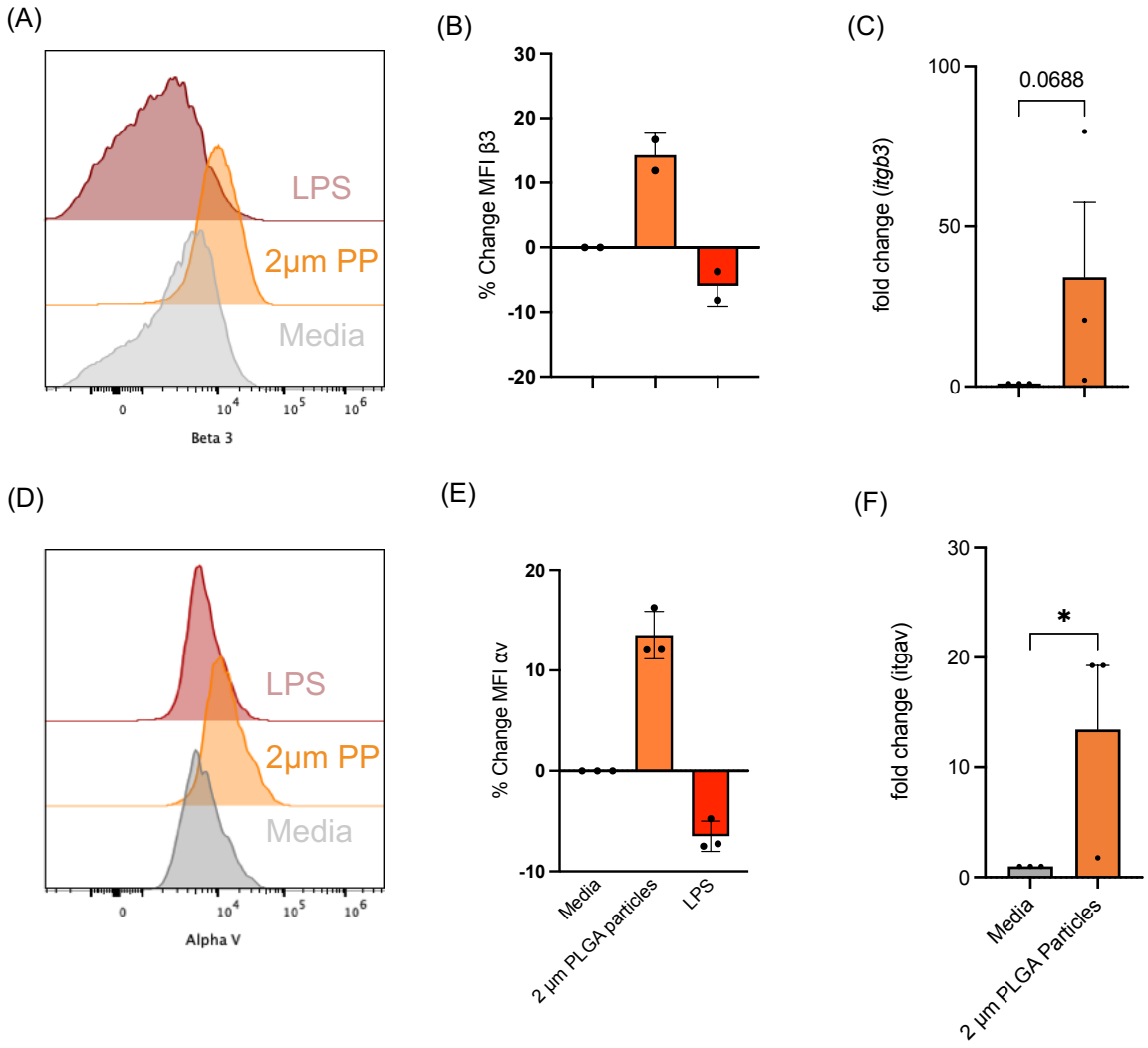

Figure 4.6.1 BMDCs treated with 0.5-2 µm PLGA particles have enhanced expression of surface αv and β3. BMDCs cultured from bone marrow isolated from C57BL/6 female mice (1x10^6 cell/ml) were treated with 2 µm PLGA particles (300 µg/ml) or LPS (10 ng/ml) for 24 hours. Fluorescent antibodies against αv and β3 integrin were used for flow cytometry analysis. Representative stacked histograms were generated demonstrating the intensity in the expression of (A) αv and (D) β3 . MFI values were calculated by FlowJo software (BDScience) and % change of the MFI values for (B) αv and (E) β3 was compared to untreated control. The gene expression (C) *itgb3* and (D) *itgav* was measured by rt qPCR and normalised to the expression of housekeeping gene; *rsp18*. Fold change was calculated compared to untreated control. Kruskall-Wallis test was used to determine statistical significance compared to untreated control where *p<0.05. Histograms are representative of (A-B) two and (D-E) three individual biological replicate experiments. rt qPCR was carried out on three individual biological replicates.

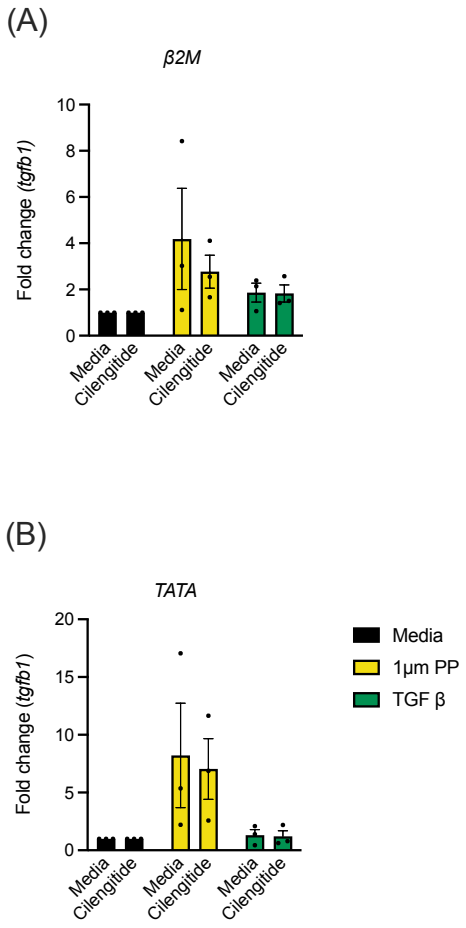

Figure 4.6.2 Inhibiting αvβ3 does not affect *tgfb1* gene expression. BMDCs (6.25x10 ^{5} cell/ml) were pre-treated with Cilengitide (150 μg/ml) and an hour later, treated with 1 μm PLGA particles (300 μg/ml) or TGFβ (25 ng/ml) for 24 hours. mRNA was isolated and cDNA was prepared for rt qPCR. Expression of *tgb1* was normalised to HKG's (A) *β2M* and (B) *Tbp*. Two-way ANOVA with Šídák multiple comparison test was used to determine statistical significance as compared to untreated control. Error bars show mean ± SEM for three individual experiments.

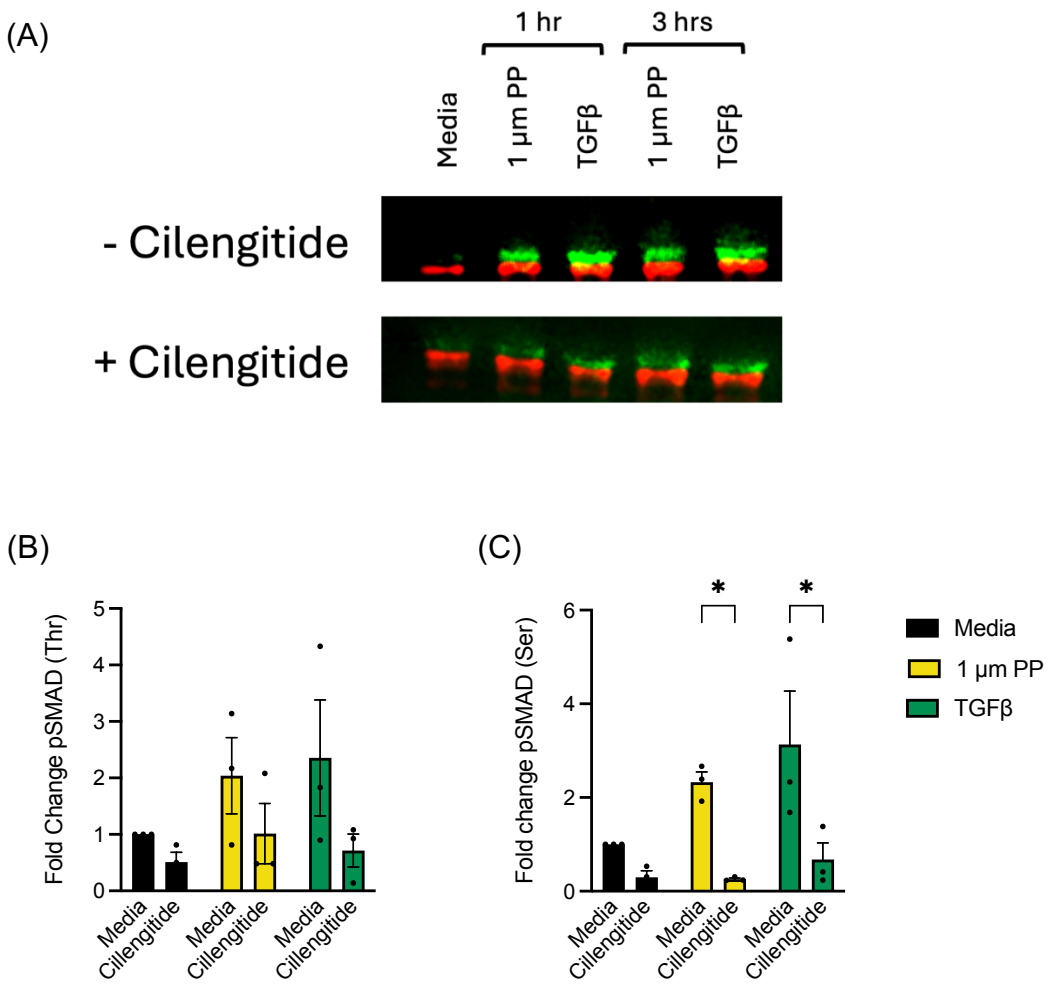

Figure 4.6.3. Blocking αvβ3 downregulates the phosphorylation of Smad2/3 in BMDCs treated with 1µm PLGA particles (PP). BMDCs (6.25x10 ^{5} cell/ml) were pre-treated with Cilengitide (150 µg/ml) and an hour later, treated with 1µm PLGA particles (300 µg/ml), TGFβ (25 ng/ml) or LPS (10 ng/ml) for 30 mins, 1 or 3- hours. Protein was isolated, denatured and separated based on size by gel electrophoresis. Proteins were transferred to a nitrocellulose membrane and quantified using antibodies specific to; pSmad2 (Ser465/467) pSmad 3 (Ser423/425) and pSmad2/3 (Thr8). Secondary antibodies were used with IR fluorescence to detect protein bands. Densitometry analysis of fluorescent signal for each band was performed using EmpiriaStudio software (Li-Cor) and normalised against β-actin and Total Smad2/3. Representative blots portray bands specific to (A) pSmad2/3 (Ser) from inhibited and uninhibited groups with corresponding β-actin bands at 3 hours. Fold change of normalised fluorescent signal for (B) pSmad2/3 (Thr) and (C) pSmad2/3 (Ser) were calculated against untreated control. Two-way ANOVA with Šídáks multiple comparison test was used to determine statistical significance as compared to untreated control, where *p<0.05. Error bars show mean ± SEM for three individual biological replicates

4.7 BMDC-derived TGFβ is required for the expansion of OVA-specific T-regs in co-culture.

With TGFβ having a fundamental role in establishing T-reg differentiation, it was hypothesised that the induction of T-regs by BMDCs treated with 2 μm PLGA particles could be attributed to the enhancement in TGFβ expression, as well as enhanced TGFβ activation by αvβ3. To test this hypothesis, an anti-TGFβ nAb was used during co-culture to evaluate the extent of T-reg expansion in the absence of TGFβ. BMDCs were treated with or without OVA, and 2 μm PLGA particles or TGFβ for 24 hours as previously described. Anti-TGFβ nAb was added to the co-culture at the same time as CFSE stained naïve $CD4^+$ T-cells from OTII mice for 72 hours. Flow cytometry of cells stained with FVS and antibodies against CD3, CD4, FoxP3 was carried out and the gating strategy described in Figure 4.3.1B was used to measure cell populations.

Preliminary results demonstrated that neutralising TGFβ resulted in less $FoxP3^+$ $CD4^+$ T-cells compared to the uninhibited BMDCs treated with TGFβ + OVA and 2 μm particles + OVA (Figure 4.7.1B). The number of live cells and $CD3/CD4^+$ T-cells was unaffected in the 2 μm particles + OVA treated groups, demonstrating that the anti-TGFβ antibody only affected T-reg priming and not the number of T-cells. (Figure 4.7.1A). In addition to the decrease in $FoxP3^+$ $CD4^+$ T-cells, neutralising TGFβ resulted in a reduction in the number of proliferating cells primed by BMDCs treated with 2 μm particles + OVA and TGFβ+ OVA (Figure 4.7.1 E), which can be seen when comparing the CFSE histograms for (F) uninhibited and (G) inhibited groups.

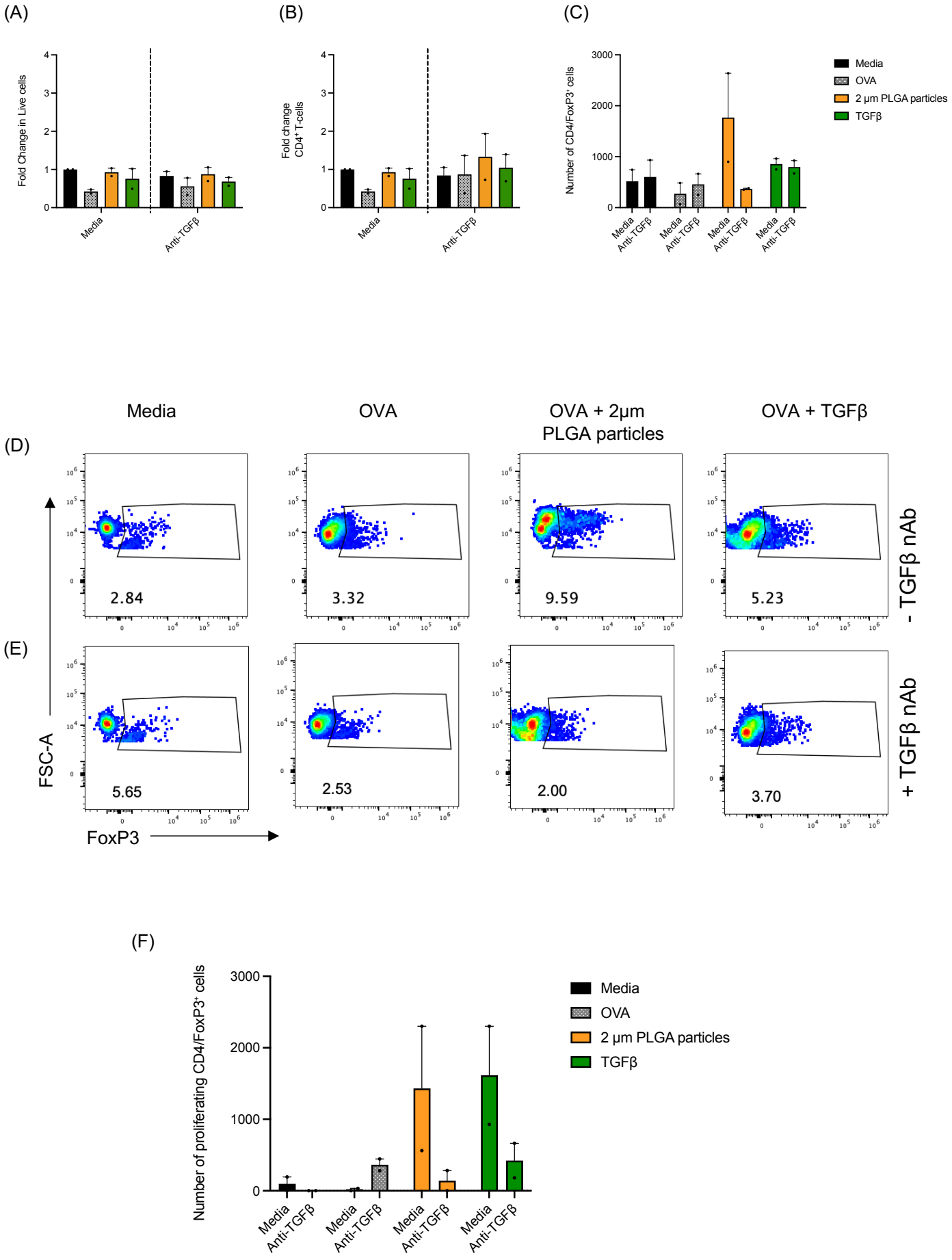
(A)
Fold Change in Live cells
Media
Anti-TGFβ
(B)
Fold change CD4+ T-cells
Media
Anti-TGFβ
(C)
Number of CD4/FoxP3+ cells
Media
OVA
2 µm PLGA particles
TGFβ
Media
Anti-TGFβ
Media
Anti-TGFβ
Media
Anti-TGFβ
Media
Anti-TGFβ
Media
OVA
OVA + 2µm PLGA particles
OVA + TGFβ
(D)
2.84
3.32
9.59
5.23
- TGFβ nAb
(E)
5.65
2.53
2.00
3.70
+ TGFβ nAb
FSC-A
FoxP3
(F)
Number of proliferating CD4/FoxP3+ cells
Media
OVA
2 µm PLGA particles
TGFβ
Media
Anti-TGFβ
Media
Anti-TGFβ
Media
Anti-TGFβ
Media
Anti-TGFβ

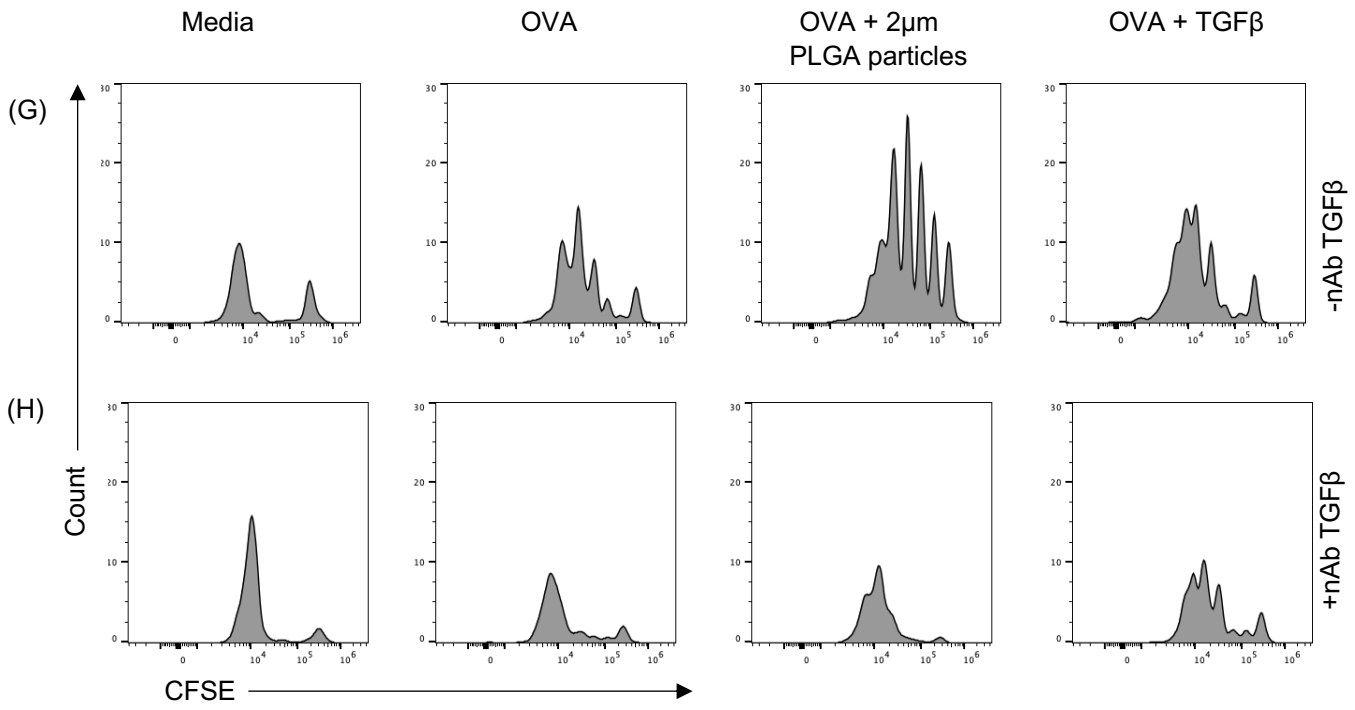

Figure 4.7.1 Neutralising TGFβ during co-culture affected T-reg expansion. BMDCs cultured from bone marrow isolated from C57BL/6 mice ($2x10^5$ cell/ml) were treated with 2µm PLGA particles (300 µg/ml), TGFβ (25 ng/ml) or LPS (10 ng/ml) with or without OVA (25 µg/ml) for 24 hours. Media was removed and enriched CFSE stained $CD4^+$ T-cells isolated from splenocytes from OTII mice ($4x10^5$) were added and co-cultured for 72 hours with or without anti-TGFβ nAb (50 µg/ml). Cells were stained with FVS, as well as fluorescent antibodies specific to CD3, CD4, CD25 and FoxP3. Fold change in the number of (A) live and (B) $CD3/CD4^+$ compared to uninhibited control was calculated and the number of (C) $CD3/CD4/FoxP3^+$ were determined. The representative dot plots of FSC-A vs FoxP3 are shown for (D) uninhibited and (E) inhibited groups. CFSE modelling was carried out using FlowJo Software (BDSciences) and the (F) the number of proliferating cells was calculated for inhibited and uninhibited groups. Proliferation modelling is shown for (G) uninhibited and (H) inhibited groups. Error bars show mean ± SEM for two individual co-culture experiments.

4.8 BMDCs require αvβ3 to expand OVA-specific T-regs in co-culture

Having established that 1-2 μm PLGA particles promote TGFβ production from BMDCs, which is appears to be required to modulate T-reg expansion in co-culture with $CD4^+$ T-cells, we speculated that blocking αvβ3 would impede T-reg priming. To evaluate this hypothesis, a monoclonal neutralising β3 antibody (nAb) was included in the previously described co-culture model (Section 4.3) to inhibit signalling dependent on β3. Selective inhibition of the β3 dimer of the αvβ3 integrin complex was tested since β3 only dimerises with αv or αIIb, and only the αvβ3 dimer has been implicated in the regulation of TGFβ. Furthermore, the β dimer of integrins is indispensable for bi-directional signalling, as it acts as a docking station for adaptor and signalling proteins. This is covered in detail in section 1.3.4.

Dendritic cells were pre-treated with the β3 nAb for one hour prior to treatment with 2 μm PLGA particles or TGFβ, with or without OVA. CFSE stained $CD4^+$ T-cells isolated from OTII splenocytes were added 24 hours later and cultured together for 72 hours. Flow cytometry on cells stained with FVS and antibodies against CD3, CD4, FoxP3 was carried out and the gating strategy depicted in figure 4.3.1 B was used to quantify cell populations.

The β3 nAb did not affect the number of live or CD3/$CD4^+$ T-cells during co-culture. There was a slight decrease in the number of $FoxP3^+$ T-cells observed when the β3 neutralising antibody was used prior the treatment of BMDCs with 2 μm particle + OVA. However, this decrease was not found to be statistically significant. Comparing the representative dot plots of the inhibited and uninhibited counterparts in Figure 4.8.1 D and E does, however, demonstrated that there are fewer T-regs being primed by these BMDCs.

The number of proliferating T-regs was significantly decreased in the 2 μm particle + OVA group when β3 was inhibited (Figure 4.8.2 A). Looking at the CFSE histograms, the proliferation of CD3/CD4/$FoxP3^+$ was brought back down to basal levels (Figure 4.8.2 B-C).

To ensure equal BMDC viability across inhibited and uninhibited groups, an LDH assay was carried out on BMDCs treated with the nAb against β3. The LDH assay measures the concentration of LDH released into the supernatant because of cell damage. It is indirectly measured spectrophotometrically based on the conversion of NAD^+ to NADH by lactate , and subsequent reduction of water soluble tetrazolium salt

dye (WTS) which can be measured spectrophotometrically. There was a slight increase in cell death from BMDCs treated with the nAb, compared to untreated cells, however this was not found to be statistically significant. The increase in cell death was approximately 18% (Figure 4.8.3 A) which we do not believed to account for the decrease in T-reg proliferation.

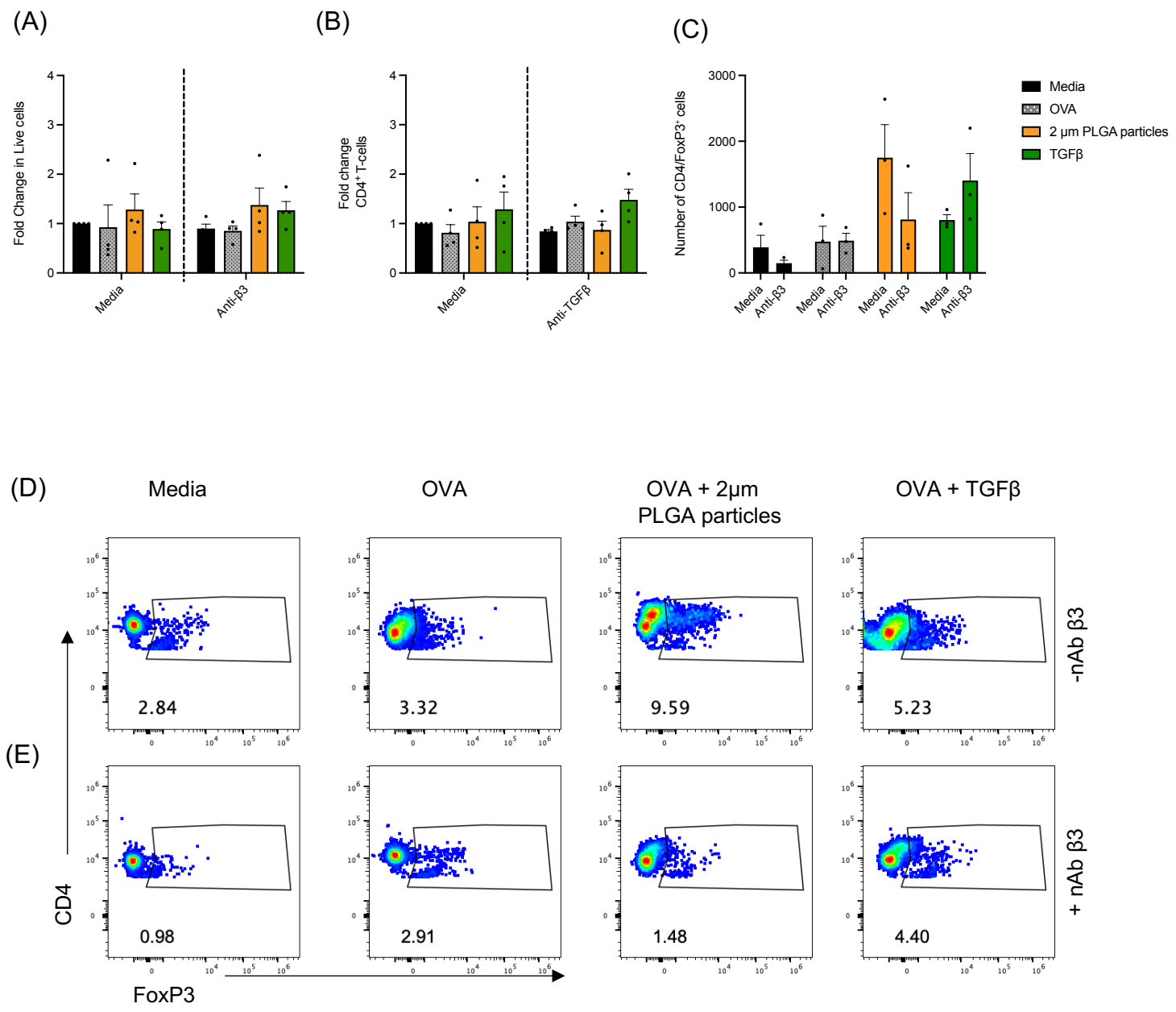

Figure 4.8.1 β3 blockade does not affect OVA-specific CD4⁺ T-reg number. BMDCs ($2x10^5$ cell/ml) were first incubated with β3 nAb (50 µg/ml) for one hour prior to treatment with 2µm PLGA particles (300 µg/ml) or TGFβ (25 ng/ml) with or without OVA (25 µg/ml) for 24 hours. Media was removed and enriched, CFSE stained, CD4⁺ T-cells isolated from splenocytes from OTII mice were added and co-cultured for 72 hours. Cells were stained with FVS, as well as fluorescent antibodies specific to CD3, CD4, CD25 and FoxP3. The same gating strategy presented in Figure 4.2.1.B was used. The fold change in the number of (A) live and (B) CD3/CD4⁺ T-cells were calculated compared to the number of each in the uninhibited media control. (C) The number of CD3/CD4/FoxP3⁺ T-cells were compared for each group with and without nAb. Representative dot plots are shown depicting (D) uninhibited and (E) inhibited FSC vs FoxP3 plots. Two-way ANOVA with Dunnet's multiple comparison was used to determine statistical significance as compared to the uninhibited counterpart for each treatment. Error bars show mean ± SEM for three individual experiments performed on three individual co-culture experiments.

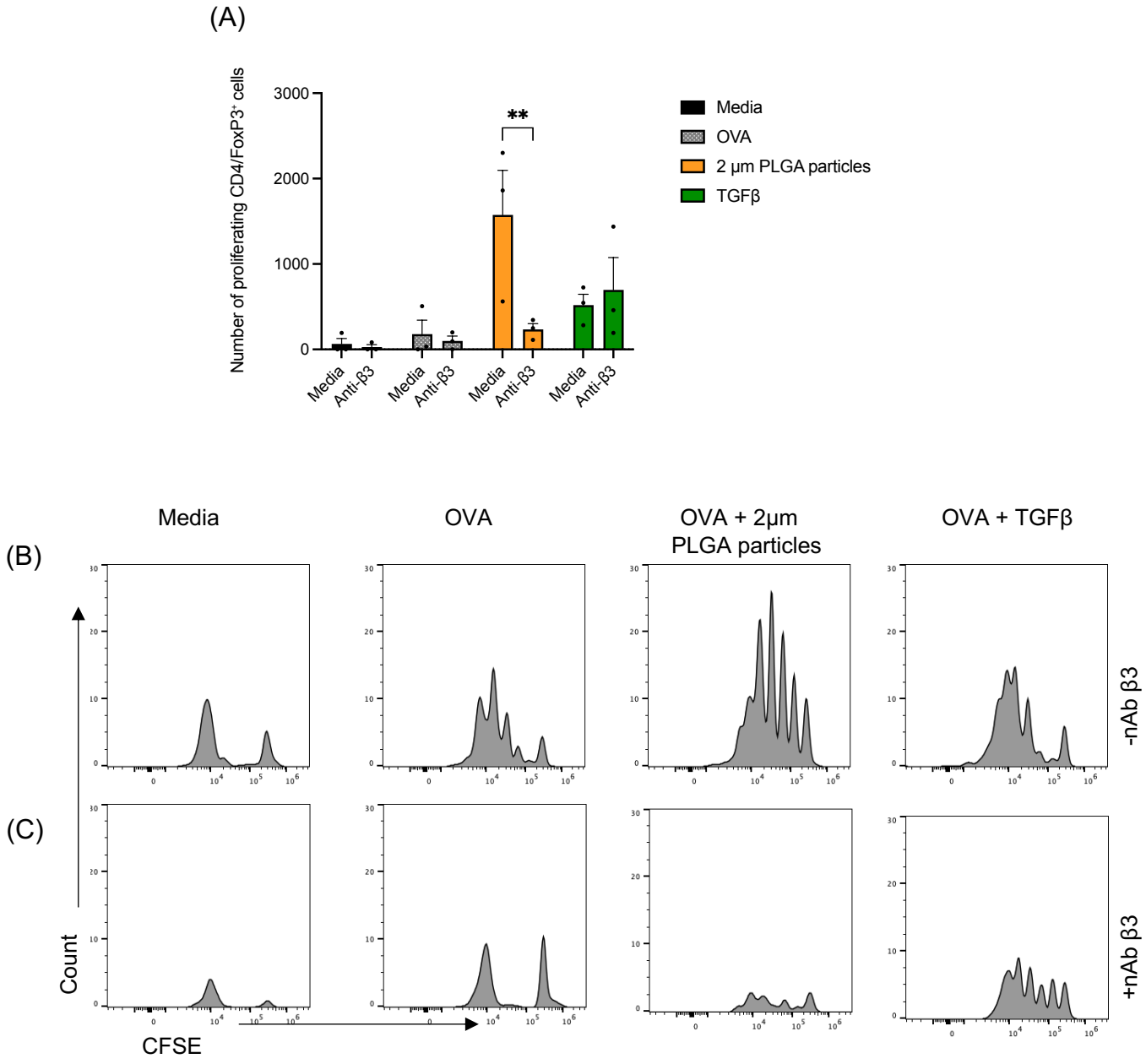

Figure 4.8.2 β3 blockade hinders T-reg proliferation. BMDCs (2x10^5 cell/ml) were first incubated with β3 nAb (50 µg/ml) for one hour, prior to treatment with 2µm PLGA particles (300 µg/ml) or TGFβ (25 ng/ml) with or without OVA (25 µg/ml) for 24 hours. Media was removed and enriched, CFSE stained, $CD4^+$ T-cells isolated from splenocytes from OTII mice were added and co-cultured for 72 hours. CFSE modelling was carried out using FlowJo Software (BDSciences) and the (A) number of proliferating cells was calculated for inhibited and uninhibited groups. Proliferation modelling is shown for (B) uninhibited and (C) inhibited groups. Two-way ANOVA with Dunnett's multiple comparison test was used to determine statistical significance as compared to the uninhibited counterpart for each treatment, where *p<0.05 and **p<0.01. Error bars show mean ± SEM for three individual co-culture experiments.

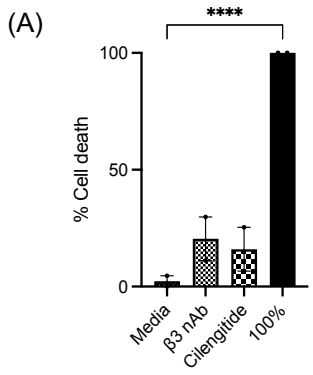

Figure 4.6.3 Anti- β3 nAb and Cilengitide induces minimal cell death. BMDCs ($6.25x10^5$ cell/ml) were treated with anti-β3 nAb (50 µg/ml) or Cilengitide (150 µg/ml) for 24 hours. A 100% cell death control was prepared 20 mins prior to the LDH assay. The % cell death was calculated as a percentage of the 100% cell death control. One way ANOVA was used to determine statistical significance as compared to untreated control, where *p<0.05 **p<0.01 ***p<0.001 and **** p<0.0001. Error bars show mean ± SEM for two individual biological replicates.

4.9 Blocking β3 inhibits expansion of OVA-specific T-regs *in-vivo*

To address the role of αvβ3 in the induction of antigen-specific Tregs in mice vaccinated with 2 μm PLGA particles and OVA, mice were injected intraperitoneally (i.p) with nAb specific to β3 (5mg/kg) 24 hours prior to i.m vaccination, and again, prior to the boost on day 14. The vaccination protocol is schematically depicted in Figure 4.9.1 A. Mice not receiving nAb, were injected i.p with Armenian hamster IgG isotype control. Splenocytes and blood were collected and splenic lymphocytes were stimulated *ex-vivo* with OVA for 72 hours to identify OVA-reactive T-regs. Cells were then stained with FVS as well as antibodies against CD3, CD4, CD8, CD25, FoxP3 and Helios for analysis of Treg cell populations.

The number of $CD4^+$ T-cells were relatively unaffected by β3 inhibition, despite some variation in the number of $CD4^+$ cells in the OVA injected group (Figure 4.9.1 B). The number of $CD25^+$ T-cells was not significantly reduced (Figure 4.9.1 C), however the number of $CD25^+$, $FoxP3^+$ and $CD25/FoxP3/Helios^+$ CD4 T-cells decreased drastically in the mice receiving β3 nAb compared to the group receiving the IgG isotype control (Figure 4.9.1 D-E). Comparing the dot plots of the double (Figure 4.9.1 F) and triple positive (Figure 4.9.1G) T-reg populations, there is a notable reduction in the density of the both T-reg populations in the mice which received the β3 nAb. These results suggest an integral role for β3 in the mechanism by which vaccination with antigen and 2 μm particles enhanced OVA-specific T-reg expansion.

In section 4.4, it was demonstrated that only the splenic lymphocytes cultured *ex-vivo* from mice vaccinated with OVA + 2 μm particles produced heightened IL-10. The role of β3 was assessed by comparing the secretion of IL-10 from splenic lymphocytes isolated from mice which received β3 nAb i.p prior to vaccination with 2μm particles + OVA. However, inhibition of β3 did not appear to affect the amount of IL-10 produced by these cells (Figure 4.9.2 A). Interestingly, vaccine induced serum IgG responses were also unaffected by injection of the neutralising antibody (Figure 4.9.3 A-B), indicating a relatively specific effect on directing Treg cell differentiation.

(A)

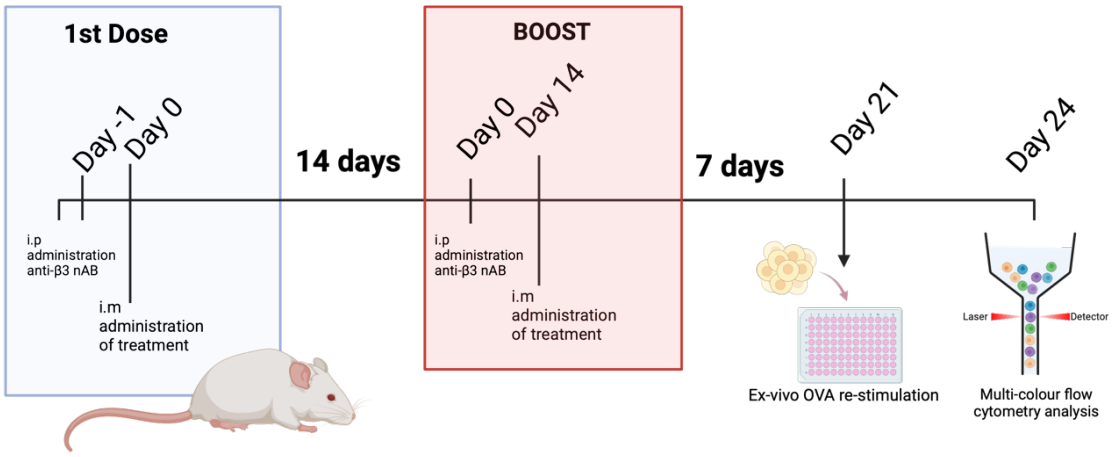
1st Dose
Day -1
Day 0
i.p
administration
anti-β3 nAB
i.m
administration
of treatment
14 days
BOOST
Day 0
Day 14
i.p
administration
anti-β3 nAB
i.m
administration
of treatment
7 days
Day 21
Day 24
Ex-vivo OVA re-stimulation
Laser
Detector
Multi-colour flow
cytometry analysis

(B)

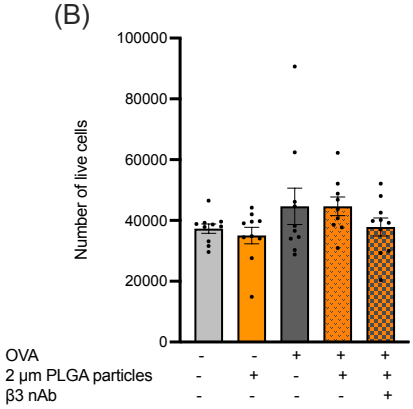
Number of live cells
100000
80000
60000
40000
20000
0
OVA
2 µm PLGA particles
β3 nAb

(C)

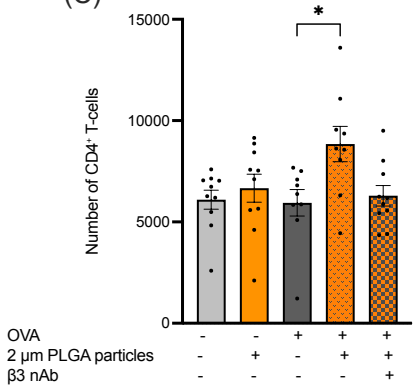
Number of CD4⁺ T-cells
15000
10000
5000
0
*
OVA
2 µm PLGA particles
β3 nAb

(D)

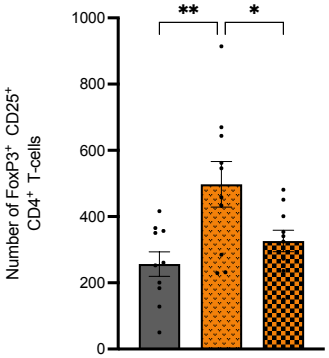
Number of FoxP3⁺ CD25⁺
CD4⁺ T-cells
1000
800
600
400
200
0
**
*

(E)

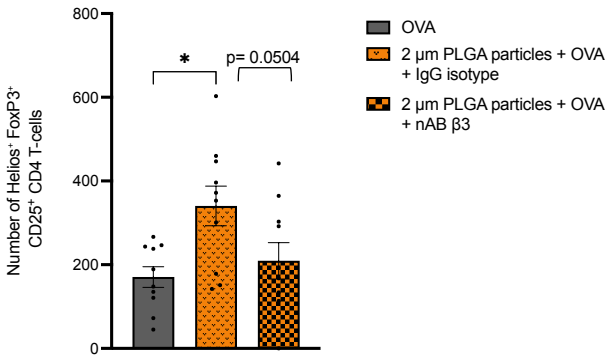
Number of Helios⁺ FoxP3⁺
CD25⁺ CD4 T-cells
800
600
400
200
0
*
p= 0.0504
OVA
2 µm PLGA particles + OVA
+ IgG isotype
2 µm PLGA particles + OVA
+ nAB β3

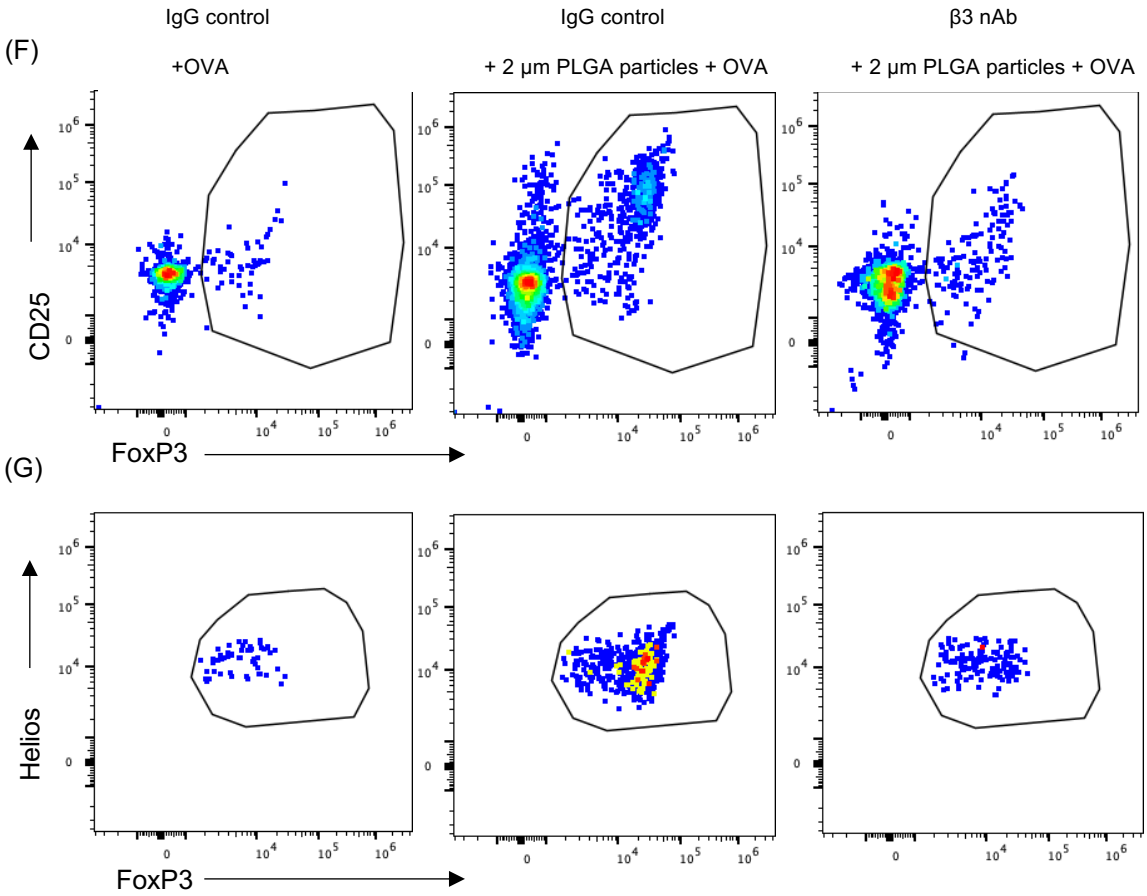

Figure 4.9.1 Intraperitoneal injection of β3 nAb inhibits the expansion of OVA-specific T-regs induced by vaccination with 2 µm PLGA particles and OVA. C57BL/6 mice were injected i.p with either anti-β3 nAb or IgG isotype control (5 mg/kg) 24 hours prior to i.m injection with PBS, OVA (10 µg/mouse), 2 µm PLGA particles (1 mg/mouse) or OVA + 2 µm particle combination. On day 13, i.p injections were repeated prior to boost on day 14. On day 21, mice were sacrificed and spleens were collected. Lymphocytes were isolated and re-stimulated with OVA (25 µg/ml) *ex-vivo* for 72 hours. The schematic of the vaccination protocol is depicted in (A). Lymphocytes were stained with FVS and antibodies specific to CD3, CD4, CD8, CD25, FoxP3 and Helios and cell populations were quantified by flow cytometry. The same gating strategy presented in Figure 4.3.1B was used. The number of (B) live single cells positive for (C) CD3/CD4 (D) CD4/CD25/FoxP3 and (E) CD4/CD25/FoxP3/Helios were quantified for each experimental group. Representative dot plots of splenic lymphocytes gated on (F) CD25 vs FoxP3 and (E) Helios vs FoxP3, from mice which received the IgG isotype control (first and middle row) or β3 nAb (last row). Statistical significance was determined using (B-C) One-Way ANOVA or (D-E) Two-way ANOVA with Dunnett's multiple comparison against OVA treated group (B-C) or OVA+ 2 µm PP group (D-E). Data are represented as mean ± SEM. Asterisks (*) represent *p < 0.05 and **p < 0.01. Mouse injection regime was performed on a total of 9 C57BL/6 female mice per group.

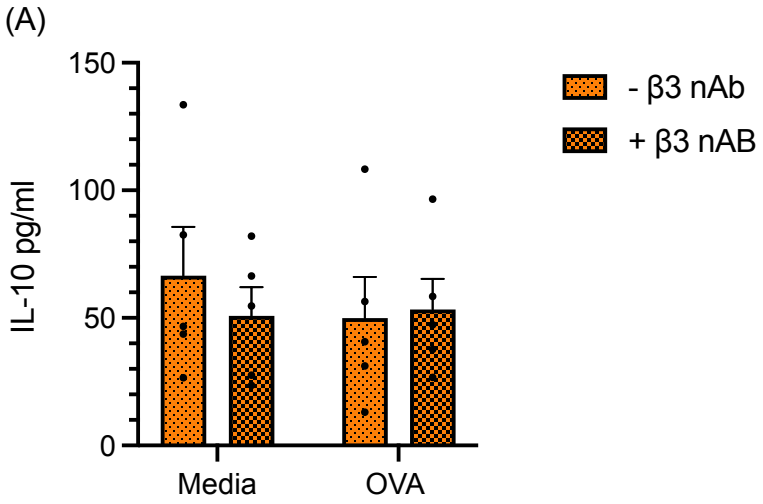

Figure 4.9.2 The secretion of IL-10 from splenic lymphocytes isolated from mice vaccinated with OVA + 2 µm PLGA particles and re-stimulated ex-vivo with media or OVA was not affected by i.p injection with anti-β3 nAb. C57BL/6 mice were injected i.p with β3 nAb a day prior to i.m vaccination with OVA + 2 µm PLGA particles on day 1 and 14. On day 21, splenic lymphocytes were isolated and cultured ex-vivo with media or OVA (25 µg/ml) 72 hours. Supernatants were collected and the secretion of IL-10 was quantified by ELISA. Statistical significance was determined using Two-Way ANOVA with Dunnett's multiple comparison against OVA treated group. Data are represented as mean ± SEM. Mouse injection regime was performed on a total of 5 C57BL/6 female mice per group. Supernatants were only collected from the second *in-vivo* experiment which was carried out on 5 mice.

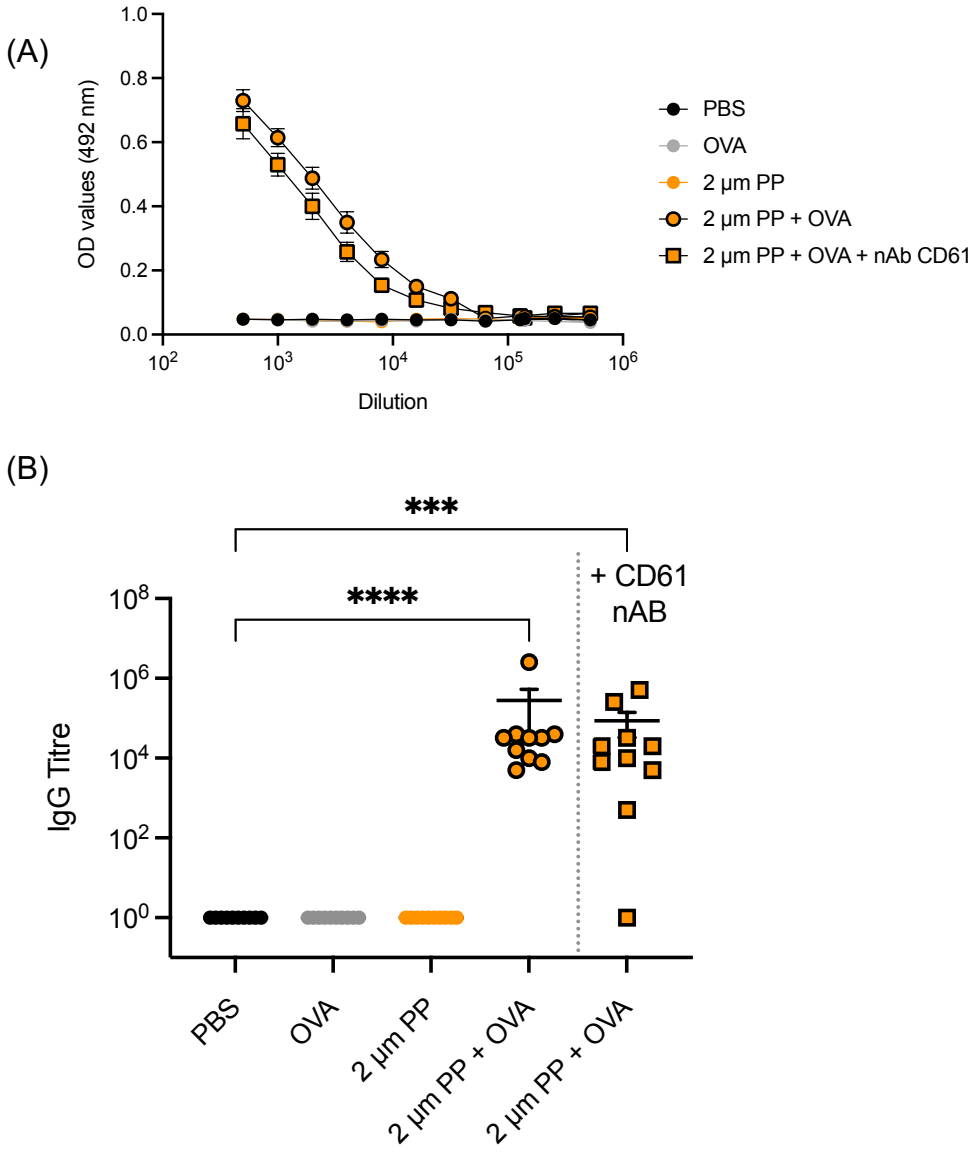

Figure 4.9.3 Intraperitoneal injection with anti-β3 nAb does not affect the enhancement of OVA-specific IgG. C57BL/6 mice were injected i.p with β3 nAb a day prior to i.m vaccination with OVA, 2 µm PLGA particles or in combination on day 1 and 14. On day 21, mice were sacrificed and blood was collected. Blood serum was isolated and OVA-specific IgG ELISA was performed. (A) The OD value of each dilution was measured and dilution curves were created. (B) From the OD values at each dilution, IgG titres were calculated. The vaccination regime was performed on a total of 10 C57BL/6 female mice per group. Kruskal-Wallis test was used to determine statistical significance as compared to untreated control, where *p<0.05 **p<0.01 ***p<0.001 and **** p<0.0001. Error bars show mean ± SEM for three individual co-culture experiments.

4.10. Chapter 4 - Discussion

The results presented here, further substantiate the capacity of 0.5-2 μm PLGA particles to drive anti-inflammatory and pro-tolerance responses. PLGA particles in this size range enhanced the production of TGFβ and IL-10, whilst having no effect on IL-6 or TNFα secretion from BMDCs. The enhancement in TGFβ was found to be critical in the capacity of 2 μm PLGA particles to expand antigen-specific T-regs. Furthermore, exploring the mechanism by which innate immune cells respond differentially to particles based on size, implicated the αvβ3 integrin in modulating antigen-specific T-regs in a co-culture setting and *in-vivo*.

In chapter 3, the effect of particle size on macrophages was explored. Whilst both macrophages and DCs are antigen presenting cells, DCs are significantly more proficient at priming naive T cells. Whilst previous work has been carried out assessing the cytokine profile of BMDCs exposed to PLGA particles in the 0.5-2 μm range, it focused on assessing Th1/Th2 polarising cytokines. Instead, the focus here, was on how PLGA particle size might influence priming of T-regs.

The production of IL-10 and TGFβ is characteristic of tolDCs and these cytokines act to modulate T-reg polarisation. Interestingly, PLGA particles, specifically in the 0.5-2 μm size range promoted significant enhancement in the secretion of IL-10 when co-stimulated with LPS. In addition, 1 μm PLGA particles alone were able to enhance the expression of *tgfb1* mRNA. The activation of the canonical signalling pathway downstream of the TGFβ receptor was also assessed by measuring the phosphorylation of transcription factors pSmad2 and 3, which upon phosphorylation can translocate to the nucleus and promote TGFβ-dependent gene expression. Since secreted TGFβ must first dissociate from its LAP protein to become active and signal via the TGFβ receptor, it provides a method of measuring how much active TGFβ is available to the cell [563]. Western blot analysis of the Smad2/3 proteins from BMDCs treated with 1 μm PLGA particles, demonstrated a significant increase in the levels of pSmad2/3 when compared to untreated BMDCs. This led to the hypothesis that not only do 1 μm particle treated BMDCs increase the expression of the TGFβ gene, but also facilitate the activation of latent TGFβ. In addition to immunosuppressive cytokines, it was critical to assess the propensity to modulate pro-inflammatory cytokines IL-6 and TNFα. DCs exposed to fungi and bacteria upregulate the secretion of TGFβ, IL-6 and IL-23

which during cross-presentation can promote Th17 differentiation, critical to resolving infection, but are also involved in aggravating auto-immunity [564]. BMDCs treated with a PLGA particles in the range of 0.5-20 μm on their own, did not enhance basal levels of IL-6 or TNFα production. Assessing their response in the presence of the bacterial ligand; LPS, also indicated no significant promotion of either cytokine above baseline.

On account of the effects of 0.5-2 μm PLGA particles we theorised that DCs would facilitate the differentiation of naïve T-cells towards T-regs. T-regs mitigate T-eff functions through the secretion of immunosuppressive cytokines; IL-10 and TGFβ, depletion of IL-2, interference of T-eff metabolism, amongst other functions covered in detail in section 1.2.2. The underlying pathology of auto-immune diseases is usually perpetuated by dysfunctions in the capacity to expand functional antigen-specific T-regs. As such, there is huge interest in identifying methods to enhance stable functional T-regs to overcome the detrimental effects of auto-immunity. Vaccination offers an attractive opportunity, which could be harnessed to expand antigen-specific T-regs *in-vivo,* rather than relying on autologous tolDC or T-reg cell transfusion therapy or non-specific immunosuppressive drugs. One of the challenges faced in developing vaccines against auto-immune diseases, is identifying a robust method to specifically direct the expansion of antigen-specific T-regs, rather than T-eff cells. This could be achieved by including “anti-inflammatory” adjuvants in vaccines, alongside a disease specific antigen. A ideal anti-inflammatory adjuvant would be able to promote the polarisation of DCs towards tolDCs and subsequently, increase T-reg activation.

To test the ability of BMDCs treated with 0.5-2 μm PLGA particles to expand T-reg populations a co-culture model was devised to compare the priming capacity of BMDCs treated with OVA alone or with 2 μm PLGA particles, TGFβ or LPS. An important substitution which was made for this model was the use of serum-free media to minimise the interference of TGFβ found in animal-derived serum. The conventionally used cRPMI containing foetal calf serum was gradually substituted with X-VIVO serum free hematopoietic cell medium (Lonza) over the course of the BMDC culturing protocol. However, when $CD4^+$ T-cells were added, conventional T-cell media (refer to table 2.1.2 for full list of components) was used to support T-cell proliferation. $CD4^+$ T-cells used here were isolated from the spleens of the

OTII mouse strain which are genetically engineered to produce T-cells which possess α/β chains complementary to the OVA protein.

BMDCs were treated with TGFβ in conjunction with OVA as a positive control to promote T-reg expansion. Indeed, BMDCs treated with TGFβ promoted an increase in the number of OVA-specific CD4/CD3/FoxP3^{+} cells referred to herein as FoxP3 T-regs. Impressively, BMDCs cultured with 2 μm PLGA particles and OVA were able to upregulate the number of FoxP3 T-regs to a similar extent as the positive control. T-regs have also been demonstrated to enhance the TGFβ membrane anchor GARP. GARP supports the suppressive functions of T-regs by further stabilising FoxP3 expression [109], and presenting latent TGFβ to its surface facilitating its release from LAP [111]. The MFI of GARP was assessed on T-cells primed by BMDCs treated with OVA and 2 μm particles or TGFβ and compared to the untreated controls. Interestingly, only T-cells cultured with OVA + 2 μm particles had enhanced surface expression of GARP. The expression of LAP was also investigated, as a measure of the amount of inactivated latent TGFβ presented on the T-cell surface by GARP. The OVA specific CD3/CD4^{+} population primed by BMDCs treated with OVA + 2 μm particles displayed significantly less LAP, despite the increase in GAPR. This could indicate an increase in the activation of TGFβ.

CFSE staining of the initial population of naïve CD4^{+} T-cells allowed us to track the proliferation of expanded cells. Expansion of T-reg populations, is fundamental to disseminate immunosuppressive capacity past the confines of lymphoid organs *in-vivo*. Indeed, there was an significant increase in the number of proliferating OVA-specific FoxP3 T-regs following activation by BMDCs treated with 2 μm PLGA particles, and TGFβ.

Of course, the *in-vitro* co-culture does not accurately represent the complexity of T-reg induction and heterogeneity *in-vivo.* To assess T-reg expansion *in-vivo* C57BL/6 female mice were vaccinated intra-muscularly with OVA, 2 μm PLGA particles or a combination of the two on day 0 and boosted on day 14. In order to expand OVA-specific T-regs, lymphocytes were isolated and cultured *ex-vivo* with OVA for a 72 hour period. The results substantiated the capacity of 2 μm PLGA particles to promote OVA-specific T-reg expansion. In fact, mice injected with OVA+ 2 μm PLGA particles produced almost double the number of OVA- specific T-regs compared to mice injected with one or the other. Helios has recently been identified as a supplementary marker to FoxP3 for the identification of T-regs, in

particular natural T-regs which are generated in the thymus [565],[566]. The FoxP3/Helios double positive phenotype has been attributed to having greater immunosuppressive capacity and provide superior protection against auto-immunity, in part due to the enhanced phenotypic stability as a result of Helios and FoxP3 co-expression [105]. Interestingly, out of the population of CD25/FoxP3^{+} T-regs isolated from the vaccinated mice, the majority also expressed Helios . This could suggest that the OVA + 2 μm PLGA particle vaccination promoted a significant expansion of thymus derived T-regs rather than peripherally activated T-regs.

The results presented here are encouraging, demonstrating the potential of 2 μm PLGA particles as an "anti-inflammatory adjuvant" capable of promoting antigen-specific T-reg expansion. However, in order to assess the immunosuppressive capacity of these T-regs, a co-culture with antigen-specific T-effs would be required demonstrate the ability to induce T-eff anergy and tolerance. Even better, an in-vivo disease model, for example a therapeutic model of EAE, would put the capacity of 2 μm PLGA particles to induce tolerance into perspective [567].

With PLGA particles lacking a ligand known to interact with any PRRs, it could be inferred that the elicited immune responses are driven by mechanical cues, especially considering polystyrene particles of the same 0.5-2 μm size range enhanced BMDC-derived IL-10 [501]. This is further supported by the remarkable morphological changes observed in BMDCs treated with 0.5-2 μm PLGA particles. Innate immune cells have a dynamic cell membrane and cytoskeleton which allow the cell to respond to environmental factors including, pH, osmolarity, substrate stiffness, compression and cell-cell interactions [190]. This allows the cell to adapt its mechanical features in order to survive for instance; in response to swelling and shrinkage without rupturing, and carry out functions which require altered morphology for instance; extravasation from blood and lymphatic vessels . These morphological alterations also result in changes to the cells phenotype and inflammatory responses [529]. In DCs and T-cells, communication via mechanical cues plays a crucial role in T-cell activation. For instance DC experience cell cortex stiffening during maturation and increased stiffness coincides with less antigen required to prime T-cells [568]. During antigen presentation, T-cells place a certain amount of force back on the APCs via the TCR-MHC bond, generated by the

formation of T-cell protrusions, microvilli and ruffling. Theoretical work carried out by Marco Fritzsche and Karsten Kruse have proposed the idea of kinetic proof-reading. This theorises that T-cells can sense force imposed on their TCR which provides a method for T-cell to discriminate between self- and non-self-antigens. This force is directly linked to the level of phosphorylation events at the intracellular portion of the TCR, which activates signalling events resulting in T-cell activation and phenotypic commitment [569].

During the culture of DCs with PLGA particles in the 0.5-2 μm range, it was observed that DCs became smaller and more granular, in a manner similar to that seen in BMDMs (Figure 3.6.2). Again, this was only observed in BMDCs treated with particles within the specific 0.5-2 μm size, with larger or smaller PLGA particles having no significant effect on the BMDCs morphology. It was, therefore, hypothesised that PLGA particles in this size apply some form of mechanical force or stress on the cell, promoting a shift its physical attributes. Based on previous work, it was also hypothesised that these mechanical cues are effected prior to the initiation of phagocytosis, during the early cell-particle interaction. As previously mentioned, the size range between 0.5-2 μm tend to be phagocytosed with relative ease [400,399], and we have observed internalised particles in BMDMs after 30 mins. However, Dr McCluskey demonstrated that upregulated IL-10 from BMDCs treated with 0.5 μm PLGA particles, was not inhibited when actin polymerisation was blocked [501]. This demonstrates that phagocytosis is not crucial to downstream signalling. However, when cholesterol was depleted using MβCD, which removes the ability of the cell membrane to stiffen or form lipid rafts, the secretion of IL-10 was inhibited. Changes to membrane stiffness, therefore, seems to be the critical step in generating downstream signalling. In fact, changes to the cell membrane were recorded within 30 minutes of exposure to 1 μm PLGA particles by FRAP analysis. This increase in membrane rigidity was similar to BMDCs treated with hyper-osmolar media.

Delving further into how particles alter membrane fluidity, Dr McCluskey previously found that 0.5 μm PLGA particles promoted lipid raft formation, which not only impacts of membrane rigidity but can alter the spatiotemporal arrangements of surface bound receptors such as GCPRs, calcium channels and integrins. In fact, sequestration of receptors into lipid rafts, can initiate downstream signalling events such as PI3K and Src/MEK/ERK signalling [532]. For instance, integrins can undergo

both inside-out and out-side in activation in response to sequestration into lipid rafts promoting the activation of signalling via pathways such as PI3K/ERK. Interestingly Dr McCluskey demonstrated that IL-10 secretion from BMDCs treated with 0.5-2 μm PLGA particles was modulated by Syk/p38, and partially through PI3K/ERK pathway. The exact receptor promoting downstream signalling was not identified, however, it was proposed to be regulated by the formation of lipid raft in response to mechanical stress imposed by particles in this size range. It is possible, therefore, that a surface bound protein, such as an integrin, could act as the mechano-receptor, sensing changes to the cell membrane rigidity and in response, initiating downstream PI3K/ERK signalling required for anti-inflammatory cytokine production.

In chapter 3, the role of the mechanoreceptive αvβ3 integrin in promoting anti-inflammatory responses from BMDMs was identified. It was, therefore, explored for its involvement the induction of tolerogenic immune responses from BMDCs treated with 2 μm PLGA particles. Interestingly, gene and surface expression of both αv and β3 dimers was significantly enhanced on BMDCs which were treated with 2 μm PLGA particles. One of the main immunomodulatory roles of αv containing integrins, such as αvβ3, is in the activation of TGFβ [107]. This is due to their strong affinity for RGD motifs, a motif which is found on the LAP of inactive TGFβ complex [537, 231]. Binding of integrins to this motif, mechanically alters the conformation of LAP, facilitating the release of bioactive TGFβ [570]. Having previously identified that 2 μm PLGA particles amplify signalling via the TGFβ axis, the role of the upregulated αvβ3 in modulating the TGFβ signalling was assessed. αvβ3 was inhibited in BMDCs using the chemical inhibitor Cilengitide prior to treatment with PLGA particles. Whilst the gene expression of *tgfb1* was unaffected when αvβ3 was inhibited, the capacity of 2 μm PLGA particles to enhance pSmad2/3 signalling was eliminated. Taken together, these results could indicate a dual role for αvβ3, acting as both a mechano-sensor responding to the mechanical alterations to the cell membrane caused by 0.5-2 μm PLGA particles and in the regulation of TGFβ activation.

The mechanism by which αvβ3 enhances TGFβ activation, could explain the propensity of 2 μm PLGA particle-treated BMDCs to prime T-regs. As previously

discussed, TGFβ plays a fundamental role in polarising T-cell activation towards T-regs, therefore, neutralising TGFβ during co-culture between BMDCs and T-cells was tested to investigate this hypothesis. Preliminary results indicate a reduction in proliferating OVA-specific FoxP3^{+} T-regs when TGFβ derived from BMDCs treated with 2 μm PLGA particles was inhibited. Whilst there is no novelty in demonstrating that blocking TGFβ would reduce T-reg expansion, the capacity of 2 μm PLGA particles to promote the enhancement in sufficient TGFβ to enable T-reg polarisation has not previously been demonstrated. Indeed, this could be a novel approach, to enhance TGFβ secretion from BMDCs and the expansion of T-regs without using immunosuppressive drugs or bioactive components.

Next we investigated if αvβ3 is critical for priming T-regs. A co-culture was carried out using a neutralising antibody specific to the β3 integrin portion to block αvβ3 on BMDCs . When αvβ3 was blocked, the number of proliferating FoxP3^{+} T-regs declined appreciably. Additionally, i.p injection of β3 nAb 24 hours prior to i.m vaccination with OVA and PLGA particles prevented the induction of OVA-specific T-regs, with a significant decrease in the numbers of OVA-specific T-reg populations positive for CD25, FoxP3 and Helios. These compelling results, demonstrate a role for αvβ3 in generating antigen-specific tolerance by 2 μm PLGA particles. In contrast to the effect on T-regs, i.p injection with β3 nAb, did not alter the capacity of vaccination with particles and OVA to promote antigen-specific IgG antibodies.

The significance of understanding the role of PLGA particle size on immune responses is two-fold. For one, this provides further evidence to demonstrate how imperative it is to study the effects of physico-chemical properties of commonly used biomaterials. Research needs to be carried out to identify the optimal properties to promote desirable immune responses to take full advantage of biomaterials for medical purposes. This is especially relevant in the use of particles as drug delivery vehicles which are becoming more popular for the delivery of immuno-regulatory cargo. On the other hand, the work provides a new perspective, demonstrating how PLGA particles could, themselves, drive robust immune responses which could be used to design new immunomodulatory therapies and vaccines. Current approaches to overcoming the pathology brought about by auto-immunity focuses heavily on non-specific immune suppression to lessen the

inflammation and tissue damage brought about by auto-reactive T-eff cells. As a consequence, there is a significant risk of global immunosuppression and unnecessary adverse effects. Next generation therapies must, therefore, provide a level of specificity to mitigate auto-reactive T-cells whilst allowing the immune system to retain the capacity to fight infection, for instance through the development of specific vaccines to combat auto-reactive T-cells.

The work presented here proposes that PLGA particles, specifically in the 0.5-2 μm range, could function as anti-inflammatory adjuvants to expand antigen-specific T-regs. The enhanced production of IL-10 and TGFβ is thought to promote activation of tolDCs, which in turn promote T-reg priming. The mechanism by which PLGA particles in this size range were able to promote these responses was found to be modulated by the mechanical stress imposed on the cell membrane in the early particle-cell interaction. The current hypothesis is that this mechanical stimulus modulates the upregulation of activated αvβ3, which enhances the kinetics of TGFβ activation and promotes the priming of T-regs. Together these findings are encouraging for the use of 1-2 μm particles as novel anti-inflammatory adjuvants.

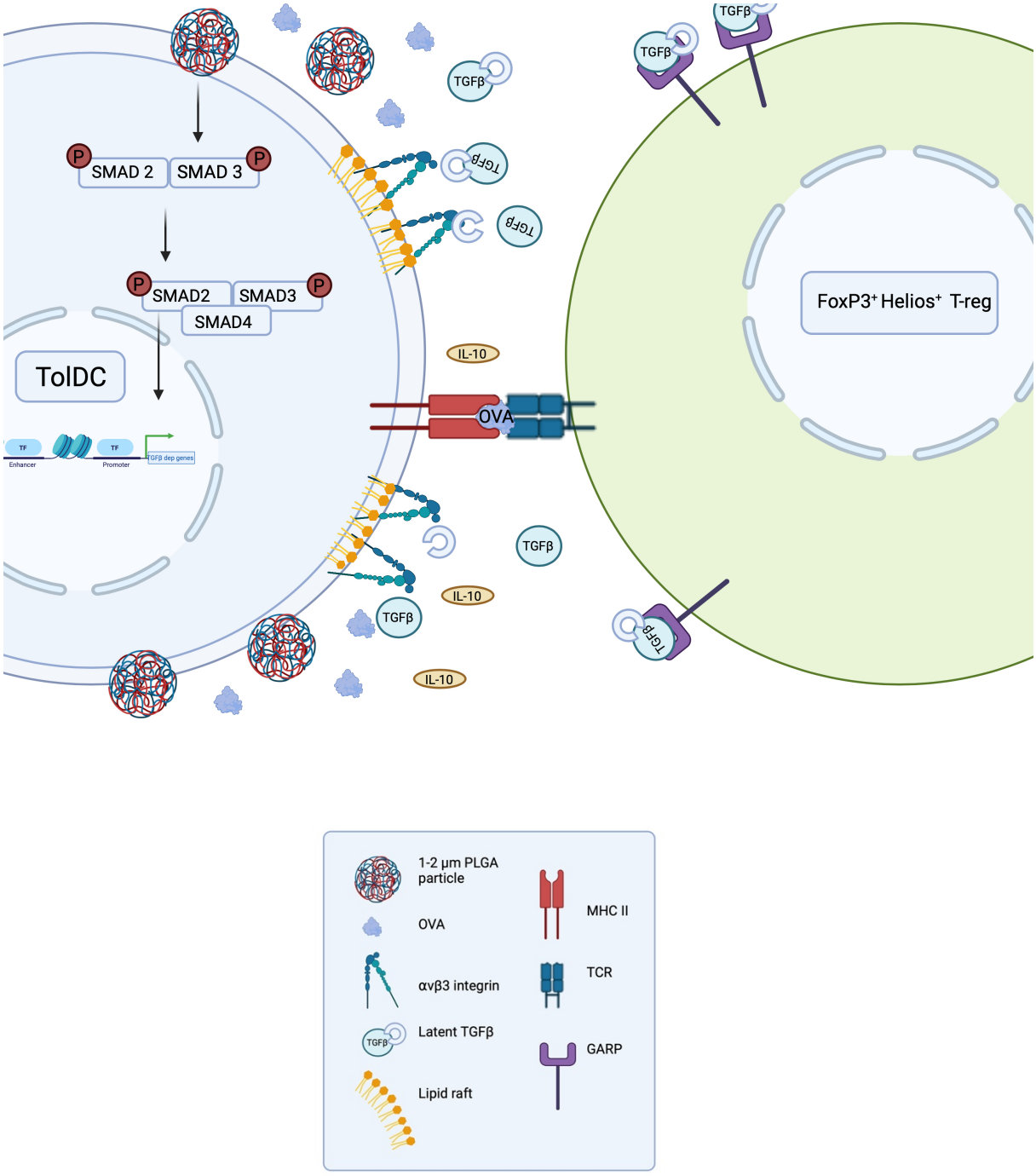

Figure 4.10.1 Proposed mechanism of 2 µm PLGA particle induced T-reg expansion. PLGA particles in the 1-2 µm size range interact with the cell membrane of BMDCs, inducing mechanical stress and formation of lipid rafts. This is translated to downstream biochemical signalling which results in increased αvβ3 surface expression as well as TGFβ and IL-10 secretion. Due to the enhanced activation of αvβ3, there is increased activation of latent TGFβ. DCs are therefore able to provide co-stimulatory signals to naïve $CD4^+$ cells which prime an OVA-specific T-reg population.

Chapter 5 - General Discussion

5.1 General discussion

The findings of this research highlight the critical role of PLGA particle size in modulating innate immune responses and by default, adaptive immune responses. In particular this work highlights in the capacity of 0.5-2 μm particles to promote anti-inflammatory responses which could be harnessed to treat chronic inflammation and auto-immunity. Whilst PLGA has been widely used in drug delivery and for other biomedical applications, the present study emphasizes that particle size is not merely a structural variable but a functional determinant in shaping immune outcomes. This underscores the importance of tailoring particle size to achieve specific therapeutic goals in immune modulation.

The seminal discovery of PAMPs, DAMPs and PRRs by Charles Janeway and Polly Matzinger revolutionised the field of immunology and has led to a significant growth in our understanding of how immune cells are able to respond to pathogens[139, 7]. Indeed, this is one of the key features providing innate immune cells with the capacity to differentiate between self and non-self and mount appropriate immune responses to a given insult. Over the last decade, a novel immune-cell sensing mechanism has been identified and has created an overlap in the field of immunology and mechano-biology. It has become increasingly clear than immune cells are sensitive to mechanical stimuli, which allows the cell to "feel" their surroundings as well as physical features of pathogenic and foreign targets. Mechano-sensitive channels were first described in skeletal muscle of chick embryos by Falguni Guharay and Frederick Sachs in 1984 [571]. This has since, led to the identification of the role of calcium-gated mechanoreceptors; Piezo1 and TRPV4 , adhesion molecules; cadherins and integrins, as well as the cell membrane and cytoskeleton in translating mechanical signals to downstream biochemical signals [572, 179, 228]. This mechano-transduction has been linked to changes in gene expression and epigenetic modifications which in turn alter immune cell phenotypes. The myriad of immune sensing mechanisms allows cells to integrate a number of signals in order to mount a highly specialised response. Indeed, this is likely what gives rise to the extensive phenotypic heterogeneity within immune cell subtypes.

The Lavelle lab has been interested in understanding the role of particle physico-chemical properties on immune responses, which can be used for the rational design of vaccine adjuvants [421]. Particulates and nano/micro particles have been

highly regarded as vaccine adjuvants and drug delivery vehicles. In particular, particle size has been shown to be a fundamental in influencing innate immune responses. For instance, work in the lab has recognised the capacity for 50-60 nm PLGA particles to enhance $CD8^+$ cytotoxic immune responses [414]. The work presented here, however, describes how particles can promote responses on the other end of the spectrum, with larger 0.5-2 μm PLGA particles, steering innate immune cells to take on an anti-inflammatory and pro-tolerance phenotype. Examining the effect of a range of PLGA particles on responses from BMDMs and BMDCs demonstrated that particles within this specific size window amplified IL-10 from both cell types, IL-1Ra from macrophages and TGFβ from DCs in response to LPS. Interestingly, 0.5-2 μm particles were also able to enhance IL-1Ra and TGFβ from respective cell types, in the absence of a TLR agonist. Examining the propensity of particles over this size range to amplify pro-inflammatory IL-6 and TNFα, exhibited no effect on either cell type when cultured without a TLR agonist and with LPS. Cumulatively this provides strong evidence of a mechanism by which particles can sense particle size, and respond to this size range in an anti-inflammatory manner.

Both macrophages and DCs are key innate immune cells which detect and respond to infection, injury and activate the adaptive immune response. Whilst they are crucial modulators of effector functions against pathogens and the generation of immunity, they are also implicated in the development of dysfunctional inflammation which underlies various pathologies [1]. Macrophages are one of the first responders to a site of inflammation and are key effector cells carrying out phagocytosis of pathogens and debris, recruiting additional immune cell types via secretion of cytokines and chemokines and production of bactericidal ROS and degradative enzymes [20]. This arsenal of defence mechanisms are non-specific and abrasive, and if left unresolved can result in a positive feedback loop inciting chronic inflammation [573]. Chronic inflammation promotes tissue damage which underpins various diseases which can affect every tissue type, and can even result in whole organ failure [343, 485, 341]. Whilst a variety of immunosuppressive drugs are routinely used to mitigate the damage caused by inflammation, this interferes with the body's ability to defend itself from infection. Therefore, there is a need to identify novel methods to mitigate inflammation without shutting down the entire immune system.

The benefit of targeting macrophages lies in their plasticity [10,343]. Here we propose that PLGA particles in this anti-inflammatory size range could be applied to direct macrophage polarisation towards a pro-resolving anti-inflammatory phenotype based on the capacity of particles in the size range to promote IL-10 and IL-1Ra secretion from BMDMs. IL-10 and IL-1Ra are both immunosuppressive cytokines which interfere with the effector function of activated, macrophages, dendritic cells, T-eff cells and NK cells. IL-10 can also act on naïve T-cells and macrophages promoting activation towards tolerogenic phenotypes, inciting a pro-resolution feedback loop [325] . The capacity of IL-1Ra to modulate inflammation has been highly regarded, and the recombinant form of IL-1Ra, Anakinra, has been used extensively as a treatment in chronic inflammatory diseases such as RA and CAPs [495, 515]. Instead of acting on cells through a cytokine receptor and inducing downstream signalling, IL-1Ra antagonises IL-1 signalling, putting the brakes on the propagation of inflammation [367].

The anti-inflammatory phenotype of BMDMs induced by PLGA particles in the 0.5-2 μm size range was also further ascertained by examining their metabolic phenotype. In order for macrophages to carry out effector functions such as cytokine production, they undergo metabolic re-programming during activation. Anti-inflammatory macrophages utilise OxPhos as their main source of energy [299, 312]. When the rates of OxPhos and glycolysis were compared to macrophages polarised towards a pro-inflammatory or anti-inflammatory phenotype, BMDMs treated with 1 μm particles exhibited a metabolism akin to the anti-inflammatory BMDMs.

Metabolic re-programming of innate immune cells has also been implicated as a crucial feature required in establishing innate immune memory [55, 574, 54]. The idea that innate immune cells carry out effector functions and then perish, without providing the host with any long term memory has been overturned by Mihai Neeta's influential work [502]. It was demonstrated that the innate immune system can retain a form of immune memory to a primary insult, re-programming the cell to amplify a given response upon re-stimulation with a secondary unrelated stimulus. Innate immune memory can pre-dispose the host to heightened inflammation when faced with a new threat, which in many cases has been shown to have a protective role against new infections [575, 576, 43, 40]. Recently, non-microbial particulates such as pristine graphene (pGr) have been demonstrated to

promote innate immune training in macrophages. What was striking, was that pGr did not invoke any inflammatory response acutely, but upon re-stimulation seven day later macrophages promoted significantly greater levels of IL-6 and TNFα compared to untrained BMDMs [62, 60]. This raises concerns about the role biomaterial particulates could have in promoting immune training and the long term repercussions this could have in driving inflammatory pathologies [577, 60]. The implication of innate immune training on the long-term responses of BMDMs treated with PLGA particles in the "anti-inflammatory" range was, therefore, examined. Remarkably, BMDMs which were trained with 0.5-2 μm PLGA particles amplified the production of IL-1Ra and IL-10 compared to untrained BMDMs when re-stimulated with a variety of TLR agonists. In addition, these BMDMs did not amplify IL-6 or TNFα. The metabolic phenotype of 1 μm particle-trained BMDMs was also altered, but did not possess the same attributes as conventionally activated β-glucan BMDMs. Whilst β-glucan re-programmed cells to maintain heightened levels of both glycolysis and OxPhos compared to untrained BMDMs, 1 μm particles retained heighted OxPhos and moderate level of glycolysis.

These results supplemented the body of work demonstrating the immuno-regulatory role of particles in this size range. What's more, these results indicate an alternative form of innate immune training, which differs from the conventional phenotype of immune memory [41, 577, 578]. Immune training is generally understood to either enhance inflammatory immune responses or suppress them through tolerization. However, the concept of innate immune training that promotes anti-inflammatory responses has received less attention. Identifying factors capable of inducing such anti-inflammatory training presents a promising strategy for managing chronic inflammation. Notably, anti-inflammatory immune training has been observed in response to certain helminth-derived products. Quinn et al. demonstrated that *Fasciola hepatica* total extract (FHTE) can reprogram macrophages to adopt an anti-inflammatory phenotype, characterized by increased production of IL-10 and IL-1Ra, alongside reduced levels of TNFα and IL-12p40 following TLR agonist restimulation. Additionally, pre-treatment with FHTE significantly reduced the clinical severity of experimental autoimmune EAE in mice and suppressed MOG-reactive Th17 cells [579]. The potential of PLGA particles within the 0.5–2 μm range to promote anti-inflammatory immune training

by increasing IL-10 and IL-1Ra could, therefore, be investigated as a strategy to mitigate autoreactive T-cells in autoimmune models. Furthermore, these results underscore the ability of non-microbial components to induce anti-inflammatory innate immune training based on physico-chemical properties.

The cumulative evidence that PLGA particles in this size range can promote anti-inflammatory responses acutely and invoke anti-inflammatory memory is compelling and demonstrates how particles could prove advantageous on their own, or in conjunction with immunosuppressive drugs. Indeed, particles also offer the added benefit of offering a method to encapsulate anti-inflammatory drugs or bioactive components, increasing their safety, tolerability, tissue targeting and stability of the cargo [439, 381, 580, 498].

DCs, like macrophages are phagocytic cells and play a part in modulating local inflammatory responses, however, they are renowned for their role in directing the activation of the adaptive immunity. As such, vaccines and various other immunotherapies have been designed to target DCs to promote the differentiation of T-eff cells which can provide protection from bacterial, fungal and parasitic pathogens, cytotoxic T-cells which are highly specialised to protect from viruses and cancer, or T-regs which promote tolerance towards a specific antigen [1]. BMDCs which were incubated with 0.5 -2 μm PLGA particles exhibited increased IL-10 and TGFβ which are commonly produced by tolerogenic DCs. The production of these cytokines, preferentially direct the activation of antigen-specific T-regs during antigen presentation. When BMDCs treated with 2 μm PLGA particles and OVA were cultured with naïve $CD4^+$ cells, they were able to significantly expand OVA-specific $FoxP3^+$ T-regs populations. Furthermore, when C57BL/6 mice were vaccinated intra-muscularly with 2 μm PLGA particles and OVA, there was a significant enhancement in splenic OVA-specific $FoxP3^+$ and $Helios^+$ T-regs.

It was hypothesised that the capacity of BMDCs to activate T-regs was most likely attributed to the enhancement in the TGFβ signalling axis. In addition to the enhanced expression of *tgfb1*, signalling via the smad2/3 dependent canonical TGFβ pathway was examined. Culturing BMDCs with 1 μm PLGA particles enhanced the phosphorylation of key signalling molecules smad2/3 indicating an increase in the ligation of active TGFβ to its receptor. This suggested a mechanism by which particles of this size range could amplify the production and activation of TGFβ from BMDCs. This hypothesis was supported by the significant drop in the

capacity of BMDCs to expand T-regs when TGFβ signalling between BMDCs and naïve $CD4^+$ cells was blocked during co-culture.

T-regs are crucial for the establishment of peripheral tolerance and to mitigate the damage perpetuated in the event of auto-immunity. Therefore, there has been a focus on developing novel methods to enhance T-regs as a means to treat auto-immunity. Current therapeutic options remain sub-par due to their non-specific suppression of the immune system as a whole, therefore the specificity of T-regs offers an advantage to selectively blocking a subset of antigen-specific T-eff cells. An "inverse vaccine" model has been proposed as an approach to generating tolerance by expanding antigen specific T-regs [462, 448, 450, 444]. Inverse vaccines would provide DCs with a disease specific antigen, which can either itself promote the features of tolerogenic antigen presentation, or contain an anti-inflammatory pro-tolerance adjuvant to direct the polarisation of DCs towards tolDCs. This is one of the major challenges faced in designing safe and efficacious inverse vaccines. In fact, delivering a disease specific antigen in the absence of tolerogenic stimuli can result in the generation of auto-reactive T-eff cells which could pose a significant risk. The work presented here examining the capacity PLGA particles to promote tolerogenic DC responses and direct the expansion of T-regs provides encouraging evidence to implicate 0.5-2 μm particles are potential adjuvants for inverse vaccines. The *in-vivo* expansion of OVA-specific $FoxP3^+$ and $Helios^+$ cells provides a good basis for future work to explore its therapeutic or prophylactic capacity in a disease model such as murine EAE or T1D.

These compelling results indicate a highly beneficial role of incorporating 0.5-2 μm PLGA particles in the treatment of inflammatory diseases. However, to garner confidence, their mechanism of action (MoA) needs to be understood. Understanding the MoA can help identify potential side effects of a novel therapeutic modality and contribute to the rational design of future therapies [421].

Due to the size-dependency of the anti-inflammatory effects of PLGA particles, it was hypothesised that mechano-sensing was likely attributed to the activation of innate immune cells. This is supported by the fact that previous work has identified a size dependent capacity of polystyrene particles in the same 0.5-2 μm size range to enhance the secretion of IL-10 from BMDCs [501]. What's more, during the culture of BMDMs and BMDCs with PLGA particles, the morphology of cells incubated

with 0.5-2 μm size range was remarkably different to cells cultured with TLR agonists or particles outside of the 0.5-2 μm size range. In fact, their morphology is comparable to cells incubated in hypo-osmolar media, demonstrating a significant decrease in size and increase in granularity. These changes in cell size and shape implied significant actin re-arrangement as well as likely modifications to the structure of the cell membrane. This was confirmed by FRAP analysis to assess changes to membrane fluidity of BMDMs and BMDCs cultured with 1-2 μm PLGA particles which demonstrated a significant decrease to membrane fluidity, likely due to the increased compactness of the phospholipid bilayer. It is also reasonable to hypothesise, that the changes to the cell membrane are likely to play a role in the activation of a potential mechanosensors, either directly as a result of the compression of the cell membrane, or through the formation of lipid rafts.

As previously mentioned, cells are highly attuned to mechanical stimuli, and various mechano-sensors have been identified to play a role in modulating innate immune cell functions [188, 581, 170]. In fact, it is probable that innate immune cells evolved to utilise mechano-sensors to supplement PRR in gaining the information required to respond and contain pathogens appropriately. The anti-inflammatory responses elicited by both macrophages and dendritic cells to particles in this size range could also contribute to how some pathogens evade the immune system.

Various mechanosensors were investigated to identify potential mechanosensors involved in modulating size dependent anti-inflammatory responses. The αvβ3 integrin was found to be significantly upregulated specifically on the surface of BMDMs and BMDCs cultured with 0.5- 2 μm PLGA particles. Integrins, which were once considered to merely provide cell-cell and cell-ECM adhesion, have gained recognition for modulating immune cell signalling, most notably for their involvement in activating TGFβ [540]. Indeed, when the αvβ3 signalling was blocked, 2 μm particle + OVA treated BMDCs were no longer able to expand FoxP3 T-regs in the co-culture model. Moreover, when the nAb against β3 was injected into mice intraperitoneally a day prior to intra-muscular vaccination with 2 μm PLGA particles and OVA, the expansion of OVA-specific $FoxP3^+$ and $Helios^+$ T-regs was abrogated.

In light of the capacity of αvβ3 to activate TGFβ and 2 μm PLGA particles to promote *tgfb1* expression from BMDCs, the involvement of the integrin in activating

the TGFβ produced by BMDCs was hypothesised, contributing to the expansion of OVA specific T-regs during antigen presentation. This hypothesis was supported by the reduction in TGFβ signalling via Smad2/3 when αvβ3 was blocked in BMDCs cultured with 2 μm PLGA particles. How exactly 2 μm PLGA particles promoted heightened expression of *tgfb1* and the increased surface expression of αvβ3 is yet to be answered. However, prior work by Dr McCluskey provides hints to some signalling events which could be involved.

Firstly, it was found that PLGA particles in the 0.5-2 μm size range interact with the cell membrane of BMDCs for a period of time prior to phagocytosis and in this time promote lipid raft formation. The formation of lipid rafts was also demonstrated to activate Syk and subsequently, MAPKs; p38, ERK and PI3K which go on to activate transcription factors such as CREB. The formation of lipid rafts has previously been described to sequester integrins into the rafts, and in doing so promote inside-out integrin activation and downstream signalling via PI3K and Src/MEK/ERK [532]. Based on these separate findings, we propose that the early interaction between 0.5- 2 μm PLGA particles with the cell membrane places mechanical stress on the membrane, causing cell shrinkage, lipid raft assembly and increased membrane rigidity. The formation of lipid rafts sequesters αvβ3 and mechanically forces its activation, which causes downstream MAPK signalling events which result in upregulation in the gene expression of anti-inflammatory cytokines. When TGFβ is then secreted in its latent form, it interacts with activated αvβ3, providing a means to mechanically activate TGFβ. Moreover, TGFβ signalling has been shown to promote the upregulation in the expression of αv containing integrins via the c-syk and p38 MAPK signalling pathway. This provides a positive feedback loop, whereby increased TGFβ can promote an increase in its own activation [582], [583], [584].

A schematic representation of this proposed mechanism is presented in Figure 5.1.A. Future work would need to be carried out in order to demonstrate the link between lipid rafts and integrin activation, as well as the downstream signalling via MAPKs which could be responsible for the increased expression of TGFβ and subsequently αvβ3.

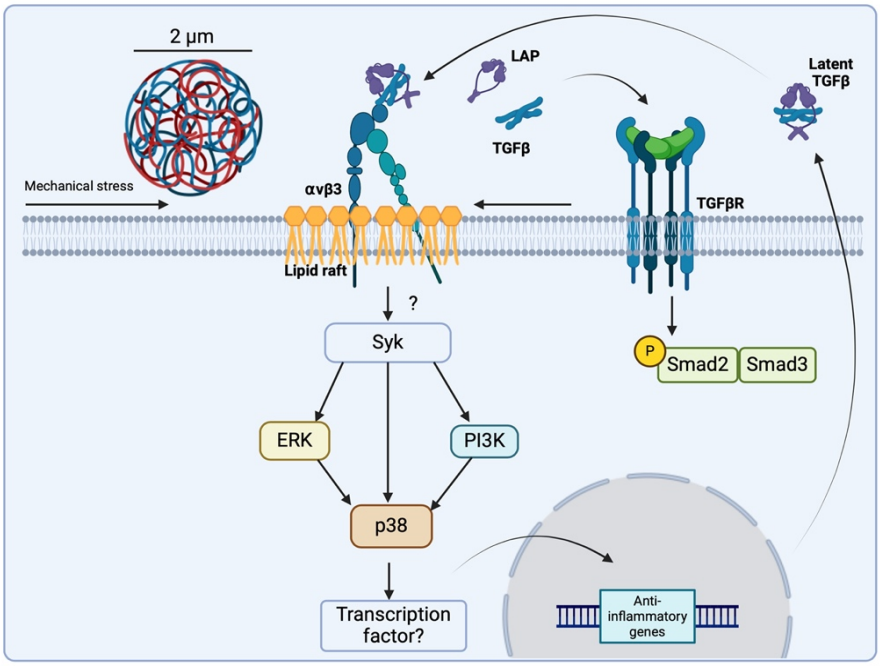

Figure 5.1.A Hypothesised schematic representation of potential mechanism of action for the enhancement of TGFβ expression and signalling from BMDCs by 2 µm PLGA particles. Early interaction between 2 µm PLGA particles and the BMDC cell membrane causes mechanical stress, which alters the cell morphology and promotes lipid raft formation. αvβ3 integrins are sequestered into lipid rafts and mechanically activated. Activated αvβ3 creates a platform for downstream signalling events via Syk and MAPKs (ERK, PI3K and p38) which activate transcription factors involved in the expression of *tgfb1* gene. Secreted latent TGFβ can then be released from the LAP complex by αvβ3 on the cell surface releasing active TGFβ which can bind the TGFβR. This initiates downstream Smad2/3 and MAPK signalling promoting the expression of TGFβ dependent genes and potentially αvβ3.

Another downstream signalling pathway which was identified to play a role in anti-inflammatory responses to 2 µm PLGA particles was mTOR. The secretion of IL-1Ra from BMDMs treated with PLGA particles in the 0.5-2 µm size range was found to inhibited when BMDMs were pretreated with the selective mTORC1 inhibitor; rapamycin. In fact, blocking mTORC1 also prevented innate immune training and the re-programmed metabolic phenotype of BMDMs. Given the mTORC1 signalling pathway has a broad regulatory role in nutrient sensing and various metabolic pathways, this is not surprising [281, 585]. However, how mTORC1 is activated by particles in this size range has not yet been identified. The capacity of lipid rafts to activate MAPK signalling could, however, provide a potential insight into the mechanical activation of mTOR. Activated ERK and PI3K signalling molecules are able to inhibit the function of Tsc, which maintains mTOR in its

inactive form. As such, it is plausible that the activation of MAPK signalling by lipid raft formation, or even αvβ3 activation, could inhibit the function of Tsc, resulting in signalling downstream of mTORC1. Again, future work would need to be carried out to substantiate a link between changes in the dynamic of the cell membrane or αvβ3 with the activation of mTOR.

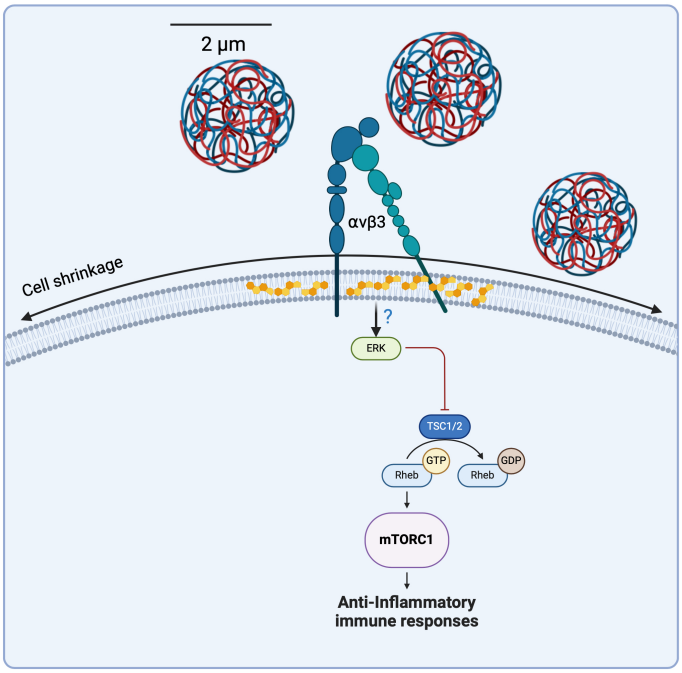

Figure 5.1 B. Hypothesised schematic representation of potential mechanism of action linking mechanical stress imposed by 0.5-2 µm PLGA particles on cell membrane and mTOR activation. Mechanical stress imposed on the cell membrane by 0.5-2 µm PLGA particles promotes the assembly of lipid rafts which activates downstream MAPKs such as ERK. ERK inhibits is then able to inhibit Tsc, preventing the de-phosphorylation of RhebGTP, which can go on to activate mTOR.

Cumulatively the work presented here provides evidence to support the use of PLGA particles in the 0.5 -2 µm range to promote anti-inflammatory immune responses. This could be applied to overcome non-specific inflammation perpetuated by macrophages during chronic inflammation, or promote tolDCs which are able prime a tolerogenic adaptive immune response via the expansion of antigen-specific T-regs. In particular, the induction of antigen-specific T-regs by PLGA particles in the 0.5-2 µm size presents desirable adjuvant properties to formulate novel inverse vaccines against auto-immune conditions. How macrophages and DCs respond differentially to particles based on their size was

explored and the involvement of the mechano-sensory αvβ3 in regulating downstream signalling resulting in enhanced IL-1Ra and TGFβ was discovered. In fact, αvβ3 was found to be indispensable for the expansion of T-regs by BMDCs treated with particles in this size range, through its contribution to the activation of the pro-tolerance inducer TGFβ. This implicates αvβ3 induction as a potential mechanism to promote tolerance in auto-immunity. The work which has been presented here draws a clear link between particle size and immune cell behaviour, which provides new insights into the design of particle-based therapies aimed at minimising inflammation while promoting tissue repair and regeneration.

5.2 Future work

- Testing the efficacy of PLGA particles in the 0.5-2 μm size range as an adjuvant in a therapeutic vaccine in a murine auto-immune disease model will be carried out to ascertain its capacity of promote disease modifying T-regs. The EAE model would present an attractive approach, whereby MOG and 2 μm PLGA particles could be injected into diseased mice to measure the improvement in disease severity and production of MOG-specific T-regs. An alternative model would be the non-obese diabetic (NOD) mouse model, which develops spontaneous T1D. Vaccination of 2 μm PLGA particles with insulin or pro-insulin peptide would be used to measure any decrease in β-cell damage or improvements in blood glucose levels. The generation of antigen-specific T-regs would also be measured.
- A prophylactic model could also be carried out to investigate if 0.5-2 μm PLGA particles can induce tolerance to an antigen prior to disease onset. This would involve the injection of antigen + particles prior to the onset of disease and comparing the development of disease to unvaccinated cohort, in either the EAE model or NOD-mice over time.

- Access the signalling pathways involved in the upregulated expression of TGFβ. MAPK/p38 and mTOR signalling pathways will be explored using specific inhibitors of key signalling molecules and measuring the expression of TGFβ. Additionally western blot analysis or Flow cytometry could be used to detect the phosphorylation of MAPK signalling proteins; ERK, PI3K and p38, and downstream mTOR signalling proteins; 4EBP1 and S6K1 in response to 0.5-2 μm PLGA particles.

- The mechanism of action by which PLGA particles in the anti-inflammatory size enhance the surface expression and activation of $\alpha v\beta 3$ will need to be delineated. The positive feedback between TGFβ signalling and $\alpha v\beta 3$ will also be explored.

- Address if αvβ3 gets sequestered into lipid rafts. This could be assessed by live high resolution confocal microscopy imaging of cells with fluorescent antibody against αvβ3 and lipid rafts to measure co-localisation.

- Finally, assess if particles of different compositions within the same size range can drive pro-tolerance and anti-inflammatory immune responses through αvβ3. This would further substantiate the the size-dependent mechanical MoA theory.

Bibliography

1. Janeway, C. A.Travers,P. Walport, M. *Immunobiology: The immune system in health and Disease*. (Garland Science, 2001).
2. Carpenter, S. & O'Neill, L. A. J. From periphery to center stage: 50 years of advancements in innate immunity. *Cell* **187**, 2030–2051 (2024).
3. Niethammer, P. The Early Wound Signals. *Curr. Opin. Genet. Dev.* **40**, 17 (2016).
4. Marin, V. *et al.* The IL-6-Soluble IL-6Rα Autocrine Loop of Endothelial Activation as an Intermediate Between Acute and Chronic Inflammation: an Experimental Model Involving Thrombin. *J. Immunol.* **167**, 3435–3442 (2001).
5. Chen, G. Y. & Nuñez, G. Sterile inflammation: sensing and reacting to damage. *Nat. Publ. Gr.* (2010) doi:10.1038/nri2873.
6. Kim, W. J., Gittes, G. K. & Longaker, M. T. Signal transduction in wound pharmacology. *Arch. Pharm. Res.* **21**, 487–95 (1998).
7. Matzinger, P. Tolerance, danger, and the extended family. *Annual Review of Immunology* vol. 12 991–1045 (1994).
8. Amarante-Mendes, G. P. *et al.* Pattern recognition receptors and the host cell death molecular machinery. *Frontiers in Immunology* vol. 9 2379 (2018).
9. Krzyszczyk, P., Schloss, R., Palmer, A. & Berthiaume, F. The role of macrophages in acute and chronic wound healing and interventions to promote pro-wound healing phenotypes. *Frontiers in Physiology* vol. 9 (2018).
10. Rodríguez-Morales, P. & Franklin, R. A. Macrophage phenotypes and functions: resolving inflammation and restoring homeostasis. *Trends Immunol.* **44**, 986–998 (2023).
11. Mellman, I. & Steinman, R. M. Dendritic cells: specialized and regulated antigen processing machines. *Cell* **106**, 255–258 (2001).
12. Park, M. D., Silvin, A., Ginhoux, F. & Merad, M. Macrophages in health and disease. *Cell* **185**, 4259 (2022).
13. Italiani, P. & Boraschi, D. From monocytes to M1/M2 macrophages: Phenotypical vs. functional differentiation. *Frontiers in Immunology* vol. 5 514 (2014).
14. Davies, L. C., Jenkins, S. J., Allen, J. E. & Taylor, P. R. Tissue-resident macrophages. *Nat. Immunol. 2013 1410* **14**, 986–995 (2013).
15. Akashi, K., Traver, D., Miyamoto, T. & Weissman, I. L. A clonogenic common myeloid progenitor that gives rise to all myeloid lineages. *Nat. 2000 4046774* **404**, 193–197 (2000).
16. Fogg, D. K. *et al.* A clonogenic bone harrow progenitor specific for macrophages and dendritic cells. *Science (80-.).* **311**, 83–87 (2006).
17. Sica, A., Erreni, M., Allavena, P. & Porta, C. Macrophage polarization in pathology. *Cellular and Molecular Life Sciences* vol. 72 4111–4126 (2015).
18. Mosser, D. M. & Edwards, J. P. Exploring the full spectrum of macrophage activation. *Nature Reviews Immunology* vol. 8 958–969 (2008).

19. Mills, C. D., Kincaid, K., Alt, J. M., Heilman, M. J. & Hill, A. M. M-1/M-2 Macrophages and the Th1/Th2 Paradigm. *J. Immunol.* **164**, 6166–6173 (2000).
20. Martinez, F. O., Sica, A., Mantovani, A. & Locati, M. Macrophage activation and polarization. *Frontiers in Bioscience* vol. 13 453–461 (2008).
21. Ye, Y., Gaugler, B., Mohty, M. & Malard, F. Plasmacytoid dendritic cell biology and its role in immune-mediated diseases. *Clin. Transl. Immunol.* **9**, (2020).
22. Kabashima, K. *et al.* Intrinsic lymphotoxin-β receptor requirement for homeostasis of lymphoid tissue dendritic cells. *Immunity* **22**, 439–450 (2005).
23. Manz, M. G. *et al.* Dendritic Cell Development from Common Myeloid Progenitors. *Ann. N. Y. Acad. Sci.* **938**, 167–174 (2001).
24. Geissmann, F. The origin of dendritic cells. *Nat. Immunol. 2007 86* **8**, 558–560 (2007).
25. Eisenbarth, S. C. Dendritic cell subsets in T cell programming: location dictates function. *Nat. Rev. Immunol. 2018 192* **19**, 89–103 (2018).
26. Merad, M., Sathe, P., Helft, J., Miller, J. & Mortha, A. The dendritic cell lineage: Ontogeny and function of dendritic cells and their subsets in the steady state and the inflamed setting. *Annu. Rev. Immunol.* **31**, 563–604 (2013).
27. Hilligan, K. L. & Ronchese, F. Antigen presentation by dendritic cells and their instruction of CD4+ T helper cell responses. *Cell. Mol. Immunol. 2020 176* **17**, 587–599 (2020).
28. Dalod, M., Chelbi, R., Malissen, B. & Lawrence, T. Dendritic cell maturation: functional specialization through signaling specificity and transcriptional programming. *EMBO J.* **33**, 1104 (2014).
29. Hewitt, E. W. The MHC class I antigen presentation pathway: strategies for viral immune evasion. *Immunology* **110**, 163 (2003).
30. Shin, J. Y., Wang, C. Y., Lin, C. C. & Chu, C. L. A recently described type 2 conventional dendritic cell (cDC2) subset mediates inflammation. *Cell. Mol. Immunol. 2020 1712* **17**, 1215–1217 (2020).
31. Schlitzer, A. *et al.* Identification of cDC1- and cDC2-committed DC progenitors reveals early lineage priming at the common DC progenitor stage in the bone marrow. *Nat. Immunol. 2015 167* **16**, 718–728 (2015).
32. Bourque, J. & Hawiger, D. Life and death of tolerogenic dendritic cells. *Trends Immunol.* **44**, 110 (2023).
33. Milutinović, B. & Kurtz, J. Immune memory in invertebrates. *Seminars in Immunology* vol. 28 328–342 (2016).
34. Kurtz, J. Specific memory within innate immune systems. *Trends Immunol.* **26**, 186–192 (2005).
35. Sherwood, E. R. *et al.* Innate Immune Memory and the Host Response to Infection. *J. Immunol.* **208**, 785–792 (2022).
36. Netea, M. G., Schlitzer, A., Placek, K., Joosten, L. A. B. & Schultze, J. L. Innate and Adaptive Immune Memory: an Evolutionary Continuum in the Host's Response to Pathogens. *Cell Host Microbe* **25**, 13–26 (2019).
37. Quintin, J. *et al.* Candida albicans infection affords protection against reinfection via functional reprogramming of monocytes. *Cell Host Microbe* **12**, 223–232 (2012).
38. Bistoni, F. *et al.* Immunomodulation by a low-virulence, agerminative

variant of candida albicans. Further evidence for macrophage activation as one of the effector mechanisms of nonspecific anti-infectious protection. *Med. Mycol.* **26**, 285–299 (1988).
39. Chan, L. C. *et al.* Protective immunity in recurrent Staphylococcus aureus infection reflects localized immune signatures and macrophage-conferred memory. *Proc. Natl. Acad. Sci. U. S. A.* **115**, E11111–E11119 (2018).
40. Nankabirwa, V. *et al.* Child survival and BCG vaccination: A community based prospective cohort study in Uganda. *BMC Public Health* **15**, 1–10 (2015).
41. Kaufmann, E. *et al.* BCG Educates Hematopoietic Stem Cells to Generate Protective Innate Immunity against Tuberculosis. *Cell* **172**, 176-190.e19 (2018).
42. Mitroulis, I. *et al.* Modulation of Myelopoiesis Progenitors Is an Integral Component of Trained Immunity. *Cell* **172**, 147-161.e12 (2018).
43. Cirovic, B. *et al.* BCG Vaccination in Humans Elicits Trained Immunity via the Hematopoietic Progenitor Compartment. *Cell Host Microbe* **28**, 322-334.e5 (2020).
44. Netea, M. G. *et al.* Trained immunity: A program of innate immune memory in health and disease. *Science* vol. 352 427 (2016).
45. Waddington, C. H. Genetic Assimilation of the Bithorax Phenotype. *Evolution (N. Y).* **10**, 1 (1956).
46. Jaenisch, R. & Bird, A. Epigenetic regulation of gene expression: How the genome integrates intrinsic and environmental signals. *Nat. Genet.* **33**, 245–254 (2003).
47. Bernstein, B. E., Meissner, A. & Lander, E. S. The Mammalian Epigenome. *Cell* **128**, 669–681 (2007).
48. Li, E. Chromatin modification and epigenetic reprogramming in mammalian development. *Nat. Rev. Genet.* **3**, 662–673 (2002).
49. Almouzni, G. & Cedar, H. Maintenance of epigenetic information. *Cold Spring Harb. Perspect. Biol.* **8**, 19372–19373 (2016).
50. Italiani, P., Della Camera, G. & Boraschi, D. Induction of Innate Immune Memory by Engineered Nanoparticles in Monocytes/Macrophages: From Hypothesis to Reality. *Front. Immunol.* **11**, 2324 (2020).
51. Penkov, S., Mitroulis, I., Hajishengallis, G. & Chavakis, T. Immunometabolic Crosstalk: An Ancestral Principle of Trained Immunity? *Trends in Immunology* vol. 40 1–11 (2019).
52. Donohoe, D. R. & Bultman, S. J. Metaboloepigenetics: Interrelationships between energy metabolism and epigenetic control of gene expression. *Journal of Cellular Physiology* vol. 227 3169–3177 (2012).
53. Fanucchi, S., Domínguez-Andrés, J., Joosten, L. A. B., Netea, M. G. & Mhlanga, M. M. The Intersection of Epigenetics and Metabolism in Trained Immunity. *Immunity* **54**, 32–43 (2021).
54. Arts, R. J. W. *et al.* Immunometabolic Pathways in BCG-Induced Trained Immunity. *Cell Rep.* **17**, 2562–2571 (2016).
55. Bekkering, S. *et al.* Metabolic Induction of Trained Immunity through the Mevalonate Pathway. *Cell* **172**, 135-146.e9 (2018).
56. Liu, P. S. *et al.* α-ketoglutarate orchestrates macrophage activation through metabolic and epigenetic reprogramming. *Nat. Immunol.* **18**, 985–994 (2017).
57. Ding, Y. *et al.* JMJD3: a critical epigenetic regulator in stem cell fate. *Cell*

Communication and Signaling vol. 19 1–9 (2021).
58. Mills, E. L. *et al.* Itaconate is an anti-inflammatory metabolite that activates Nrf2 via alkylation of KEAP1. *Nature* **556**, 113–117 (2018).
59. Domínguez-Andrés, J. *et al.* The Itaconate Pathway Is a Central Regulatory Node Linking Innate Immune Tolerance and Trained Immunity. *Cell Metab.* **29**, 211-220.e5 (2019).
60. Muñoz-Wolf, N. & Lavelle, E. C. Promotion of trained innate immunity by nanoparticles. *Semin. Immunol.* **56**, (2021).
61. Wegmann, M. Trained immunity in allergic asthma. (2023) doi:10.1016/j.jaci.2023.02.023.
62. Lebre, F. *et al.* Pristine graphene induces innate immune training. *Nanoscale* **12**, 11192–11200 (2020).
63. Gorman, A. L. Modulation of macrophage responses by the vaccine adjuvant alum. (TCD, 2020).
64. Alberts, B., Johnson, A. & Lewis, J. *Molecular Biology of the Cell 4th Edition*. (Garland Science, 2002).
65. Miller, J. D. *et al.* Human effector and memory CD8+ T cell responses to smallpox and yellow fever vaccines. *Immunity* **28**, 710–722 (2008).
66. H Gudmundsdottir, A. D. W. Dynamics and requirements of T cell clonal expansion in vivo at the single-cell level: effector function is linked to proliferative capacity. *J. Immunol. Sci.* **162**, 5212–23 (1999).
67. Kumar, B. V., Connors, T. J. & Farber, D. L. Human T cell development, localization, and function throughout life. *Immunity* **48**, 202 (2018).
68. Woodland, D. L. & Dutton, R. W. Heterogeneity of CD4+ and CD8+ T cells. *Curr. Opin. Immunol.* **15**, 336–342 (2003).
69. Koh, C. H., Lee, S., Kwak, M., Kim, B. S. & Chung, Y. CD8 T-cell subsets: heterogeneity, functions, and therapeutic potential. *Exp. Mol. Med. 2023 5511* **55**, 2287–2299 (2023).
70. Crotty, S. T follicular helper cell differentiation, function, and roles in disease. *Immunity* **41**, 529 (2014).
71. Shevyrev, D. & Tereshchenko, V. Treg Heterogeneity, Function, and Homeostasis. *Front. Immunol.* **10**, (2020).
72. Yu, X. *et al.* Reducing affinity as a strategy to boost immunomodulatory antibody agonism. *Nat. 2023 6147948* **614**, 539–547 (2023).
73. Rosser, E. C. & Mauri, C. Regulatory B cells: origin, phenotype, and function. *Immunity* **42**, 607–612 (2015).
74. Shen, P. & Fillatreau, S. Antibody-independent functions of B cells: a focus on cytokines. *Nat. Rev. Immunol.* **15**, 441–451 (2015).
75. Xing, Y. & Hogquist, K. A. T-Cell Tolerance: Central and Peripheral. *Cold Spring Harb. Perspect. Biol.* **4**, 1–15 (2012).
76. Owen, D. L., Sjaastad, L. E. & Farrar, M. A. Regulatory T Cell Development in the Thymus. *J. Immunol.* **203**, 2031–2041 (2019).
77. Hsieh, C. S., Lee, H. M. & Lio, C. W. J. Selection of regulatory T cells in the thymus. *Nat. Rev. Immunol. 2012 123* **12**, 157–167 (2012).
78. Romagnani, S. Immunological tolerance and autoimmunity. *Intern. Emerg. Med.* **1**, 187–196 (2006).
79. Labrecque, N., Baldwin, T. & Lesage, S. Molecular and genetic parameters defining T-cell clonal selection. *Immunol. Cell Biol.* **89**, 16–26 (2011).
80. Vojdani, A., Gushgari, L. R. & Vojdani, E. Interaction between food antigens and the immune system: Association with autoimmune disorders.

Autoimmun. Rev. **19**, (2020).
81. Sokolova, M. V., Schett, G. & Steffen, U. Autoantibodies in Rheumatoid Arthritis: Historical Background and Novel Findings. *Clin. Rev. Allergy Immunol.* **63**, 138 (2022).
82. Yamada, R., Suzuki, A., Chang, X. & Yamamoto, K. Citrullinated proteins in rheumatoid arthritis. *Front. Biosci.* **10**, 54–64 (2005).
83. Martins, Y. C., Jurberg, A. D. & Daniel-Ribeiro, C. T. Visiting Molecular Mimicry Once More: Pathogenicity, Virulence, and Autoimmunity. *Microorganisms* **11**, (2023).
84. Bhagavati, S. Autoimmune Disorders of the Nervous System: Pathophysiology, Clinical Features, and Therapy. *Front. Neurol.* **12**, 664664 (2021).
85. Romagnani, S. Immunological tolerance and autoimmunity. *Intern. Emerg. Med.* **1**, 187–196 (2006).
86. Brunkow, M. E. *et al.* Disruption of a new forkhead/winged-helix protein, scurfin, results in the fatal lymphoproliferative disorder of the scurfy mouse. *Nat. Genet. 2001 271* **27**, 68–73 (2001).
87. Hadaschik, E. N. *et al.* Regulatory T cell-deficient scurfy mice develop systemic autoimmune features resembling lupus-like disease. *Arthritis Res. Ther.* **17**, (2015).
88. Mahmud, S. A. *et al.* Costimulation via the tumor-necrosis factor receptor superfamily couples TCR signal strength to the thymic differentiation of regulatory T cells. *Nat. Immunol. 2014 155* **15**, 473–481 (2014).
89. Grover, P., Goel, P. N. & Greene, M. I. Regulatory T Cells: Regulation of Identity and Function. *Front. Immunol.* **12**, (2021).
90. Hori, S., Nomura, T. & Sakaguchi, S. Control of regulatory T cell development by the transcription factor Foxp3. *Science* **299**, 981–985 (2003).
91. Gootjes, C., Zwaginga, J. J., Roep, B. O. & Nikolic, T. Defining Human Regulatory T Cells beyond FOXP3: The Need to Combine Phenotype with Function. *Cells 2024, Vol. 13, Page 941* **13**, 941 (2024).
92. Zemmour, D. *et al.* Single-cell analysis of FOXP3 deficiencies in humans and mice unmasks intrinsic and extrinsic CD4+ T cell perturbations. *Nat. Immunol. 2021 225* **22**, 607–619 (2021).
93. Brun, V., Bastian, H., Neveu, V. & Foussat, A. Clinical grade production of IL-10 producing regulatory Tr1 lymphocytes for cell therapy of chronic inflammatory diseases. *Int. Immunopharmacol.* **9**, 609–613 (2009).
94. Passerini, L. *et al.* Functional type 1 regulatory T cells develop regardless of FOXP3 mutations in patients with IPEX syndrome. *Eur. J. Immunol.* **41**, 1120–1131 (2011).
95. Scurr, M. *et al.* Highly prevalent colorectal cancer-infiltrating LAP+ Foxp3− T cells exhibit more potent immunosuppressive activity than Foxp3+ regulatory T cells. *Mucosal Immunol.* **7**, 428–439 (2014).
96. Thornton, A. M. & Shevach, E. M. CD4+CD25+ Immunoregulatory T Cells Suppress Polyclonal T Cell Activation In Vitro by Inhibiting Interleukin 2 Production. *J. Exp. Med.* **188**, 287 (1998).
97. Coleman, M. M. *et al.* The immunoregulatory role of CD4+FoxP3+CD25− regulatory T cells in lungs of mice infected with Bordetella pertussis. *FEMS Immunol. Med. Microbiol.* **64**, 413–424 (2012).
98. Ono, M., Shimizu, J., Miyachi, Y. & Sakaguchi, S. Control of Autoimmune

Myocarditis and Multiorgan Inflammation by Glucocorticoid-Induced TNF Receptor Family-Related Proteinhigh, Foxp3-Expressing CD25+ and CD25− Regulatory T Cells. *J. Immunol.* **176**, 4748–4756 (2006).
99. Lindqvist, C. A. *et al.* T regulatory cells control T-cell proliferation partly by the release of soluble CD25 in patients with B-cell malignancies. *Immunology* **131**, 371 (2010).
100. Zelenay, S. *et al.* Foxp3+ CD25– CD4 T cells constitute a reservoir of committed regulatory cells that regain CD25 expression upon homeostatic expansion. *Proc. Natl. Acad. Sci. U. S. A.* **102**, 4091 (2005).
101. Morina, L. *et al.* Co-expression of Foxp3 and Helios facilitates the identification of human T regulatory cells in health and disease. *Front. Immunol.* **14**, 1114780 (2023).
102. Thornton, A. M. *et al.* Helios + and Helios − Treg subpopulations are phenotypically and functionally distinct and express dissimilar TCR repertoires. *Eur. J. Immunol.* **49**, 398–412 (2019).
103. Chougnet, C. & Hildeman, D. Helios—controller of Treg stability and function. *Transl. Cancer Res.* **5**, S338 (2016).
104. Morina, L. *et al.* Co-expression of Foxp3 and Helios facilitates the identification of human T regulatory cells in health and disease. *Front. Immunol.* **14**, (2023).
105. Thornton, A. M. *et al.* Helios+ and Helios− Treg subpopulations are phenotypically and functionally distinct and express dissimilar TCR repertoires. *Eur. J. Immunol.* **49**, 398–412 (2019).
106. Esebanmen, G. E. & Langridge, W. H. R. The role of TGF-beta signaling in dendritic cell tolerance. *Immunol. Res.* **65**, 987–994 (2017).
107. Shi, M. *et al.* Latent TGF-β structure and activation. *Nat. 2011 4747351* **474**, 343–349 (2011).
108. Marie, J. C., Letterio, J. J., Gavin, M. & Rudensky, A. Y. TGF-β1 maintains suppressor function and Foxp3 expression in CD4+CD25+ regulatory T cells. *J. Exp. Med.* **201**, 1061–1067 (2005).
109. Wang, R., Wan, Q., Kozhaya, L., Fujii, H. & Unutmaz, D. Identification of a Regulatory T Cell Specific Cell Surface Molecule that Mediates Suppressive Signals and Induces Foxp3 Expression. *PLoS One* **3**, e2705 (2008).
110. Sun, L., Jin, H. & Li, H. GARP: a surface molecule of regulatory T cells that is involved in the regulatory function and TGF-β releasing. *Oncotarget* **7**, 42826 (2016).
111. Metelli, A. *et al.* Immunoregulatory functions and the therapeutic implications of GARP-TGF-β in inflammation and cancer. *J. Hematol. Oncol. 2018 111* **11**, 1–11 (2018).
112. Kanamori, M., Nakatsukasa, H., Okada, M., Lu, Q. & Yoshimura, A. Induced Regulatory T Cells: Their Development, Stability, and Applications. *Trends Immunol.* **37**, 803–811 (2016).
113. Min, H. *et al.* Differentiation and homeostasis of effector Treg cells are regulated by inositol polyphosphates modulating Ca2+ influx. *Proc. Natl. Acad. Sci. U. S. A.* **119**, e2121520119 (2022).
114. Fukazawa, T. *et al.* Egress of Mature Murine Regulatory T Cells from the Thymus Requires RelA. *J. Immunol.* **194**, 3020–3028 (2015).
115. Koizumi, S. I. & Ishikawa, H. Transcriptional Regulation of Differentiation and Functions of Effector T Regulatory Cells. *Cells* **8**, 939 (2019).

116. Smigiel, K. S. *et al.* CCR7 provides localized access to IL-2 and defines homeostatically distinct regulatory T cell subsets. *J. Exp. Med.* **211**, 121–136 (2014).
117. Liston, A. & Gray, D. H. D. Homeostatic control of regulatory T cell diversity. *Nat. Rev. Immunol. 2014 143* **14**, 154–165 (2014).
118. Pot, C., Apetoh, L. & Kuchroo, V. K. Type 1 Regulatory T cells (Tr1) in autoimmunity. *Semin. Immunol.* **23**, 202 (2011).
119. Levings, M. K. *et al.* Differentiation of Tr1 cells by immature dendritic cells requires IL-10 but not CD25+CD4+ Tr cells. *Blood* **105**, 1162–1169 (2005).
120. Gandhi, R. *et al.* Cutting Edge: Human Latency-Associated Peptide + T Cells: A Novel Regulatory T Cell Subset. *J. Immunol.* **184**, 4620–4624 (2010).
121. Duan, W., So, T., Mehta, A. K., Choi, H. & Croft, M. Inducible CD4+LAP+ Foxp3 negative Regulatory T cells Suppress Allergic Inflammation. *J. Immunol.* **187**, 6499 (2011).
122. Rosenblum, M. D., Way, S. S. & Abbas, A. K. Regulatory T cell memory. *Nature Reviews Immunology* vol. 16 90–101 (2016).
123. Khantakova, J. N., Bulygin, A. S. & Sennikov, S. V. The Regulatory-T-Cell Memory Phenotype: What We Know. (2022) doi:10.3390/cells11101687.
124. Robb, R. J. *et al.* Identification and expansion of highly suppressive CD8+FoxP3+ regulatory T cells after experimental allogeneic bone marrow transplantation. *Blood* **119**, 5898–5908 (2012).
125. Vieyra-Lobato, M. R., Vela-Ojeda, J., Montiel-Cervantes, L., López-Santiago, R. & Moreno-Lafont, M. C. Description of CD8+ Regulatory T Lymphocytes and Their Specific Intervention in Graft-versus-Host and Infectious Diseases, Autoimmunity, and Cancer. *J. Immunol. Res.* **2018**, (2018).
126. Kulkarni, A. B. *et al.* Transforming growth factor beta 1 null mutation in mice causes excessive inflammatory response and early death. *Proc. Natl. Acad. Sci.* **90**, 770–774 (1993).
127. Turner, J. A. *et al.* Regulatory T Cell-Derived TGF-β1 Controls Multiple Checkpoints Governing Allergy and Autoimmunity. *Immunity* **53**, 1202-1214.e6 (2020).
128. Rubtsov, Y. P. *et al.* Regulatory T Cell-Derived Interleukin-10 Limits Inflammation at Environmental Interfaces. *Immunity* **28**, 546–558 (2008).
129. Arumugham, V. B. & Baldari, C. T. cAMP: a multifaceted modulator of immune synapse assembly and T cell activation. *J. Leukoc. Biol.* **101**, 1301–1316 (2017).
130. Bopp, T. *et al.* Cyclic adenosine monophosphate is a key component of regulatory T cell–mediated suppression. *J. Exp. Med.* **204**, 1303–1310 (2007).
131. Bodor, J. *et al.* Cyclic AMP underpins suppression by regulatory T cells. *Eur. J. Immunol.* **42**, 1375–1384 (2012).
132. Goldmann, O., Nwofor, O. V., Chen, Q. & Medina, E. Mechanisms underlying immunosuppression by regulatory cells. *Front. Immunol.* **15**, 1328193 (2024).
133. Grossman, W. J. *et al.* Human T regulatory cells can use the perforin pathway to cause autologous target cell death. *Immunity* **21**, 589–601 (2004).
134. Akkaya, B. *et al.* Regulatory T cells mediate specific suppression by

depleting peptide–MHC class II from dendritic cells. *Nat. Immunol. 2019 202* **20**, 218–231 (2019).
135. Read, S. *et al.* Blockade of CTLA-4 on CD4+CD25+ Regulatory T Cells Abrogates Their Function In Vivo. *J. Immunol.* **177**, 4376–4383 (2006).
136. Walker, L. S. K. & Sansom, D. M. The emerging role of CTLA4 as a cell-extrinsic regulator of T cell responses. *Nat. Rev. Immunol. 2011 1112* **11**, 852–863 (2011).
137. Beutler, B. *et al.* Genetic analysis of host resistance: Toll-like receptor signaling and immunity at large. *Annu. Rev. Immunol.* **24**, 353–389 (2006).
138. Medzhitov, R. & Janeway, C. A. Innate immunity: Impact on the adaptive immune response. *Curr. Opin. Immunol.* **9**, 4–9 (1997).
139. Janeway, C. A. Approaching the asymptote? Evolution and revolution in immunology. *Cold Spring Harb. Symp. Quant. Biol.* **54**, 1–13 (1989).
140. Mogensen, T. H. Pathogen recognition and inflammatory signaling in innate immune defenses. *Clin. Microbiol. Rev.* **22**, 240–273 (2009).
141. Ghosh, S., May, M. J. & Kopp, E. B. NF-kappa B and Rel proteins: evolutionarily conserved mediators of immune responses. *Annu. Rev. Immunol.* **16**, 225–260 (1998).
142. O'Neill, L. A. J. & Bowie, A. G. The family of five: TIR-domain-containing adaptors in Toll-like receptor signalling. *Nat. Rev. Immunol. 2007 75* **7**, 353–364 (2007).
143. Zelensky, A. N. & Gready, J. E. The C-type lectin-like domain superfamily. *FEBS J.* **272**, 6179–6217 (2005).
144. Brown, G. D., Willment, J. A. & Whitehead, L. C-type lectins in immunity and homeostasis. *Nat. Rev. Immunol. 2018 186* **18**, 374–389 (2018).
145. Sharma, A., Steichen, A. L., Jondle, C. N., Mishra, B. B. & Sharma, J. Protective Role of Mincle in Bacterial Pneumonia by Regulation of Neutrophil Mediated Phagocytosis and Extracellular Trap Formation. *J. Infect. Dis.* **209**, 1837–1846 (2014).
146. Behler-Janbeck, F. *et al.* C-type Lectin Mincle Recognizes Glucosyl-diacylglycerol of Streptococcus pneumoniae and Plays a Protective Role in Pneumococcal Pneumonia. *PLOS Pathog.* **12**, e1006038 (2016).
147. Naqvi, K. F. & Endsley, J. J. Myeloid C-Type Lectin Receptors in Tuberculosis and HIV Immunity: Insights Into Co-infection? *Front. Cell. Infect. Microbiol.* **10**, 525104 (2020).
148. Van Kooyk, Y. & Geijtenbeek, T. B. H. DC-SIGN: escape mechanism for pathogens. *Nat. Rev. Immunol. 2003 39* **3**, 697–709 (2003).
149. Iliev, I. D. *et al.* Interactions between commensal fungi and the C-type lectin receptor dectin-1 influence colitis. *Science (80-.).* **336**, 1314–1317 (2012).
150. Kimura, Y. *et al.* The innate immune receptor Dectin-2 mediates the phagocytosis of cancer cells by Kupffer cells for the suppression of liver metastasis. *Proc. Natl. Acad. Sci. U. S. A.* **113**, 14097–14102 (2016).
151. Chiba, S. *et al.* Recognition of tumor cells by Dectin-1 orchestrates innate immune cells for anti-tumor responses. *Elife* **3**, 1–20 (2014).
152. Lafouresse, F., Bellard, E., Blood, C. L.-, Journal, T. & 2015, undefined. L-selectin controls trafficking of chronic lymphocytic leukemia cells in lymph node high endothelial venules in vivo. *ashpublications.orgF Lafouresse, E Bellard, C Laurent, C Moussion, JJ Fournié, L Ysebaert, JP GirardBlood, J. Am. Soc. Hematol. 2015•ashpublications.org*.
153. Seifert, L. *et al.* The necrosome promotes pancreatic oncogenesis via

CXCL1 and Mincle-induced immune suppression. *Nat. 2016 5327598* **532**, 245–249 (2016).
154. Daley, D. *et al.* Dectin 1 activation on macrophages by galectin 9 promotes pancreatic carcinoma and peritumoral immune tolerance. *Nat. Med. 2017 235* **23**, 556–567 (2017).
155. Cáliz, R. *et al.* Gender-Specific Effects of Genetic Variants within Th1 and Th17 Cell-Mediated Immune Response Genes on the Risk of Developing Rheumatoid Arthritis. *PLoS One* **8**, e72732 (2013).
156. Zou, X. Z. *et al.* Involvement of epithelial-mesenchymal transition afforded by activation of LOX-1/ TGF-β1/KLF6 signaling pathway in diabetic pulmonary fibrosis. *Pulm. Pharmacol. Ther.* **44**, 70–77 (2017).
157. Baccala, R. *et al.* Sensors of the innate immune system: Their mode of action. *Nature Reviews Rheumatology* vol. 5 448–456 (2009).
158. Rehwinkel, J. & Gack, M. U. RIG-I-like receptors: their regulation and roles in RNA sensing. *Nat. Rev. Immunol. 2020 209* **20**, 537–551 (2020).
159. Zahid, A., Ismail, H., Li, B. & Jin, T. Molecular and Structural Basis of DNA Sensors in Antiviral Innate Immunity. *Frontiers in Immunology* vol. 11 3094 (2020).
160. Ishikawa, H. & Barber, G. N. STING an Endoplasmic Reticulum Adaptor that Facilitates Innate Immune Signaling. *Nature* **455**, 674 (2008).
161. Vance, R. E. Cytosolic DNA Sensing: The Field Narrows. *Immunity* vol. 45 227–228 (2016).
162. Kong, L. Z. *et al.* Understanding nucleic acid sensing and its therapeutic applications. *Exp. Mol. Med. 2023 5511* **55**, 2320–2331 (2023).
163. Zahid, A., Ismail, H., Li, B. & Jin, T. Molecular and Structural Basis of DNA Sensors in Antiviral Innate Immunity. *Front. Immunol.* **11**, 613039 (2020).
164. Fernandes-Alnemri, T., Yu, J. W., Datta, P., Wu, J. & Alnemri, E. S. AIM2 activates the inflammasome and cell death in response to cytoplasmic DNA. *Nature* **458**, 509–513 (2009).
165. Hornung, V. *et al.* AIM2 recognizes cytosolic dsDNA and forms a caspase-1-activating inflammasome with ASC. *Nature* **458**, 514–518 (2009).
166. Proell, M., Riedl, S. J., Fritz, J. H., Rojas, A. M. & Schwarzenbacher, R. The Nod-Like Receptor (NLR) family: A tale of similarities and differences. *PLoS One* **3**, (2008).
167. Wicherska-pawłowska, K., Wróbel, T. & Rybka, J. Toll-Like Receptors (TLRs), NOD-Like Receptors (NLRs), and RIG-I-Like Receptors (RLRs) in Innate Immunity. TLRs, NLRs, and RLRs Ligands as Immunotherapeutic Agents for Hematopoietic Diseases. *Int. J. Mol. Sci.* **22**, (2021).
168. Gharagozloo, M. *et al.* NLR-dependent regulation of inflammation in multiple sclerosis- Dependent regulation of inflammation in multiple sclerosis. *Frontiers in Immunology* vol. 8 2012 (2018).
169. Huse, M. Mechanical Forces in the Immune System. *Nat. Rev. Immunol.* **17**, 679 (2017).
170. Du, H. *et al.* Tuning immunity through tissue mechanotransduction. *Nat. Rev. Immunol.* **23**, (2022).
171. Knecht, R. S. *et al.* Mechanobiological Principles Influence the Immune Response in Regeneration: Implications for Bone Healing. *Front. Bioeng. Biotechnol.* **9**, (2021).
172. Xia, K. *et al.* Roles of mechanosensitive ion channels in immune cells. *Heliyon* **10**, e23318 (2024).

173. Pageon, S. V., Govendir, M. A., Kempe, D. & Biro, M. Mechanoimmunology: Molecular-scale forces govern immune cell functions. *Mol. Biol. Cell* **29**, 1919–1926 (2018).
174. Rogers, J., Bajur, A. T., Salaita, K. & Spillane, K. M. Mechanical control of antigen detection and discrimination by T and B cell receptors. *Biophys. J.* **123**, 2234–2255 (2024).
175. Blumenthal, D., Chandra, V., Avery, L. & Burkhardt, J. K. Mouse T cell priming is enhanced by maturation-dependent stiffening of the dendritic cell cortex. *Elife* **9**, 1–44 (2020).
176. Mai, Z., Lin, Y., Lin, P., Zhao, X. & Cui, L. Modulating extracellular matrix stiffness: a strategic approach to boost cancer immunotherapy. *Cell Death Dis. 2024 155* **15**, 1–16 (2024).
177. Yu, K. X., Yuan, W. J., Wang, H. Z. & Li, Y. X. Extracellular matrix stiffness and tumor-associated macrophage polarization: new fields affecting immune exclusion. *Cancer Immunol. Immunother.* **73**, 115 (2024).
178. Renkawitz, J. & Sixt, M. Mechanisms of force generation and force transmission during interstitial leukocyte migration. *EMBO Rep.* **11**, 744–750 (2010).
179. Le Roux, A. L., Quiroga, X., Walani, N., Arroyo, M. & Roca-Cusachs, P. The plasma membrane as a mechanochemical transducer. *Philos. Trans. R. Soc. B* **374**, (2019).
180. Diz-Muñoz, A. *et al.* Membrane Tension Acts Through PLD2 and mTORC2 to Limit Actin Network Assembly During Neutrophil Migration. *PLOS Biol.* **14**, e1002474 (2016).
181. Varshney, P., Yadav, V. & Saini, N. Lipid rafts in immune signalling: current progress and future perspective. *Immunology* **149**, 13 (2016).
182. Bernard, C., Carotenuto, A. R., Pugno, N. M., Fraldi, M. & Deseri, L. Modelling lipid rafts formation through chemo-mechanical interplay triggered by receptor–ligand binding. *Biomech. Model. Mechanobiol.* **23**, 485–505 (2024).
183. Medina, F. A. *et al.* Caveolin-1-deficient mice show defects in innate immunity and inflammatory immune response during Salmonella enterica serovar typhimurium infection. *Infect. Immun.* **74**, 6665–6674 (2006).
184. Del Pozo, M. A., Lolo, F. N. & Echarri, A. Caveolae: Mechanosensing and mechanotransduction devices linking membrane trafficking to mechanoadaptation. *Curr. Opin. Cell Biol.* **68**, 113–123 (2021).
185. Sotodosos-Alonso, L., Pulgarín-Alfaro, M. & del Pozo, M. A. Caveolae Mechanotransduction at the Interface between Cytoskeleton and Extracellular Matrix. *Cells* **12**, (2023).
186. Chen, C. L., Shuan, S. H. & Jung, S. H. Cholesterol Modulates Cellular TGF-β Responsiveness by Altering TGF-β Binding to TGF-β Receptors. *J. Cell. Physiol.* **215**, 223 (2008).
187. Triantafilou, M., Miyake, K., Golenbock, D. T. & Triantafilou, K. Mediators of innate immune recognition of bacteria concentrate in lipid rafts and facilitate lipopolysaccharide-induced cell activation. *J. Cell Sci.* **115**, 2603–2611 (2002).
188. Orsini, E. M. *et al.* Stretching the Function of Innate Immune Cells. *Frontiers in Immunology* vol. 12 4507 (2021).
189. Zhang, X. *et al.* Unraveling the mechanobiology of immune cells. *Current Opinion in Biotechnology* vol. 66 236–245 (2020).

190. Huse, M. Mechanical forces in the immune system. *Nature Reviews Immunology* vol. 17 679–690 (2017).
191. Humphrey, J. D., Dufresne, E. R. & Schwartz, M. A. Mechanotransduction and extracellular matrix homeostasis. *Nat. Rev. Mol. Cell Biol.* **15**, 802–812 (2014).
192. Meli, V. S. *et al.* YAP-mediated mechanotransduction tunes the macrophage inflammatory response. *Sci. Adv.* **6**, (2020).
193. Rostam, H. M., Reynolds, P. M., Alexander, M. R., Gadegaard, N. & Ghaemmaghami, A. M. Image based Machine Learning for identification of macrophage subsets. *Sci. Reports 2017 71* **7**, 1–11 (2017).
194. McWhorter, F. Y., Davis, C. T. & Liu, W. F. Physical and mechanical regulation of macrophage phenotype and function. *Cellular and Molecular Life Sciences* vol. 72 1303–1316 (2015).
195. Coste, B. *et al.* Piezo1 and Piezo2 are essential components of distinct mechanically activated cation channels. *Science (80-.).* **330**, 55–60 (2010).
196. Watanabe, H. *et al.* Heat-evoked Activation of TRPV4 Channels in a HEK293 Cell Expression System and in Native Mouse Aorta Endothelial Cells *. *J. Biol. Chem.* **277**, 47044–47051 (2002).
197. Matthews, B. D. *et al.* Ultra-rapid activation of TRPV4 ion channels by mechanical forces applied to cell surface β1 integrins. *Integr. Biol.* **2**, 435–442 (2010).
198. Vriens, J. *et al.* Cell swelling, heat, and chemical agonists use distinct pathways for the activation of the cation channel TRPV4. *Proc. Natl. Acad. Sci. U. S. A.* **101**, 396–401 (2004).
199. Loukin, S., Zhou, X., Su, Z., Saimi, Y. & Kung, C. Wild-type and brachyolmia-causing mutant TRPV4 channels respond directly to stretch force. *J. Biol. Chem.* **285**, 27176–27181 (2010).
200. Michalick, L. & Kuebler, W. M. TRPV4—A Missing Link Between Mechanosensation and Immunity. *Front. Immunol.* **11**, 413 (2020).
201. Scheraga, R. G. *et al.* TRPV4 Protects the Lung from Bacterial Pneumonia via MAPK Molecular Pathway Switching. *J. Immunol.* **204**, 1310–1321 (2020).
202. Sharma, S., Goswami, R. & Rahaman, S. O. The TRPV4-TAZ Mechanotransduction Signaling Axis in Matrix Stiffness- and TGFβ1-Induced Epithelial-Mesenchymal Transition. *Cell. Mol. Bioeng.* **12**, 139 (2019).
203. Hamanaka, K. *et al.* TRPV4 initiates the acute calcium-dependent permeability increase during ventilator-induced lung injury in isolated mouse lungs. *Am. J. Physiol. - Lung Cell. Mol. Physiol.* **293**, 923–932 (2007).
204. Scheraga, R. G. *et al.* TRPV4 Mechanosensitive Ion Channel Regulates Lipopolysaccharide-Stimulated Macrophage Phagocytosis. *J. Immunol.* **196**, 428–436 (2016).
205. Wang, Y. *et al.* Immunoregulatory Role of the Mechanosensitive Ion Channel Piezo1 in Inflammation and Cancer. *Molecules* **28**, (2023).
206. Ge, J. *et al.* Architecture of the mammalian mechanosensitive Piezo1 channel. *Nat. 2015 5277576* **527**, 64–69 (2015).
207. Wang, Y. *et al.* Stiffness sensing via Piezo1 enhances macrophage efferocytosis and promotes the resolution of liver fibrosis. *Sci. Adv.* **10**, 3289 (2024).

208. Xu, Y. *et al.* Mechanotransductive receptor Piezo1 as a promising target in the treatment of fibrosis diseases. *Front. Mol. Biosci.* **10**, 1270979 (2023).
209. Liu, H. *et al.* Piezo1 Channels as Force Sensors in Mechanical Force-Related Chronic Inflammation. *Front. Immunol.* **13**, 816149 (2022).
210. Ma, S. *et al.* A role of PIEZO1 in iron metabolism in mice and humans. *Cell* **184**, 969-982.e13 (2021).
211. Wang, Y. *et al.* Dendritic cell Piezo1 directs the differentiation of TH1 and Treg cells in cancer. *Elife* **11**, (2022).
212. abiff, muta *et al.* Piezo1 facilitates optimal T cell activation during tumor challenge. *Oncoimmunology* **12**, (2023).
213. Jairaman, A. *et al.* Piezo1 channels restrain regulatory T cells but are dispensable for effector CD4+ T cell responses. *Sci. Adv.* **7**, (2021).
214. Hynes, R. O. Integrins: Bidirectional, Allosteric Signaling Machines. *Cell* **110**, 673–687 (2002).
215. Van der Flier, A. & Sonnenberg, A. Function and interactions of integrins. *Cell Tissue Res.* **305**, 285–298 (2001).
216. Luo, B. H., Carman, C. V. & Springer, T. A. Structural Basis of Integrin Regulation and Signaling. *Annu. Rev. Immunol.* **25**, 619 (2007).
217. Takagi, J., Petre, B. M., Walz, T. & Springer, T. A. Global conformational earrangements in integrin extracellular domains in outside-in and inside-out signaling. *Cell* **110**, 599–611 (2002).
218. Wang, J. H. Pull and push: Talin activation for integrin signaling. *Cell Res. 2012 2211* **22**, 1512–1514 (2012).
219. Calderwood, D. A. *et al.* The phosphotyrosine binding-like domain of talin activates integrins. *J. Biol. Chem.* **277**, 21749–21758 (2002).
220. Goksoy, E. *et al.* Structural Basis for the Autoinhibition of Talin in Regulating Integrin Activation. *Mol. Cell* **31**, 124–133 (2008).
221. Song, X. *et al.* A novel membrane-dependent on/off switch mechanism of talin FERM domain at sites of cell adhesion. *Cell Res. 2012 2211* **22**, 1533–1545 (2012).
222. Ludwig, B. S., Kessler, H., Kossatz, S. & Reuning, U. RGD-Binding Integrins Revisited: How Recently Discovered Functions and Novel Synthetic Ligands (Re-)Shape an Ever-Evolving Field. *Cancers (Basel).* **13**, 1711 (2021).
223. Campbell, I. D. & Humphries, M. J. Integrin Structure, Activation, and Interactions. *Cold Spring Harb. Perspect. Biol.* **3**, 1–14 (2011).
224. Pang, X. *et al.* Targeting integrin pathways: mechanisms and advances in therapy. *Signal Transduct. Target. Ther. 2022 81* **8**, 1–42 (2023).
225. Baade, T., Paone, C., Baldrich, A. & Hauck, C. R. Clustering of integrin β cytoplasmic domains triggers nascent adhesion formation and reveals a protozoan origin of the integrin-talin interaction. *Sci. Reports 2019 91* **9**, 1–13 (2019).
226. Shattil, S. J., Kim, C. & Ginsberg, M. H. The final steps of integrin activation: the end game. (2010) doi:10.1038/nrm2871.
227. Welf, E. S., Naik, U. P. & Ogunnaike, B. A. A Spatial Model for Integrin Clustering as a Result of Feedback between Integrin Activation and Integrin Binding. *Biophys. J.* **103**, 1379 (2012).
228. Ross, T. D. *et al.* Integrins In Mechanotransduction. *Curr. Opin. Cell Biol.* **25**, 613 (2013).
229. Cheng, D., Wang, J., Yao, M. & Cox, C. D. Joining forces: crosstalk

between mechanosensitive PIEZO1 ion channels and integrin-mediated focal adhesions. *Biochem. Soc. Trans.* **51**, 1897–1906 (2023).
230. Bui, T. M., Wiesolek, H. L. & Sumagin, R. ICAM-1: A master regulator of cellular responses in inflammation, injury resolution, and tumorigenesis. *J. Leukoc. Biol.* **108**, 787 (2020).
231. Lainé, A. *et al.* Regulatory T cells promote cancer immune-escape through integrin αvβ8-mediated TGF-β activation. *Nat. Commun. 2021 121* **12**, 1–14 (2021).
232. Margadant, C. & Sonnenberg, A. Integrin-TGF-B crosstalk in fibrosis, cancer and wound healing. *EMBO Rep.* **11**, 97–105 (2010).
233. Annes, J. P., Chen, Y., Munger, J. S. & Rifkin, D. B. Integrin αVβ6-mediated activation of latent TGF-β requires the latent TGF-β binding protein-1. *J. Cell Biol.* **165**, 723 (2004).
234. Wipff, P. J., Rifkin, D. B., Meister, J. J. & Hinz, B. Myofibroblast contraction activates latent TGF-β1 from the extracellular matrix. *J. Cell Biol.* **179**, 1311 (2007).
235. Annes, J. P., Chen, Y., Munger, J. S. & Rifkin, D. B. Integrin αVβ6-mediated activation of latent TGF-β requires the latent TGF-β binding protein-1. *J. Cell Biol.* **165**, 723 (2004).
236. Sarrazy, V. *et al.* Integrins αvβ5 and αvβ3 promote latent TGF-β1 activation by human cardiac fibroblast contraction. *Cardiovasc. Res.* **102**, 407 (2014).
237. Campbell, M. G. *et al.* Cryo-EM reveals integrin-mediated TGF-β activation without release from latent TGF-β. *Cell* **180**, 490 (2020).
238. Shi, M. *et al.* Latent TGF-β structure and activation. *Nat. 2011 4747351* **474**, 343–349 (2011).
239. Brooks, P. C. *et al.* Localization of matrix metalloproteinase MMP-2 to the surface of invasive cells by interaction with integrin αvβ3. *Cell* **85**, 683–693 (1996).
240. Brown, N. F. & Marshall, J. F. Integrin-Mediated TGFβ Activation Modulates the Tumour Microenvironment. *Cancers (Basel).* **11**, (2019).
241. Aluwihare, P. *et al.* Mice that lack activity of αvβ6- and αvβ8-integrins reproduce the abnormalities of Tgfb1- and Tgfb3-null mice. *J. Cell Sci.* **122**, 227–232 (2009).
242. Brown, N. F. & Marshall, J. F. Integrin-Mediated TGFβ Activation Modulates the Tumour Microenvironment. *Cancers (Basel).* **11**, (2019).
243. Mair, I. *et al.* A context-dependent role for αv integrins in regulatory T cell accumulation at sites of inflammation. *Front. Immunol.* **9**, 301122 (2018).
244. Szeto, A. C. H. *et al.* An αvβ3 integrin checkpoint is critical for efficient T H 2 cytokine polarisation and potentiating antigen-specific immunity. doi:10.1038/s41590-022-01378-w.
245. Li, X. *et al.* The DEL-1/β3 integrin axis promotes regulatory T cell responses during inflammation resolution. *J. Clin. Invest.* **130**, 6261 (2020).
246. Asano, Y. *et al.* Increased expression of integrin alpha(v)beta3 contributes to the establishment of autocrine TGF-beta signaling in scleroderma fibroblasts. *J. Immunol.* **175**, 7708–7718 (2005).
247. Mierke, C. T. The integrin alphav beta3 increases cellular stiffness and cytoskeletal remodeling dynamics to facilitate cancer cell invasion. *New J. Phys.* **15**, 015003 (2013).
248. Zhang, Q., Zhang, S., Chen, J. & Xie, Z. The Interplay between Integrins and Immune Cells as a Regulator in Cancer Immunology. *Int. J. Mol. Sci.*

24, (2023).
249. Asano, Y., Ihn, H., Yamane, K., Jinnin, M. & Tamaki, K. Increased Expression of Integrin αvβ5 Induces the Myofibroblastic Differentiation of Dermal Fibroblasts. *Am. J. Pathol.* **168**, 499–510 (2006).
250. Munger, J. S. *et al.* The integrin alpha v beta 6 binds and activates latent TGF beta 1: a mechanism for regulating pulmonary inflammation and fibrosis. *Cell* **96**, 319–328 (1999).
251. Popov, Y. *et al.* Integrin αvβ6 is a marker of the progression of biliary and portal liver fibrosis and a novel target for antifibrotic therapies. *J. Hepatol.* **48**, 453–464 (2008).
252. Moore, K. M. *et al.* Therapeutic Targeting of Integrin αvβ6 in Breast Cancer. *JNCI J. Natl. Cancer Inst.* **106**, (2014).
253. Steel, N. *et al.* TGFβ-activation by dendritic cells drives Th17 induction and intestinal contractility and augments the expulsion of the parasite Trichinella spiralis in mice. *PLoS Pathog.* **15**, (2019).
254. Worthington, J. J. *et al.* Integrin αvβ8-Mediated TGF-β Activation by Effector Regulatory T Cells Is Essential for Suppression of T-Cell-Mediated Inflammation. *Immunity* **42**, 903–915 (2015).
255. Mu, D. *et al.* The integrin αvβ8 mediates epithelial homeostasis through MT1-MMP–dependent activation of TGF-β1. *J. Cell Biol.* **157**, 493 (2002).
256. Kelly, A. *et al.* Human monocytes and macrophages regulate immune tolerance via integrin αvβ8–mediated TGFβ activation. *J. Exp. Med.* **215**, 2725 (2018).
257. Lainé, A. *et al.* Regulatory T cells promote cancer immune-escape through integrin αvβ8-mediated TGF-β activation. *Nat. Commun. 2021 121* **12**, 1–14 (2021).
258. Huang, X. *et al.* Integrin Avß8 On Dendritic Cells Regulates Airway Hyperresponsiveness Through Induction Of IL-17 In T Cells. *Am. Thorac. Soc. Int. Conf. Meet. Abstr. Am. Thorac. Soc. Int. Conf. Meet. Abstr.* A2574–A2574 (2011) doi:10.1164/AJRCCM-CONFERENCE.2011.183.1_MEETINGABSTRACTS.A2574.
259. Heldin, C. H. & Moustakas, A. Signaling Receptors for TGF-β Family Members. *Cold Spring Harb. Perspect. Biol.* **8**, (2016).
260. Huse, M., Chen, Y. G., Massagué, J. & Kuriyan, J. Crystal Structure of the Cytoplasmic Domain of the Type I TGF β Receptor in Complex with FKBP12. *Cell* **96**, 425–436 (1999).
261. Miyazawa, K. & Miyazono, K. Regulation of TGF-β Family Signaling by Inhibitory Smads. *Cold Spring Harb. Perspect. Biol.* **9**, (2017).
262. Massagué, J. & Sheppard, D. TGF-β signaling in health and disease. *Cell* **186**, 4007–4037 (2023).
263. Zhang, Y. E. Non-Smad pathways in TGF-β signaling. *Cell Res. 2009 191* **19**, 128–139 (2008).
264. Powell, J. D., Pollizzi, K. N., Heikamp, E. B. & Horton, M. R. Regulation of Immune Responses by mTOR. *Annu. Rev. Immunol.* **30**, 39 (2012).
265. Collins, S. L. *et al.* mTORC1 Signaling Regulates Proinflammatory Macrophage Function and Metabolism. *J. Immunol.* **207**, 913–922 (2021).
266. Weichhart, T. & Säemann, M. D. The multiple facets of mTOR in immunity. *Trends Immunol.* **30**, 218–226 (2009).
267. Ohtani, M. *et al.* Mammalian target of rapamycin and glycogen synthase kinase 3 differentially regulate lipopolysaccharide-induced interleukin-12

production in dendritic cells. *Blood* **112**, 635–643 (2008).
268. Haidinger, M. *et al.* A Versatile Role of Mammalian Target of Rapamycin in Human Dendritic Cell Function and Differentiation. *J. Immunol.* **185**, 3919–3931 (2010).
269. Maruyama, K., Nemoto, E. & Yamada, S. Mechanical regulation of macrophage function - Cyclic tensile force inhibits NLRP3 inflammasome-dependent IL-1β secretion in murine macrophages. *Inflamm. Regen.* **39**, 1–9 (2019).
270. You, J. S., Frey, J. W. & Hornberger, T. A. Mechanical Stimulation Induces mTOR Signaling via an ERK-Independent Mechanism: Implications for a Direct Activation of mTOR by Phosphatidic Acid. *PLoS One* **7**, e47258 (2012).
271. Yang, Q. & Guan, K. L. Expanding mTOR signaling. *Cell Research* vol. 17 666–681 (2007).
272. Reiling, J. H. & Sabatini, D. M. Stress and mTORture signaling. *Oncogene 2006 2548* **25**, 6373–6383 (2006).
273. Bond, P. Regulation of mTORC1 by growth factors, energy status, amino acids and mechanical stimuli at a glance. *Journal of the International Society of Sports Nutrition* vol. 13 8 (2016).
274. Laplante, M. & Sabatini, D. M. mTOR signaling at a glance. *J. Cell Sci.* **122**, 3589–3594 (2009).
275. Abraham, R. T. & Wiederrecht, G. J. Immunopharmacology of rapamycin. *Annual Review of Immunology* vol. 14 483–510 (1996).
276. Thomson, A. W., Turnquist, H. R. & Raimondi, G. Immunoregulatory functions of mTOR inhibition. *Nature Reviews Immunology* vol. 9 324–337 (2009).
277. Byles, V. *et al.* The TSC-mTOR pathway regulates macrophage polarization. *Nat. Commun.* **4**, (2013).
278. Ma, X. M. & Blenis, J. Molecular mechanisms of mTOR-mediated translational control. *Nature Reviews Molecular Cell Biology* vol. 10 307–318 (2009).
279. Cunningham, J. T. *et al.* mTOR controls mitochondrial oxidative function through a YY1-PGC-1α transcriptional complex. *Nature* **450**, 736–740 (2007).
280. Porstmann, T. *et al.* SREBP Activity Is Regulated by mTORC1 and Contributes to Akt-Dependent Cell Growth. *Cell Metab.* **8**, 224–236 (2008).
281. Linke, M., Fritsch, S. D., Sukhbaatar, N., Hengstschläger, M. & Weichhart, T. mTORC1 and mTORC2 as regulators of cell metabolism in immunity. *FEBS Lett.* **591**, 3089–3103 (2017).
282. Chi, H. Regulation and function of mTOR signalling in T cell fate decisions. *Nat. Rev. Immunol. 2012 125* **12**, 325–338 (2012).
283. Haidinger, M. *et al.* A Versatile Role of Mammalian Target of Rapamycin in Human Dendritic Cell Function and Differentiation. *J. Immunol.* **185**, 3919–3931 (2010).
284. Zhou, L. *et al.* Rapamycin treated tol-dendritic cells derived from BM-MSCs reversed graft rejection in a rat liver transplantation model by inducing CD8+CD45RC-Treg. *Mol. Immunol.* **137**, 11–19 (2021).
285. Passerini, L. *et al.* Treatment with rapamycin can restore regulatory T-cell function in IPEX patients. *J. Allergy Clin. Immunol.* **145**, 1262-1271.e13 (2020).

286. Dzankic, P. J. & Partridge, L. Clinical trials of mTOR inhibitors to boost immunity to viral infection in older adults. *Lancet Heal. Longev.* **2**, e232–e233 (2021).
287. Amiel, E. *et al.* Mechanistic Target of Rapamycin Inhibition Extends Cellular Lifespan in Dendritic Cells by Preserving Mitochondrial Function. *J. Immunol.* **193**, 2821–2830 (2014).
288. Cao, W. *et al.* Toll-like receptor–mediated induction of type I interferon in plasmacytoid dendritic cells requires the rapamycin-sensitive PI(3)K-mTOR-p70S6K pathway. *Nat. Immunol. 2008 910* **9**, 1157–1164 (2008).
289. Ohtani, M. *et al.* Mammalian target of rapamycin and glycogen synthase kinase 3 differentially regulate lipopolysaccharide-induced interleukin-12 production in dendritic cells. *Blood* **112**, 635–643 (2008).
290. Amiel, E. *et al.* Inhibition of Mechanistic Target of Rapamycin Promotes Dendritic Cell Activation and Enhances Therapeutic Autologous Vaccination in Mice. *J. Immunol.* **189**, 2151–2158 (2012).
291. Wu, Q. *et al.* The Tuberous Sclerosis Complex–Mammalian Target of Rapamycin Pathway Maintains the Quiescence and Survival of Naive T Cells. *J. Immunol.* **187**, 1106–1112 (2011).
292. Yang, K., Neale, G., Green, D. R., He, W. & Chi, H. The tumor suppressor Tsc1 enforces quiescence of naive T cells to promote immune homeostasis and function. *Nat. Immunol. 2011 129* **12**, 888–897 (2011).
293. Katzman, S. D. *et al.* Duration of antigen receptor signaling determines T-cell tolerance or activation. *Proc. Natl. Acad. Sci. U. S. A.* **107**, 18085–18090 (2010).
294. Turner, M. S., Kane, L. P. & Morel, P. A. Dominant Role of Antigen Dose in CD4+Foxp3+ Regulatory T Cell Induction and Expansion. *J. Immunol.* **183**, 4895–4903 (2009).
295. Chi, H. Regulation and function of mTOR signalling in T cell fate decisions. *Nat. Rev. Immunol. 2012 125* **12**, 325–338 (2012).
296. Francisco, L. M. *et al.* PD-L1 regulates the development, maintenance, and function of induced regulatory T cells. *J. Exp. Med.* **206**, 3015 (2009).
297. Fernandez, D., Bonilla, E., Mirza, N., Niland, B. & Perl, A. Rapamycin reduces disease activity and normalizes T cell activation–induced calcium fluxing in patients with systemic lupus erythematosus. *Arthritis Rheum.* **54**, 2983–2988 (2006).
298. Huang, S. C. C. *et al.* Metabolic Reprogramming Mediated by the mTORC2-IRF4 Signaling Axis Is Essential for Macrophage Alternative Activation. *Immunity* **45**, 817–830 (2016).
299. O'Neill, L. A. J., Kishton, R. J. & Rathmell, J. A guide to immunometabolism for immunologists. *Nature Reviews Immunology* vol. 16 553–565 (2016).
300. Technologies, A. *Agilent Technologies Agilent Seahorse XF Cell Mito Stress Test Kit User Guide*. https://www.agilent.com/cs/library/usermanuals/public/XF_Cell_Mito_Stress_Test_Kit_User_Guide.pdf (2019).
301. Vangapandu, H. V. & Gandhi, V. Extracellular Flux Assays to Determine Oxidative Phosphorylation and Glycolysis in Chronic Lymphocytic Leukemia Cells. *Methods Mol. Biol.* **1881**, 121–128 (2019).
302. Voss, K. *et al.* A guide to interrogating immunometabolism. *Nat. Rev. Immunol.* **21**, 637 (2021).
303. Purohit, V., Wagner, A., Yosef, N. & Kuchroo, V. K. Systems-based

approaches to study immunometabolism. *Cell. Mol. Immunol. 2022 193* **19**, 409–420 (2022).
304. Warburg, O., Wind, F. & Negelein, E. The metabolism of tumors in the body. *J. Gen. Physiol.* **8**, 519–530 (1927).
305. Vazquez, A., Liu, J., Zhou, Y. & Oltvai, Z. N. Catabolic efficiency of aerobic glycolysis: the Warburg effect revisited. *BMC Syst. Biol.* **4**, (2010).
306. Tannahill, G. M. *et al.* Succinate is an inflammatory signal that induces IL-1β through HIF-1α. *Nature* **496**, 238–242 (2013).
307. Rodríguez-Prados, J.-C. *et al.* Substrate Fate in Activated Macrophages: A Comparison between Innate, Classic, and Alternative Activation. *J. Immunol.* **185**, 605–614 (2010).
308. Everts, B. *et al.* TLR-driven early glycolytic reprogramming via the kinases TBK1-IKKε supports the anabolic demands of dendritic cell activation. *Nat. Immunol.* **15**, 323–332 (2014).
309. Wu, L. *et al.* Metabolic regulation of dendritic cell activation and immune function during inflammation. *Front. Immunol.* **14**, 1140749 (2023).
310. Krawczyk, C. M. *et al.* Toll-like receptor–induced changes in glycolytic metabolism regulate dendritic cell activation. *Blood* **115**, 4742–4749 (2010).
311. Everts, B. *et al.* TLR-driven early glycolytic reprogramming via the kinases TBK1-IKKε supports the anabolic demands of dendritic cell activation. *Nat. Immunol. 2014 154* **15**, 323–332 (2014).
312. O'Neill, L. A. J. & Pearce, E. J. Immunometabolism governs dendritic cell and macrophage function. *Journal of Experimental Medicine* vol. 213 15–23 (2016).
313. Clementi, E., Brown, G. C., Feelisch, M. & Moncada, S. Persistent inhibition of cell respiration by nitric oxide: Crucial role of S-nitrosylation of mitochondrial complex I and protective action of glutathione. *Proc. Natl. Acad. Sci. U. S. A.* **95**, 7631–7636 (1998).
314. Carroll, K. C., Viollet, B. & Suttles, J. AMPKα1 deficiency amplifies proinflammatory myeloid APC activity and CD40 signaling. *J. Leukoc. Biol.* **94**, 1113–1121 (2013).
315. Sukhbaatar, N., Hengstschläger, M. & Weichhart, T. mTOR-Mediated Regulation of Dendritic Cell Differentiation and Function. *Trends Immunol.* **37**, 778–789 (2016).
316. Frauwirth, K. A. *et al.* The CD28 signaling pathway regulates glucose metabolism. *Immunity* **16**, 769–777 (2002).
317. Chang, C. H. *et al.* Posttranscriptional control of T cell effector function by aerobic glycolysis. *Cell* **153**, 1239 (2013).
318. Sena, L. A. *et al.* Mitochondria Are Required for Antigen-Specific T Cell Activation through Reactive Oxygen Species Signaling. *Immunity* **38**, 225–236 (2013).
319. DeBerardinis, R. J., Lum, J. J., Hatzivassiliou, G. & Thompson, C. B. The Biology of Cancer: Metabolic Reprogramming Fuels Cell Growth and Proliferation. *Cell Metab.* **7**, 11–20 (2008).
320. Kidani, Y. *et al.* Sterol regulatory element–binding proteins are essential for the metabolic programming of effector T cells and adaptive immunity. *Nat. Immunol. 2013 145* **14**, 489–499 (2013).
321. Carr, E. L. *et al.* Glutamine Uptake and Metabolism Are Coordinately Regulated by ERK/MAPK during T Lymphocyte Activation. *J. Immunol.* **185**, 1037–1044 (2010).

322. Michalek, R. D. *et al.* Cutting Edge: Distinct Glycolytic and Lipid Oxidative Metabolic Programs Are Essential for Effector and Regulatory CD4+ T Cell Subsets. *J. Immunol.* **186**, 3299–3303 (2011).
323. Weinberg, S. E. *et al.* Mitochondrial complex III is essential for suppressive function of regulatory T cells. *Nat. 2019 5657740* **565**, 495–499 (2019).
324. Fu, Z. *et al.* Requirement of Mitochondrial Transcription Factor A in Tissue-Resident Regulatory T Cell Maintenance and Function. *Cell Rep.* **28**, 159-171.e4 (2019).
325. Serhan, C. N. & Savill, J. Resolution of inflammation: the beginning programs the end. *Nat. Immunol. 2005 612* **6**, 1191–1197 (2005).
326. Headland, S. E. & Norling, L. V. The resolution of inflammation: Principles and challenges. *Semin. Immunol.* **27**, 149–160 (2015).
327. Sugimoto, M. A., Sousa, L. P., Pinho, V., Perretti, M. & Teixeira, M. M. Resolution of inflammation: What controls its onset? *Front. Immunol.* **7**, 189956 (2016).
328. Das, A., Ganesh, K., Khanna, S., Sen, C. K. & Roy, S. Engulfment of Apoptotic Cells by Macrophages: A Role of MicroRNA-21 in the Resolution of Wound Inflammation. *J. Immunol.* **192**, 1120–1129 (2014).
329. Nathan, C. Neutrophils and immunity: challenges and opportunities. *Nat. Rev. Immunol. 2006 63* **6**, 173–182 (2006).
330. Vacchini, A., Locati, M. & Borroni, E. M. Overview and potential unifying themes of the atypical chemokine receptor family. *J. Leukoc. Biol.* **99**, 883–892 (2016).
331. Dean, R. A. *et al.* Macrophage-specific metalloelastase (MMP-12) truncates and inactivates ELR+ CXC chemokines and generates CCL2, -7, -8, and -13 antagonists: potential role of the macrophage in terminating polymorphonuclear leukocyte influx. *Blood* **112**, 3455–3464 (2008).
332. Xue, M. & Jackson, C. J. Extracellular Matrix Reorganization During Wound Healing and Its Impact on Abnormal Scarring. *Adv. Wound Care* **4**, 119 (2015).
333. Frantz, C., Stewart, K. M. & Weaver, V. M. The extracellular matrix at a glance. *Journal of Cell Science* vol. 123 4195–4200 (2010).
334. Tonnesen, M. G., Feng, X. & Clark, R. A. F. Angiogenesis in wound healing. *J. Investig. dermatology. Symp. Proc.* **5**, 40–46 (2000).
335. Vannella, K. M. & Wynn, T. A. Mechanisms of Organ Injury and Repair by Macrophages. *Annu. Rev. Physiol.* **79**, 593–617 (2017).
336. Akhurst, R. J. & Hata, A. Targeting the TGFβ signalling pathway in disease. *Nature Reviews Drug Discovery* vol. 11 790–811 (2012).
337. Mirza, R., DiPietro, L. A. & Koh, T. J. Selective and specific macrophage ablation is detrimental to wound healing in mice. *Am. J. Pathol.* **175**, 2454–2462 (2009).
338. Chousterman, B. G., Swirski, F. K. & Weber, G. F. Cytokine storm and sepsis disease pathogenesis. doi:10.1007/s00281-017-0639-8.
339. Qudus, M. S. *et al.* The roles of critical pro-inflammatory cytokines in the drive of cytokine storm during SARS-CoV-2 infection. *J. Med. Virol.* **95**, e28751 (2023).
340. Furman, D. *et al.* Chronic inflammation in the etiology of disease across the life span. *Nat. Med. 2019 2512* **25**, 1822–1832 (2019).
341. Chen, L. *et al.* Inflammatory responses and inflammation-associated diseases in organs. *Oncotarget* **9**, 7204 (2018).

342. Liu, C. H. *et al.* Biomarkers of chronic inflammation in disease development and prevention: challenges and opportunities. *Nat. Immunol. 2017 1811* **18**, 1175–1180 (2017).
343. Ross, E. A., Devitt, A. & Johnson, J. R. Macrophages: The Good, the Bad, and the Gluttony. *Front. Immunol.* **12**, 708186 (2021).
344. Parisi, L. *et al.* Macrophage Polarization in Chronic Inflammatory Diseases: Killers or Builders? (2018) doi:10.1155/2018/8917804.
345. Ushach, I. & Zlotnik, A. Biological role of granulocyte macrophage colony-stimulating factor (GM-CSF) and macrophage colony-stimulating factor (M-CSF) on cells of the myeloid lineage. *J. Leukoc. Biol.* **100**, 481 (2016).
346. Popova, A., Kzhyshkowska, J., Nurgazieva, D., Goerdt, S. & Gratchev, A. Pro- and anti-inflammatory control of M-CSF-mediated macrophage differentiation. *Immunobiology* **216**, 164–172 (2011).
347. Laskin, D. L., Sunil, V. R., Gardner, C. R. & Laskin, J. D. Macrophages and Tissue Injury: Agents of Defense or Destruction? *Annu. Rev. Pharmacol. Toxicol.* **51**, 267 (2011).
348. Pisetsky, D. S. Pathogenesis of autoimmune disease. *Nat. Rev. Nephrol. 2023 198* **19**, 509–524 (2023).
349. Pisetsky, D. S. Pathogenesis of autoimmune disease. *Nat. Rev. Nephrol. 2023 198* **19**, 509–524 (2023).
350. Vojdani, A., Pollard, K. M. & Campbell, A. W. Environmental Triggers and Autoimmunity. *Autoimmune Dis.* **2014**, (2014).
351. Miller, A. L., Bessho, S., Grando, K. & Tükel, Ç. Microbiome or Infections: Amyloid-Containing Biofilms as a Trigger for Complex Human Diseases. *Front. Immunol.* **12**, 638867 (2021).
352. Doyle, H. A. & Mamula, M. J. Post-translational protein modifications in antigen recognition and autoimmunity. *Trends Immunol.* **22**, 443–449 (2001).
353. Viglietta, V., Baecher-Allan, C., Weiner, H. L. & Hafler, D. A. Loss of Functional Suppression by CD4+CD25+ Regulatory T Cells in Patients with Multiple Sclerosis. *J. Exp. Med.* **199**, 971–979 (2004).
354. Dominguez-Villar, M., Baecher-Allan, C. M. & Hafler, D. A. Identification of T helper type 1–like, Foxp3+ regulatory T cells in human autoimmune disease. *Nat. Med. 2011 176* **17**, 673–675 (2011).
355. Alunno, A. *et al.* Role of regulatory t cells in rheumatoid arthritis: Facts and hypothesis. *Autoimmun. Highlights* **1**, 45–51 (2010).
356. Haseda, F., Imagawa, A., Murase-Mishiba, Y., Terasaki, J. & Hanafusa, T. CD4+CD45RA−FoxP3high activated regulatory T cells are functionally impaired and related to residual insulin-secreting capacity in patients with type 1 diabetes. *Clin. Exp. Immunol.* **173**, 207–216 (2013).
357. Schneider, A. *et al.* In active relapsing-remitting multiple sclerosis, effector T cell resistance to adaptive Tregs involves IL-6-mediated signaling. *Sci. Transl. Med.* **5**, (2013).
358. Arend, W. P. The balance between IL-1 and IL-1Ra in disease. *Cytokine Growth Factor Rev.* **13**, 323–340 (2002).
359. Xu, D., Mu, R. & Wei, X. The Roles of IL-1 Family Cytokines in the Pathogenesis of Systemic Sclerosis. *Front. Immunol.* **10**, 451830 (2019).
360. Migliorini, P., Italiani, P., Pratesi, F., Puxeddu, I. & Boraschi, D. The IL-1 family cytokines and receptors in autoimmune diseases. *Autoimmun. Rev.* **19**, 102617 (2020).

361. Martin, P., Goldstein, J. D., Mermoud, L., Diaz-Barreiro, A. & Palmer, G. IL-1 Family Antagonists in Mouse and Human Skin Inflammation. *Front. Immunol.* **12**, 652846 (2021).
362. Makaremi, S. *et al.* The role of IL-1 family of cytokines and receptors in pathogenesis of COVID-19. *Inflamm. Res.* **71**, 923 (2022).
363. Dinarello, C. A. Overview of the IL-1 family in innate inflammation and acquired immunity. *Immunol. Rev.* **281**, 8 (2018).
364. Hurme, M. & Santtila, S. IL-1 receptor antagonist (IL-1Ra) plasma levels are co-ordinately regulated by both IL-1Ra and IL-1 I genes. doi:10.1002/(SICI)1521-4141(199808)28:08.
365. Khazim, K., Azulay, E. E., Kristal, B. & Cohen, I. Interleukin 1 gene polymorphism and susceptibility to disease. *Immunol. Rev.* **281**, 40–56 (2018).
366. Ballak, D. B., Stienstra, R., Tack, C. J., Dinarello, C. A. & van Diepen, J. A. IL-1 family members in the pathogenesis and treatment of metabolic disease: Focus on adipose tissue inflammation and insulin resistance. *Cytokine* **75**, 280 (2015).
367. Colantuoni, M. *et al.* Constitutive IL-1RA production by modified immune cells protects against IL-1–mediated inflammatory disorders. *Sci. Transl. Med.* **15**, (2023).
368. Gabay, C., Smith, M. F., Eidlen, D. & Arend, W. P. Interleukin 1 receptor antagonist (IL-1Ra) is an acute-phase protein. *J. Clin. Invest.* **99**, 2930–2940 (1997).
369. Akitsu, A. *et al.* IL-1 receptor antagonist-deficient mice develop autoimmune arthritis due to intrinsic activation of IL-17-producing CCR2+Vγ6+γδ T cells. *Nat. Commun.* **6**, (2015).
370. Isoda, K., Matsuki, T., Kondo, H., Iwakura, Y. & Ohsuzu, F. Deficiency of interleukin-1 receptor antagonist induces aortic valve disease in BALB/c Mice. *Arterioscler. Thromb. Vasc. Biol.* **30**, 708–715 (2010).
371. Dong, W. *et al.* Deficiency of interleukin-1 receptor antagonist in mice differentially affects bone properties under different genomic backgrounds. *Sci. Reports 2024 141* **14**, 1–11 (2024).
372. FDA. LANREOTIDE injection, for subcutaneous use.
373. Akash, M. S. H. *et al.* Sustained delivery of IL-1Ra from pluronic F127-based thermosensitive gel prolongs its therapeutic potentials. *Pharm. Res.* **29**, 3475–3485 (2012).
374. Qiu, B., Gong, M., He, Q. T. & Zhou, P. H. Controlled release of interleukin-1 receptor antagonist from hyaluronic acid-chitosan microspheres attenuates interleukin-1 β -induced inflammation and apoptosis in chondrocytes. *Biomed Res. Int.* **2016**, (2016).
375. Biernacka, A., Dobaczewski, M. & Frangogiannis, N. G. TGF-β signaling in fibrosis. *Growth Factors* **29**, 196–202 (2011).
376. Hahm, K. B. *et al.* Loss of transforming growth factor beta signalling in the intestine contributes to tissue injury in inflammatory bowel disease. *Gut* **49**, 190–198 (2001).
377. Zhang, Y., Alexander, P. B. & Wang, X. F. TGF-β Family Signaling in the Control of Cell Proliferation and Survival. *Cold Spring Harb. Perspect. Biol.* **9**, (2017).
378. Xu, J., Lamouille, S. & Derynck, R. TGF-β-induced epithelial to mesenchymal transition. *Cell Res. 2009 192* **19**, 156–172 (2009).

379. Finnson, K. W., McLean, S., Guglielmo, G. M. Di & Philip, A. Dynamics of Transforming Growth Factor Beta Signaling in Wound Healing and Scarring. *https://home.liebertpub.com/wound* **2**, 195–214 (2013).
380. Chen, B., Mu, C., Zhang, Z., He, X. & Liu, X. The Love-Hate Relationship Between TGF-β Signaling and the Immune System During Development and Tumorigenesis. *Front. Immunol.* **13**, 891268 (2022).
381. Wang, H. *et al.* Update on Nanoparticle-Based Drug Delivery System for Anti-inflammatory Treatment. *Front. Bioeng. Biotechnol.* **9**, 630352 (2021).
382. Wang, Z. Z., Lu, W. W., Zhen, W., Yang, D. & Peng, S. Novel biomaterial strategies for controlled growth factor delivery for biomedical applications. *NPG Asia Mater.* **9**, e435–e435 (2017).
383. Jo, J., Gao, J.-Q. & Tabata, Y. Biomaterial-based delivery systems of nucleic acid for regenerative research and regenerative therapy. *Regen. Ther.* **11**, 123 (2019).
384. Montes-Cobos, E. *et al.* Targeted delivery of glucocorticoids to macrophages in a mouse model of multiple sclerosis using inorganic-organic hybrid nanoparticles. *J. Control. Release* **245**, 157–169 (2017).
385. Mansour, H. M., Sohn, M. J., Al-Ghananeem, A. & DeLuca, P. P. Materials for pharmaceutical dosage forms: Molecular pharmaceutics and controlled release drug delivery aspects. *International Journal of Molecular Sciences* vol. 11 3298–3322 (2010).
386. Zielinska, A. *et al.* Polymeric Nanoparticles: Production, Characterization, Toxicology and Ecotoxicology. *Molecules* **25**, (2020).
387. van Leent, M. M. T. *et al.* Regulating trained immunity with nanomedicine. *Nat. Rev. Mater. 2022 76* **7**, 465–481 (2022).
388. Sun, B. & Xia, T. Nanomaterial-Based Vaccine Adjuvants. *J. Mater. Chem. B* **4**, 5496 (2016).
389. Getts, D. R. *et al.* Microparticles bearing encephalitogenic peptides induce T-cell tolerance and ameliorate experimental autoimmune encephalomyelitis. *Nat. Biotechnol. 2012 3012* **30**, 1217–1224 (2012).
390. Rhodes, K. R., Meyer, R. A., Wang, J., Tzeng, S. Y. & Green, J. J. Biomimetic Tolerogenic Artificial Antigen Presenting Cells for Regulatory T Cell Induction. *Acta Biomater.* **112**, 136 (2020).
391. Giang, S., Horwitz, D. A., Bickerton, S. & La Cava, A. Nanoparticles Engineered as Artificial Antigen-Presenting Cells Induce Human CD4+ and CD8+ Tregs That Are Functional in Humanized Mice. *Front. Immunol.* **12**, 628059 (2021).
392. Sun, Y. *et al.* DNA origami–based artificial antigen-presenting cells for adoptive T cell therapy. *Sci. Adv.* **8**, 1106 (2022).
393. Lee-Chang, C. & Lesniak, M. S. Next-generation antigen-presenting cell immune therapeutics for gliomas. *J. Clin. Invest.* **133**, (2023).
394. Moorman, C. D., Sohn, S. J. & Phee, H. Emerging Therapeutics for Immune Tolerance: Tolerogenic Vaccines, T cell Therapy, and IL-2 Therapy. *Front. Immunol.* **12**, 657768 (2021).
395. Pei, W. *et al.* Direct modulation of myelin-autoreactive CD4+ and CD8+ T cells in EAE mice by a tolerogenic nanoparticle co-carrying myelin peptide-loaded major histocompatibility complexes, CD47 and multiple regulatory molecules. *Int. J. Nanomedicine* **13**, 3731–3750 (2018).
396. Rejman, J., Oberle, V., Zuhorn, I. S. & Hoekstra, D. Size-dependent internalization of particles via the pathways of clathrin-and caveolae-

mediated endocytosis. *Biochem. J.* **377**, 159–169 (2004).
397. Pratten, M. K. & Lloyd, J. B. Pinocytosis and phagocytosis: the effect of size of a particulate substrate on its mode of capture by rat peritoneal macrophages cultured in vitro. *Biochim. Biophys. Acta - Gen. Subj.* **881**, 307–313 (1986).
398. Champion, J. A., Walker, A. & Mitragotri, S. Role of Particle Size in Phagocytosis of Polymeric Microspheres. *Pharm. Res.* **25**, 1815 (2008).
399. Baranov, M. V., Kumar, M., Sacanna, S., Thutupalli, S. & van den Bogaart, G. Modulation of Immune Responses by Particle Size and Shape. *Front. Immunol.* 3854 (2021).
400. Uribe-Querol, E. & Rosales, C. Phagocytosis: Our Current Understanding of a Universal Biological Process. *Front. Immunol.* **11**, 1066 (2020).
401. Andorko, J. I. & Jewell, C. M. Designing biomaterials with immunomodulatory properties for tissue engineering and regenerative medicine. *Bioeng. Transl. Med.* **2**, 139–155 (2017).
402. Anderson, J. M., Rodriguez, A. & Chang, D. T. Foreign body reaction to biomaterials. *Seminars in Immunology* vol. 20 86–100 (2008).
403. Rabolli, V., Lison, D. & Huaux, F. The complex cascade of cellular events governing inflammasome activation and IL-1β processing in response to inhaled particles. *Part. Fibre Toxicol. 2016 131* **13**, 1–17 (2016).
404. Mitragotri, S. & Lahann, J. Physical approaches to biomaterial design. *Nat. Mater. 2009 81* **8**, 15–23 (2009).
405. Lebre, F. *et al.* The shape and size of hydroxyapatite particles dictate inflammatory responses following implantation. *Sci. Rep.* **7**, 1–13 (2017).
406. Palomäki, J. *et al.* Long, Needle-like Carbon Nanotubes and Asbestos Activate the NLRP3 Inflammasome through a Similar Mechanism. *ACS Nano* **5**, 6861–6870 (2011).
407. Niikura, K. *et al.* Gold nanoparticles as a vaccine platform: Influence of size and shape on immunological responses in vitro and in vivo. *ACS Nano* **7**, 3926–3938 (2013).
408. Sun, B., Wang, X., Ji, Z., Li, R. & Xia, T. NLRP3 Inflammasome Activation Induced by Engineered Nanomaterials. *Small* **9**, 1595–1607 (2013).
409. Seong, S. Y. & Matzinger, P. Hydrophobicity: An ancient damage-associated molecular pattern that initiates innate immune responses. *Nature Reviews Immunology* vol. 4 469–478 (2004).
410. Neumann, S. *et al.* Activation of the NLRP3 inflammasome is not a feature of all particulate vaccine adjuvants. *Immunol. Cell Biol.* **92**, 535–542 (2014).
411. Fifis, T. *et al.* Size-Dependent Immunogenicity: Therapeutic and Protective Properties of Nano-Vaccines against Tumors. *J. Immunol.* **173**, 3148–3154 (2004).
412. Oyewumi, M. O., Kumar, A. & Cui, Z. Nano-microparticles as immune adjuvants: correlating particle sizes and the resultant immune responses. *Expert Rev. Vaccines* **9**, 1095 (2010).
413. Mant, A., Chinnery, F., Elliott, T. & Williams, A. P. The pathway of cross-presentation is influenced by the particle size of phagocytosed antigen. *Immunology* **136**, 163 (2012).
414. Munoz-Wolf, Natalia, Ward, R. W. & Al., E. Non-Canonical Inflammasome Activation Mediates the Adjuvanticity of Nanoparticles. *Cell Reports Med.* (2022) doi:10.2139/SSRN.4024552.
415. Mottram, P. L. *et al.* Type 1 and 2 immunity following vaccination is

influenced by nanoparticle size: formulation of a model vaccine for respiratory syncytial virus. *Mol. Pharm.* **4**, 73–84 (2007).
416. Kanchan, V. & Panda, A. K. Interactions of antigen-loaded polylactide particles with macrophages and their correlation with the immune response. *Biomaterials* **28**, 5344–5357 (2007).
417. Shardlow, E., Mold, M. & Exley, C. From stock bottle to vaccine: Elucidating the particle size distributions of aluminum adjuvants using dynamic light scattering. *Front. Chem.* **5**, 239174 (2017).
418. Oleszycka, E. *et al.* The vaccine adjuvant alum promotes IL-10 production that suppresses Th1 responses. *Eur. J. Immunol.* **48**, 705–715 (2018).
419. Li, Y., Fujita, M. & Boraschi, D. Endotoxin contamination in nanomaterials leads to the misinterpretation of immunosafety results. *Front. Immunol.* **8**, 251213 (2017).
420. Gorbet, M. B. & Sefton, M. V. Endotoxin: The uninvited guest. *Biomaterials* **26**, 6811–6817 (2005).
421. Huete-Carrasco, J., Lynch, R. I., Ward, R. W. & Lavelle, E. C. Rational design of polymer-based particulate vaccine adjuvants. *Eur. J. Immunol* **54**, 2350512 (2024).
422. Lynch, R. I. & Lavelle, E. C. Immuno-modulatory biomaterials as anti-inflammatory therapeutics. *Biochemical Pharmacology* vol. 197 (2022).
423. Mahon, O. R. *et al.* Nano-particle mediated M2 macrophage polarization enhances bone formation and MSC osteogenesis in an IL-10 dependent manner. *Biomaterials* **239**, 119833 (2020).
424. Oró, D. *et al.* Cerium oxide nanoparticles reduce steatosis, portal hypertension and display anti-inflammatory properties in rats with liver fibrosis. *J. Hepatol.* **64**, 691–698 (2016).
425. Da Silva, C. A. *et al.* Chitin Is a Size-Dependent Regulator of Macrophage TNF and IL-10 Production. *J. Immunol.* **182**, 3573–3582 (2009).
426. Placha, D. & Jampilek, J. Chronic Inflammatory Diseases, Anti-Inflammatory Agents and Their Delivery Nanosystems. *Pharmaceutics* **13**, 1–27 (2021).
427. Wynn, T. A. & Vannella, K. M. Macrophages in Tissue Repair, Regeneration, and Fibrosis. *Immunity* vol. 44 450–462 (2016).
428. Gan, J. *et al.* Producing anti-inflammatory macrophages by nanoparticle-triggered clustering of mannose receptors. *Biomaterials* **178**, 95–108 (2018).
429. Laroui, H. *et al.* Fab'-bearing siRNA TNFα-loaded nanoparticles targeted to colonic macrophages offer an effective therapy for experimental colitis. *J. Control. Release* **186**, 41–53 (2014).
430. Rosenblum, M. D., Gratz, I. K., Paw, J. S. & Abbas, A. K. Treating Human Autoimmunity: Current Practice and Future Prospects. *Sci. Transl. Med.* **4**, 125sr1 (2012).
431. Campbell, N. K. *et al.* Naturally derived Heme-Oxygenase 1 inducers attenuate inflammatory responses in human dendritic cells and T cells: relevance for psoriasis treatment. *Sci. Reports 2018 81* **8**, 1–15 (2018).
432. Wu, J. & Horuzsko, A. Expression and function of immunoglobulin-like transcripts on tolerogenic dendritic cells. *Hum. Immunol.* **70**, 353–356 (2009).
433. Huo, C. W. *et al.* High mammographic density in women is associated with protumor inflammation. *Breast Cancer Res.* **20**, 1–16 (2018).

434. Wolfle, S. J. *et al.* PD-L1 expression on tolerogenic APCs is controlled by STAT-3. *Eur. J. Immunol.* **41**, 413–424 (2011).
435. Passeri, L., Marta, F., Bassi, V. & Gregori, S. Tolerogenic dendritic cell-based approaches in autoimmunity. *International Journal of Molecular Sciences* vol. 22 (2021).
436. Puricelli, C. *et al.* Cutting-Edge Delivery Systems and Adjuvants in Tolerogenic Vaccines: A Review. *Pharmaceutics* **14**, (2022).
437. Cifuentes-Rius, A., Desai, A., Yuen, D., Johnston, A. P. R. & Voelcker, N. H. Inducing immune tolerance with dendritic cell-targeting nanomedicines. *Nat. Nanotechnol.* **16**, 37–46 (2021).
438. Pujol-Autonell, I. *et al.* Use of Autoantigen-Loaded Phosphatidylserine-Liposomes to Arrest Autoimmunity in Type 1 Diabetes. *PLoS One* **10**, e0127057 (2015).
439. Saito, E. *et al.* Designing drug-free biodegradable nanoparticles to modulate inflammatory monocytes and neutrophils for ameliorating inflammation. *J. Control. Release* **300**, 185–196 (2019).
440. Maldonado, R. A. *et al.* Polymeric synthetic nanoparticles for the induction of antigen-specific immunological tolerance. *Proc. Natl. Acad. Sci. U. S. A.* **112**, E156–E165 (2015).
441. Yeste, A., Nadeau, M., Burns, E. J., Weiner, H. L. & Quintana, F. J. Nanoparticle-mediated codelivery of myelin antigen and a tolerogenic small molecule suppresses experimental autoimmune encephalomyelitis. *Proc. Natl. Acad. Sci. U. S. A.* **109**, 11270–11275 (2012).
442. Yeste, A. *et al.* Tolerogenic nanoparticles inhibit T cell-mediated autoimmunity through SOCS2. *Sci. Signal.* **9**, (2016).
443. Lewis, J. S. *et al.* Dual-Sized Microparticle System for Generating Suppressive Dendritic Cells Prevents and Reverses Type 1 Diabetes in the Nonobese Diabetic Mouse Model. *ACS Biomater. Sci. Eng.* **5**, 2631–2646 (2019).
444. Cappellano, G. *et al.* Subcutaneous inverse vaccination with PLGA particles loaded with a MOG peptide and IL-10 decreases the severity of experimental autoimmune encephalomyelitis. *Vaccine* **32**, 5681–5689 (2014).
445. Engman, C. *et al.* Generation of antigen-specific Foxp3+ regulatory T-cells in vivo following administration of diabetes-reversing tolerogenic microspheres does not require provision of antigen in the formulation. *Clin. Immunol.* **160**, 103–123 (2015).
446. Manolova, V. *et al.* Nanoparticles target distinct dendritic cell populations according to their size. *Eur. J. Immunol.* **38**, 1404–1413 (2008).
447. Gerner, M. Y., Torabi-Parizi, P. & Germain, R. N. Strategically localized dendritic cells promote rapid T cell responses to lymph-borne particulate antigens. *Immunity* **42**, 172–185 (2015).
448. Arnold, C. 'Inverse vaccines' could treat autoimmune disease — from multiple sclerosis to celiac disease. *Nat. Med.* **30**, 1218–1219 (2024).
449. Moorman, C. D., Sohn, S. J. & Phee, H. Emerging Therapeutics for Immune Tolerance: Tolerogenic Vaccines, T cell Therapy, and IL-2 Therapy. *Front. Immunol.* **12**, (2021).
450. Steinman, L. Inverse vaccination, the opposite of Jenner's concept, for therapy of autoimmunity. *J. Intern. Med.* **267**, 441–451 (2010).
451. Zhang, W., Rho, J. hyun, Roehrl, M. W., Roehrl, M. H. & Wang, J. Y. A

repertoire of 124 potential autoantigens for autoimmune kidney diseases identified by dermatan sulfate affinity enrichment of kidney tissue proteins. *PLoS One* **14**, (2019).
452. Kim, A., Xie, F., Abed, O. A. & Moon, J. J. Vaccines for immune tolerance against autoimmune disease. *Adv. Drug Deliv. Rev.* **203**, 115140 (2023).
453. Khoury, S. J. *et al.* Acquired tolerance to experimental autoimmune encephalomyelitis by intrathymic injection of myelin basic protein or its major encephalitogenic peptide. *J. Exp. Med.* **178**, 559–566 (1993).
454. Higgins, P. J. & Weiner', H. L. Suppression of experimental autoimmune encephalomyelitis by oral administration of myelin basic protein and its fragments. *J. Immunol.* **140**, 440–445 (1988).
455. Keijzer, C., Van der Zee, R., Van Eden, W. & Broere, F. Treg Inducing Adjuvants for Therapeutic Vaccination Against Chronic Inflammatory Diseases. *Front. Immunol.* **4**, (2013).
456. Spiering, R. *et al.* DEC205+ Dendritic Cell-Targeted Tolerogenic Vaccination Promotes Immune Tolerance in Experimental Autoimmune Arthritis. *J. Immunol.* **194**, 4804–4813 (2015).
457. Ring, S., Maas, M., Nettelbeck, D. M., Enk, A. H. & Mahnke, K. Targeting of autoantigens to DEC205^{+} dendritic cells in vivo suppresses experimental allergic encephalomyelitis in mice. *J. Immunol.* **191**, 2938–2947 (2013).
458. Wang, D. *et al.* IFN-β Facilitates Neuroantigen-Dependent Induction of CD25+ FOXP3+ Regulatory T Cells That Suppress Experimental Autoimmune Encephalomyelitis. *J. Immunol.* **197**, 2992–3007 (2016).
459. Blanchfield, J. L. & Mannie, M. D. A GMCSF-neuroantigen fusion protein is a potent tolerogen in experimental autoimmune encephalomyelitis (EAE) that is associated with efficient targeting of neuroantigen to APC. *J. Leukoc. Biol.* **87**, 509–521 (2010).
460. Puentes, F. *et al.* Immune Modulation and Prevention of Autoimmune Disease by Repeated Sequences from Parasites Linked to Self Antigens. *J. Neuroimmune Pharmacol.* **11**, 749–762 (2016).
461. Belogurov, A. A. *et al.* Liposome-encapsulated peptides protect against experimental allergic encephalitis. *FASEB J.* **27**, 222 (2013).
462. Maulloo, C. D. *et al.* Lymph Node-Targeted Synthetically Glycosylated Antigen Leads to Antigen-Specific Immunological Tolerance. *Front. Immunol.* **12**, 714842 (2021).
463. Murray, J. A. *et al.* Safety and tolerability of KAN-101, a liver-targeted immune tolerance therapy, in patients with coeliac disease (ACeD): a phase 1 trial. *lancet. Gastroenterol. Hepatol.* **8**, 735–747 (2023).
464. Cao, S. *et al.* Glycosylation-modified antigens as a tolerance-inducing vaccine platform prevent anaphylaxis in a pre-clinical model of food allergy. *Cell Reports Med.* **5**, (2024).
465. Capini, C. *et al.* Antigen-specific suppression of inflammatory arthritis using liposomes. *J. Immunol.* **182**, 3556–3565 (2009).
466. Ploix, C. *et al.* Oral administration of cholera toxin B-insulin conjugates protects NOD mice from autoimmune diabetes by inducing CD4+ regulatory T-cells. *Diabetes* **48**, 2150–2156 (1999).
467. Raz, I. *et al.* β-cell function in new-onset type 1 diabetes and immunomodulation with a heat-shock protein peptide (DiaPep277): A randomised, double-blind, phase II trial. *Lancet* **358**, 1749–1753 (2001).
468. Choi, M. Y. & Costenbader, K. H. Understanding the Concept of Pre-

Clinical Autoimmunity: Prediction and Prevention of Systemic Lupus Erythematosus: Identifying Risk Factors and Developing Strategies Against Disease Development. *Front. Immunol.* **13**, 890522 (2022).
469. Lutterotti, A., Hayward-Koennecke, H., Sospedra, M. & Martin, R. Antigen-Specific Immune Tolerance in Multiple Sclerosis—Promising Approaches and How to Bring Them to Patients. *Front. Immunol.* **12**, (2021).
470. Jabri, B., Abadie, V. & Stuphorn, V. Restoring tolerance with antigen delivery. *Science (80-.).* **383**, 30–32 (2024).
471. Kazmi, W. & Berin, M. C. Oral tolerance and oral immunotherapy for food allergy: Evidence for common mechanisms? *Cell. Immunol.* **383**, 104650 (2023).
472. Kim, W. U. *et al.* Suppression of collagen-induced arthritis by single administration of poly(lactic-co-glycolic acid) nanoparticles entrapping type II collagen: A novel treatment strategy for induction of oral tolerance. *Arthritis Rheum.* **46**, 1109–1120 (2002).
473. Keijzer, C. *et al.* PLGA nanoparticles enhance the expression of retinaldehyde dehydrogenase enzymes in dendritic cells and induce FoxP3+ T-cells in vitro. *J. Control. Release* **168**, 35–40 (2013).
474. Pan, P. *et al.* Undenatured type II collagen protects against collagen-induced arthritis by restoring gut-joint homeostasis and immunity. *Commun. Biol.* **7**, (2024).
475. Sun, X., Xu, C., Wu, G., Ye, Q. & Wang, C. Review poly(lactic-co-glycolic acid): Applications and future prospects for periodontal tissue regeneration. *Polymers* vol. 9 (2017).
476. Margerrison, E. & Lucas, S. *Medical Device Material Performance Study Polypropylene Safety Profile Prepared for Submitted to Date of Submission*. www.ecri.org (2020).
477. Makadia, H. K. & Siegel, S. J. Poly Lactic-co-Glycolic Acid (PLGA) as biodegradable controlled drug delivery carrier. *Polymers (Basel).* **3**, 1377–1397 (2011).
478. Gentile, P., Chiono, V., Carmagnola, I. & Hatton, P. V. An Overview of Poly(lactic-co-glycolic) Acid (PLGA)-Based Biomaterials for Bone Tissue Engineering. *Int. J. Mol. Sci.* **15**, 3640 (2014).
479. Grover, C. N., Cameron, R. E. & Best, S. M. Investigating the morphological, mechanical and degradation properties of scaffolds comprising collagen, gelatin and elastin for use in soft tissue engineering. *J. Mech. Behav. Biomed. Mater.* **10**, 62–74 (2012).
480. Elmowafy, E. M., Tiboni, M. & Soliman, M. E. Biocompatibility, biodegradation and biomedical applications of poly(lactic acid)/poly(lactic-co-glycolic acid) micro and nanoparticles. *J. Pharm. Investig. 2019 494* **49**, 347–380 (2019).
481. Han, F. Y., Thurecht, K. J., Whittaker, A. K. & Smith, M. T. Bioerodable PLGA-based microparticles for producing sustained-release drug formulations and strategies for improving drug loading. *Frontiers in Pharmacology* vol. 7 185 (2016).
482. Astete, C. E. & Sabliov, C. M. Synthesis and characterization of PLGA nanoparticles. *Journal of Biomaterials Science, Polymer Edition* vol. 17 247–289 (2006).
483. Huang, W. & Zhang, C. Tuning the Size of Poly(lactic-co-glycolic Acid) (PLGA) Nanoparticles Fabricated by Nanoprecipitation. *Biotechnol. J.* **13**,

(2018).
484. Zhang, X. & Mosser, D. M. Macrophage activation by endogenous danger signals. *Journal of Pathology* vol. 214 161–178 (2008).
485. Zhao, R., Liang, H., Clarke, E., Jackson, C. & Xue, M. Inflammation in chronic wounds. *International Journal of Molecular Sciences* vol. 17 (2016).
486. Rohm, T. V., Meier, D. T., Olefsky, J. M. & Donath, M. Y. Inflammation in obesity, diabetes, and related disorders. *Immunity* **55**, 31–55 (2022).
487. Rubin, D. C., Shaker, A. & Levin, M. S. Chronic intestinal inflammation: Inflammatory bowel disease and colitis-associated colon cancer. *Front. Immunol.* **3**, 22422 (2012).
488. Nedeva, C., Menassa, J. & Puthalakath, H. Sepsis: Inflammation is a necessary evil. *Front. Cell Dev. Biol.* **7**, 447614 (2019).
489. Ordikhani, F., Pothula, V., Sanchez-Tarjuelo, R., Jordan, S. & Ochando, J. Macrophages in Organ Transplantation. *Front. Immunol.* **11**, 582939 (2020).
490. Chen, H., Agrawal, D. K. & Thankam, F. G. Biomaterials-Driven Sterile Inflammation. *Tissue Engineering - Part B: Reviews* vol. 28 22–34 (2022).
491. Anderson, J. M., Rodriguez, A. & Chang, D. T. Foreign body reaction to biomaterials. *Seminars in Immunology* vol. 20 86–100 (2008).
492. Tabas, I. & Glass, C. K. Anti-inflammatory therapy in chronic disease: Challenges and opportunities. *Science (80-.).* **339**, 166–172 (2013).
493. Gordon, S. & Taylor, P. R. Monocyte and macrophage heterogeneity. *Nature Reviews Immunology* vol. 5 953–964 (2005).
494. Mosser, D. M. The many faces of macrophage activation. *J. Leukoc. Biol.* **73**, 209–212 (2003).
495. Dinarello, C. A., Simon, A. & Van Der Meer, J. W. M. Treating inflammation by blocking interleukin-1 in a broad spectrum of diseases. *Nature Reviews Drug Discovery* vol. 11 633–652 (2012).
496. Brusini, R., Varna, M. & Couvreur, P. Advanced nanomedicines for the treatment of inflammatory diseases. *Adv. Drug Deliv. Rev.* **157**, 161–178 (2020).
497. Calafiore, R., Basta, G. & Montanucci, P. Microencapsulation of islets for the treatment of type 1 diabetes mellitus (T1D). in *Methods in Molecular Biology* vol. 1479 283–304 (Humana Press Inc., 2017).
498. Anselmo, A. C. & Mitragotri, S. Nanoparticles in the clinic: An update. *Bioeng. Transl. Med.* **4**, (2019).
499. Silva, A. L., Soema, P. C., Slütter, B., Ossendorp, F. & Jiskoot, W. PLGA particulate delivery systems for subunit vaccines: Linking particle properties to immunogenicity. *Hum. Vaccin. Immunother.* **12**, 1056 (2016).
500. Shanley, L. C. *et al.* Macrophage Metabolic Profile is Altered by Hydroxyapatite Particle Size. *SSRN Electron. J.* (2022) doi:10.2139/ssrn.4243936.
501. McCluskey S. Size regulates particulate adjuvant induced IL-10 and IL-12p70 production. (TCD, 2018).
502. Netea, M. G., Quintin, J. & Van Der Meer, J. W. M. Trained Immunity: A Memory for Innate Host Defense. *Cell Host Microbe* **9**, 355–361 (2011).
503. Italiani, P. & Boraschi, D. Induction of innate immune memory by engineered nanoparticles: A hypothesis that may become true. *Front. Immunol.* **8**, 734 (2017).
504. Lund, M. E., To, J., O'Brien, B. A. & Donnelly, S. The choice of phorbol 12-

myristate 13-acetate differentiation protocol influences the response of THP-1 macrophages to a pro-inflammatory stimulus. *J. Immunol. Methods* **430**, 64–70 (2016).
505. Park, E. K. *et al.* Optimized THP-1 differentiation is required for the detection of responses to weak stimuli. *Inflamm. Res.* **56**, 45–50 (2007).
506. Wang, S. *et al.* β-Glucan attenuates inflammatory responses in oxidized LDL-induced THP-1 cells via the p38 MAPK pathway. *Nutr. Metab. Cardiovasc. Dis.* **24**, 248–255 (2014).
507. Chanput, W. *et al.* β-Glucans are involved in immune-modulation of THP-1 macrophages. *Mol. Nutr. Food Res.* **56**, 822–833 (2012).
508. Elmore, S. Apoptosis: A Review of Programmed Cell Death. *Toxicol. Pathol.* **35**, 495 (2007).
509. Xiang, J., Wan, C., Guo, R. & Guo, D. Is Hydrogen Peroxide a Suitable Apoptosis Inducer for All Cell Types? *Biomed Res. Int.* **2016**, (2016).
510. Mezu-Ndubuisi, O. J. & Maheshwari, A. The role of integrins in inflammation and angiogenesis. *Pediatr. Res. 2020 897* **89**, 1619–1626 (2020).
511. Kreuter, J. Possibilities of using nanoparticles as carriers for drugs and vaccines. *Journal of Microencapsulation* vol. 5 115–127 (1988).
512. Wang, Y., Wen, Q. & Choi, S. FDA's Regulatory Science Program for Generic PLA/ PLGA-Based Drug Products | American Pharmaceutical Review - The Review of American Pharmaceutical Business & Technology. *Am Pharm Rev.* **19**, 5–9 (2016).
513. Champion, J. A. & Mitragotri, S. Role of target geometry in phagocytosis. *Proc. Natl. Acad. Sci. U. S. A.* **103**, 4930–4934 (2006).
514. Tahtinen, S. *et al.* IL-1 and IL-1ra are key regulators of the inflammatory response to RNA vaccines. *Nat. Immunol. 2022 234* **23**, 532–542 (2022).
515. Center watch. Kineret (anakinra) | CenterWatch. https://www.centerwatch.com/directories/1067-fda-approved-drugs/listing/3720-kineret-anakinra#:~:text=Kineret (anakinra) - 3 indications&text=for the treatment of Rheumatoid Arthritis%3B approved November 2001.
516. Carlini, V. *et al.* The multifaceted nature of IL-10: regulation, role in immunological homeostasis and its relevance to cancer, COVID-19 and post-COVID conditions. *Front. Immunol.* **14**, 1161067 (2023).
517. Tynan, G. A., McNaughton, A., Jarnicki, A., Tsuji, T. & Lavelle, E. C. Polymyxin B Inadequately Quenches the Effects of Contaminating Lipopolysaccharide on Murine Dendritic Cells. *PLoS One* **7**, e37261 (2012).
518. Verdeguer, F. & Aouadi, M. Macrophage heterogeneity and energy metabolism. *Exp. Cell Res.* **360**, 35–40 (2017).
519. Bomans, K. *et al.* Sepsis induces a long-lasting state of trained immunity in bone marrow monocytes. *Front. Immunol.* **9**, 2685 (2018).
520. HogenEsch, H., O'Hagan, D. T. & Fox, C. B. Optimizing the utilization of aluminum adjuvants in vaccines: you might just get what you want. *npj Vaccines* vol. 3 1–11 (2018).
521. Jentho, E. *et al.* Trained innate immunity, long-lasting epigenetic modulation, and skewed myelopoiesis by heme. *Proc. Natl. Acad. Sci. U. S. A.* **118**, (2021).
522. Mestas, J. & Hughes, C. C. W. Of Mice and Not Men: Differences between Mouse and Human Immunology. *J. Immunol.* **172**, 2731–2738 (2004).

523. Bjornson-Hooper, Z. B. *et al.* A Comprehensive Atlas of Immunological Differences Between Humans, Mice, and Non-Human Primates. *Front. Immunol.* **13**, 867015 (2022).
524. Tedesco, S. *et al.* Convenience versus biological significance: Are PMA-differentiated THP-1 cells a reliable substitute for blood-derived macrophages when studying in vitro polarization? *Front. Pharmacol.* **9**, 318678 (2018).
525. Certo, M., Llibre, A., Lee, W. & Mauro, C. Understanding lactate sensing and signalling. (2022) doi:10.1016/j.tem.2022.07.004.
526. Caslin, H. L., Abebayehu, D., Pinette, J. A. & Ryan, J. J. Lactate Is a Metabolic Mediator That Shapes Immune Cell Fate and Function. *Front. Physiol.* **12**, 688485 (2021).
527. Lim, Y. W. *et al.* Challenges and Complications of Poly(lactic-co-glycolic acid)-Based Long-Acting Drug Product Development. *Pharmaceutics* **14**, (2022).
528. Mohammad, A. K. & Reineke, J. J. Quantitative detection of PLGA nanoparticle degradation in tissues following intravenous administration. *Mol. Pharm.* **10**, 2183–2189 (2013).
529. Patel, N. R. *et al.* Cell Elasticity Determines Macrophage Function. *PLoS One* **7**, e41024 (2012).
530. Rys, J. P. *et al.* Discrete spatial organization of TGFβ receptors couples receptor multimerization and signaling to cellular tension. *Elife* **4**, (2015).
531. Green, J. M. *et al.* Role of Cholesterol in Formation and Function of a Signaling Complex Involving αvβ3, Integrin-Associated Protein (Cd47), and Heterotrimeric G Proteins. *J. Cell Biol.* **146**, 673–682 (1999).
532. Lietha, D. & Izard, T. Roles of Membrane Domains in Integrin-Mediated Cell Adhesion. *Int. J. Mol. Sci.* **21**, 1–19 (2020).
533. Ge, Y., Gao, J., Jordan, R. & Naumann, C. A. Changes in Cholesterol Level Alter Integrin Sequestration in Raft-Mimicking Lipid Mixtures. *Biophys. J.* **114**, 158–167 (2018).
534. Decker, L. & Ffrench-Constant, C. Lipid Rafts and Integrin Activation Regulate Oligodendrocyte Survival. *J. Neurosci.* **24**, 3816–3825 (2004).
535. Desai, A. J. & Miller, L. J. Changes in the plasma membrane in metabolic disease: impact of the membrane environment on G protein-coupled receptor structure and function. *Br. J. Pharmacol.* **175**, 4009 (2018).
536. Hoffmann, E. J. & Ponik, S. M. Biomechanical Contributions to Macrophage Activation in the Tumor Microenvironment. *Front. Oncol.* **10**, 787 (2020).
537. McEntee, C. P., Gunaltay, S. & Travis, M. A. Regulation of barrier immunity and homeostasis by integrin-mediated transforming growth factor β activation. *Immunology* **160**, 139 (2020).
538. Wilder, R. L. Integrin alpha V beta 3 as a target for treatment of rheumatoid arthritis and related rheumatic diseases. in *Annals of the Rheumatic Diseases* vol. 61 (BMJ Publishing Group, 2002).
539. Kelly, A. *et al.* Human monocytes and macrophages regulate immune tolerance via integrin αvβ8–mediated TGFβ activation. *J. Exp. Med.* **215**, 2725–2736 (2018).
540. Zhang, Y. & Wang, H. Integrin signalling and function in immune cells. *Immunology* **135**, 268 (2012).
541. Asano, Y. *et al.* Increased Expression of Integrin αvβ3 Contributes to the Establishment of Autocrine TGF-β Signaling in Scleroderma Fibroblasts. *J.*

Immunol. **175**, 7708–7718 (2005).
542. Antonov, A. S. *et al.* αVβ3 Integrin Regulates Macrophage Inflammatory Responses via PI3 Kinase/Akt-Dependent NF-κB Activation. *J. Cell. Physiol.* **226**, 469 (2011).
543. Inaba, K., Metlay, J. P., Crowley, M. T. & Steinman, R. M. Dendritic cells pulsed with protein antigens in vitro can prime antigen-specific, MHC-restricted T cells in situ. *J. Exp. Med.* **172**, 631–640 (1990).
544. Zhuang, Q. *et al.* Tolerogenic Dendritic Cells: The Pearl of Immunotherapy in Organ Transplantation. *Front. Immunol.* **11**, (2020).
545. Sun, L., Su, Y., Jiao, A., Wang, X. & Zhang, B. T cells in health and disease. *Signal Transduct. Target. Ther. 2023 81* **8**, 1–50 (2023).
546. Sumida, T. S., Cheru, N. T. & Hafler, D. A. The regulation and differentiation of regulatory T cells and their dysfunction in autoimmune diseases. *Nat. Rev. Immunol. 2024* 1–15 (2024) doi:10.1038/s41577-024-00994-x.
547. Giannoukakis, N., Phillips, B., Finegold, D., Harnaha, J. & Trucco, M. Phase I (safety) study of autologous tolerogenic dendritic cells in type 1 diabetic patients. *Diabetes Care* **34**, 2026–2032 (2011).
548. Bell, G. M. *et al.* Autologous tolerogenic dendritic cells for rheumatoid and inflammatory arthritis. *Ann. Rheum. Dis.* **76**, 227–234 (2017).
549. Amini, L. *et al.* Clinical adoptive regulatory T Cell therapy: State of the art, challenges, and prospective. *Front. Cell Dev. Biol.* **10**, (2023).
550. Bluestone, J. A., McKenzie, B. S., Beilke, J. & Ramsdell, F. Opportunities for Treg cell therapy for the treatment of human disease. *Front. Immunol.* **14**, (2023).
551. Hartemann, A. *et al.* Low-dose interleukin 2 in patients with type 1 diabetes: a phase 1/2 randomised, double-blind, placebo-controlled trial. *lancet. Diabetes Endocrinol.* **1**, 295–305 (2013).
552. Mekala, D. J. & Geiger, T. L. Immunotherapy of autoimmune encephalomyelitis with redirected CD4+CD25+ T lymphocytes. *Blood* **105**, 2090–2092 (2005).
553. Rana, J. & Biswas, M. Regulatory T cell therapy: Current and future design perspectives. *Cell. Immunol.* **356**, 104193 (2020).
554. He, J. *et al.* Low-dose interleukin-2 treatment selectively modulates CD4(+) T cell subsets in patients with systemic lupus erythematosus. *Nat. Med.* **22**, 991–993 (2016).
555. Roemhild, A. *et al.* Regulatory T cells for minimising immune suppression in kidney transplantation: phase I/IIa clinical trial. *BMJ* **371**, (2020).
556. Zhang, Y. & Wang, H. Integrin signalling and function in immune cells. *Immunology* **135**, 268 (2012).
557. Fu, S. *et al.* TGF-β Induces Foxp3 + T-Regulatory Cells from CD4 + CD25 − Precursors. *Am. J. Transplant.* **4**, 1614–1627 (2004).
558. Ward, R. Particulate adjuvants for use in cancer vaccination. (2023).
559. Chakraborty, S. & Sa, G. Development, maintenance and functions of CD8+ T-regulatory cells: Molecular orchestration of FOXP3 transcription. *J. Immunol. Sci.* **2**, 8–12 (2018).
560. Beres, A. J. *et al.* CD8+ Foxp3+ regulatory T cells are induced during graft-versus-host disease and mitigate disease severity. *J. Immunol.* **189**, 464–474 (2012).
561. Pang, X. *et al.* Targeting integrin pathways: mechanisms and advances in

therapy. *Signal Transduct. Target. Ther. 2022 81* **8**, 1–42 (2023).
562. Worthington, J. J. *et al.* Integrin αvβ8-Mediated TGF-β Activation by Effector Regulatory T Cells Is Essential for Suppression of T-Cell-Mediated Inflammation. *Immunity* **42**, 903–915 (2015).
563. Chen, P. Y., Qin, L. & Simons, M. TGFβ signaling pathways in human health and disease. *Front. Mol. Biosci.* **10**, 1113061 (2023).
564. Hilligan, K. L. & Ronchese, F. Antigen presentation by dendritic cells and their instruction of CD4+ T helper cell responses. *Cell. Mol. Immunol.* **17**, 587 (2020).
565. Lourenço, E. V. & La Cava, A. Natural regulatory T cells in autoimmunity. *Autoimmunity* **44**, 33 (2011).
566. Schmitt, E. G. & Williams, C. B. Generation and function of induced regulatory T cells. *Front. Immunol.* **4**, 54995 (2013).
567. Catalán, D. *et al.* Immunosuppressive Mechanisms of Regulatory B Cells. *Front. Immunol.* **12**, 611795 (2021).
568. Blumenthal, D., Chandra, V., Avery, L. & Burkhardt, J. K. Mouse T cell priming is enhanced by maturation-dependent stiffening of the dendritic cell cortex. *Elife* **9**, 1–44 (2020).
569. Fritzsche, M., Kruse, K., Edited, I. D. & Garcia, K. Mechanical force matters in early T cell activation. *Proc. Natl. Acad. Sci.* **121**, e2404748121 (2024).
570. Worthington, J. J., Fenton, T. M., Czajkowska, B. I., Klementowicz, J. E. & Travis, M. A. Regulation of TGFβ in the immune system: An emerging role for integrins and dendritic cells. *Immunobiology* **217**, 1259–1265 (2012).
571. Guharay, F. & Sachs, F. Stretch-activated single ion channel currents in tissue-cultured embryonic chick skeletal muscle. *J. Physiol.* **352**, 685–701 (1984).
572. Saika, S., Veldhuis, N., Križaj, D. & Rahaman, S. O. Editorial: New Insights into Mechanotransduction by Immune Cells in Physiological and Pathological Conditions. *Front. Immunol.* **13**, 930362 (2022).
573. Khanna, S. *et al.* Macrophage Dysfunction Impairs Resolution of Inflammation in the Wounds of Diabetic Mice. *PLoS One* **5**, e9539 (2010).
574. Lundahl, M. L. E. *et al.* Macrophage innate training induced by IL-4 and IL-13 activation enhances OXPHOS driven anti-mycobacterial responses. *Elife* **11**, e74690 (2022).
575. Andersen, A. *et al.* National Immunization Campaigns with Oral Polio Vaccine Reduce All-Cause Mortality: A Natural Experiment within Seven Randomized Trials. *Front. public Heal.* **6**, (2018).
576. Rieckmann, A. *et al.* Vaccinations against smallpox and tuberculosis are associated with better long-term survival: a Danish case-cohort study 1971-2010. *Int. J. Epidemiol.* **46**, 695–705 (2017).
577. Ochando, J., Mulder, W. J. M., Madsen, J. C., Netea, M. G. & Duivenvoorden, R. Trained immunity — basic concepts and contributions to immunopathology. *Nat. Rev. Nephrol. 2022 191* **19**, 23–37 (2022).
578. Divangahi, M. *et al.* Trained immunity, tolerance, priming and differentiation: distinct immunological processes. *Nat. Immunol. 2020 221* **22**, 2–6 (2020).
579. Quinn, S. M. *et al.* Anti-inflammatory trained immunity mediated by helminth products attenuates the induction of T cell-mediated autoimmune disease. *Front. Immunol.* **10**, 459836 (2019).
580. Brannon, E. R. *et al.* Polymeric particle-based therapies for acute

inflammatory diseases. *Nat. Rev. Mater. 2022 710* **7**, 796–813 (2022).
581. Lee, M., Du, H., Winer, D. A., Clemente-Casares, X. & Tsai, S. Mechanosensing in macrophages and dendritic cells in steady-state and disease. *Front. Cell Dev. Biol.* **10**, 1044729 (2022).
582. Pechkovsky, D. V. *et al.* Transforming growth factor β1 induces αvβ3 integrin expression in human lung fibroblasts via a β3 integrin-, c-Src-, and p38 MAPK-dependent pathway. *J. Biol. Chem.* **283**, 12898–12908 (2008).
583. Mamuya, F. A. & Duncan, M. K. aV integrins and TGF-β-induced EMT: a circle of regulation. *J. Cell. Mol. Med.* **16**, 445–455 (2012).
584. Mori, S. *et al.* Enhanced Expression of Integrin αvβ3 Induced by TGF-β Is Required for the Enhancing Effect of Fibroblast Growth Factor 1 (FGF1) in TGF-β-Induced Epithelial-Mesenchymal Transition (EMT) in Mammary Epithelial Cells. *PLoS One* **10**, 137486 (2015).
585. Weichhart, T., Hengstschläger, M. & Linke, M. Regulation of innate immune cell function by mTOR. *Nature Reviews Immunology* vol. 15 599–614 (2015).